

AD736469

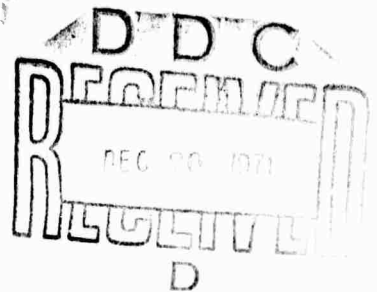
RADC-TR-71-276
Final Technical Report
November 1971



POLAR FOX II STUDY PHASE
Analytical Systems Corporation

Sponsored by
Advanced Research Projects Agency
ARPA Order No. 1765

Approved for public release;
distribution unlimited.



The views and conclusions contained in this document are those of the authors and should not be interpreted as necessarily representing the official policies, either expressed or implied, of the Advanced Research Projects Agency or the U. S. Government.

Rome Air Development Center
Air Force Systems Command
Griffiss Air Force Base, New York

Reproduced by
NATIONAL TECHNICAL
INFORMATION SERVICE
Springfield, Va 22151

**BEST
AVAILABLE COPY**

UNCLASSIFIED

Security Classification

DOCUMENT CONTROL DATA - R & D

(Security classification of title, body of abstract and indexing annotation must be entered when the overall report is classified)

1. ORIGINATING ACTIVITY (Corporate author)		2a. REPORT SECURITY CLASSIFICATION	
Analytical Systems Corp. 11 Ray Avenue Burlington, MA 01803		UNCLASSIFIED	
3. REPORT TITLE		2b. GROUP	
Polar Fox II Study Phase			
4. DESCRIPTIVE NOTES (Type of report and inclusive dates)			
Final Report			
5. AUTHOR(S) (First name, middle initial, last name)			
John R. Herman R. Vargas-Vila			
6. REPORT DATE	7a. TOTAL NO. OF PAGES	7b. NO. OF REFS	
November 1971	226 246	69	
8a. CONTRACT OR GRANT NO.	9a. ORIGINATOR'S REPORT NUMBER(S)		
F30602-71-C-0250			
b. PROJECT NO.	9b. OTHER REPORT NO(S) (Any other numbers that may be assigned this report)		
ARPA Order 1765	RADC-TR-71-276		
c.			
d. Program Code Nr. IE 90			
10. DISTRIBUTION STATEMENT			
Approved for public release; distribution unlimited			
11. SUPPLEMENTARY NOTES		12. SPONSORING MILITARY ACTIVITY	
MONITORED BY: Donald S. Luczak RADC/GCSE Griffiss AFB NY 13440		Advanced Research Projects Agency 1400 Wilson Blvd Arlington VA 22209	
13. ABSTRACT			
<p>Auroral phenomena related to HF radiowave propagation are investigated to establish regions where and times when spectral spreading, backscatter echoes and radiowave absorption may be expected on signals propagating in polar latitudes.</p> <p>The spatial and temporal patterns of energetic particle precipitation are summarized in relation to ionospheric effects observed in the D, E and F regions to provide a background for the analysis of similar patterns in auroral ionospheric phenomena.</p> <p>Synoptic spread F occurrence maps are projected to a mid-solar cycle period by interpolating between IGY (solar maximum) and IQSY (solar minimum) data. The occurrence probability is still high in middle sunspot years and exhibits a strong auroral oval-type pattern. Contours of occurrence probability are converted to the oblique incidence case to illustrate range/azimuth variations in spreading and possible backscatter as observed at a fixed location. To complete the F region study, the effects of ionospheric troughs on HF ray trajectories are investigated. Under certain conditions pronounced vertical and lateral deviations in ray path may be expected and these may lead to significant bearing and range errors in echo source location.</p> <p>Since high latitude HF propagation can be strongly influenced</p>			

(Cont'd)

DD FORM 1473
1 NOV 65

UNCLASSIFIED

Security Classification

14 KEY WORDS	LINK A		LINK B		LINK C	
	ROLE	WT	ROLE	WT	ROLE	WT
Electromagnetic Waves						
Ionospheric Propagation						
Electromagnetic Absorption						
Ionospheric & Atmospheric Models						
Atmospheric Sounding						
Abstract Con't						

by the occurrence of sporadic E (E_s), a prediction of anticipated E_s as would be seen near the geomagnetic pole is given. The occurrence of E_s is described as a function of time of day for three different conditions of magnetic activity. A method was developed for the computation of auroral absorption of HF radiowaves propagating in the polar ionosphere and used to generate isocontour maps showing the probability of absorption being less than or equal to some specified level for various frequencies, levels of absorption and times of day.

--	--	--	--	--	--	--

RADC-TR-71-276
Final Technical Report
November 1971



POLAR FOX II STUDY PHASE
Analytical Systems Corporation

Sponsored by
Advanced Research Projects Agency
ARPA Order No. 1765

Approved for public release;
distribution unlimited.

The views and conclusions contained in this document are those of the authors and should not be interpreted as necessarily representing the official policies, either expressed or implied, of the Advanced Research Projects Agency or the U. S. Government.

Rome Air Development Center
Air Force Systems Command
Griffiss Air Force Base, New York

When US Government drawings, specifications, or other data are used for any purpose other than a definitely related government procurement operation, the government thereby incurs no responsibility nor any obligation whatsoever; and the fact that the government may have formulated, furnished, or in any way supplied the said drawings, specifications, or other data is not to be regarded, by implication or otherwise, as in any manner licensing the holder or any other person or corporation, or conveying any rights or permission to manufacture, use, or sell any patented invention that may in any way be related thereto.

Do not return this copy. Retain or destroy.

POLAR FOX II STUDY PHASE

John R. Herman
R. Vargas-Vila

Contractor: Analytical Systems Corporation
Contract Number: F30602-71-C-0250
Effective Date of Contract: 26 January 1971
Contract Expiration Date: July 1971
Amount of Contract: \$45,274.00
Program Code Number : IE90

Principal Investigator: J. Herman
Phone: 617 272-7910

Project Engineer: V. Coyne
Phone: 315 330-3107

Contracting Engineer: D. Luczak
Phone: 315 330-3231

Approved for public release;
distribution unlimited.

This research was supported by the Advanced Research
Projects Agency of the Department of Defense and was
monitored by Donald S. Luczak RADC (OCSE), GAFB, NY
13440 under contract F30602-71-C-0250.

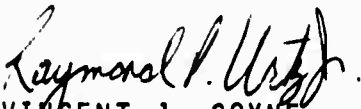
FOREWORD

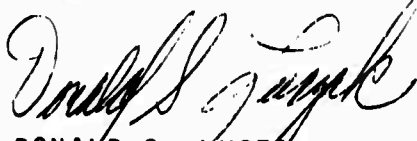
This final report summarizes the investigations carried out in the study phase of the Polar Fox II, and contains technical discussions of pertinent auroral phenomena related to HF propagation. To facilitate its use, the report is presented in four major parts. Part I considers auroral precipitating particles and spread F; Part II contains sporadic E results; Part III summarizes auroral absorption effects; and Part IV treats effects of ionospheric troughs on HF propagation. Each part is separately organized with self-contained references & figures.

The work has benefited from several formal and informal technical discussions held with Dr. M. Balser of Xonics Corp.; Mr. B. Nichols and Mr. J. Chisholm of Lincoln Laboratory; and Messrs. A. Briggs, D. Luczak and V. Coyne of RADC.

PUBLICATION REVIEW

This technical report has been reviewed and is approved.


for VINCENT J. COYNE
RADC Project Engineer


DONALD S. LUCZAK
RADC Contract Engineer

ABSTRACT

Auroral phenomena related to HF radiowave propagation are investigated to establish regions where and times when spectral spreading, backscatter echoes and radiowave absorption may be expected on signals propagating in polar latitudes.

The spatial and temporal patterns of energetic particle precipitation are summarized in relation to ionospheric effects observed in the D, E and F regions to provide a background for the analysis of similar patterns in auroral ionospheric phenomena.

Synoptic spread F occurrence maps are projected to a mid-solar cycle period by interpolating between IGY (solar maximum) and IQSY (solar minimum) data. The occurrence probability is still high in middle sunspot years and exhibits a strong auroral oval-type pattern. Contours of occurrence probability are converted to the oblique incidence case to illustrate range/ azimuth variations in spreading and possible backscatter as observed at a fixed location. To complete the F region study, the effects of ionospheric troughs on HF ray trajectories are investigated. Under certain conditions pronounced vertical and lateral deviations in ray path may be expected and these may lead to significant bearing and range errors in echo source location.

Since high latitude HF propagation can be strongly influenced by the occurrence of sporadic E (E_s), a prediction of anticipated E_s as would be seen near the geomagnetic pole is given. The occurrence of E_s

is described as a function of time of day for three different conditions of magnetic activity. A method was developed for the computation of auroral absorption of HF radiowaves propagating in the polar ionosphere and used to generate isocontour maps showing the probability of absorption being less than or equal to some specified level for various frequencies, levels of absorption and times of day.

TABLE OF CONTENTS

PART I AURORAL PRECIPITATING PARTICLES AND SPREAD F

1.0	Introduction	I-2
2.0	High Latitude Particle Precipitation	I-4
2.1	Background	I-4
2.2	Phenomenological Patterns.....	I-5
2.3	Polar Precipitation Summary Model.....	I-13
2.3.1	D Region.....	I-14
2.3.2	E Region.....	I-16
2.3.3	F Region.....	I-17
2.3.4	Precipitation Model Meridional Cross Section.....	I-22
2.4	References for Section 2	I-24
3.0	High Latitude Spread F	I-25
3.1	Background.....	I-25
3.2	Data Base.....	I-29
3.3	Projection to Mid Solar Cycle.....	I-33
3.4	Application to Oblique Incidence Ray Paths.....	I-43
3.5	References for Section 3.....	I-46

PART II AURORAL SPORADIC E PREDICTIONS

1.0	Introduction	II-2
2.0	Data Base	II-4
3.0	Discussion.....	II-9
4.0	Summary.....	II-11
5.0	References.....	II-12

PART III AURORAL ABSORPTION

1.0	Introduction	III-2
2.0	Data Base	III-3
3.0	Method.....	III-9
4.0	Discussion.....	III-15
5.0	Summary	III-17
6.0	References.....	III-18

PART IV HIGH LATITUDE IONOSPHERIC TROUGHS

1.0	Introduction.....	IV-2
2.0	Historical Background.....	IV-3
3.0	Trough Characteristics.....	IV-6
3.1	General Features.....	IV-6
3.2	Diurnal and Latitudinal Variations.....	IV-6
3.3	Seasonal and Solar Cycle Variations.....	IV-8
3.4	Trough Structure.....	IV-10
4.0	Application to Ray Tracing.....	IV-13
5.0	Summary	IV-16
6.0	References.....	IV-17

LIST OF FIGURES

PART I

Fig. 1 Hartz and Brice (1967) zones of auroral particle precipitation in geomagnetic latitude and time. Dots are diffuse events and drizzle precipitation and triangles are discrete events and associated splash-type precipitation..... I-47

Fig. 2 Various zones of auroral particle precipitation as deduced by Eather and Mende (1971)..... I-48

Fig. 3 Occurrence of 5 keV-electron precipitation for energy fluxes $\geq 2.5 \text{ erg (cm}^2 \text{ sec sr)}^{-1}$ (after Craven (1971))..... I-49

Fig. 4 Meridional model of precipitating particles and associated ionospheric phenomena for typical night time along 75°W longitude..... I-50

Fig. 5 Typical spectral spread on a polar path compared to a mid-latitude path (reproduced from Hunsucker and Bates, 1969)..... I-51

Fig. 6 Spectral spread on an Antarctic path with spread F at the midpoint (after Jones, 1970)..... I-52

Fig. 7 Auroral oval component of spread F occurrence interpolated to mid solar cycle for July presented in geomagnetic latitude/local time coordinates..... I-53

Fig. 8 Spread F permanent maximum component projected to July 1971/72 for 1500 UT and 1800 UT..... I-54

Fig. 9 Permanent maximum component for July 1971/72, for 0900 UT..... I-55

Fig. 10 Probability of overhead spread F occurrence projected to July 1971/72 in geomagnetic coordinates for 0000UT.. I-56

Fig. 11 Same as Fig. 10 for 0300 UT..... I-57

Fig. 12 Same as Fig. 10 for 0600 UT..... I-58

Analytical Systems CORPORATION

Fig. 13	Same as Fig. 10 for 0900 UT.....	I-59
Fig. 14	Same as Fig. 10 for 1200 UT.....	I-60
Fig. 15	Same as Fig. 10 for 1500 UT.....	I-61
Fig. 16	Same as Fig. 10 for 1800 UT.....	I-62
Fig. 17	Same as Fig. 10 for 2100 UT.....	I-63
Fig. 18	Probability of overhead spread F occurrence projected to September 1971/72 in geomagnetic coordinates for 0000 UT.....	I-64
Fig. 19	Same as Fig. 18 for 0300 UT.....	I-65
Fig. 20	Same as Fig. 18 for 0600 UT.....	I-65
Fig. 21	Same as Fig. 18 for 0900 UT.....	I-67
Fig. 22	Same as Fig. 18 for 1200 UT.....	I-68
Fig. 23	Same as Fig. 18 for 1500 UT.....	I-69
Fig. 24	Same as Fig. 18 for 1800 UT.....	I-70
Fig. 25	Same as Fig. 18 for 2100 UT.....	I-71
Fig. 26	Factors to convert July spread F occurrence percentages to Winter conditions (reproduced from Penndorf, 1960).....	I-72
Fig. 27	Probability of overhead spread F occurrence projected to Winter (January 1971/72) in geomagnetic coordinates for 0000 UT.....	I-73
Fig. 28	Same as Fig. 27 for 0300 UT.....	I-74
Fig. 29	Same as Fig. 27 for 0600 UT.....	I-75
Fig. 30	Same as Fig. 27 for 0900 UT.....	I-76
Fig. 31	Same as Fig. 27 for 1200 UT.....	I-77
Fig. 32	Same as Fig. 27 for 1500 UT.....	I-78
Fig. 33	Same as Fig. 27 for 1800 UT.....	I-79
Fig. 34	Same as Fig. 27 for 2100 UT.....	I-80

Fig. 35	Range/Azimuth grid with origin at 46° 58'N, 68° 0'W (geographic coordinates) showing relative locations of geophysical ground stations.....	I-81
Fig. 36	Spread F occurrence probability at midpoint of path terminating at indicated range and azimuth: projected to July 1971/72 for 0000 UT.....	I-82
Fig. 37	Same as Fig. 36 for 0300 UT.....	I-83
Fig. 38	Same as Fig. 36 for 0600 UT.....	I-84
Fig. 39	Same as Fig. 36 for 0900 UT.....	I-85
Fig. 40	Same as Fig. 36 for 1200 UT.....	I-86
Fig. 41	Same as Fig. 36 for 1500 UT.....	I-87
Fig. 42	Same as Fig. 36 for 1800 UT.....	I-88
Fig. 43	Same as Fig. 36 for 2100 UT.....	I-89
Fig. 44	Spread F occurrence probability at midpoint of path terminating at indicated range and azimuth. Projected to September 1971/72 for 0000 UT.....	I-90
Fig. 45	Same as Fig. 44 for 0300 UT.....	I-91
Fig. 46	Same as Fig. 44 for 0600 UT.....	I-92
Fig. 47	Same as Fig. 44 for 0900 UT.....	I-93
Fig. 48	Same as Fig. 44 for 1200 UT.....	I-94
Fig. 49	Same as Fig. 44 for 1500 UT.....	I-95
Fig. 50	Same as Fig. 44 for 1800 UT.....	I-96
Fig. 51	Same as Fig. 44 for 2100 UT.....	I-97
Fig. 52	Spread F occurrence probability at midpoint of path terminating at indicated range and azimuth. Projected to Winter (January 1971/72) for 0000 UT....	I-98

Fig. 53 Same as Fig. 52 for 0300 UT..... I-99

Fig. 54 Same as Fig. 52 for 0600 UT..... I-100

Fig. 55 Same as Fig. 52 for 0900 UT..... I-101

Fig. 56 Same as Fig. 52 for 1200 UT..... I-102

Fig. 57 Same as Fig. 52 for 1500 UT..... I-103

Fig. 58 Same as Fig. 52 for 1800 UT..... I-104

Fig. 59 Same as Fig. 52 for 2100 UT..... I-105

PART II

Fig. 1 Percent Occurrences of $fE_s > 3,6$
and 9 MHz for Quiet Magnetic Conditions
in CGL/CGT Coordinates..... II-6

Fig. 2 Percent Occurrences of $fE_s > 3,6$
and 9 MHz for Moderate Magnetic Conditions
in CGL/CGT Coordinates..... II-7

Fig. 3 Percent Occurrences of $fE_s > 3,6$
and 9 MHz for Disturbed Magnetic Conditions
in CGL/CGT Coordinates.....II-8

Fig. 4 Low Magnetic Activity % Occurrence $fE_s > 3\text{MHz}$ 00UT.....II-13

Fig. 5 Low Magnetic Activity % Occurrence $fE_s > 3\text{MHz}$ 03 UT.....II-14

Fig. 6 Low Magnetic Activity % Occurrence $fE_s > 3\text{MHz}$ 06 UT.....II-15

Fig. 7 Low Magnetic Activity % Occurrence $fE_s > 3\text{MHz}$ 09 UT.....II-16

Fig. 8 Low Magnetic Activity % Occurrence $fE_s > 3\text{MHz}$
12-21 UT.....II-17

Fig. 9 Low Magnetic Activity % Occurrence $fE_s > 6\text{MHz}$
00-21 UT.....II-18

Fig. 10 Low Magnetic Activity % Occurrence $fE_s > 9\text{MHz}$
00-21 UT.....II-19

Fig. 11 Moderate Magnetic Activity % Occurrence $fE_s > 3\text{MHz}$
00 UT.....II-20

Fig. 12 Moderate Magnetic Activity % Occurrence $fE_s > 3\text{MHz}$
03 UT.....II-21

Fig. 13 Moderate Magnetic Activity % Occurrence $fE_s > 3\text{MHz}$
06 UT.....II-22

Fig. 14 Moderate Magnetic Activity % Occurrence $fE_s > 3\text{MHz}$
12 UT..... II-23

Analytical Systems CORPORATION

Fig. 15	Moderate Magnetic Activity % Occurrence $fE_S > 3\text{MHz}$ 12 UT.....	II-24
<u>Fig. 16</u>	Moderate Magnetic Activity % Occurrence $fE_S >$ 3MHz 15-21 UT.....	II-25
<u>Fig. 17</u>	Moderate Magnetic Activity % Occurrence $fE_S >$ 6MHz 00 UT.....	II-26
<u>Fig. 18</u>	Moderate Magnetic Activity % Occurrence $fE_S >$ 6MHz 03 UT.....	II-27
<u>Fig. 19</u>	Moderate Magnetic Activity % Occurrence $fE_S >$ 6MHz 06 UT.....	II-28
<u>Fig. 20</u>	Moderate Magnetic Activity % Occurrence $fE_S >$ 6MHz 09 UT	II-29
<u>Fig. 21</u>	Moderate Magnetic Activity % Occurrence $fE_S >$ 6MHz 12-21 UT.....	II-30
<u>Fig. 22</u>	Moderate Magnetic Activity % Occurrence $fE_S >$ 9MHz 00 UT.....	II-31
<u>Fig. 23</u>	Moderate Magnetic Activity % Occurrence $fE_S >$ 9MHz 03 UT.....	II-32
<u>Fig. 24</u>	Moderate Magnetic Activity % Occurrence $fE_S >$ 9MHz 06 UT.....	II-33
<u>Fig. 25</u>	Moderate Magnetic Activity % Occurrence $fE_S >$ 9MHz 09 UT.....	II-34
<u>Fig. 26</u>	Moderate Magnetic Activity % Occurrence $fE_S >$ 9MHz 12-21 UT.....	II-35
<u>Fig. 27</u>	Very Disturbed Magnetic Activity % Occurrence $fE_S > 3\text{MHz}$ 00 UT.....	II-36
<u>Fig. 28</u>	Very Disturbed Magnetic Activity % Occurrence $fE_S > 3\text{MHz}$ 03 UT.....	II-37
<u>Fig. 29</u>	Very Disturbed Magnetic Activity % Occurrence $fE_S > 3\text{MHz}$ 06 UT.....	II-38
<u>Fig. 30</u>	Very Disturbed Magnetic Activity % Occurrence $fE_S > 3\text{MHz}$ 09 UT.....	II-39
<u>Fig. 31</u>	Very Disturbed Magnetic Activity % Occurrence $fE_S > 3\text{MHz}$ 12 UT.....	II-40
<u>Fig. 32</u>	Very Disturbed Magnetic Activity % Occurrence $fE_S > 3\text{MHz}$ 15 UT.....	II-41
<u>Fig. 33</u>	Very Disturbed Magnetic Activity % Occurrence $fE_S > 3\text{MHz}$ 18 UT.....	II-42

Analytical Systems CORPORATION

Fig. 34	Very Disturbed Magnetic Activity & Occurrence $fE_s > 3\text{MHz}$ 21 UT.....	II-43
Fig. 35	Very Disturbed Magnetic Activity & Occurrence $fE_s > 6\text{MHz}$ 00 UT.....	II-44
Fig. 36	Very Disturbed Magnetic Activity & Occurrence $fE_s > 6\text{MHz}$ 03 UT.....	II-45
Fig. 37	Very Disturbed Magnetic Activity & Occurrence $fE_s > 6\text{MHz}$ 06 UT.....	II-46
Fig. 38	Very Disturbed Magnetic Activity & Occurrence $fE_s > 6\text{MHz}$ 09 UT.....	II-47
Fig. 39	Very Disturbed Magnetic Activity & Occurrence $fE_s > 6\text{MHz}$ 12 UT.....	II-48
Fig. 40	Very Disturbed Magnetic Activity & Occurrence $fE_s > 6\text{MHz}$ 15-18 UT.....	II-49
Fig. 41	Very Disturbed Magnetic Activity & Occurrence $fE_s > 6\text{MHz}$ 21 UT.....	II-50
Fig. 42	Very Disturbed Magnetic Activity & Occurrence $fE_s > 9\text{MHz}$ 00 UT.....	II-51
Fig. 43	Very Disturbed Magnetic Activity & Occurrence $fE_s > 9\text{MHz}$ 03 UT.....	II-52
Fig. 44	Very Disturbed Magnetic Activity & Occurrence $fE_s > 9\text{MHz}$ 06 UT.....	II-53
Fig. 45	Very Disturbed Magnetic Activity & Occurrence $fE_s > 9\text{MHz}$ 09-21 UT.....	II-54

PART III

Fig. 1	Probability of Occurrence of Auroral Absorption $\geq 0.42\text{dB}$ in Corrected Geomagnetic Coordinates.....	III-5
Fig. 2	Probability of Occurrence of Auroral Absorption $\geq 1.0\text{dB}$ in Corrected Geomagnetic Coordinates.....	III-6
Fig. 3	Probability of Occurrence of Auroral Absorption $\geq 3.0\text{dB}$ in Corrected Geomagnetic Coordinates.....	III-7
Fig. 4	Cumulative Probability Distribution Showing Percentage of Time That a Given Level of Absorption is Equaled or Exceeded.....	III-8
Fig. 5	Range Azimuth Fan Graph In Corrected Geomagnetic Coordinates.....	III-10

Analytical Systems CORPORATION

Fig. 6	Flat Earth Geometry with Relation Between Path Loss and Equivalent Vertical Incidence Absorption.....	III-11
Fig. 7	Auroral Absorption Occurrence F=10MHz, T=04UT L=10dB, L=20dB.....	III-19
Fig. 8	Auroral Absorption Occurrence F=10MHz, T =04UT L=30dB, L=40dB.....	III-20
Fig. 9	Auroral Absorption Occurrence F=10MHz, T=12UT L=10dB, L=20dB.....	III-21
Fig. 10	Auroral Absorption Occurrence F=10MHz, T=12UT, L=30dB, L=40dB.....	III-22
Fig. 11	Auroral Absorption Occurrence F=10MHz, T=20UT, L=10dB, L=20dB.....	III-23
Fig. 12	Auroral Absorption Occurrence F=10MHz, T=20UT L=30dB, L=40dB.....	III-24
Fig. 13	Auroral Absorption Occurrence F=15MHz, T=04UT, L=10dB, L=20dB.....	III-25
Fig. 14	Auroral Absorption Occurrence F=15MHz, T=-4 UT, L=30dB, L=40dB.....	III-26
Fig. 15	Auroral Absorption Occurrence F=15MHz, T=12UT, L=10dB, L=20dB.....	III-27
Fig. 16	Auroral Absorption Occurrence F=15MHz, T=12UT, L=30dB, L=40dB.....	III-28
Fig. 17	Auroral Absorption Occurrence F=15MHz, T=20UT, L=10dB, L=20dB.....	III-29
Fig. 18	Auroral Absorption Occurrence F=15MHz, T=20UT, L=30dB, L=40dB.....	III-30
Fig. 19	Auroral Absorption Occurrence, F=20MHz, T=04UT, L=10dB, L=20dB.....	III-31
Fig. 20	Auroral Absorption Occurrence F=20MHz, T=04UT, L=30dB, L=40dB.....	III-32
Fig. 21	Auroral Absorption Occurrence F=20MHz, T=12UT, L=10dB, L=20dB.....	III-33
Fig. 22	Auroral Absorption Occurrence F=20MHz, T=12UT, L=30dB, L=40dB.....	III-34
Fig. 23	Auroral Absorption Occurrence F=20MHz, T=20UT, L=10dB, L=20dB.....	III-35

Analytical Systems CORPORATION

Fig. 24	Auroral Absorption Occurrence F=20MHz, T=20UT, L=30dB, L=40dB.....	III-36
Fig. 25	Auroral Absorption Occurrence F=25MHz, T=04UT, L=10dB, L=30dB.....	III-37
Fig. 26	Auroral Absorption Occurrence F=25MHz, T=04UT, L=30dB, L=40dB.....	III-38
Fig. 27	Auroral Absorption Occurrence F=25MHz, T=12UT, L=10dB, L=20dB.....	III-39
Fig. 28	Auroral Absorption Occurrence F=25MHz, T=12UT, L=30dB, L=40dB.....	III-40
Fig. 29	Auroral Absorption Occurrence F=25MHz, T=20UT, L=10dB, L=20dB.....	III-41
Fig. 30	Auroral Absorption Occurrence F=25MHz, T=20UT, L=30dB, L=40dB.....	III-42

PART IV

Fig. 1	Contour map of $f_x F_2$ observed by Alouette 1 on consecutive passes spanning 16 UT Oct. 30 to 05UT Oct. 31, 1962, presented in geographic coordinates and approximately constant local time (reproduced from Muldrew, 1965).....	IV-19
Fig. 2	Mean Position of Main trough (after Jelly and Petrie, 1969, and Muldrew, 1965).....	IV-20
Fig. 3	Variation in peak electron density (plasma frequency) with latitude showing main trough and high latitude troughs (Muldrew, 1965).....	IV-21
Fig. 4	Observed distribution of electron density (plasma frequency) in a bottomside trough deduced by Bowman (1969).....	IV-22
Fig. 5	Model of main trough (electron density expressed as plasma frequency contours) utilized by Thompson (1970)	IV-23
Fig. 6	Ray path projections on Earth's surface showing lateral deviations of 6MHz rays through main trough with elevation angle of 60° (after Thompson, 1970).....	IV-24
Fig. 7	Ray path projections on Earth's surface showing lateral deviations of 6MHz rays through main trough with elevation angle of 30° (after Thompson, 1970).....	IV-25

**PART I: AURORAL PRECIPITATING PARTICLES
AND SPREAD F**

by

John R. Herman

1.0 INTRODUCTION

High frequency (HF) radio or radio signals propagating in high latitude regions are beset with a number of difficulties imposed by the complex polar ionosphere. The major phenomena affecting such propagation are irregularities in F-region electron density as typified by spread F, enhanced ionization patches in the E-Region identified as sporadic E (E_s) and excessive electron densities in the D region. The HF propagation effects include spectral spreading and backscatter echoes introduced by F-region irregularities, anomalous propagation support and/or shielding of certain portions of the upper ionosphere by E_s patches and absorption of the radiowaves by D-region electron enhancements.

In examining other polar geophysical phenomena for their possible import, it has been discovered that ionospheric troughs may have a significant effect on the propagation of HF signals leading to errors in the interpretation of observational data, particularly in the assessment of range and bearing of observed echoes. These troughs are defined as latitudinally narrow bands of much lower (3X or more) electron density than that in regions to the north or south of them.

The objective of this final report is to assess known characteristics of these various polar ionospheric phenomena and express them in terms allowing for the prediction of the effects to be expected in HF polar propagation experiments.

For convenience in presentation, the report is divided into four parts: Part I deals with spread F and ionospheric irregularities; Part II covers the E region and sporadic E; Part III assesses auroral absorption effects; and Part IV deals with ionospheric troughs. In the first three parts temporal and spatial variations in the occurrence statistics of spread F, sporadic E and auroral absorption are formulated in range/ azimuth coordinates with the origin at a typical observing location. Because ray tracing is an integral part of any examination of ionospheric trough effects, Part IV summarizes the geophysical characteristics of this phenomenon without any attempt to project it into range/azimuth space.

In the following pages, which constitute Part I of the final report, a summary is given on the phenomenological characteristics of precipitating energetic particles from the magnetosphere into the polar ionosphere. Since these particles are apparently largely responsible for the production of auroral ionospheric phenomena, it is believed that such a summary will afford the framework within which the characteristics of these phenomena and their spatial relationships may be viewed in an integrated way. It serves also as background for the material presented in all parts of the final report. Following this (section 2), the characteristics of spread F and their application to oblique propagation experiments are presented (section 3).

2.0 HIGH LATITUDE PARTICLE PRECIPITATION

2.1 BACKGROUND

It has become apparent in recent years that many of the auroral ionospheric phenomena leading to radiowave propagation disturbances are intimately related to energetic charged particle precipitation from the magnetosphere. Although the detailed correlations are far from complete, gross phenomenological patterns have emerged to reveal diurnal and geographic variations in particle precipitation which are similar to those for auroral phenomena (Hartz and Brice, 1967).

Consideration of the precipitation patterns may, therefore, lead to greater insight into the characteristics and variations of polar geophysical phenomena of importance to Polar Fox II. These phenomena include spread F, sporadic E, auroral absorption and high latitude troughs, all of whose characteristics vary with time at a fixed location and with location at a fixed time.

If the correlations of precipitating particles with these ionospheric phenomena of interest are sufficiently well behaved it should be possible to utilize particle measurements for indirect verification of geophysical events as observed by the experimental radar and thus lead to improved prediction of how an operational radar may be expected to behave.

2.2 PHENOMENOLOGICAL PATTERNS

The basis for the current picture of the morphology of auroral precipitation includes both direct measurements of energetic particles and indirect measurements of the consequent effects of those particles precipitating into the upper atmosphere (Hartz and Brice, 1967; Pudovkin and Barsukov, 1971; Eather and Mende, 1971).

In a simplistic way it may be presumed that the energetic particles will penetrate to a certain depth and produce ionization and excitation of the upper atmospheric constituents through collisions and heating. The depth of penetration is a function of the particle species, pitch angle distribution and energy spectrum; within the loss cone the highest energies penetrate to the lowest heights. The magnitude of ionization and excitation effects are proportional to the amount of energy deposited and therefore to the intensity or number flux of the precipitating particles as well as their initial energy.

In establishing patterns and precipitation zones, most reliance has been placed upon indirect measurements of the ionization and excitation effects, including:

- Optical aurora (visual and subvisual)
- Radio aurora
- Radiowave absorption (riometer measurements)
- Sporadic E
- Spread F (topside and bottomside)

Since these phenomena occur over a range of altitudes it is evident that the precipitating particles must deposit their energy over a similar range of altitudes. This behavior suggests that the energetic particles responsible for riometer absorption are "harder" (have higher energies) than those producing spread F. For a complete phenomenological pattern, then, particle energies and their heights of maximum effects should be taken into account.

Utilizing indirect measurements augmented with Alouette 1 and Injun III particle measurements ($E_0 \geq 40$ keV and ≥ 10 keV), Hartz and Brice (1967), established that there are at least two major zones of precipitation in auroral regions. They showed also that the character of the precipitation process and associated ionospheric effects are different in the two zones. An idealized representation of the Hartz and Brice model is depicted in Fig. 1, where the two zones are separated according to the processes within them; that is "splash" events and "drizzle" events.

The drizzle zone is nearly circular at about 65° geomagnetic latitude and its maximum intensity occurs in the morning hours (about 0600 - 1000 LT). The types of events occurring here are:

- a) a consistent, moderately intense flux of electrons of energy $E_0 \sim 40$ keV which precipitates in a quasi-steady manner (hence "drizzle").

b) diffuse upper atmospheric events including:

- i) diffuse aurora
- ii) slowly varying riometer absorption
- iii) sporadic E echoes from 80 to 90 km heights

The "splash" zone pattern is quite similar in appearance to the optical auroral oval defined by Feldstein (1963), being about 76° geomagnetic latitude on the dayside and 10° lower on the midnight side. The precipitating flux intensity maximizes at about 2200 LT, and the splash zone overlaps the drizzle zone in the midnight sector. The events observed here are:

a) soft electron fluxes ($E \sim 10$ keV) which precipitate in short bursts of a few seconds to a few minutes (hence "splash" events)

b) discrete upper atmospheric events including

(according to Hartz and Brice):

- i) localized fluctuating aurora
- ii) abrupt auroral riometer absorption
- iii) intense sporadic E at 100 km or greater
- iv) spread F on ionograms

The Hartz and Brice results do not contain estimates for establishing occurrence-percentage contours, and the gross patterns are significantly different from our spread F occurrence patterns. As will be seen later, spread F occurs both equatorward and poleward of the Hartz/Brice zones on the night side. The general

patterns as well as the evening and morning maximums do, however, agree rather well with the sporadic E (evening) and absorption (morning) peaks, as discussed elsewhere in this report.

It may be noted in passing that in deriving these phenomenological patterns, Hartz and Brice (1967) analyzed a large and diverse data base without discriminating between local time and local geomagnetic time or between geomagnetic and invariant latitudes. For case-by-case studies, this may be a dangerous practice, but for morphological and statistical comparison of gross data the distinctions are unimportant. This is especially true along the 75° West Meridian, where invariant latitude up to 300 km height is within $\pm 0.5^\circ$ of geomagnetic latitude except in the immediate vicinity of the pole and local geomagnetic time is within about 15 to 20 minutes (depending on season) of local sun time.

For correlating particle precipitation with spread F occurrence it must be remembered that we are dealing with an F-region phenomenon so it might be expected that electron energies lower than 10 keV are more important than the harder fluxes of 10 or 40 keV. The Hartz and Brice results, though comprehensive in many respects, are insufficient to correlate with spread F.

More recent investigations of phenomenological patterns utilizing both direct and indirect observations (Pudovkin and Barsukov, 1971; Eather and Mende, 1971), do take into account measurements of lower energy electrons and soft proton precipitation. As illustrated in Fig. 2 (Eather and Mende, 1971), soft particle precipitation occurs both above and below the auroral oval, more in keeping with observed spread F occurrence.

The important features to note in Fig. 2 are:

- a) A dayside soft zone (~ 0.15 keV electrons and low energy protons) is located poleward of the auroral oval (and hard electron precipitation zone), implying that F-region effects may be expected;
- b) The nightside softzone (electrons ~ 0.5 keV) is poleward of the oval, extending up to about 80° geomagnetic latitude;
- c) The night side proton aurora associated with ~ 10 keV protons is equatorward of the oval near midnight, overlapping it after midnight.

As in the Hartz and Brice (1967) results, these later studies show only the gross features of the particle precipitation zones, without any quantitative indication of the fraction of time (how many nights of the month, for example) that such precipitation takes place, or how long an individual event might last. However, they do show that soft particles which may be expected to produce F-region ionization effects do precipitate in regions outside of the Feldstein oval.

Recent measurements by Injun 4 have been analyzed by Craven (1970) to show the quantitative phenomenology of electron precipitation for energies $E_0 \sim 5\text{keV}$, expressed as occurrence frequency as a function of time and latitude. One example of Craven's analysis is illustrated in Fig. 3, where the percentage of time that an energy flux greater than $2.5 \text{ erg } (\text{cm}^2 \text{ sec sr})^{-1}$ was observed.

Maximum precipitation (10% contours) of this large energy flux occurs on the postmidnight side, in the time intervals 00-02LT and again at 04-06LT. Both maximums are centered at about 65° , just at the southern edge of the Feldstein oval, and they overlap the 10 keV proton zone described by Eather and Mende (1971). The 1% probability contour covers the latitude range from about 60° to 73° .

As the threshold energy flux is decreased to 4×10^{-2} erg $(\text{cm}^2 \text{ sec sr})^{-1}$ (Craven, 1970), the general shape of the contours in Fig. 3 is maintained, but covers a larger area. For example, this amount of flux precipitates for more than 50% of the time on the night side beginning at about 22LT centered at about 65° and covering both of the 10% contour areas of Fig. 3. The 1% occurrence contour covers the latitude range of 55° to 75° .

At a still lower threshold of 5×10^{-3} erg $(\text{cm}^2 \text{ sec sr})^{-1}$ Craven (1970) found that precipitation occurs more than 80% of the time at all hours of the day in a narrow belt centered about 70° on the dayside and 65° on the post midnight side.

Gross comparison of the Craven results with those of Hartz and Brice indicates that precipitation of 5 keV electrons maximizes 3 to 5 hours earlier than that for 40 keV electrons. The day/night and dawn/dusk ratios of occurrence are greater than unity for 40 keV and less than unity for 5 keV electrons (Craven 1970), which is indicative of the differences in precipitation patterns of the soft (5 keV) compared to the hard electron fluxes. Measurements of 80 eV electrons (Sharp and Johnson, 1968) shows an occurrence pattern similar to the soft electron pattern of Craven.

The major import of the soft particle studies (Pudovkin and Barsukov, 1971; Eather and Mende, 1971; Craven 1970) is that soft electrons and protons precipitate in regions both poleward and equatorward of the Feldstein oval, maximum intensity occurs on the post midnight side, and that at least a low flux precipitates 80% or more of the time. It appears that the overall pattern of soft precipitation agrees qualitatively with spread F occurrence.

There are, however, important limitations applicable to the past phenomenological precipitation studies. These are:

- a) Only gross precipitation zones have been defined, with little information on occurrence frequency except for Craven's (1970) Injun 4 results;
- b) The energies of the particles treated are by and large greater than those required for F region effects except for the work by Eather and Mende (1971);
- c) All of the studies have been directed toward the definition of statistical zones of precipitation and do not show the morphology of individual events. (Hartz and Brice, 1967, have cited some evidence indicating that a close correlation does exist between ionospheric phenomena and precipitation

events on a case-by-case basis, but the data are too sparse for quantitative arguments);

- d) of major importance to F region phenomena, there seems to be no observational data by rocket or satellite in the geographic area of the spread F permanent maximum, so the possibility of its existence being due to a quasi-continuous influx of charged particles (electrons, protons or both) creating field-aligned irregularities is still open to question.

These limitations notwithstanding, the results of the past phenomenological studies may be used as the basis for formulating a working model of high latitude particle precipitation and associated ionospheric phenomena. Such a model in three dimensions (local time, geomagnetic latitude and altitude) is summarized in the following section.

2.3 POLAR PRECIPITATION SUMMARY MODEL

The precipitation model presented here is admittedly an oversimplification of complex auroral processes, phenomena and their interrelationships; it is designed to provide the framework within which detailed observations may be interpreted and correlated. Being separated into the layered regimes of the ionosphere, this model may serve as a guide in unravelling the complexities of the polar ionospheric phenomena of importance to Polar Fox II.

2.3.1 D REGION

The principal process assumed to be at work in the 60-90 km height region is direct ionization by precipitating energetic electrons having energies in the 10-40 keV range, with additional ionization being created by secondary electrons (c.f., Chamberlain, 1961). This enhanced ionization in the D region produces radiowave absorption of the non-deviative type in accordance with standard magnetic theory, wherein the absorption coefficient, α is given by (Davies, 1965):

$$\alpha = \frac{2\pi e^2}{mc} \frac{N\nu}{\nu^2 + (\omega - \omega_L)^2} \quad (2.1)$$

N = electron density

ν = electron collision frequency

ω = angular frequency of the radiowave

ω_L = longitudinal component of angular electron gyrofrequency.

e,m = charge and mass of electron, respectively

c = speed of light

Integration of the absorption coefficient along a path, s, yields the total absorption L:

$$L = 8.7 \int \alpha ds \quad (2.2)$$

where the constant 8.7 yields L in decibels (dB).

The spatial extent and time variation of this absorption are dictated by those of the energetic electron precipitation.

Following Hartz and Brice (1967), two gross types of precipitation

affect the D region creating impulsive, discrete intense absorption in one zone and quasi-steady moderate absorption in the other.

The discrete zone (A) is marked by intense 10-keV electron precipitation. Spatially, this zone corresponds closely to the auroral oval; on the dayside it is about 2° wide latitudinally (76°-78°), on the premidnight side it extends roughly from 68° to 75° and on the post midnight side the zone is at its lowest latitude (63° to 70°). Although 10 keV precipitation can be expected at all hours of the day, its maximum intensity occurs in the local time period of 2000 to 2400; the occurrence frequency is roughly a factor of 5 or 6 greater near 2200LT than near local noon.

The quasi-steady zone (B) describes the region where 40 keV electrons precipitate on a more or less continuous basis. It is an annular region symmetric about the geomagnetic pole, centered at 65° latitude and extending approximately +4° latitude on the morning side and +2° on the evening side. Diurnally, maximum intensity of the 40-keV precipitation occurs in the period 0600-1000LT, while a pronounced minimum in occurrence appears in the evening (1900-2300LT).

Zones A and B overlap in the sector bounded by approximately 2300 to 0300LT and 62° to 66° geomagnetic latitude. During this time period the 10-keV electron precipitation is observed up to 70° and occurs more often than the 40-keV precipitation. At

all other times of the day, zone B (40 keV electrons) is found at a lower latitude than A, and the largest latitudinal separation occurs near local noon. The spatial patterns of precipitating electrons for D-region heights are depicted in Fig. 1.

2.3.2 E REGION

The discrimination between D and E region here must be made on the basis of the observed ionospheric effects presumed to be due to energetic particle influx. Thus the E region height range of approximately 80 to 140 km overlaps that of the D region. Ionization in the 80 to 90 km interval is considered to be a D region phenomenon when causing absorption and an E region one when observed as low-lying sporadic E.

Past measurements of energetic electrons with energies of 5, 10 and 40 keV as discussed above all apply to the E region, since 5-keV electrons penetrate to this depth, too. While the intense fluxes of 40 keV electrons in drizzle events produce low-lying sporadic E (Hartz and Brice, 1967), those for 5-keV are expected to have maximum effect ≥ 100 km altitude (Chamberlain 1961). The principal ionospheric effect of these energetic particles in the E region is the production of sporadic E. The type of sporadic layer so produced may range from a flat, thin layer of 300-1000 meter thickness ("auroral" E_s) to a thick layer some 20 or more km in vertical extent which can introduce significant group delay in a probing radio signal ("retarding" E_s). The thickness of the layer in a particular situation is dependent upon

the energy spectrum of the precipitating particles - e.g. a near-monoenergetic spectrum would produce a thin layer - and upon the conditions of the ambient E region. No distinction of E_s type is made, however, in this summary model.

Since all energies \geq 5-keV are important, as said before, we find a 3-zone spatial pattern at E-region heights. These include zones A and B (Fig. 1) where 10-keV electrons precipitate maximally around 2200 LT (A) and 40-KeV drizzle maximizes around 0800LT(B). The third zone (C) is defined as the region where 5-keV electrons have been observed to precipitate by Injun 4 (Craven 1970). From about 2300LT to 0400LT zone C overlaps A and from 0400 to 1000LT this zone is located in the gap between zones A and B.

2.3.3 F REGION

Energetic particles of a few keV and above give up very little of their energy when precipitating downward through the F region because the collisional ionization cross-section of the upper atmospheric constituents is strongly energy dependent and their density is small in the F region. In addition, the incident particle gives up most of its energy near its stopping altitude. Thus electrons with energies of 5keV and above deposit most of their energy (and produce ionization) in and below the E region. Depending upon pitch angle distribution, however, these electrons may contribute a small amount of F region ionization. According to Kamiyama (1966), precipitating electrons of energies 1 KeV and lower will deposit most of their energy at and above about

150km, so for direct ionization effects in the F layer, electrons of energies less than about 1keV must be considered. As discussed below, indirect effects might still be expected from hard electrons.

The F-region effect of principal concern here is the production of field-aligned irregularities in the electron density distribution. These irregularities, whose spatial extent transverse to the guiding magnetic field lines ranges from a few hundred meters to a few kilometers, produce radiowave effects observed as spread F (detected by bottomside and topside sounders) amplitude scintillations in radio star or satellite signals traversing the F region, HF backscatter echoes and, more than likely, spectral spreading.

Details of the production mechanism or mechanisms for field aligned F-region irregularities in high latitudes are not completely resolved. Possible mechanisms include direct ionization along field lines by precipitating protons (Herman, 1966a) or electrons (Frihagen, 1969), redistribution of electron density by magnetospheric electric fields or perhaps by electrostatic coupling along field lines of E region (dynamo region) irregularities to the F layer (Reid, 1968). If the mechanism suggested by Reid (1968) is correct, then precipitating energetic electrons with energies in the keV range would be important to the production of spread F provided they first created small scale (~1km) ionization enhancements in the E region. It is probable that "drizzle" events (Hartz and Brice, 1967) do not produce the

required small scale structure. Regardless of the details, the production of high latitude F region irregularities depends either directly or indirectly upon energetic particle precipitation; probably both direct and indirect processes are at work. This being the case, it is important to include all energies of energetic electrons in the present summary precipitation model for F layer heights.

For direct ionization production, the Eather and Mende (1971) model is appropriate (Fig. 2). In this model we find a dayside soft zone of 0.15 keV electrons and low energy (<10 keV) protons extending longitudinally from about 78° to 82° and from at least 0900 to 1500 LT (zone I). A second zone (II) consisting of 0.5 keV electrons is on the night side between 70° and 80° and 1800 to 0600 LT; it lies immediately poleward of the Feldstein oval during the entire period. Zone III, consisting of protons ($E_0 \sim 10\text{keV}$) is on the evening and night side, centered at about 70° at 1800 LT and about 65° near local midnight. In the postmidnight hours the probability of proton precipitation in Zone III apparently decreases (see Fig. 2).

On the basis of these patterns, direct production of field-aligned ionization and spread F can be expected poleward of the Feldstein oval at night by low energy (0.5 keV) electrons and equatorward of it by protons (~ 10 keV); on the dayside both electrons and protons contribute to the spread F production centered at about 80° geomagnetic latitude, just inside the oval.

Indirect production of spread F irregularities through Reid's (1968) mechanism may be expected in those regions where electrons of $E_0 \gtrsim 5$ keV precipitate and produce small scale E region irregularities. Thus, the 10-keV splash region (Fig. 1) coinciding essentially with the Feldstein oval (Hartz and Brice, 1967) and the 5-keV region defined by Craven (1970) (c.f., Fig. 3) are presumed to be applicable. Since the 10-keV precipitation maximizes on the pre-midnight side and that for 5 keV maximizes on the post midnight side, it is expected that F region effects would be produced at all hours of the night.

Taking into account all energetic electron energies and the possibility of both direct and indirect irregularity production, the overall F region precipitation model can be summarized in geomagnetic-latitude/local-time space. At about 1800 LT precipitation covers the latitude range from approximately 70°

to 80° and as midnight is approached the lower boundary gradually moves equatorward to about 60° . In the postmidnight hours ($\approx 0100 - 0300$ LT) the precipitation of 5-keV electrons intensifies and the total latitudinal extent is perhaps 60° to 80° . By sunrise (approximately 0600 LT) the lower boundary (fixed by the 5-keV pattern) is $\approx 62^\circ$ or 63° and the poleward boundary remains at about 80° geomagnetic latitude. Proceeding toward 1200 LT the equatorward boundary recedes to about 75° while the inner boundary shrinks to roughly 83° .

The whole-day picture is characterized by an inner boundary staying with ± 2 or 3 degrees of 80° latitude, and an outer boundary that moves equatorward from 75° at noon through 70° near 1800 LT to 60° at midnight. The pattern bulges toward the equator in the midnight to noon plane compared to the noon to midnight plane.

This gross F-region model lacks percentage-occurrence contours, at least partly because no account has been taken of magnetic activity influence, and it does not directly allow prediction of possible variations in ionospheric irregularity strength or scale size. It does, however, give an indication of the polar geographic region and time periods in which F-region precipitation and associated ionospheric effects can be expected for some portion of the time. Occurrence probability contours of the ionospheric effects are deduced from spread F data in the next chapter.

2.3.4 PRECIPITATION MODEL MERIDIONAL CROSS SECTION

In summarizing the relationship between precipitating particles of various energies and ionospheric phenomena of interest to the present effort, it is illuminating to view a meridional slice of the polar region along a representative longitude. This view, presented in Fig. 4, depicts a typical nighttime situation, at say 0200 LT along 75° West Meridian.

The sketch in Fig. 4 is largely self-explanatory. It should be noted though, that the indicated latitudes can be taken as either geomagnetic or invariant latitudes since the two are nearly the same above $\approx 50^\circ$. The relationship between invariant latitude and McIlwain's L shell parameter is

$$\Lambda = \arccos \left(\sqrt{\frac{1}{L}} \right) \quad (2.3)$$

where L is expressed in terms of earth radii.

Going north from midlatitude, the lower latitude boundary of topside spread F (Calvert and Schmid, 1964) and the scintillation boundary (c.f., Aarons, et al, 1971) are encountered first at about 50° . These phenomena are observed alone in association with ≤ 0.2 keV energetic electrons up to about 58° , where penetration of precipitating particles to below the peak of the F layer adds bottomside spread F. Then, in the Feldstein oval from 64° to 72° auroral sporadic E and absorption due to energetic electrons of energies 5 keV and higher appear in conjunction with the F-region phenomena. Further north, from about 72 to 80° , bottomside and topside spread F still persist.

It must be emphasized that the sketch in Fig. 4 is only qualitatively accurate; details of the structure may change when magnetic activity and occurrence frequencies of the various phenomena are taken into account.

2.4 REFERENCES FOR SECTION 2

- Aarons, J., et al, 1971, Proc. IEEE, 59, P. 159.
- Calvert, W., and C. W. Schmidt, 1964, J. Geophys. Res., 69, p. 1839.
- Chamberlain, J. W., 1961, Physics of the Aurora and Ainglow, Academic Press, New York
- Craven, J. D., 1970, J. Geophys. Res., 75, p. 2468.
- Davies, K., 1965, Ionospheric Radio Propagation, NBS Monograph 80, U. S. Govt. Printing Office, Washington, D. C.
- Eather, R. H. and S. B. Mende, 1971, J. Geophys. Res., 76, p 1746.
- Feldstein, Y. I., 1963, Geomag. and Aeron. (English Ed) 3, p. 183. (see also, Akasofu, S. I., Polar and Magnetospheric Substorms, Springer Verlag New York, Inc., New York, 1968).
- Frihagen, J., 1969, J. Atmos Terr. Phys., 31, p 81.
- Hartz, T. R. and N. M. Brice, 1967, Planet Space Sci., 15, p. 301.
- Herman, John R., 1966a, Spread F and its Effects Upon Radiowave Propagation and Communication, P. Newman Ed., Technavision Press, p. 567.
- Kamiyama, H. 1966 Rpt. Ionosphere Space Res. Japan, 20, p. 374.
- Pudovkin, M. I. and v. M. Barsukov, 1971, Planet Space Sci., 19, p. 525.
- Reid, G. C., 1968, J. Geophys. Res., 73, p. 1627.
- Sharp, R. D. and R. G. Johnson, 1968, J. Geophys. Res., 73, p. 969.

3.0 HIGH LATITUDE SPREAD F

3.1 BACKGROUND

Inhomogenities in the density distribution of F-region electrons have been known to be a prominent feature of the polar ionosphere for a number of years (c.f., the review article by Herman, 1966b). These irregularities have long been a plague to high frequency (HF) radio communications and direction-finding in the Arctic, because they introduce rapid fluctuations in amplitude (Flutter fading) and apparent arrival direction of received signals.

Two additional adverse effects imposed by the irregularities are observed as frequency spreading (spectral spread) on signals propagated through the disturbed region and backscatter echoes from field-aligned irregularities. These effects are of importance in certain types of radar operation. It is, therefore, imperative to establish the regions where and the times when such spreading or backscatter can be expected in order to predict and verify the results of radar experiments in polar regions.

There is no doubt that F-region field-aligned irregularities in the polar ionosphere produce spread echoes, commonly called spread F, on vertical incidence ionograms (Herman, 1966b). Since there exists an abundance of data and analysis revealing the temporal and spatial variations in spread F occurrence as well as its correlations with other polar geophysical phenomena, contrasted with a dearth of similar information on spectral spreading,

the questions of "where" and "when" can best be answered by appropriate interpretation of spread F observations. The case for this approach is further strengthened by the results of Jones (1970) and Lomax (quoted in Hunsucker and Bates, 1969).

Lomax measured spectral spread on signals received in California from transmissions on about 15 MHz in Thule and Fort Monmouth. The Thule-California path crosses the whole of the auroral zone, where spread F often occurs, while the Fort Monmouth-California path is entirely in midlatitude, where spread F is seldom seen. Typical spectral spreading on these two paths is compared in Fig. 5 where the polar path is seen to have a spread of about 20 Hz (+10 Hz) while the midlatitude spread is confined to about +2Hz. These results at least suggest that spread F and spectral spreading are highly correlated.

Jones (1970) measurements were made in Antarctica over a one-year period on a 1200 km path from South Pole to McMurdo, with an observing frequency of about 6MHz. Jones showed that spectral spreading and spread F are very definitely correlated on both a statistical and a case-by-case basis. The seasonal variation in a spectral spreading followed that for Antarctic spread F as determined by Penndorf (1966) and further, the spread was much greater for F-layer than E-layer propagation. An example of spectral spreading measured by Jones at a time when spread F was known to be present is shown in Fig. 6. Here it is seen in an average of several records (bottom curve) that the power is only 30 dB down with a frequency displacement of about 35Hz. A

straight line extrapolation indicates that at the -60dB level, the spectral width would be about 70 Hz. The top half of Fig. 6 depicting power spectra taken over a period of 6 minutes at 2-min intervals, illustrates that the spreading persists with only minor variations in structure over minutes rather than seconds. We conclude that severe spectral spreading will persist as long as spread F is present on the propagation path. It is intuitively expected that the spectral width is directly proportional to the severity (or intensity) of spread F; however, this expectation has not been examined in detail in the present effort.

To answer the question of where and when backscatter echoes may be expected, knowledge of the locations and periods of occurrence of spread F field-aligned irregularities is necessary but insufficient. Because such echoes are strongly aspect-sensitive (i.e. the wave normal has to be nearly perpendicular to the long, field-aligned dimension of the irregularity), the magnetic field geometry and the effects of wave refraction by the ionosphere must be taken into account. Measurements by Bates and Albee (1969) indicate that the decrease in echo strength is approximately 6 dB per degree of off-perpendicularity. There appears to be no clear-cut relationship between echo strength and irregularity intensity ($\frac{\Delta N}{N}$) but again, one might expect a direct correlation between the two.

The above complications notwithstanding, there is ample evidence to support the contention that spread F irregularities produce strong backscatter echoes on HF when the geometry is right. (Baggaley, 1970; Bates and Albee, 1970; Hower, et al, 1966; Au and Hower, 1970).

Thus for both spectral spreading and backscatter, we are inexorably led to consideration of spread F characteristics.

3.2 DATA BASE

Spread F data from vertical incidence ionosonde observations contain no quantitative measure of the irregularity intensity; however, tabulation of the international scaling symbol "F" when a critical frequency (foF2) cannot be read is indicative of strong irregularities since these produce severe frequency spread on polar ionograms. As mentioned above, strong irregularities imply wide spectral spread and strong backscatter.

The chief advantages in utilizing spread F data for ascertaining when and where spectral spreading and backscatter may occur are: (a) continuous data over many years from a large number of polar ionospheric stations are available; b) several careful and comprehensive analyses of that data have already been made to determine the morphology of spread F (Penndorf, 1960, 1962a; Singleton, 1960, 1968; Shimazaki, 1959, 1962; Tao, 1965). These analyses were made for sunspot maximum and sunspot minimum years; for application to the present problem they need to be interpolated to a middle sunspot era.

The work by Penndorf (1960, 1962a) serves as our starting point. His analysis is based on IGY (1957-58) ionospheric data from 34 stations north of 50° N geomagnetic latitude. At each station the percentage occurrence of spread F in a month was determined for each hour of the day. Hours having equipment outage, obscuring noise, and blackout were excluded from the count and in addition, the basic data were rescaled in many

instances to minimize variations in scaling practices between stations. With the data thus statistically homogenized, Penndorf constructed smoothed diurnal curves of occurrence percentage for each station, converted to the corresponding universal time (UT) and plotted the percentage every 3 hours on base maps at the appropriate geographic location.

Isocontours of equal percentage at 20, 40, 60, 80 and 100% were then drawn with some further smoothing to maintain continuity. The result was a "snapshot" for a given UT hour showing the geographic distribution of spread F occurrence during sunspot maximum in polar stereographic projection and geographic coordinates. Only the months of July and September, 1957 were analyzed and published in this manner. Additional analysis of winter months at some stations provided a correction factor for converting the July maps to winter maps.

A similar analysis for a sunspot minimum year (IQSY) was conducted by Singleton (1968) except that he confined attention to ionospheric stations near 75° W meridian (the so-called "American chain") and plotted the percent-occurrence contours in graphs of geomagnetic latitude versus local time.

Tao (1965) utilized a similar statistical approach with 70 stations to determine spread F occurrence in a sunspot minimum year (1954) and maximum year (1958) on a world wide basis for four seasons at 3-hour intervals. His results were plotted in modified cylindrical projection with geographic coordinates.

Supporting evidence for modelling the projected contours of spread F occurrence frequency as presented in this document has been obtained from the scintillation boundary as given by Aarons, et al (1971), the ionospheric fine structure boundaries deduced by Dyson (1969) and the topside spread F regions as reported by Petrie (1966).

The main features of polar spread F occurrence stand out clearly in the three cited analyses. Most obvious (except in Singleton's presentation) are two occurrence maximums in the geographical distribution. One, the "permanent maximum" (Penndorf 1960), is found over Foxe Basin, Canada, near the dip pole and it remains there throughout the day. The second, a "travelling maximum" (Penndorf, 1960), moves along the auroral zone on the night side of the earth, approximately centered on the local midnight meridian. Penndorf (1966) also found the double maximum in the Antarctic for IGY and Tao (1965) showed that they both exist during sunspot minimum, too (at least in the northern hemisphere).

Diurnal and seasonal variations in occurrence frequency are explainable in terms of the two geographic maximums, as discussed earlier by Herman (1966b). Briefly, at stations near the dip pole (in Penndorf's permanent maximum region) the occurrence frequency in summer is about 90 to 100% at night but still 50-60% during daytime, and in winter spread F occurs nearly 100% of the time both night and day. Thus there is little or no diurnal variation in the permanent maximum region. At stations near the auroral zone, in the path of the travelling maximum, the diurnal variation is quite pronounced, being 60 to 100% occurrence at night and about 20% during daytime. In the inner arctic away from the permanent maximum region the diurnal variation is greater than that within the permanent maximum but less than that along the travelling maximum path. The above percentages apply to solar maximum years.

Quite similar diurnal and seasonal variations are evident in solar minimum years (Tao, 1865; Singleton, 1968), but there are differences in detail between maximum and minimum years as revealed by synoptic map displays.

3.3 PROJECTION TO MID-SOLAR CYCLE

Expected spread F occurrence distributions for periods near the middle of the solar cycle (1971-72) are deduced in this section by graphically interpolating between maximum and minimum synoptic patterns. To do this, it was necessary to convert the base data to a common coordinate system and format.

A format gaining increased popularity is the so-called " Λ/M space" plotted in polar stereographic projection where Λ is invariant latitude and M is magnetic local time. Two visual advantages accruing from this system are that; a) latitudinal and time variations are readily discerned; and b) ionospheric phenomenological patterns plotted in Λ/M space can be viewed as fixed relative to the sun while the earth rotates beneath them. Further, this system allows ready comparison with published precipitating particle patterns (Section 2.) A disadvantage is that longitudinal variations are hidden. As mentioned in section 2, in the high latitude regions of interest to the present study geomagnetic latitude (G) is agreeably close to invariant latitude and geomagnetic local time is within 15 or 20 minutes of local sun time (T); we therefore, propose to utilize G/T space interchangeably with Λ/M space.

To begin, Penndorf's (1960) maps for each UT and available month were scaled to obtain sufficient geographic points to describe each percentage-occurrence contour line. For each geographic longitude, the UT hour was converted to geomagnetic local time through Hakura's (1965) tables, and the corresponding geographic latitude was re-expressed as corrected geomagnetic latitude (Hakura, 1965). The converted points were then plotted in G/T space, but it was found that in the longitude sector from about 30° to 105° W the existence of the permanent maximum obscured the patterns. Consequently the data outside of this sector were grouped together, plotted in G/T space and graphically averaged to obtain a single contour for each percentage occurrence level.

The result of this manipulation yielded a picture quite similar to that in Fig. 7. That is, there is a very strong auroral oval component in spread F occurrence which has been identified in the past as the travelling maximum. This pattern, when viewed as fixed with respect to the sun with the earth rotating beneath it, readily yields the observed diurnal variation at a fixed station in the auroral zone. The shape of this pattern strongly suggests energetic particle precipitation as the production mechanism for spread F irregularities in the travelling maximum region; henceforth, it is referred to as the "auroral oval component" (AOC) of high latitude spread F. Further remarks are devoted to Fig. 7 later in this section.

Having now defined an auroral oval component, comparison was made with G/T maps constructed from data along longitudes spaced 15° apart in the $30-105^\circ\text{W}$ longitude sector. Graphical subtraction of the AOC from the contours in these latter maps ultimately yielded a permanent maximum (or dip pole) component (DPC) of spread F occurrence plotted in geomagnetic coordinates at 3 hourly intervals throughout the UT day.

The same treatment was applied to the sunspot minimum data of Singleton (1968) with some guidance being afforded by the 1954 data of Tao (1965). Then, with the auroral oval and dip pole components separated, it was possible to graphically interpolate approximately halfway between sunspot max and min to obtain patterns appropriate for mid-solar cycle years (1971-72).

To illustrate the results of this process, the auroral oval component in G/T space projected to July 1971/72 is depicted in Fig. 7. Noteworthy is the narrow band of high occurrence probability (80%) even in middling sunspot years, to be found between about 0100 to 0300 LT and centered at about 70° . Almost symmetric in time about this core are the lower percentage contours of 60% and 40%. In the postmidnight sector equatorward of the core there is a steady progression southward in decreasing occurrence probability, roughly 6% per degree of latitude. The shape of the 20% contour is reminiscent of the scintillation boundary except that it is located about 8° north of the boundary on the night side; this, coupled with the latitudinal gradient noted above indicates that 0%

contour might lie at about 50° geomagnetic latitude on the night side. To the north of the 80% core, a negative latitudinal gradient in occurrence probability is evident; it is less steep from the 80% to 60% contours but sharper from 60% to 40% compared to the equatorward gradient. Within the polar cap region the occurrence probability is between 20% and 40%.

The overall shape of the AOC pattern corresponds qualitatively to the phenomenological particle precipitation model deduced in Section 2.3.3 for the F region, but now we have a measure of the occurrence statistics. It is suspected, though no substantiating investigation has been made in the present effort, that the expansion in G/T space of the coverage area as the percent occurrence decreases is closely related to magnetic activity. That is, for geomagnetically disturbed days, of which there are few, one may expect to see spread F over the whole G/T region encompassed by the 20% contour line, whereas on the quietest days spread F may be expected only in the hours 00-03 LT in the narrow latitude band from about 68° to 71°. The areas covered by 60% and 40% should correspond to spread F occurrence on moderately quiet and moderately disturbed days, respectively.

Similar auroral oval component patterns (not illustrated) have been projected for mid-solar cycle September and "winter". It is presumed that the September AOC is reasonably representative of both fall and spring equinox conditions, and the July AOC (Fig. 7) is representative of Summer. Comparing these three,

it is found that spread F is most pronounced in the Equinox followed next by Winter and finally by Summer, in agreement with Shimazaki's (1962) results.

It should be noted that the present patterns are principally influenced by Penndorf's (1960) results. His analysis was made in terms of geographic coordinates at a time when polar spread F was widely believed to be a nocturnal phenomenon and strongly solar controlled, and there was only a hint that charged particles might play a role (Shimazaki, 1959). The remarkable agreement between the projections in G/T space and present concepts of precipitating particles attests to the care and insight with which Penndorf's early analysis was conducted. We may therefore proceed with confidence in the present analysis.

Patterns of the dip pole maximum region obtained as described above and projected to mid-solar cycle in geomagnetic coordinates exhibit diurnal and seasonal variations in both maximum occurrence frequency and effective coverage area. In general, both are smallest on the day side and largest on the night side, and more pronounced in Winter and Equinox compared to Summer. Although maps of the DPC were generated for each 3-hour UT time in July and September, for utilization in constructing spread F occurrence projections covering the polar regions, it is felt that two examples will suffice for this report.

In July 1971/1972 the dip pole maximum during daytime (1500 UT and 1800 UT) is found between about 75° to 85° geomagnetic latitude and 310° to 40° E geomagnetic longitude (Fig. 8) as defined by the 40% occurrence contour. (The method of analysis precluded establishment of a 20% contour). Within this region one may expect to see 60% spread F occurrence in a small area centered at about 82° N.

Going into the nightside (the relative motion of the sun is clockwise with respect to the map,) the coverage area expands and the maximum occurrence probability increases, as can be seen in Fig. 9. The area of highest occurrence probability (80% or more) is still centered at about 82° N, and the 40% poleward boundary remains at about 85° N. The percentage falls off more rapidly going poleward than equatorward. The lower border of the 40% region is now at about 67° (Fig. 9) compared to 77° on the dayside (Fig. 8). The largest coverage area defined by the 40% contour appears at 0600 UT (0100 LT in the dip pole maximum region).

Throughout the day, the maximum-occurrence core is centered at about 81 or 82° N and the poleward 40% border remains at about 85° N. The southern border apparently varies from about 64° N (at 0600 UT) to 77° N on the dayside; however, on the night side there may be some contamination by auroral effects in the southern part of the dip pole component deduced here. In the composite spread F maps to be discussed below, this possible contamination will be of no real consequence.

Composite spread F maps applicable to mid-solar cycle have been generated for eight UT hours of the day (00, 03... 21 UT) for a Summer, an Equinoctial and a Winter month, to depict the spatial and temporal variations in occurrence of overhead spread F. These maps have been derived by superimposing the auroral oval component (as in Fig. 7) on the dip pole component (e.g., Figs. 8 or 9).

For a given UT hour the relative orientation of the AOC is fixed by overlaying the geomagnetic local time at 0° geomagnetic longitude corresponding to that UT hour onto the 0° geomagnetic meridian of the appropriate DPC map. The common reference point for the two displays is the geomagnetic pole. In regions where AOC and DPC overlap, the larger of the two occurrence percentage contour values was chosen. Some smoothing was required in constructing composite contours in the vicinity of overlapping junction points.

In the superposition process, any errors present in the areal coverage of the dip pole component deduced earlier will be largely cancelled. The result of this merging technique is a fairly idealized representation of spread F occurrence percentage displayed in geomagnetic coordinates. It should be noted that in a limited-distribution preliminary report on this subject (Herman, 1971, unpublished), the longitude was erroneously identified as geographic longitude. That notation is correct only along 60° N geomagnetic latitude and should not be used. It has been corrected in this report. The first map, for 00 UT, July 1971/72 (Fig. 10) serves to illustrate the results.

2. DATA BASE

Collection of the data used in this study was made by the airborne ionospheric laboratory of AFCRL (Pittenger and Gassmann, 1971). In that effort, all E_s events were lumped together and no attempt was made to classify E_s , night E was considered to be the same as E_s . This is a good assumption with respect to oblique radio propagation insofar as the effects of E_s and night E are similar on oblique transmissions. The Pittenger and Gassmann data, used in this analysis, are presented in the form of maps giving the probability of occurrence of E_s with top frequencies (fE_s) being greater than 3, 6 and 9 MHz. Three such maps were made for each of three different conditions of magnetic activity. These maps, shown in figures 1 through 3 are plotted in corrected geomagnetic latitude and local time. For purposes of oblique HF radio propagation, the parameter fE_s was chosen because it is closely related to this phenomenon. For the phenomenon of interruption of normal F layer propagation, the corresponding parameter to be investigated is the blanketing frequency ($f_b E_s$) which correlates closely to the maximum electron density of the E_s cloud.

From the probability of occurrence maps it can be seen that for quiet magnetic conditions, the chances of observing E_s are uniformly distributed around the auroral oval, with the highest probability being naturally for the lowest value of fE_s . For conditions of moderate magnetic activity, the overall

chances of finding E_s increases with a tendency to predominate in the late evening hours. During very disturbed magnetic conditions there is a strong preference for E_s to concentrate in a period centered approximately two hours before midnight in corrected geomagnetic time.

In order to translate these maps into probability contours on a radar fan plot, a fan in range azimuth space at the geographic coordinates of interest was plotted onto the corresponding coordinates of corrected geomagnetic latitude and corrected geomagnetic time. This graph is then superimposed on a given data base map. Then the probability of occurrence of E_s as seen at path midpoint for some range and azimuth is recorded. This process is then repeated for several ranges and azimuth. After a sufficient number of points have been gathered, they are transferred to the radar fan plot and points of equal probability are connected into smooth contours.

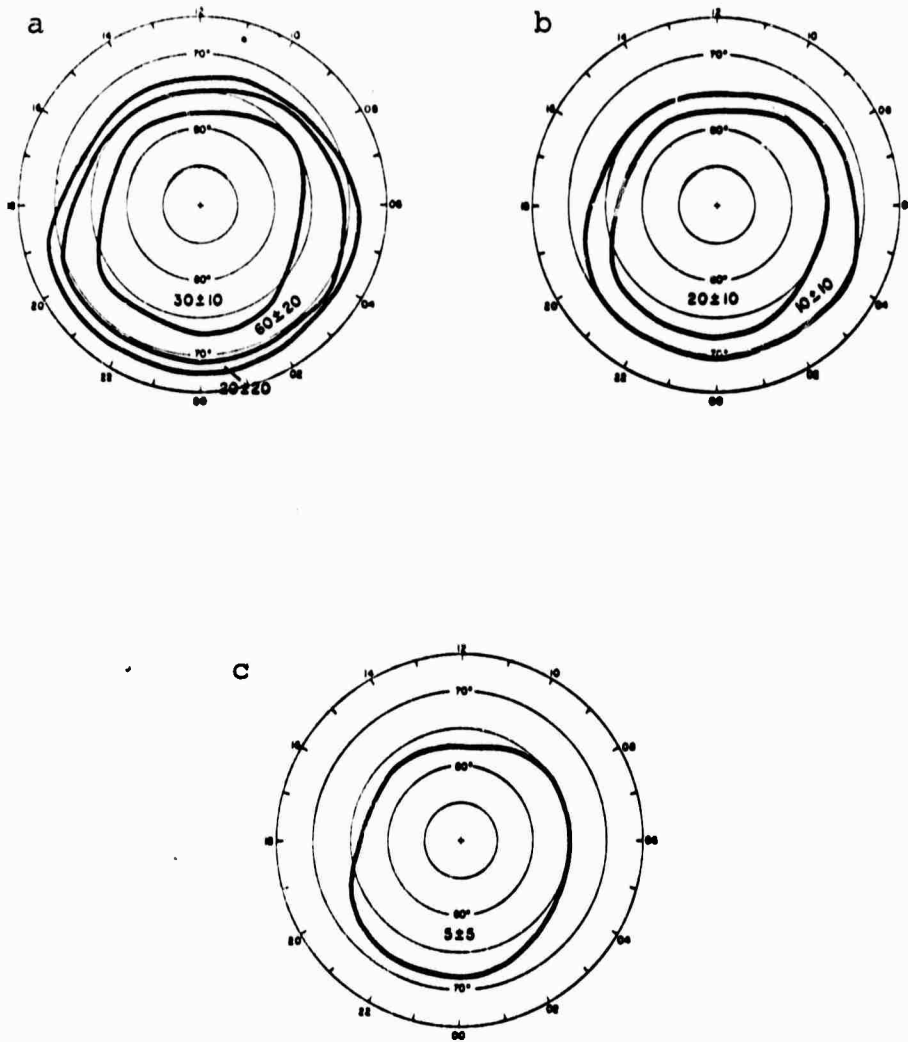


Figure 1 Schematic Presentation a, b, c of Occurrence in Percent of fEs Larger Than 3, 6, 9 MHz Respectively for Quiet Magnetic Conditions in CGL/CGT Coordinates

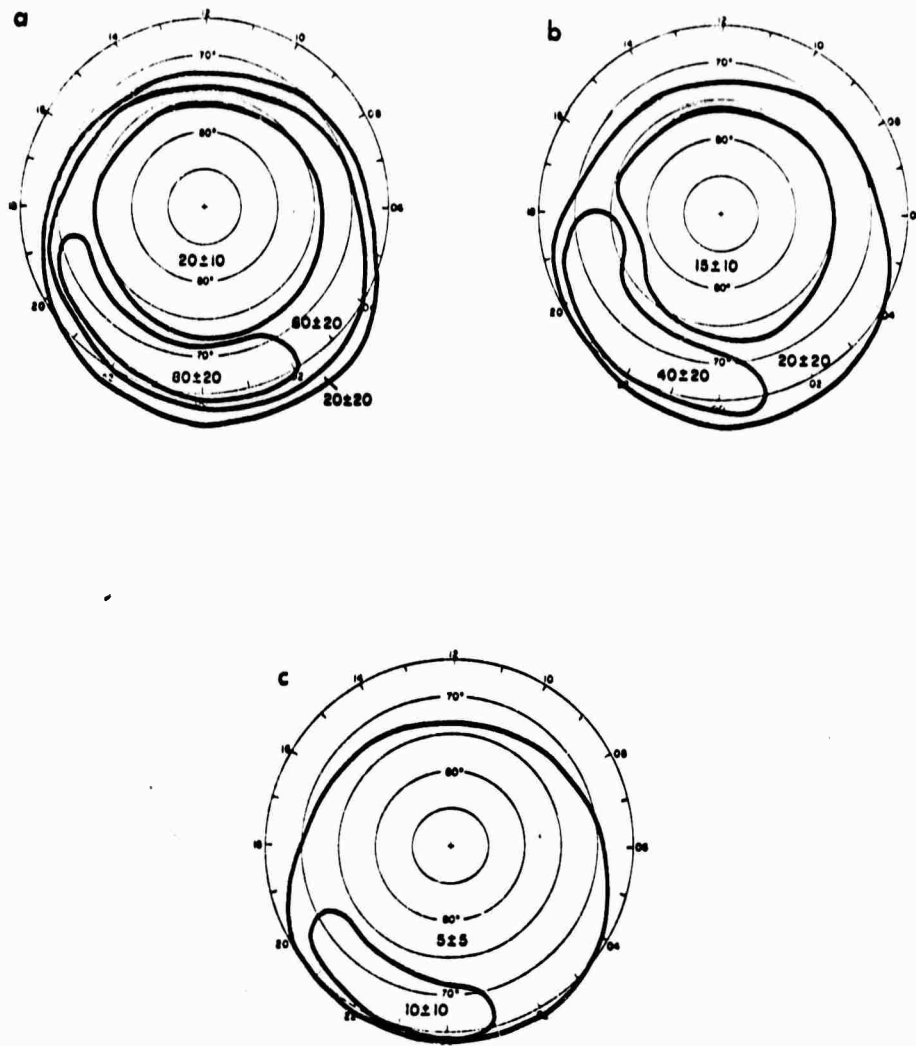


Figure 2 Schematic Presentation a, b, c of Occurrence in Percent of fE_s Larger Than 3, 6, 9 MHz, Respectively, for Moderate Magnetic Conditions in CGL/CGT Coordinates

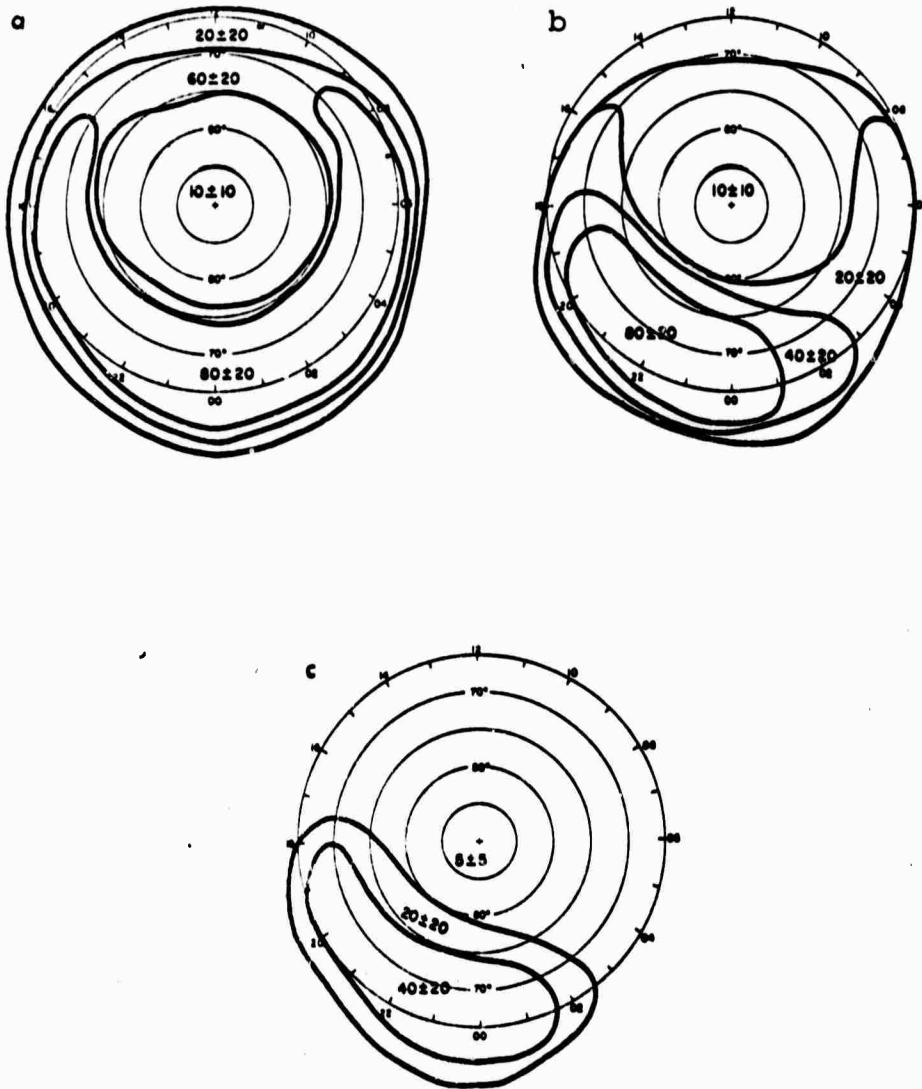


Figure 3 Schematic Presentation a, b, c of Occurrence in Percent of fE_s Larger Than 3, 6, 9 MHz, respectively, for Very Disturbed Magnetic Conditions in CGL/CGT Coordinates

3. DISCUSSION

Range azimuth fan graphs shown in Figures 4 through 45 are arranged in three groups in order of increasing magnetic activity. Within each group the plots are ordered in terms of increasing fE_s . For any given level of magnetic activity and top frequency, plots are shown every three hours, giving the diurnal variation of the probability of occurrence of sporadic E as seen at the midpoint of the path from the transmitter to some point in the range azimuth sector.

For conditions of low magnetic activity from about 00UT through 09 UT patches of fE_s greater than 3MHz occur in the range of 1000 km from the transmitter (apex of fan) that would support HF propagation to distances of 2000 km roughly due north for about 20 to 40% of the time. If one assumes a secant law behavior for oblique E_s propagation, then for a reflection height of 100 km and a path length of 2000 km the secant of the incidence angle is ten. In other words, HF forward scatter up to 30 MHz would be supported by this E_s . Most likely, the upper frequency limit is not 30 MHz but is probably lower, since this forward scatter mechanism, which is not clearly understood, does not appear to follow a simple secant relationship (Herman 1969). For days of low magnetic activity fE_s greater than 6MHz and 9MHz occurs less 10% of the time in the fan. All such periods where the incidence of E_s is less than some minimum percentage of time are indicated in the maps.

During periods of moderate magnetic activity, the appearance of fE_s greater than 3 MHz comes into the fan for about a 12 hour period from about 00UT to 12UT. It is strongest during the hours 03UT to 06UT where it occurs over large portions of the fan for 60% of the time or more. As time progresses from night to day, the occurrence of E_s tends to move towards the northwest or nighttime sector of the fan in almost all cases. Auroral sporadic E is predominantly a nighttime phenomena hence, in the northeast or daytime sector of the fan there is less E_s . As expected the probability of observing $fE_s > 9\text{MHz}$ is less than for $fE_s > 6\text{MHz}$ which in turn is less than that for finding $fE_s > 3\text{MHz}$. In addition, the higher the top frequency, the shorter the portion of the evening that E_s is observed this is so because the occurrence of E_s is no longer uniformly distributed around the auroral oval.

Only at times of very disturbed magnetic activity does $fE_s > 3\text{MHz}$ appear continuously in the fan throughout a 24 hour period. During much of the evening hours it is present 80% of the time while throughout the day it is present at least 20% of the time. Even $fE_s > 6\text{MHz}$ is prevalent in the evening hours between 40 and 80% of the time over most of the fan and during about half of the daytime it is found 20% of the time. During 20% to 40% of the evening hours $fE_s > 9\text{MHz}$ is present in the fan. Additional details of E_s supported propagation in the area of interest are evident in the maps.

4. SUMMARY

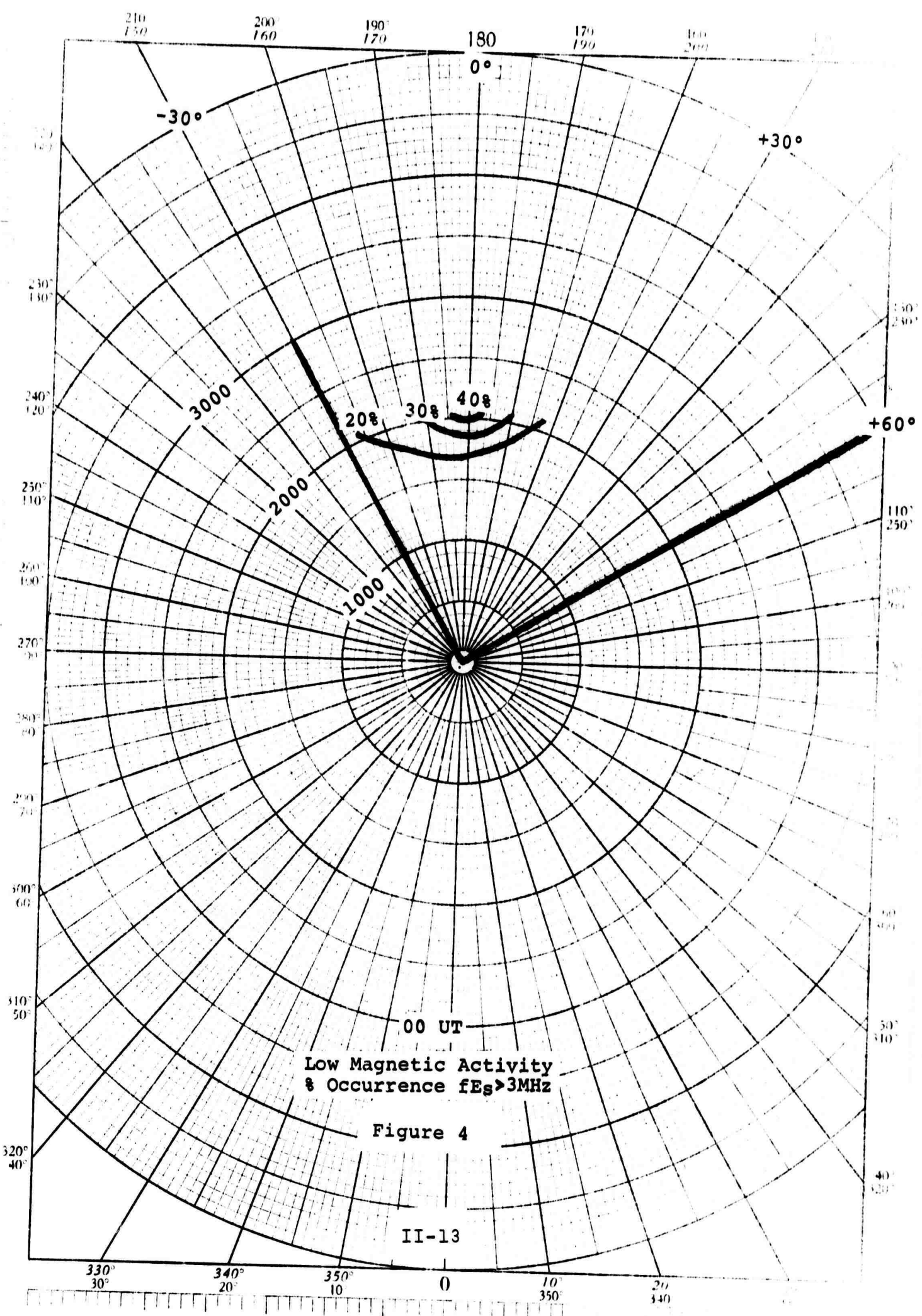
It has been shown that HF radio wave propagation in the polar ionosphere is significantly influenced by the occurrence of sporadic E. During the evening hours local magnetic time (00UT through 06UT) the prevalence of E_s is greatest. Although E_s is strongest during periods of very disturbed magnetic activity, $fE_s > 3\text{MHz}$ during moderately disturbed magnetic conditions occurs with a high probability (60% and 80%) in the fan. This will support HF forward scatter propagation up to about 30 MHz, and provide coverage during those periods when normal F layer propagation may have been interrupted.

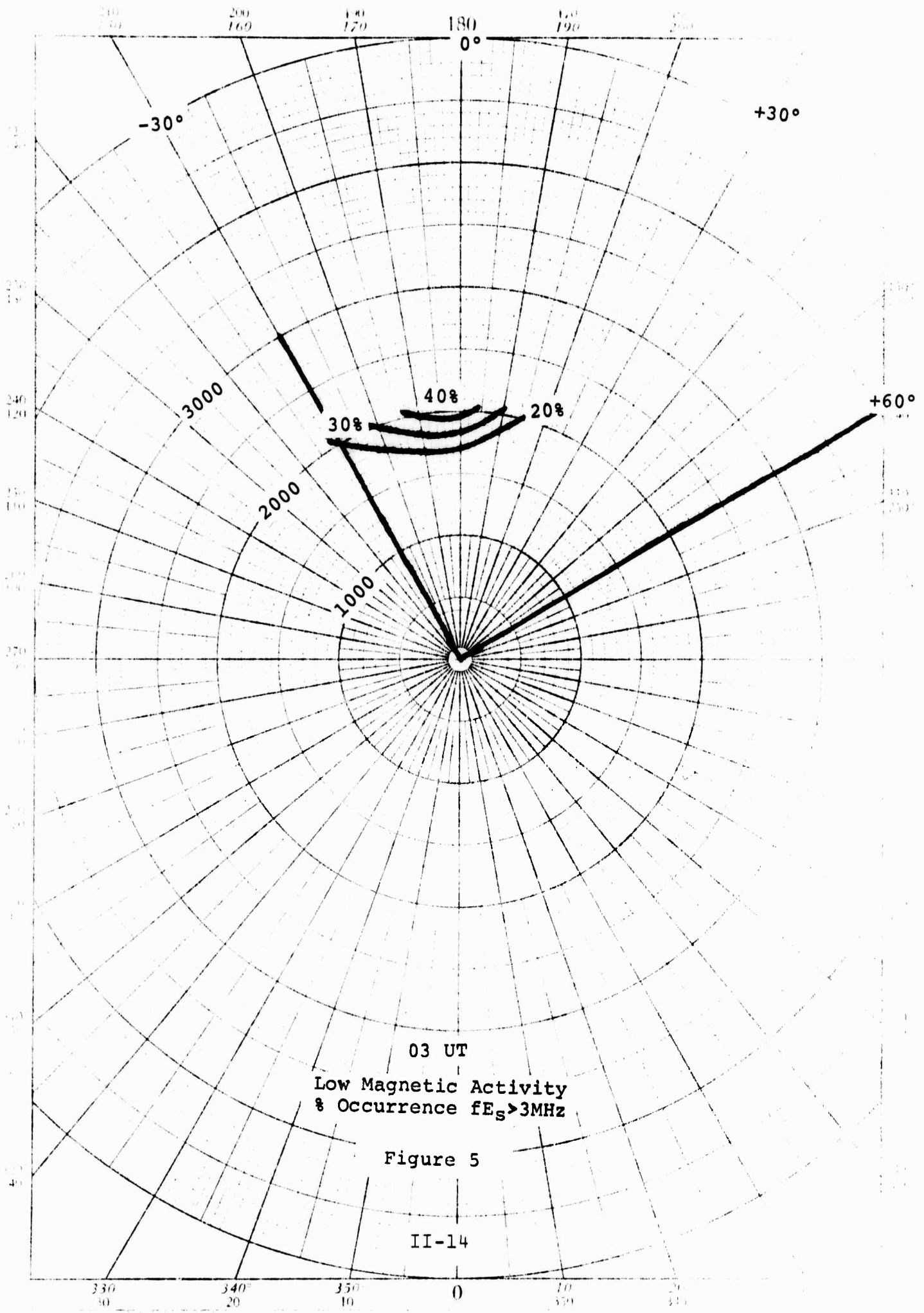
Since the parameter under consideration in this study is fE_s , which is not necessarily correlated with $f_b E_s$, it should be remembered that a simultaneous F layer mode of propagation is possible. Therefore, conditions may arise where interfering modes exist. This could cause degrading effects such as amplitude fluctuations and Doppler shifts.

REFERENCES

- 1 Herman, J. R., "High Latitude Sporadic E,"
Final Report, Con. No. F19628-68-C-0263, January, 1969.
- 2 Penndorf, R., "High Latitude Propagation Study,"
Final Report, Con. No. F30602-69-C-0201,
September, 1970.
- 3 Pittenger, E.W. and Gassmann, G. H., "High
Latitude Sporadic E," AFCRL-71-0032, Environmental
Research Paper, 347, February 1971.

RZ POLAR COORDINATE 46 3412
KEUFFEL & BRUNNEN

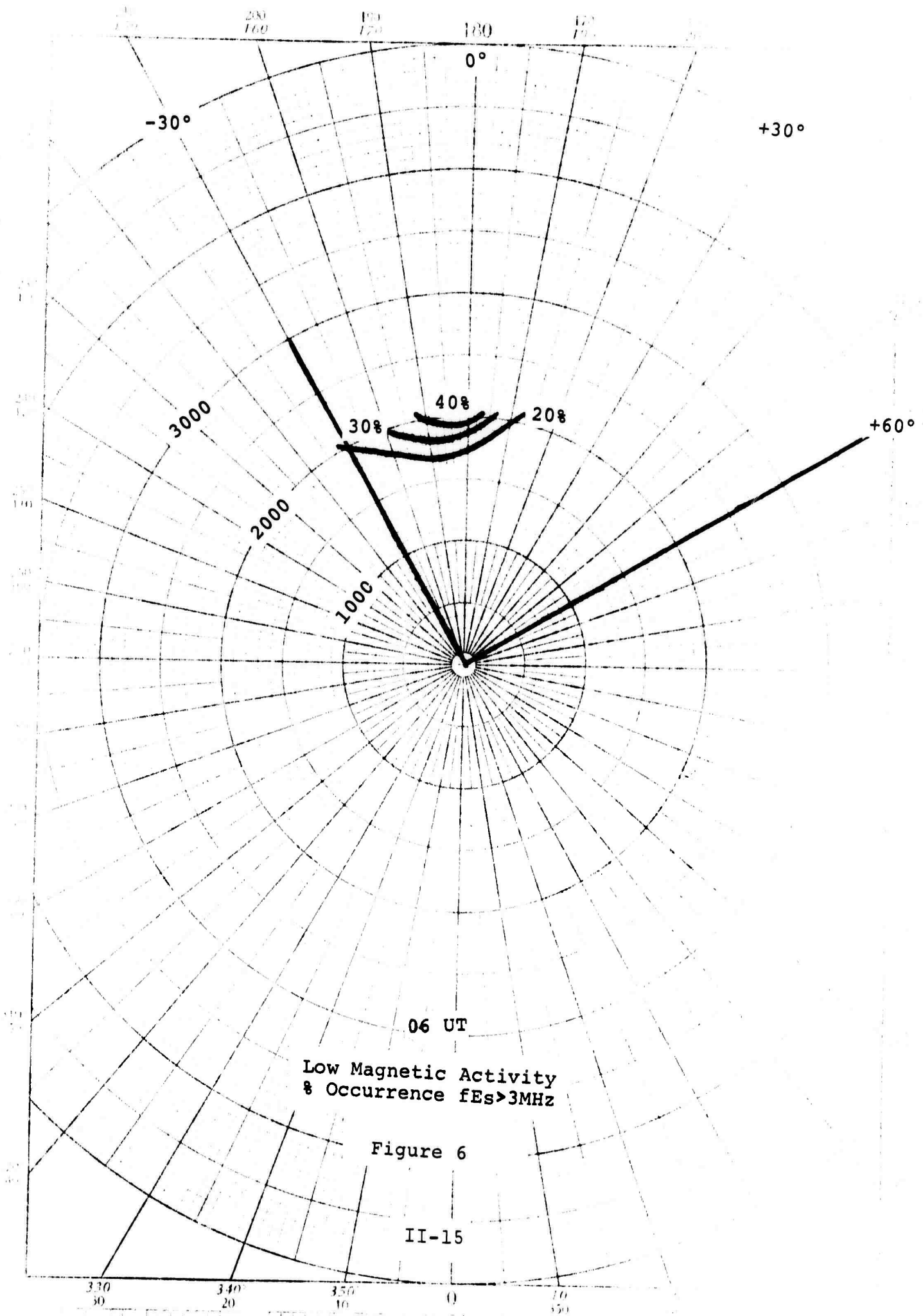


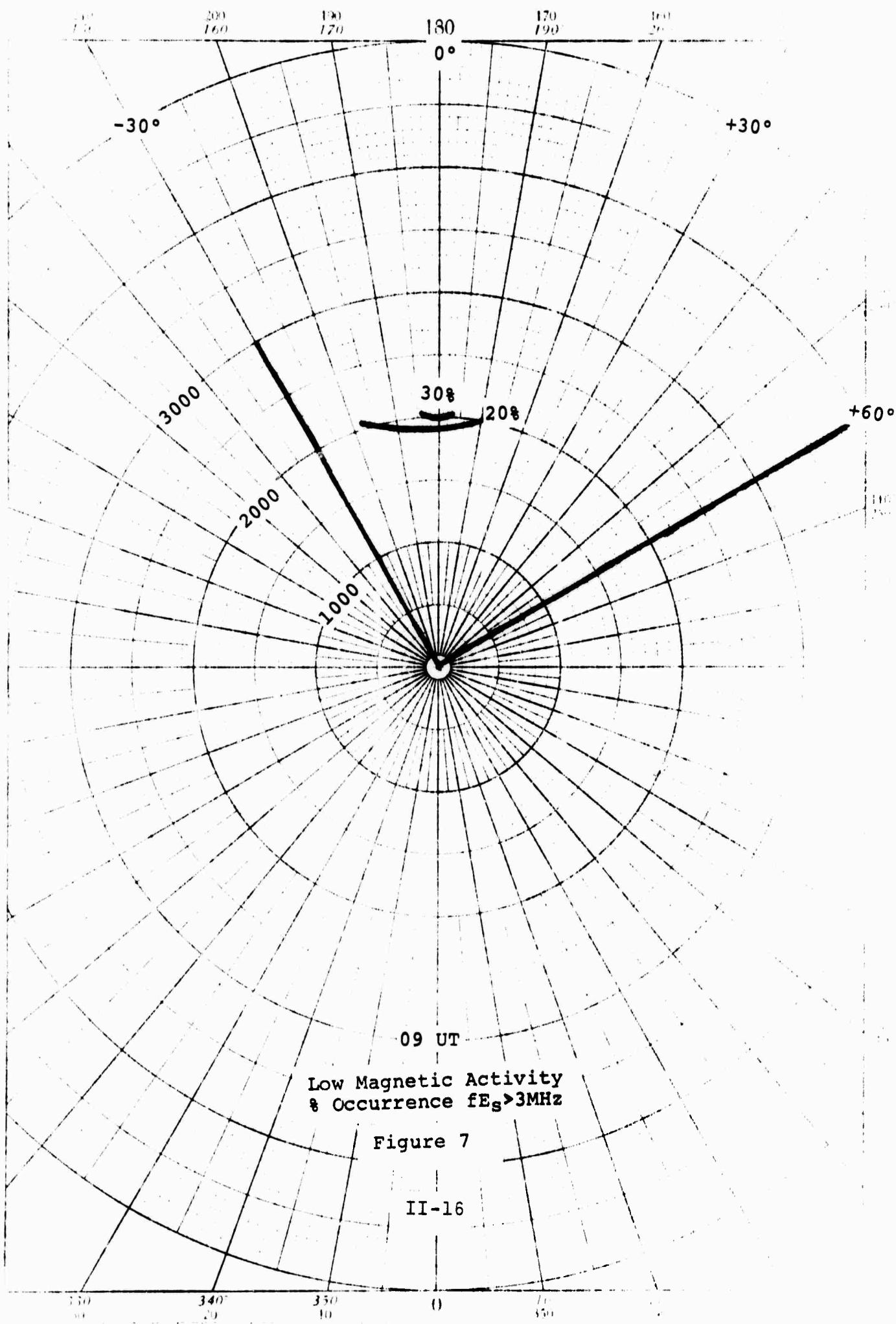


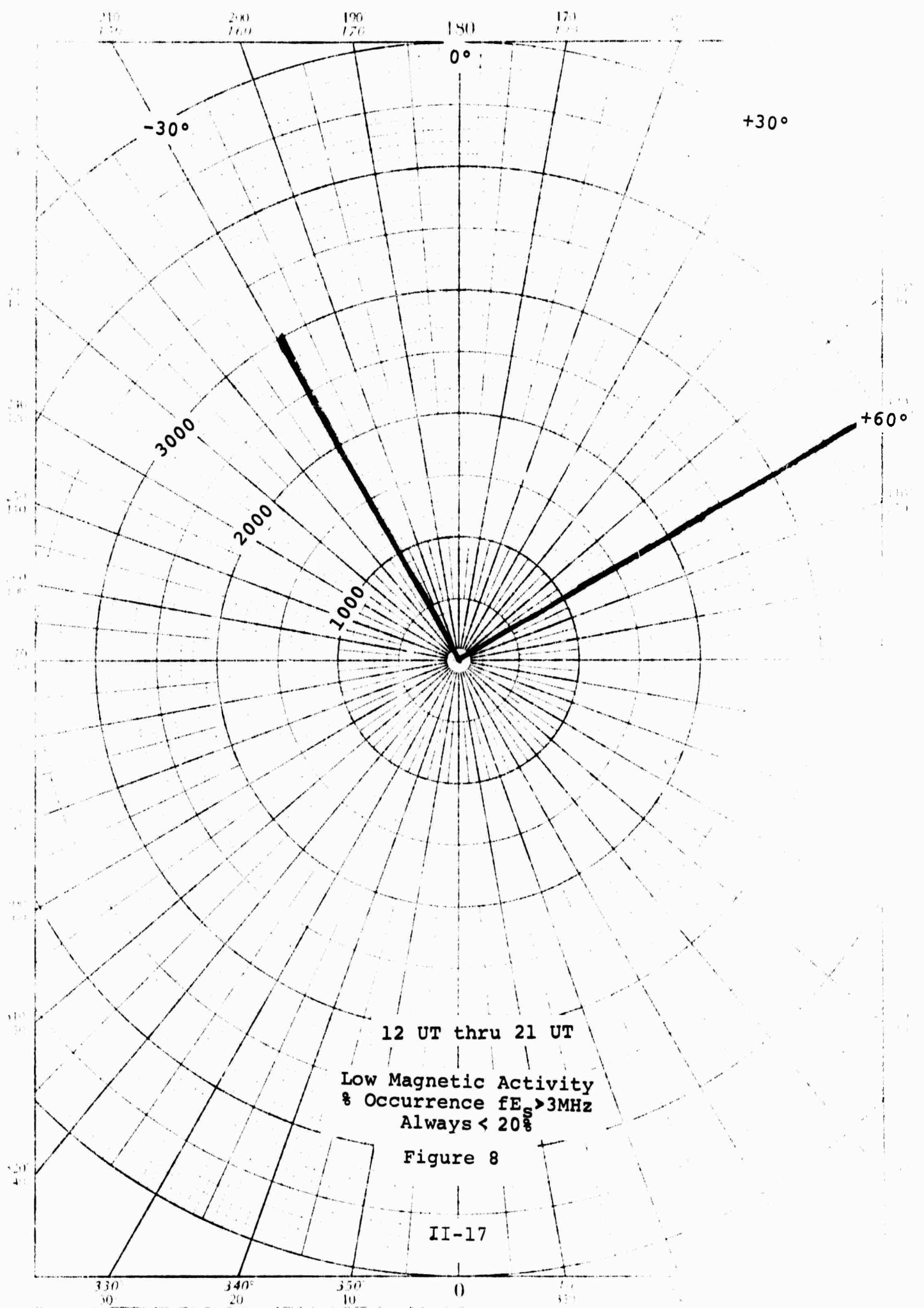
03 UT
Low Magnetic Activity
% Occurrence $fE_s > 3\text{MHz}$

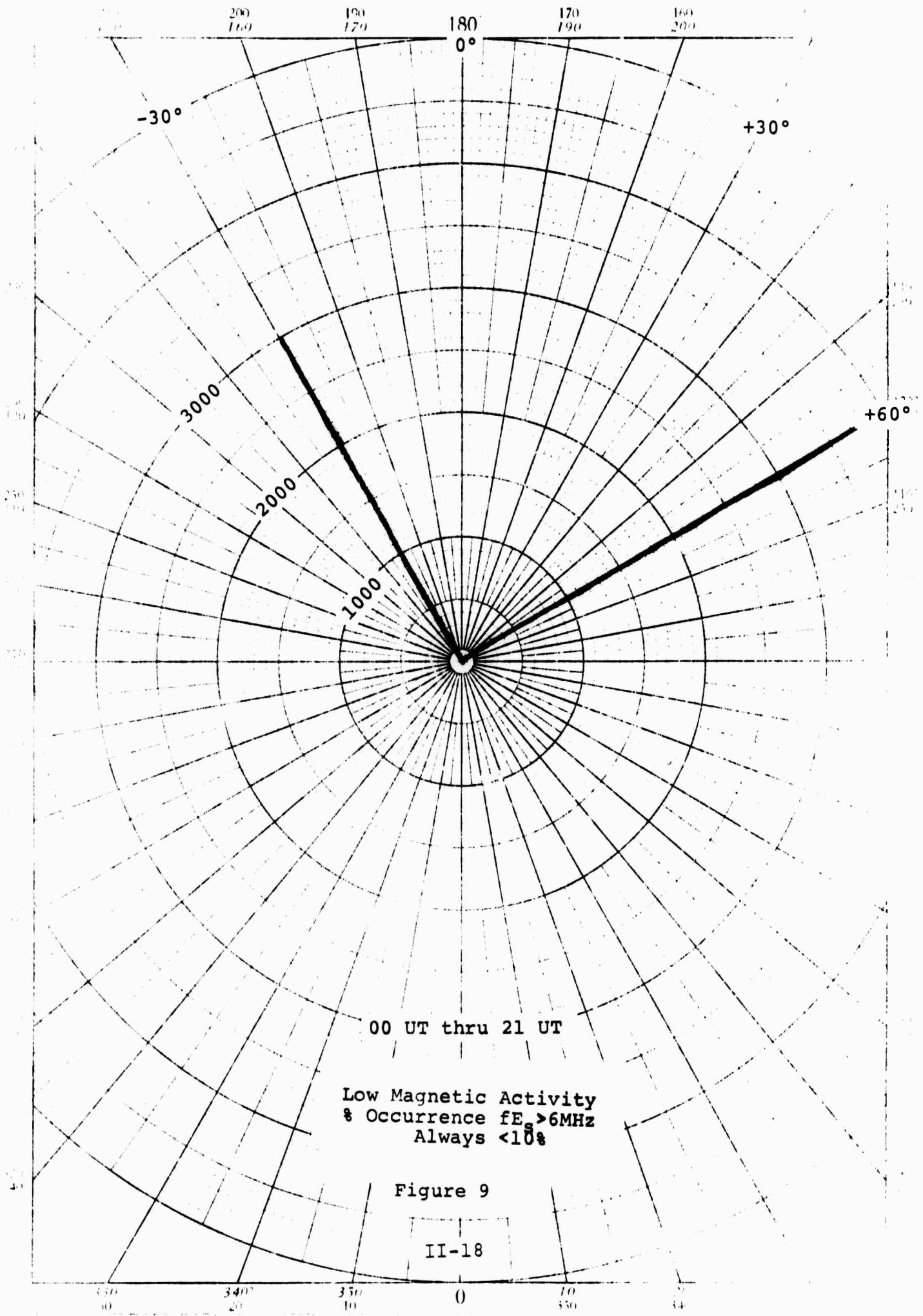
Figure 5

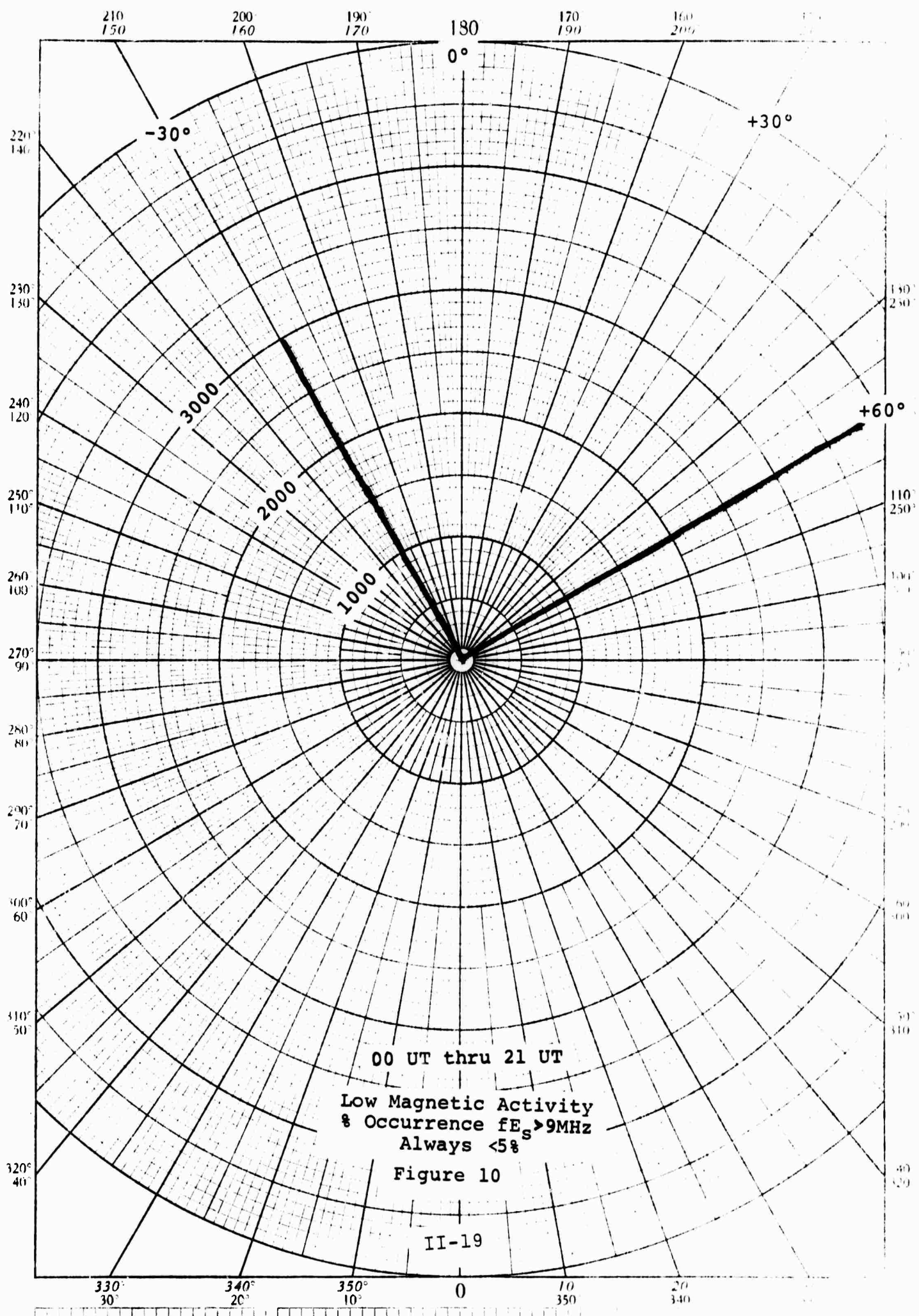
II-14









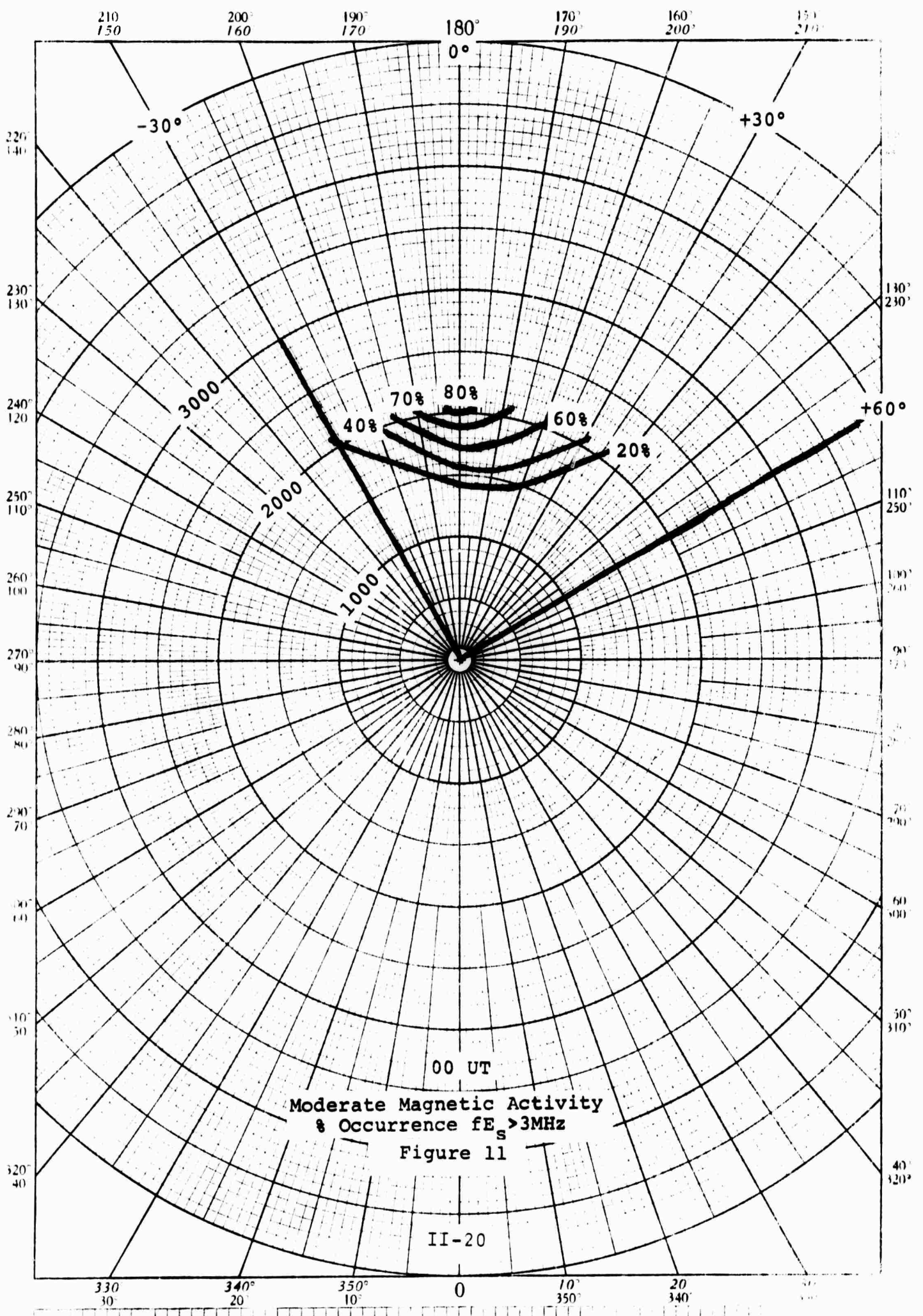


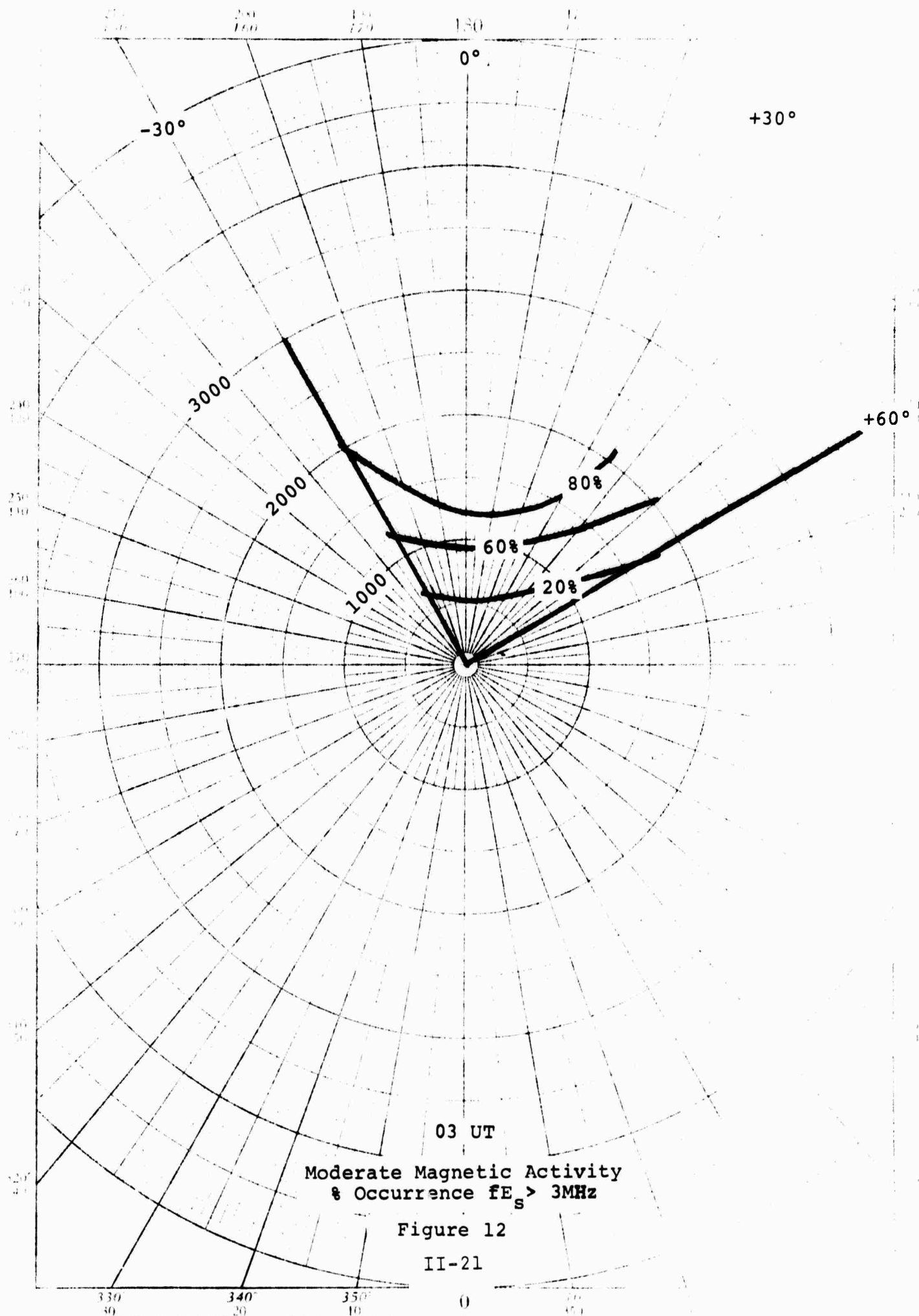
210 150 200 160 190 170 180 170 190 160 200

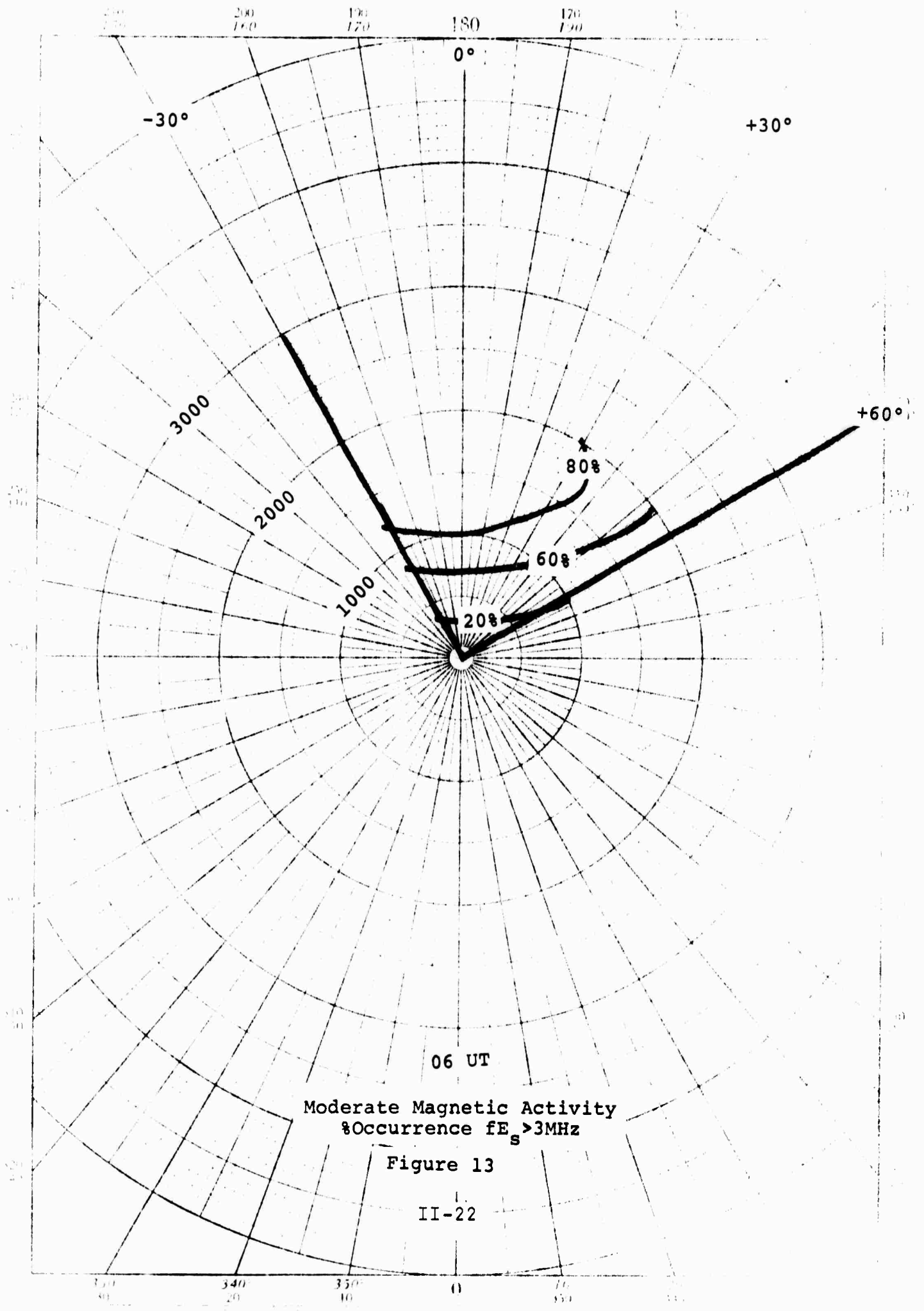
220 140
230 130
240 120
250 110
260 100
270 90
280 80
290 70
300 60
310 50
320 40

0°
+30°
+60°
150° 250°
110° 250°
100°
90°
80°
70°
60°
50°
40°

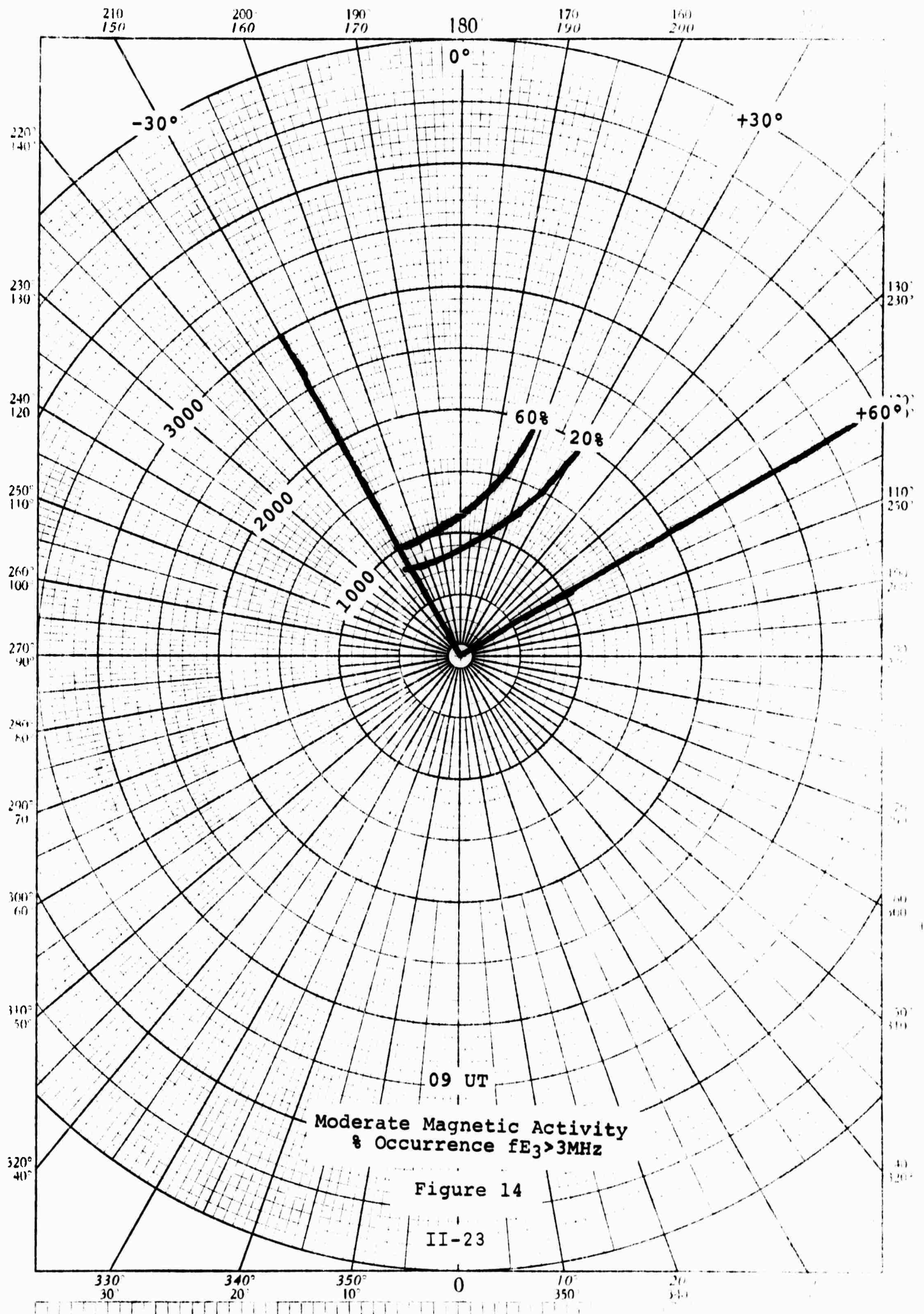
330° 30° 340° 20° 350° 10° 0 10 350 20 340

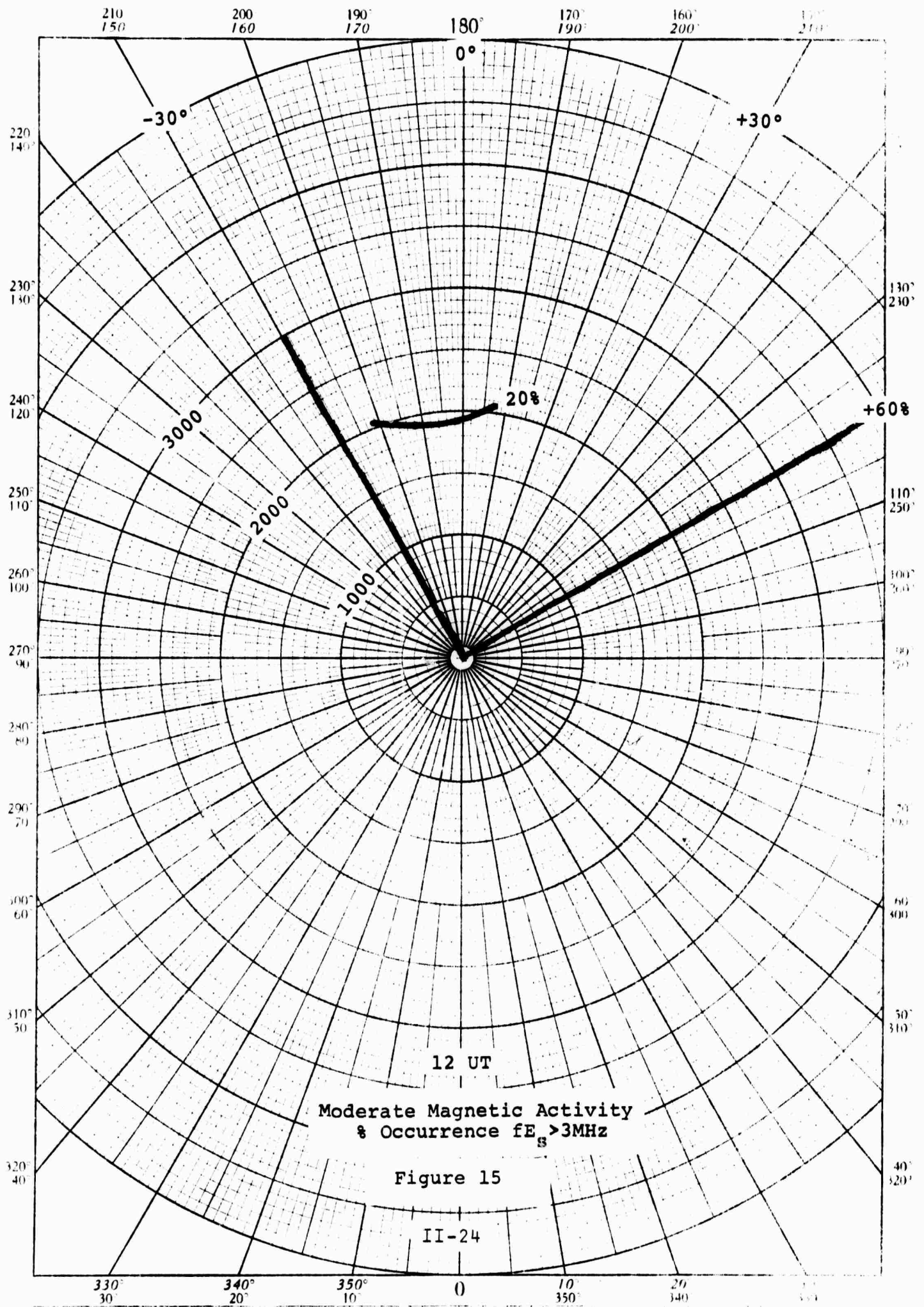


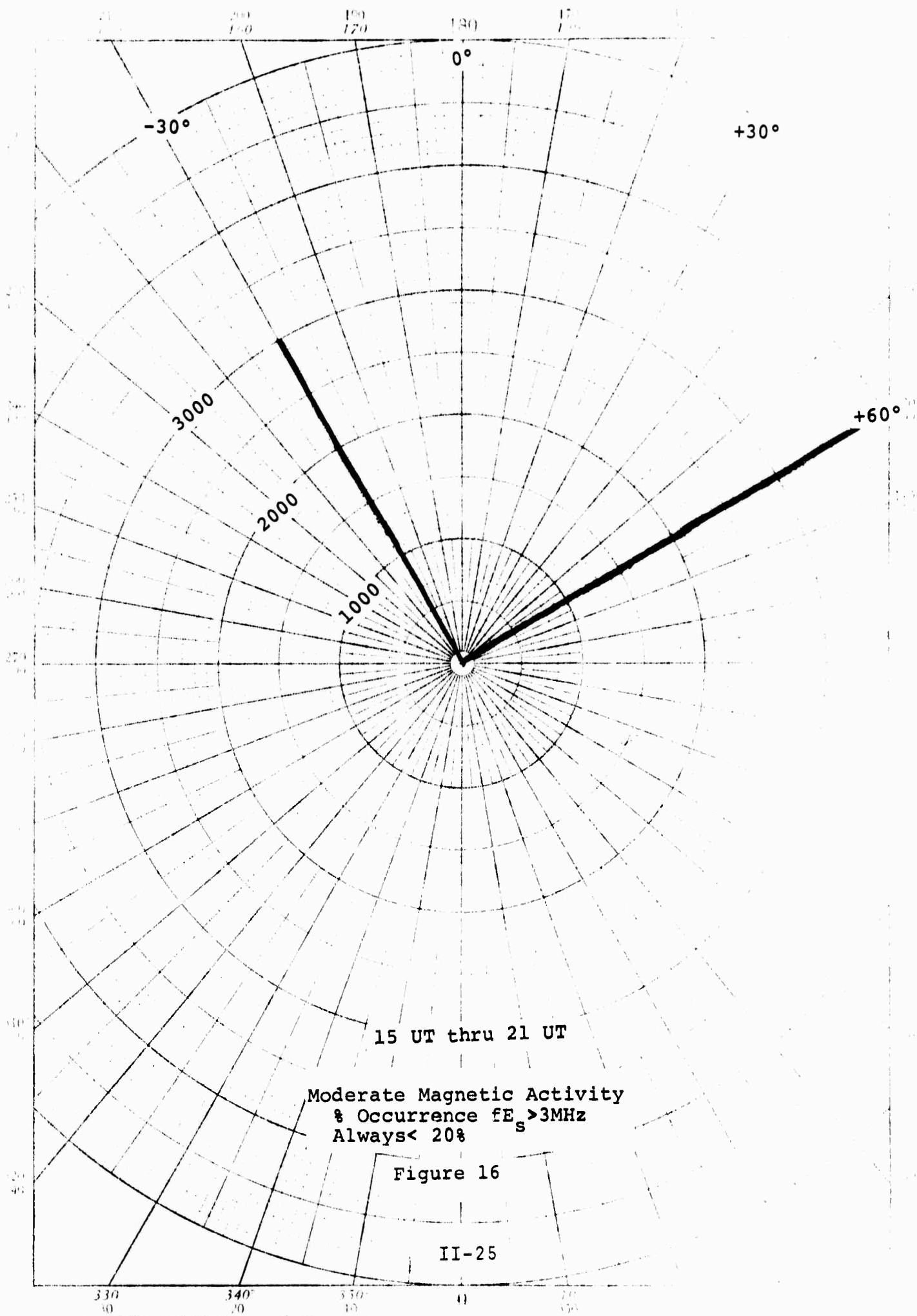


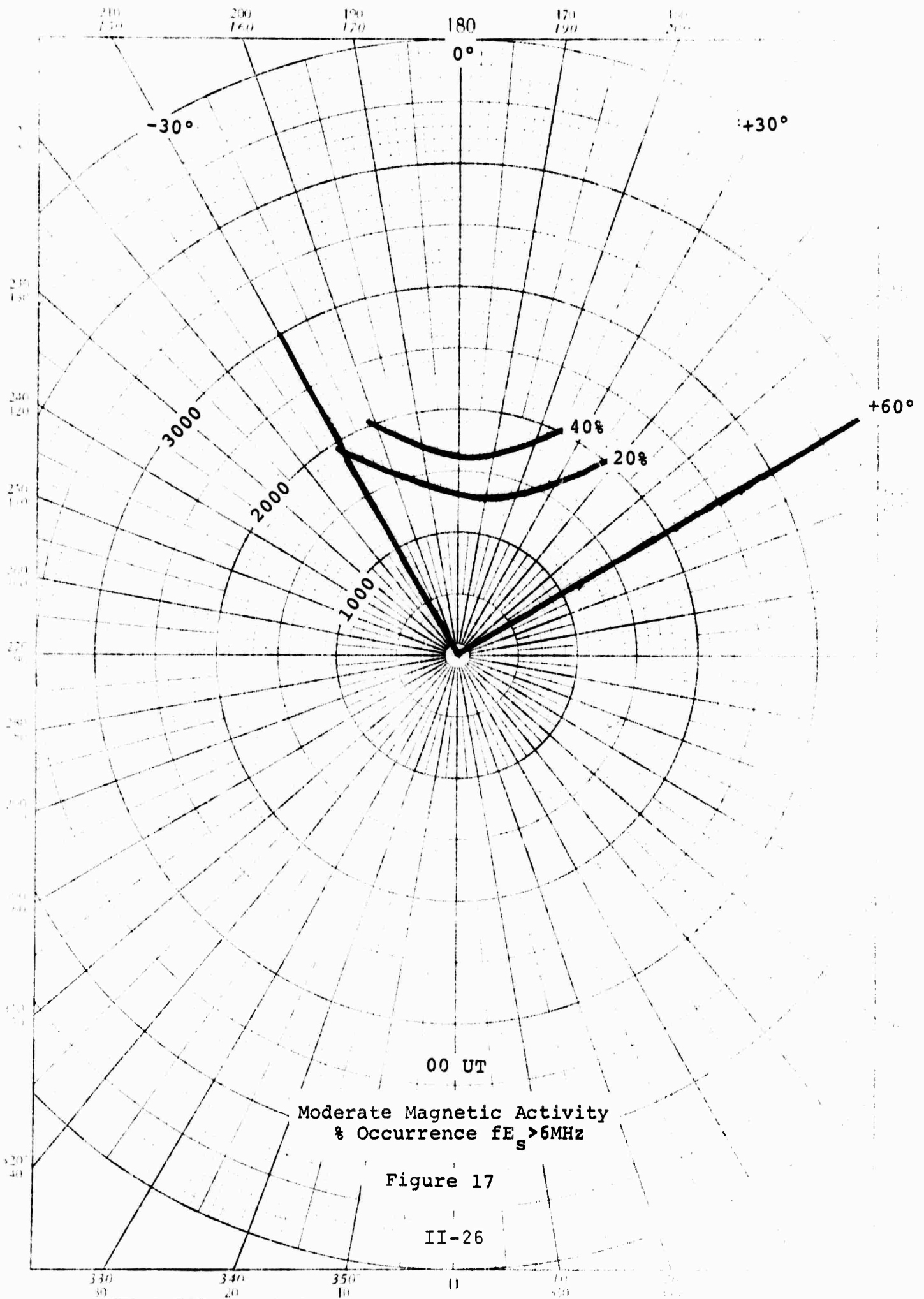


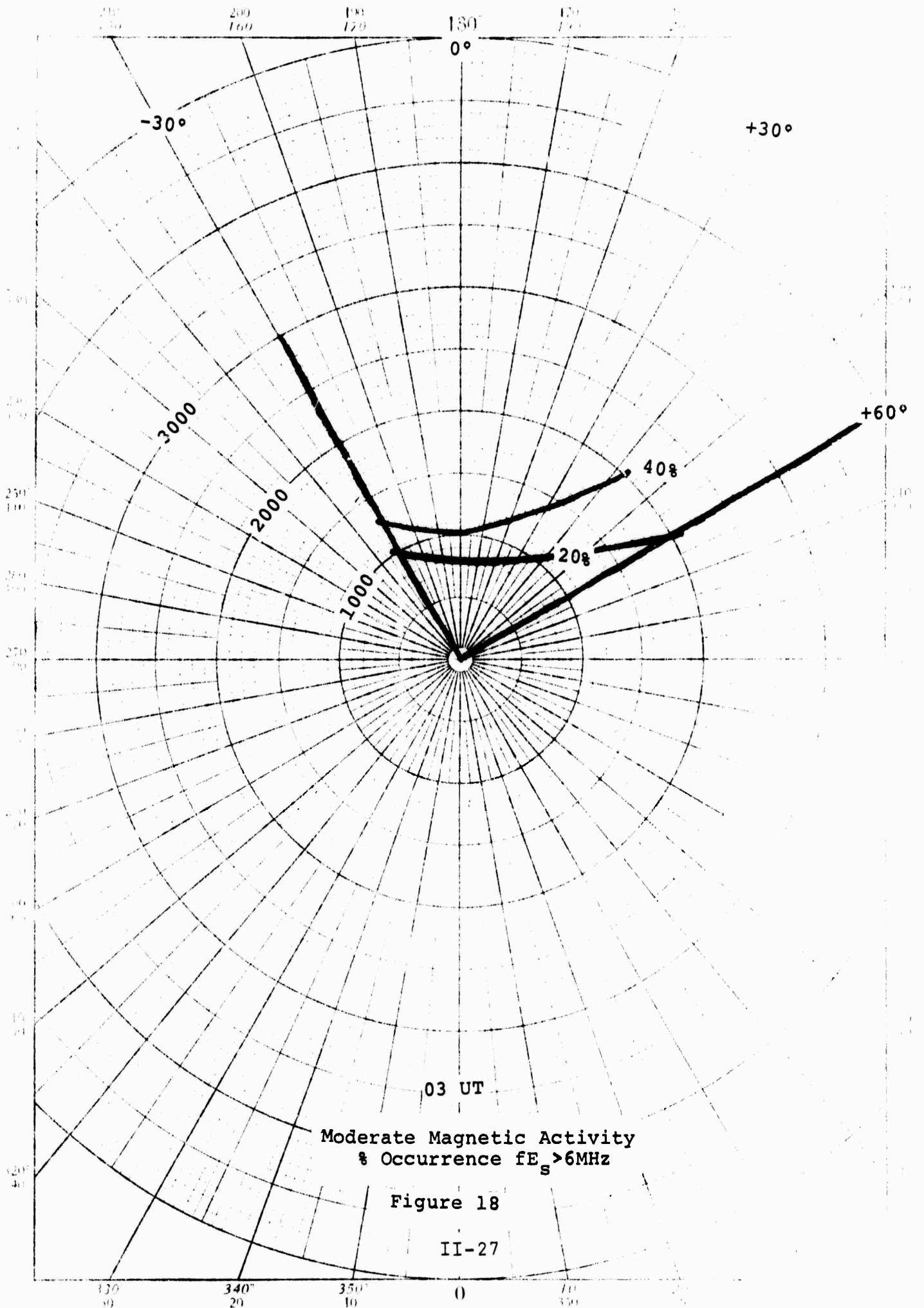
K&E POLAR COORDINATE 46-4412
HEUFFEL & CO.

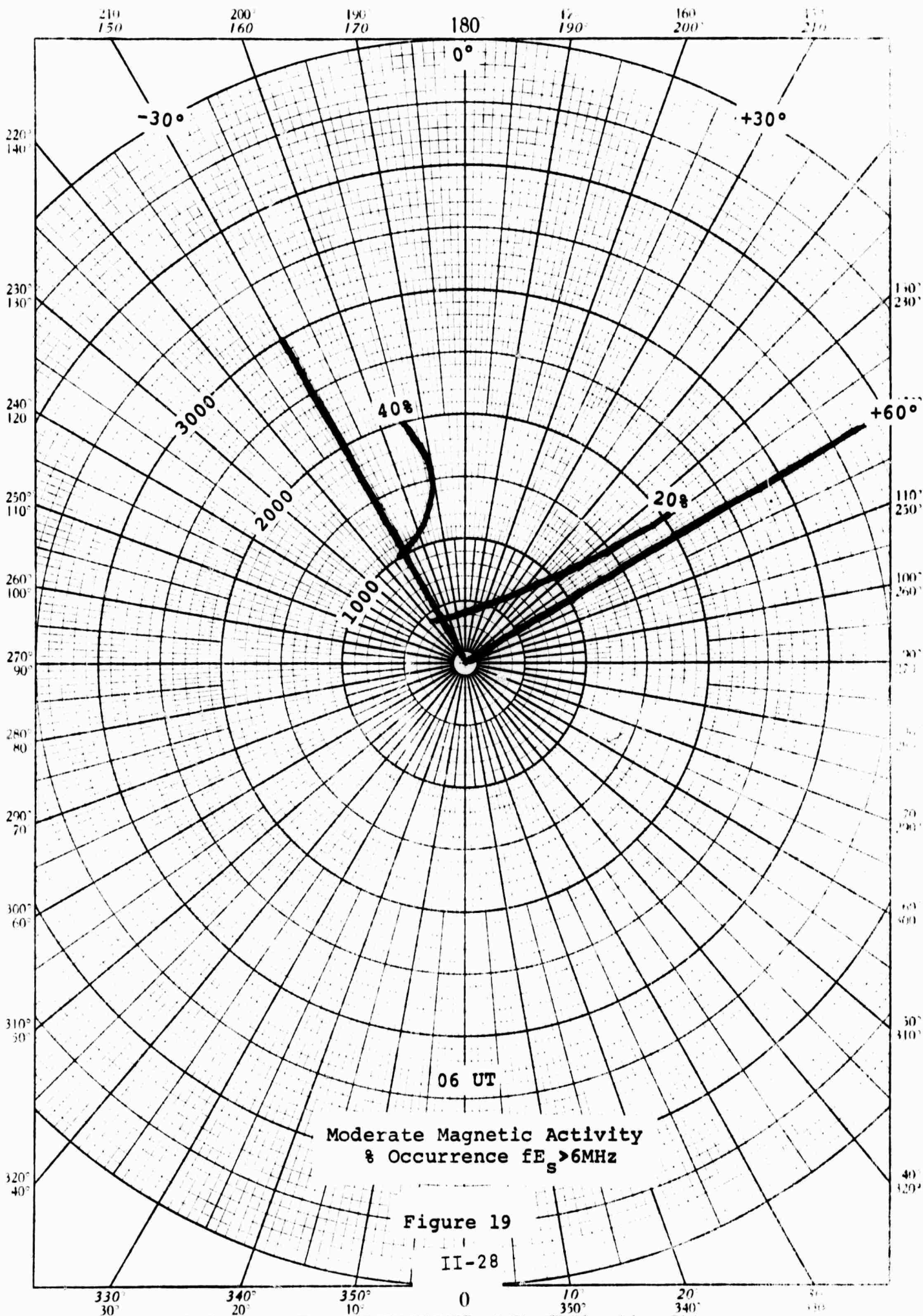


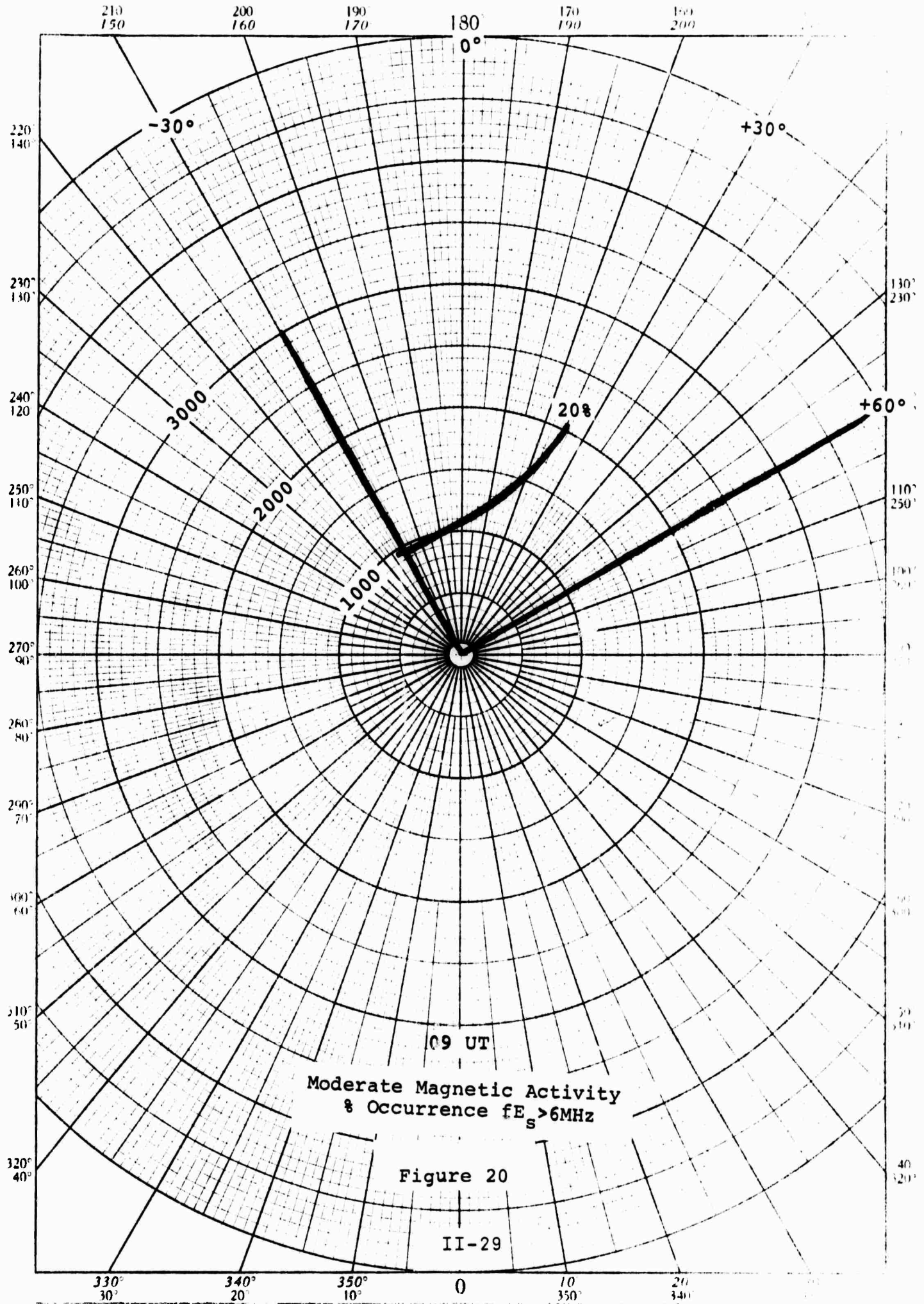


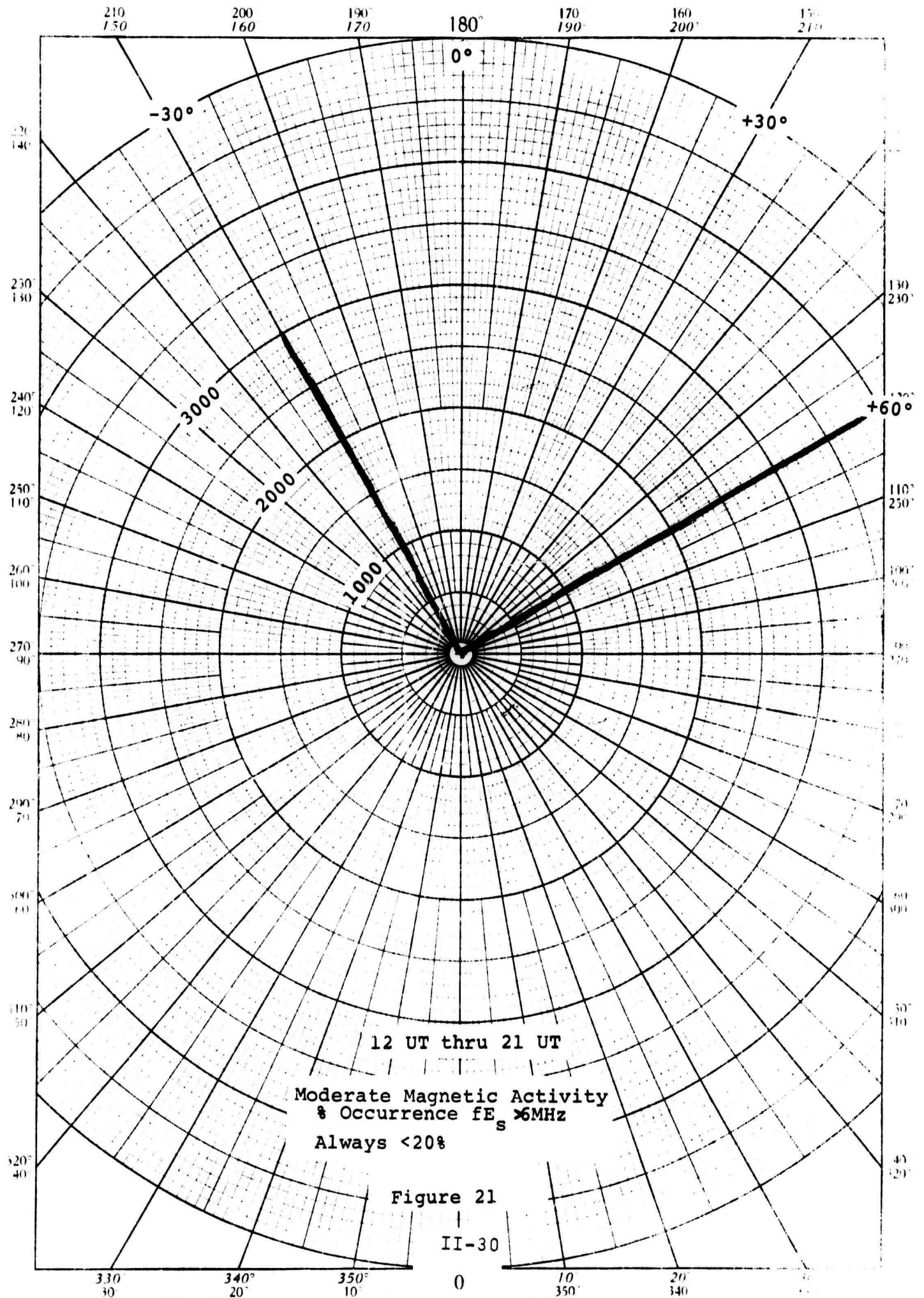


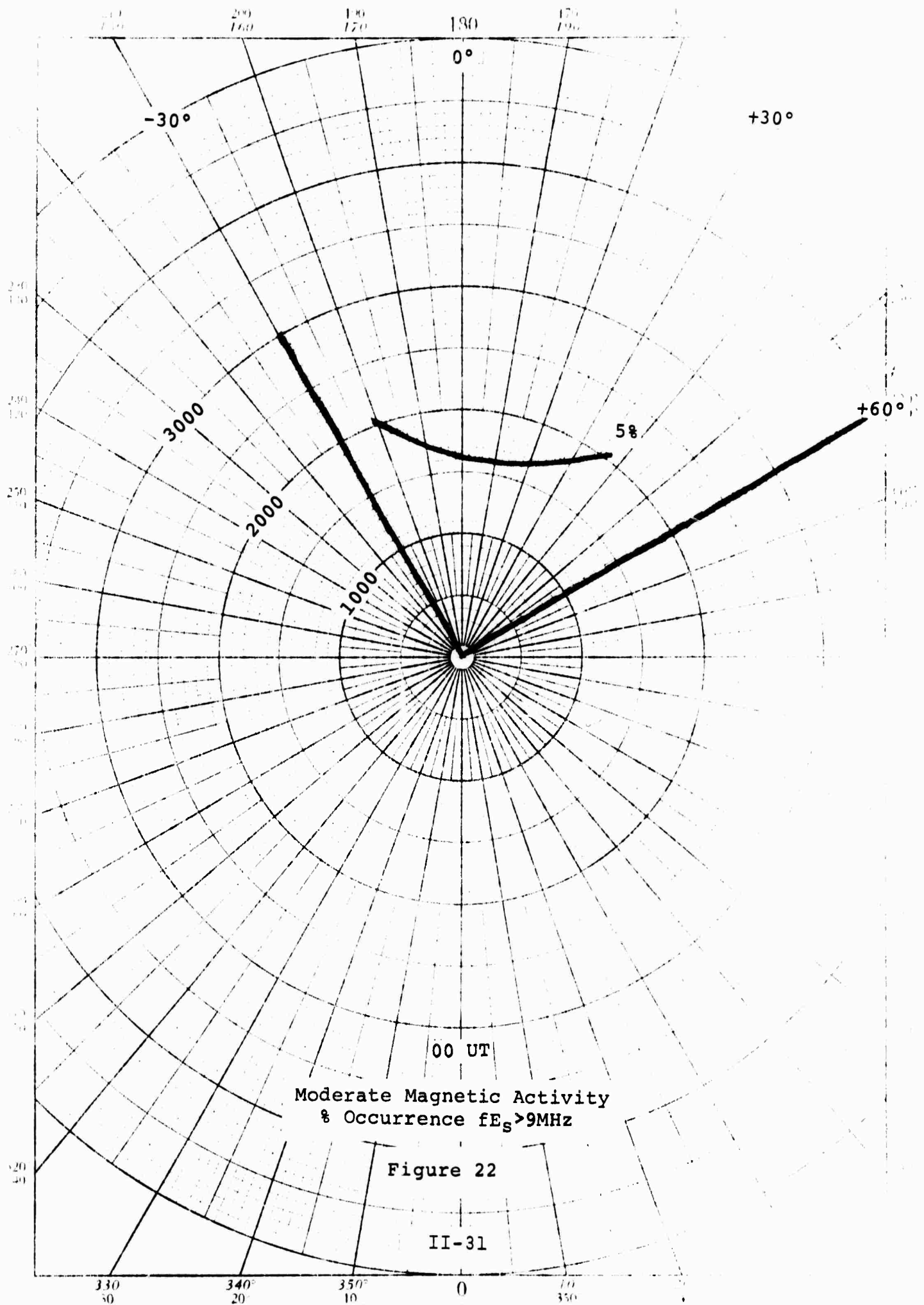


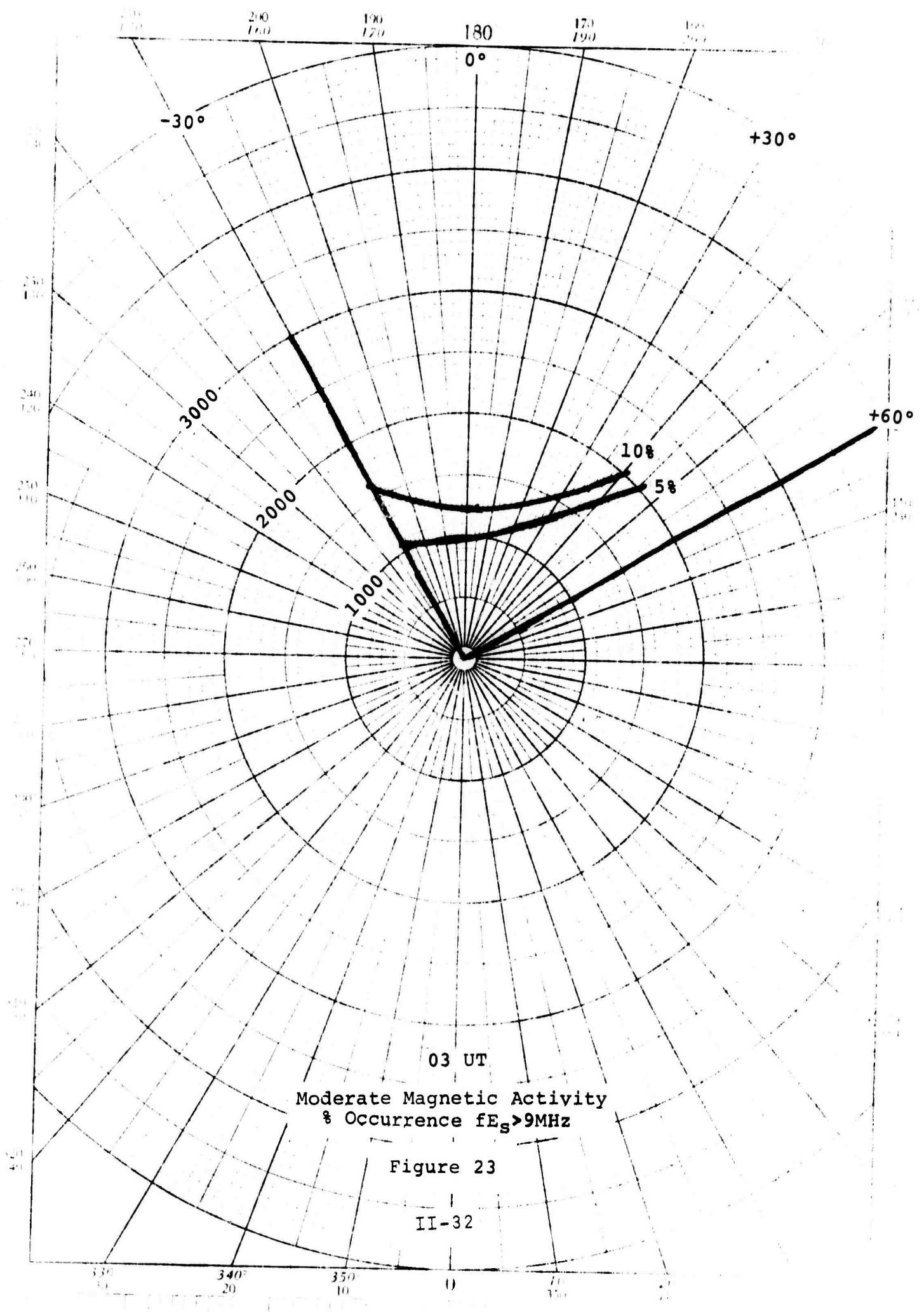


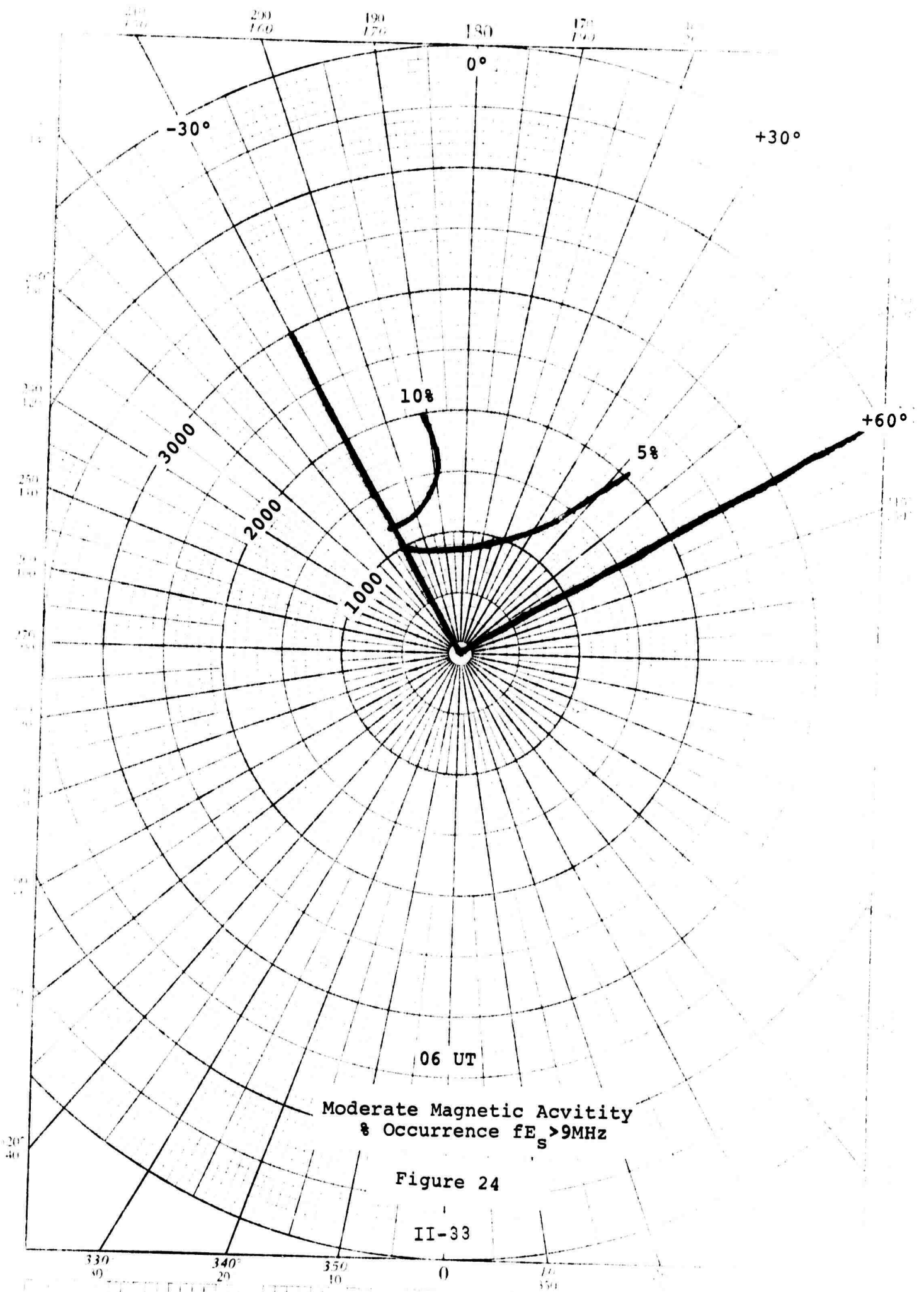


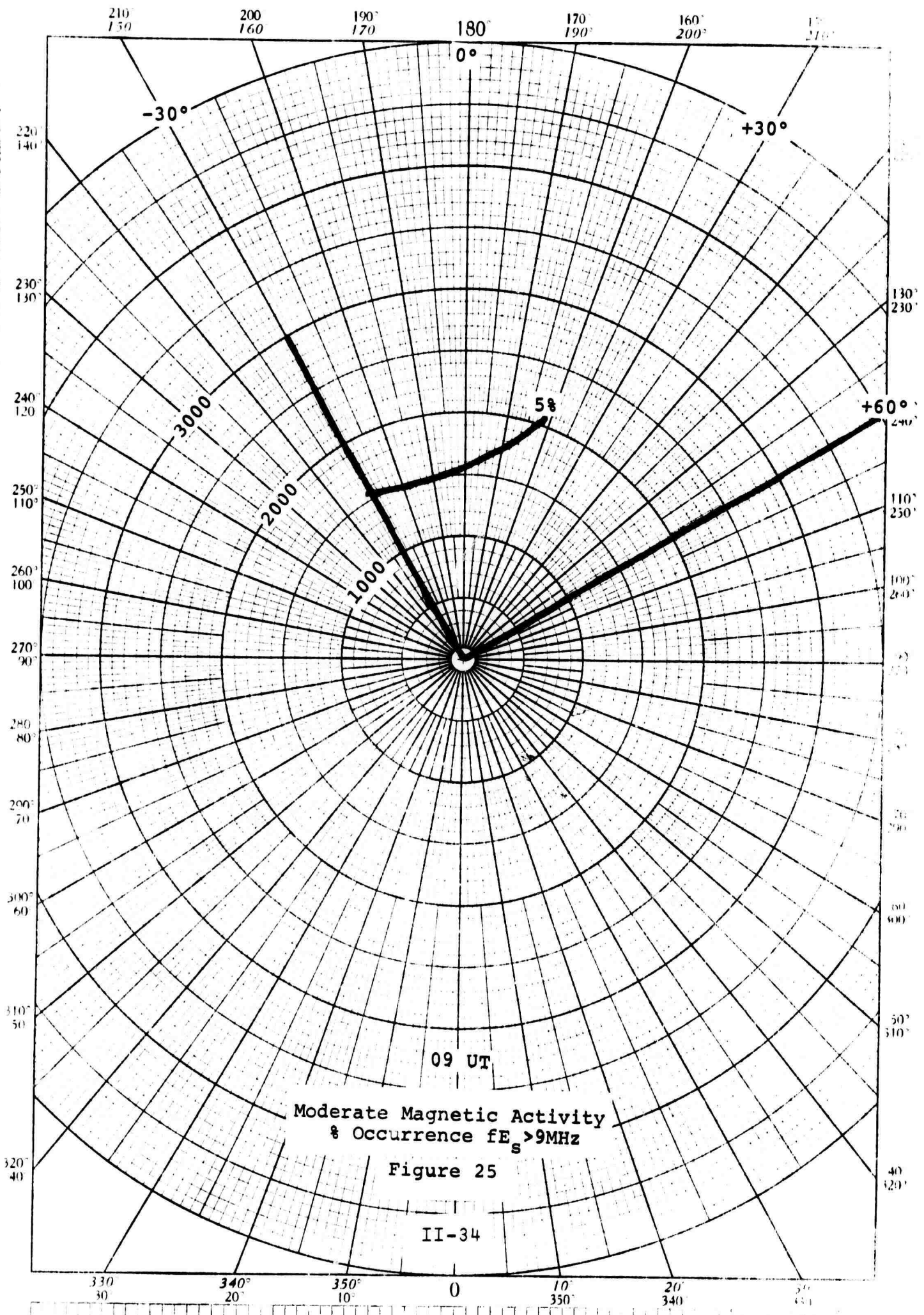












45 4112

POLAR COORDINATE



© KUPFER & BROSCH CO

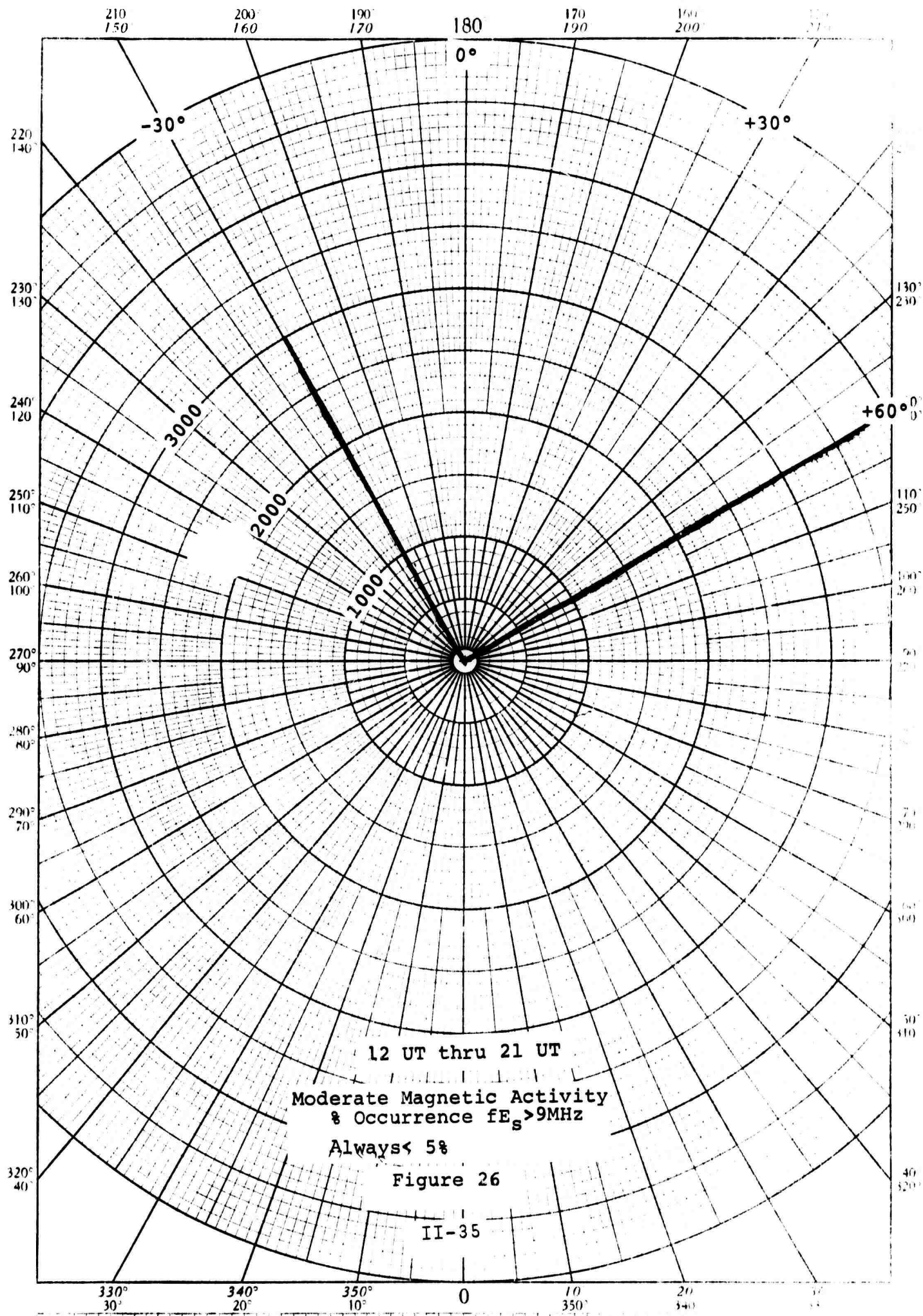
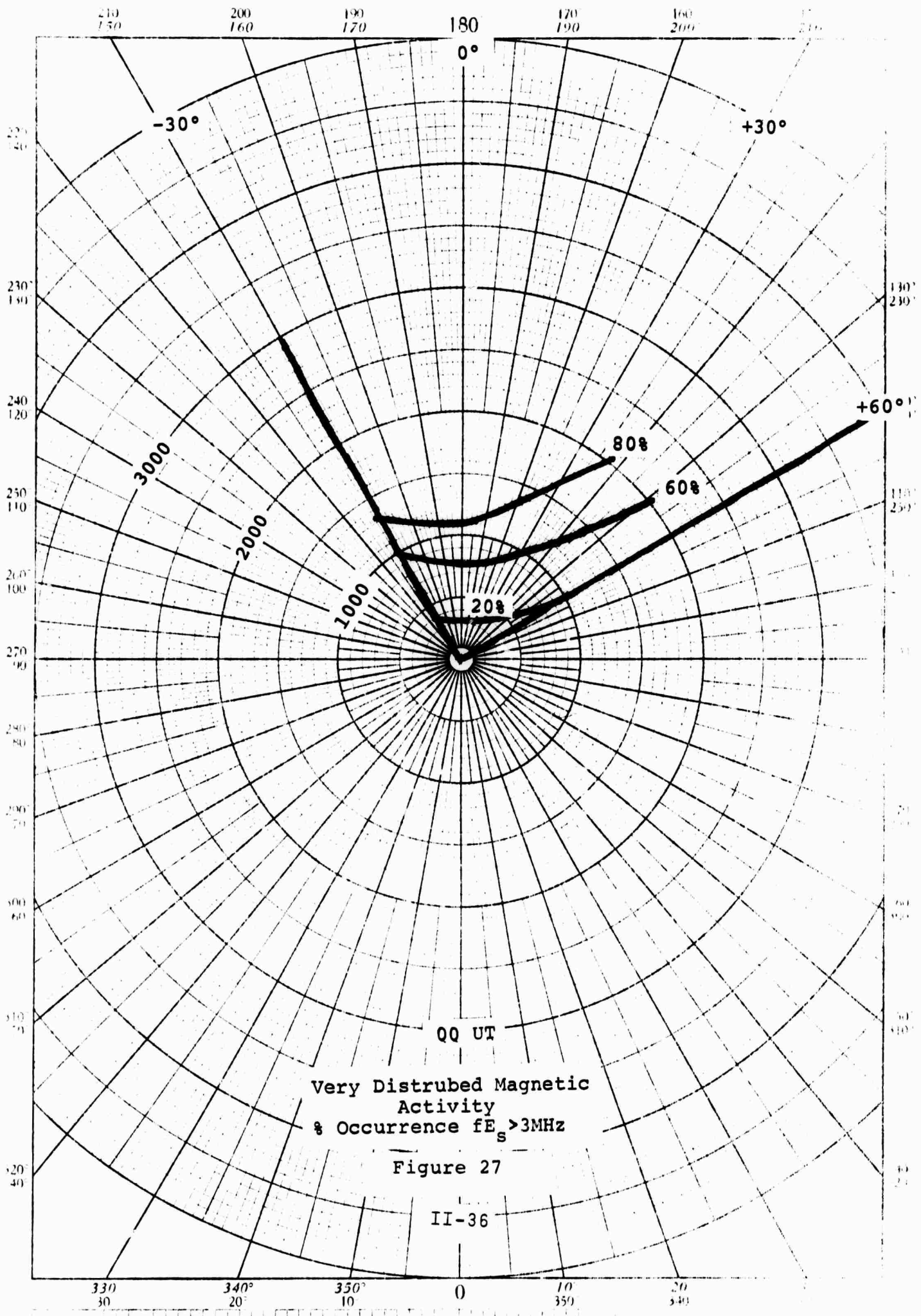
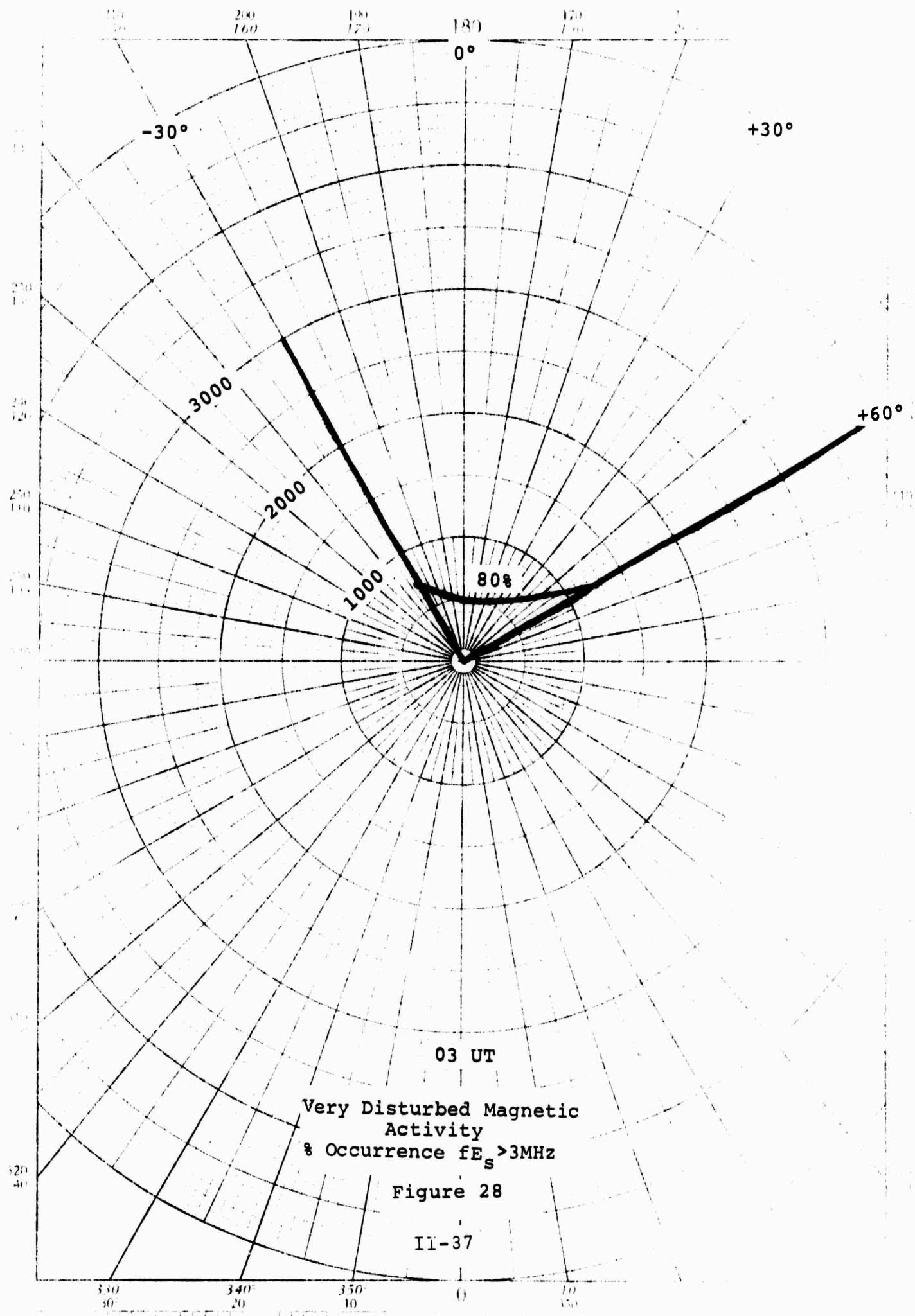
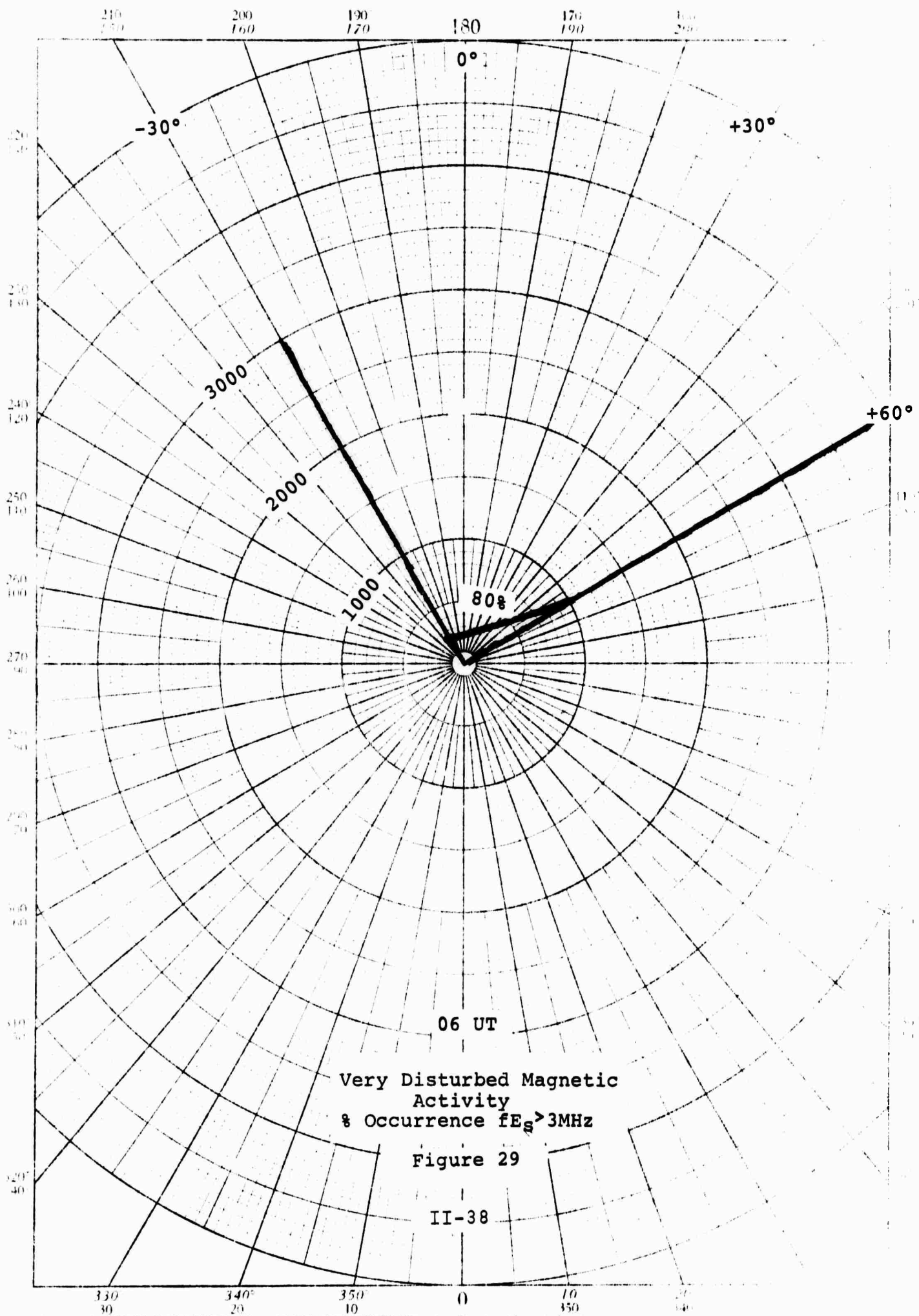


Figure 26

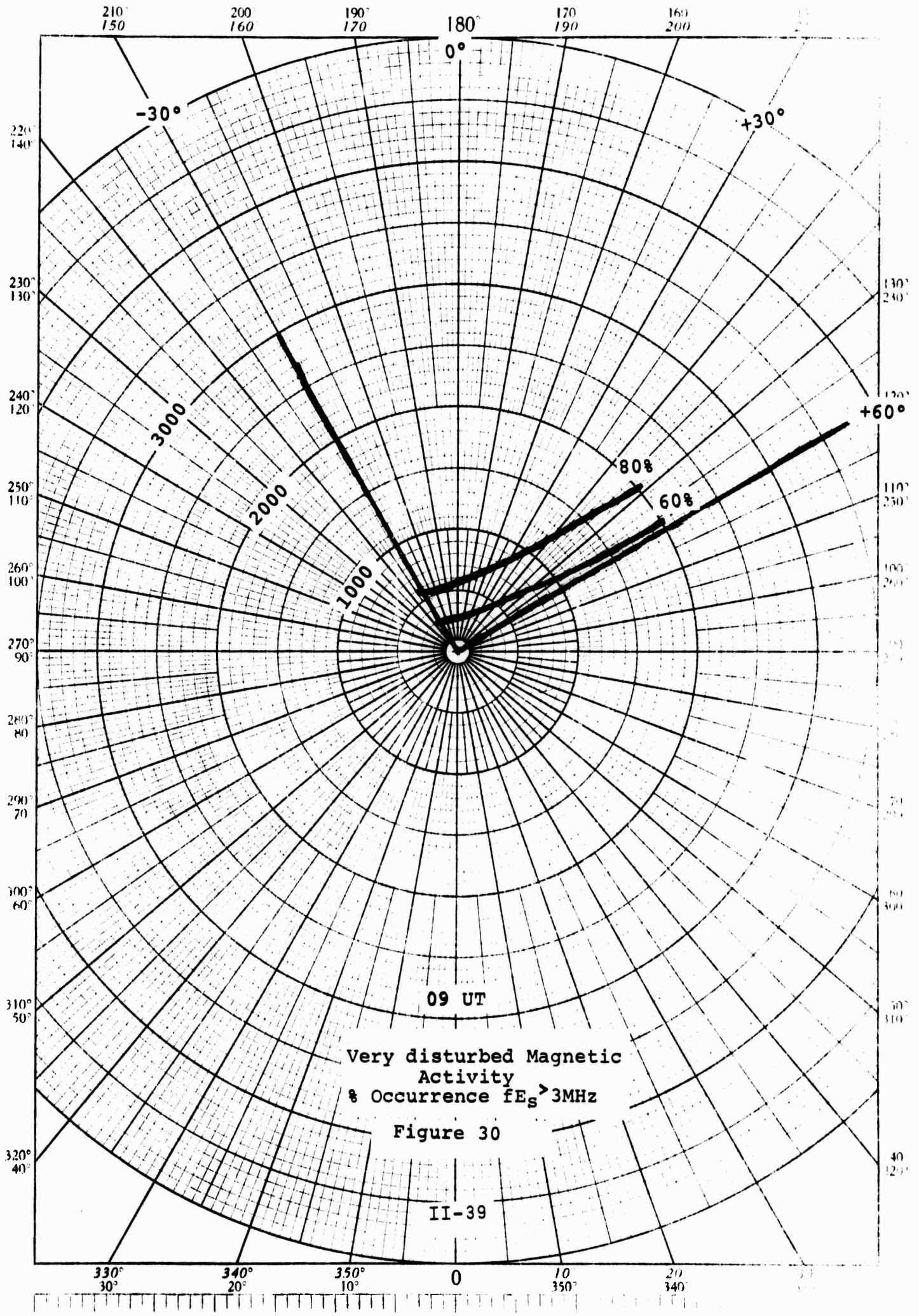
II-35

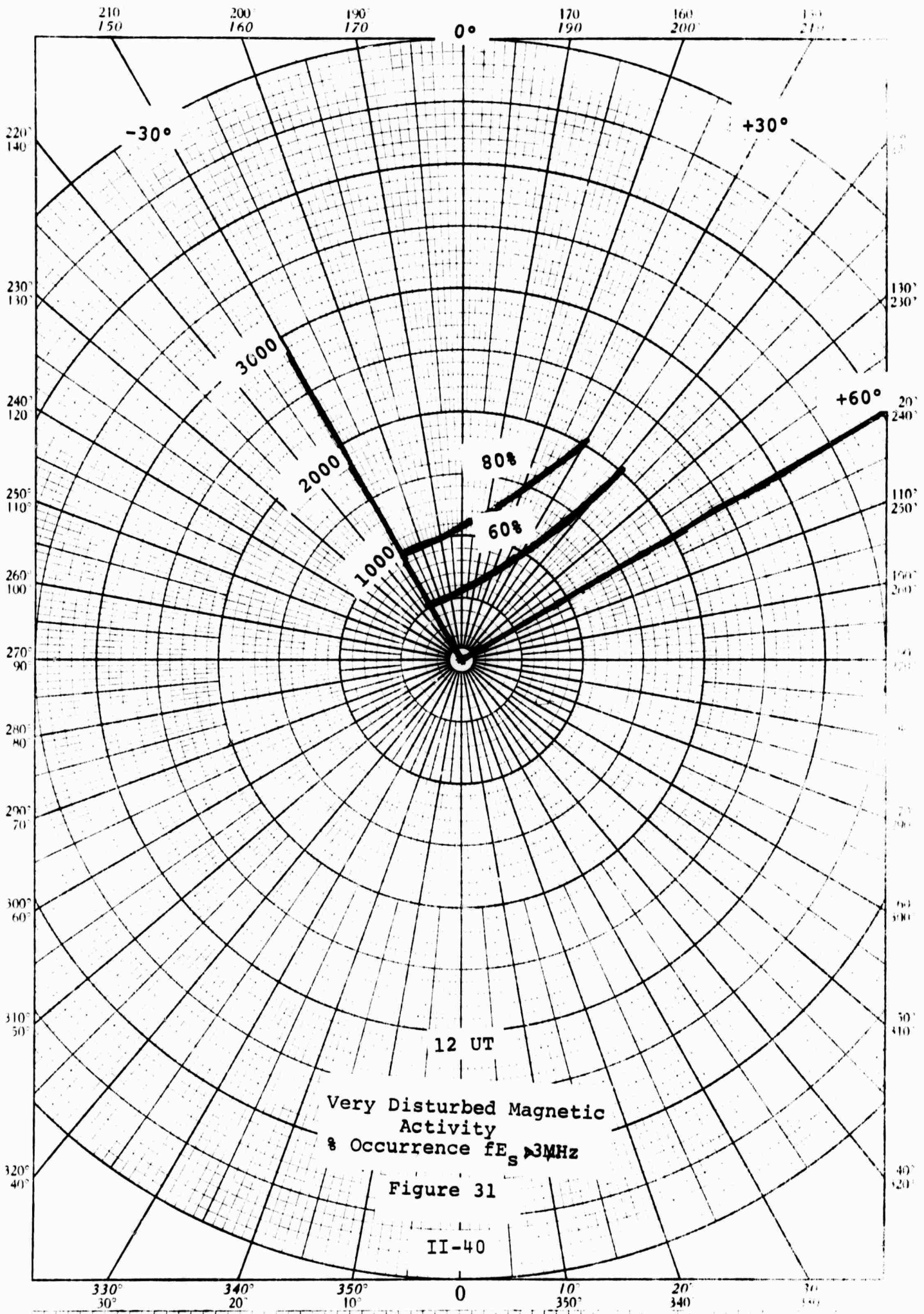


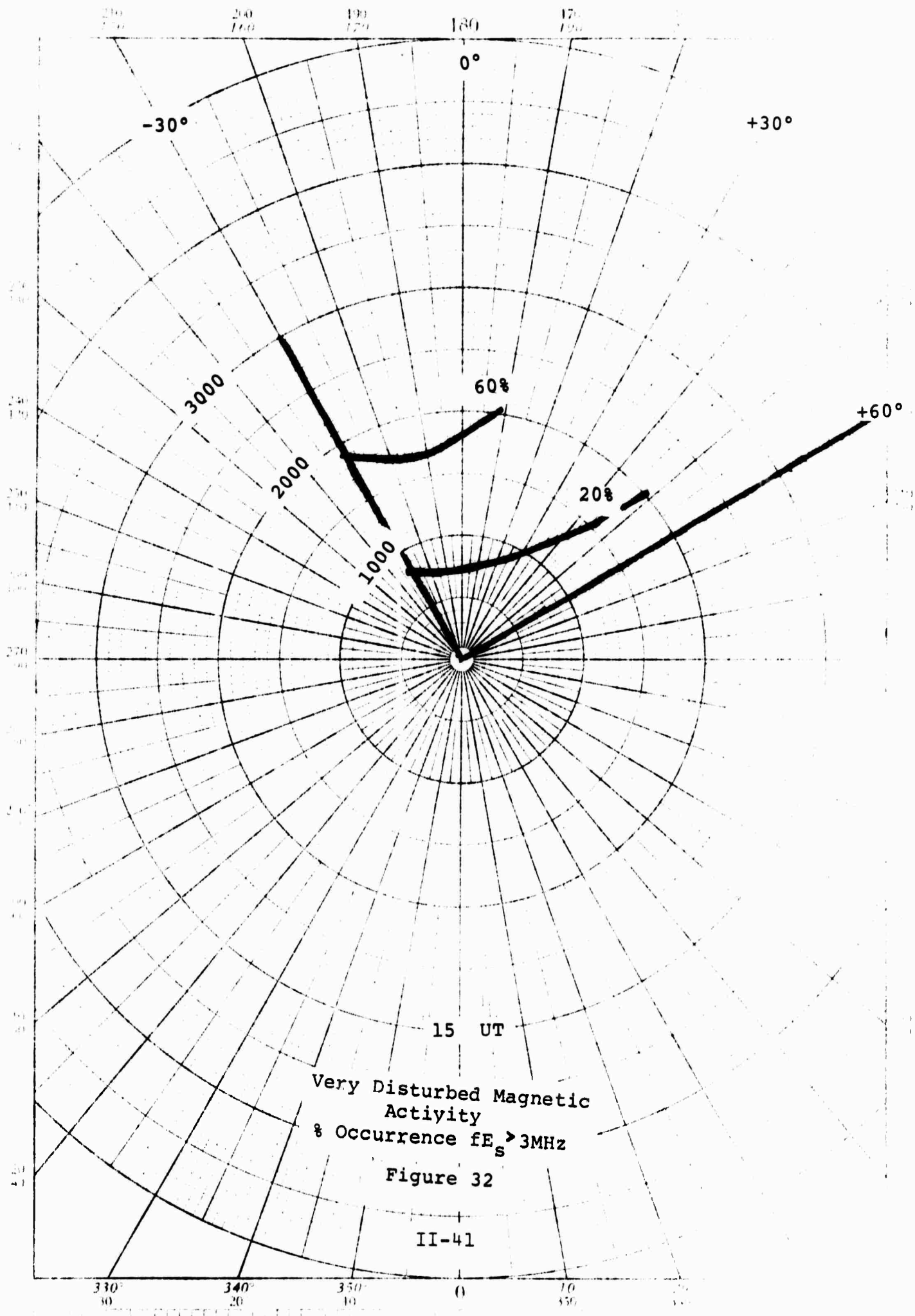


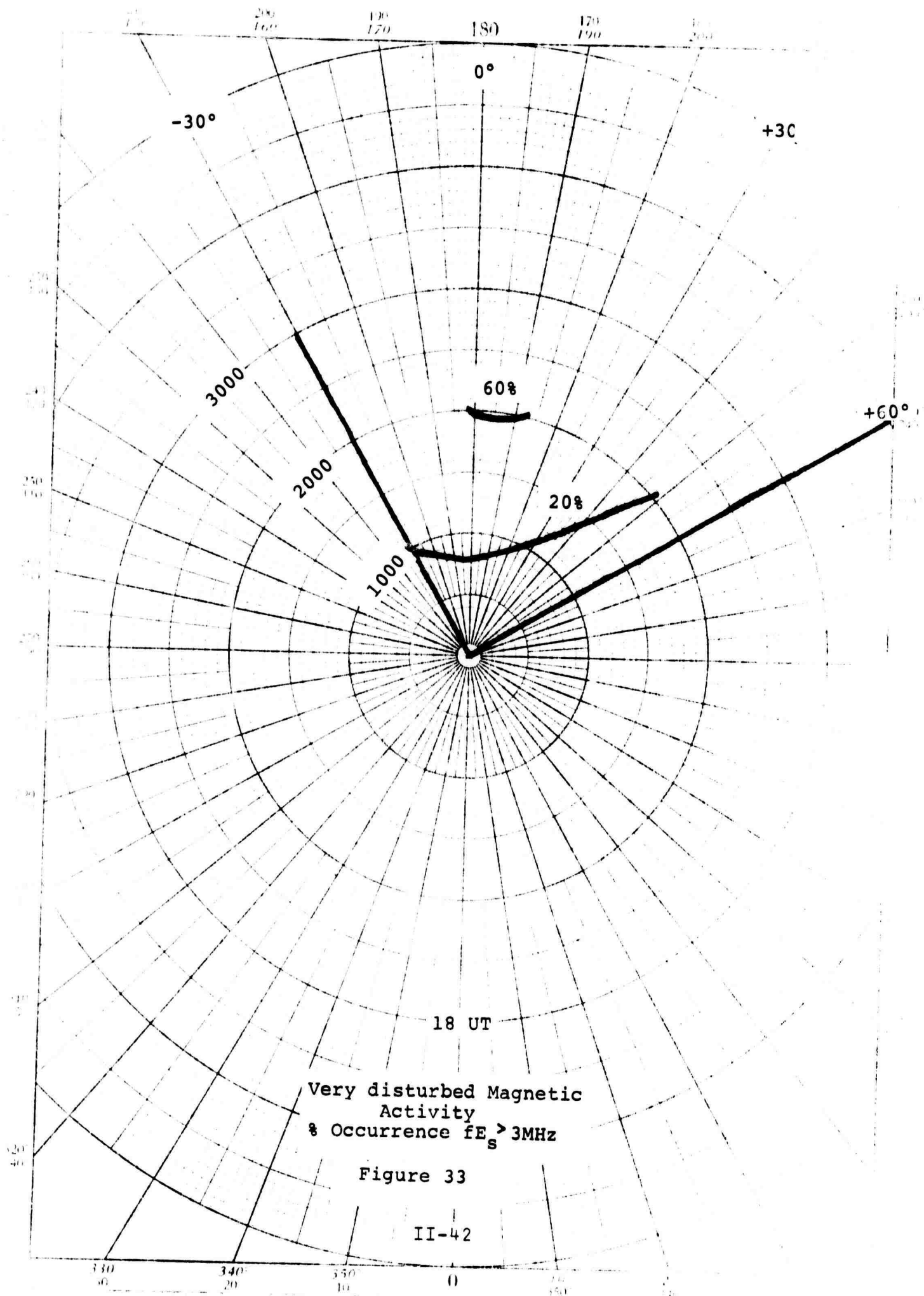


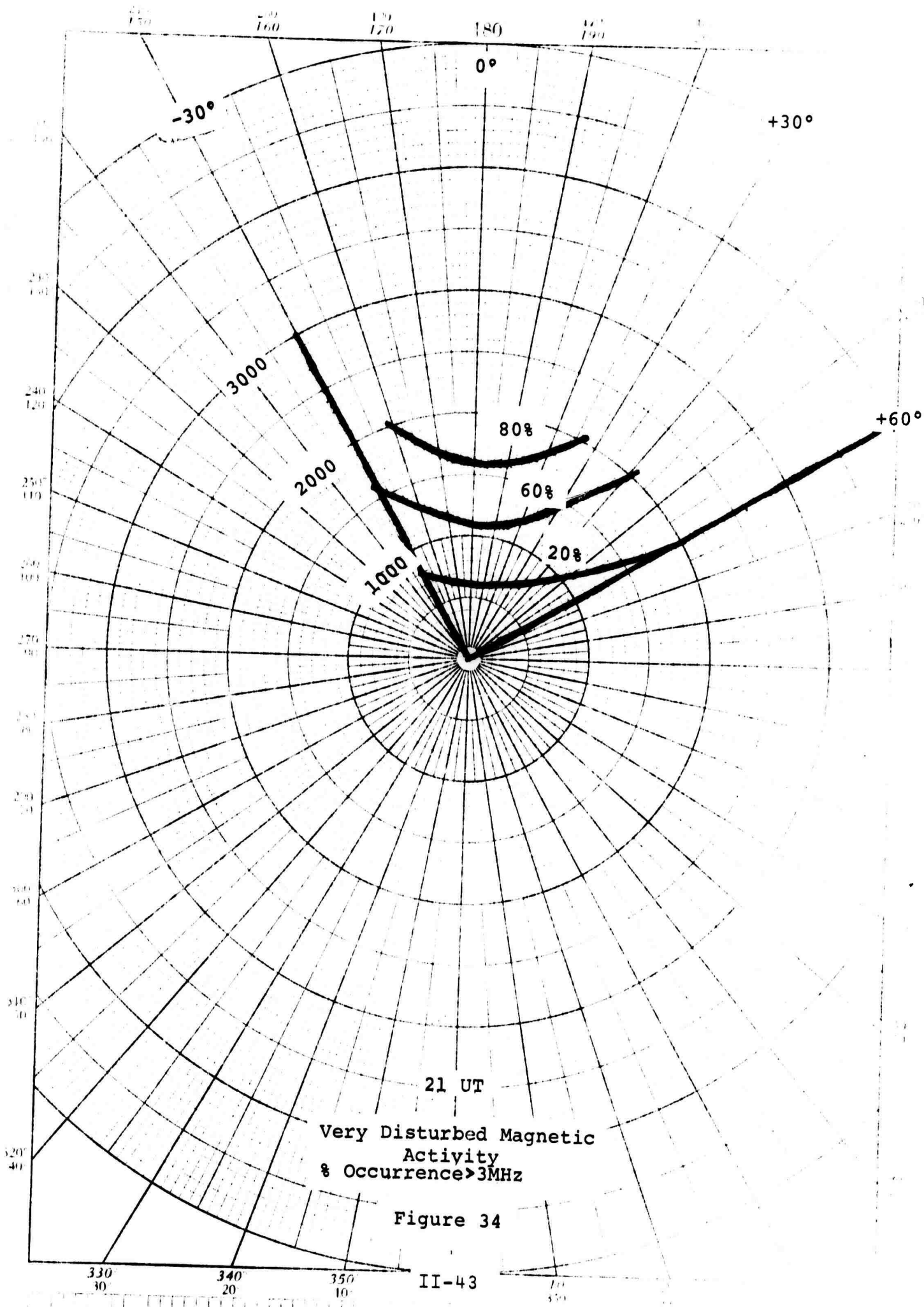
POLAR COORDINATE 45 4412
KEUFFEL & ESSER CO.



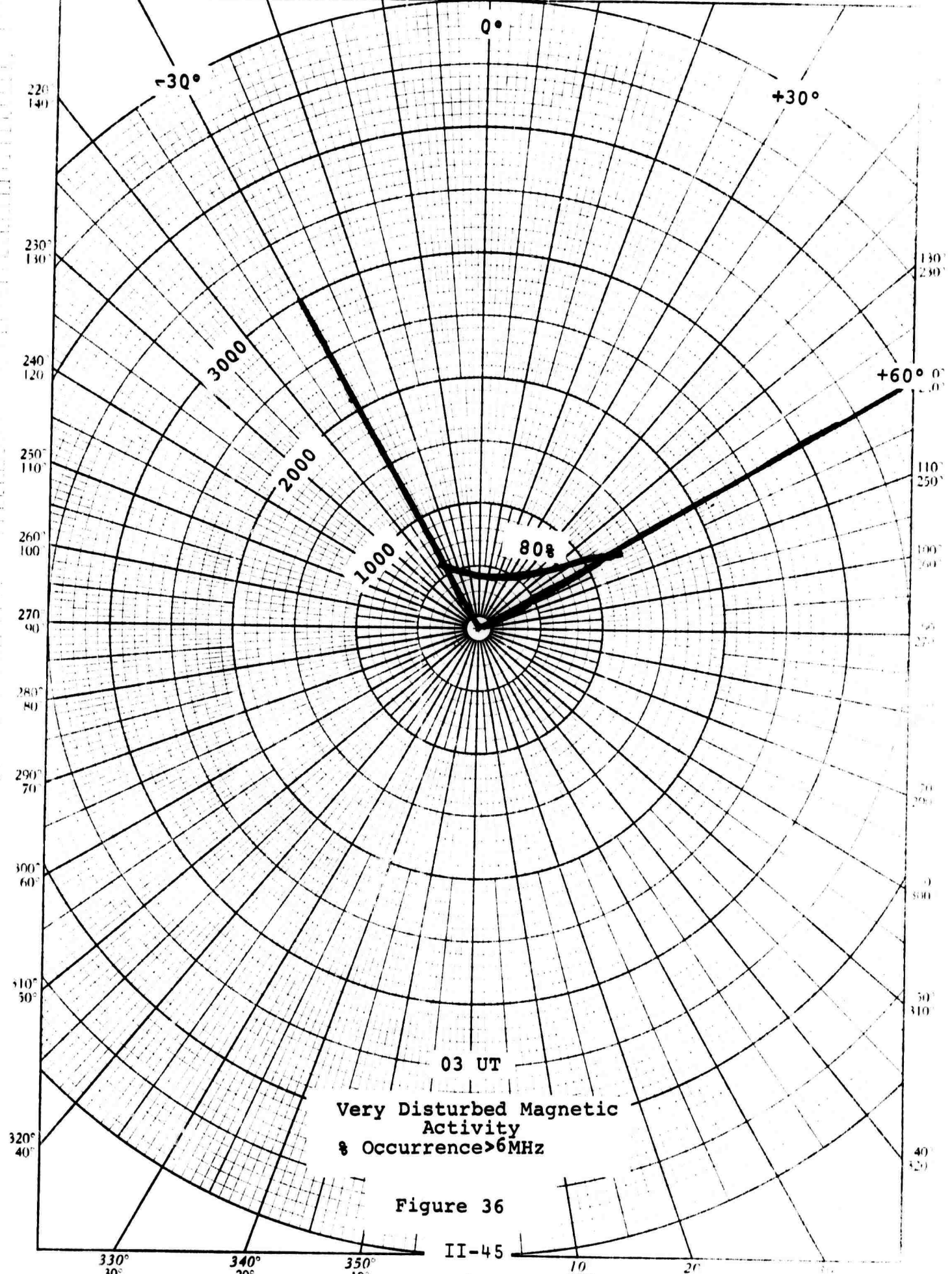








210 200 190 180 170 160



220
140
230
130
240
120
250
110
260
100
270
90
280
80
290
70
300
60
310
50
320
40

230
200
110
250
100
200
70
200
50
310
40
320

-30°

+30°

+60°

0°

3000

2000

1000

80%

03 UT

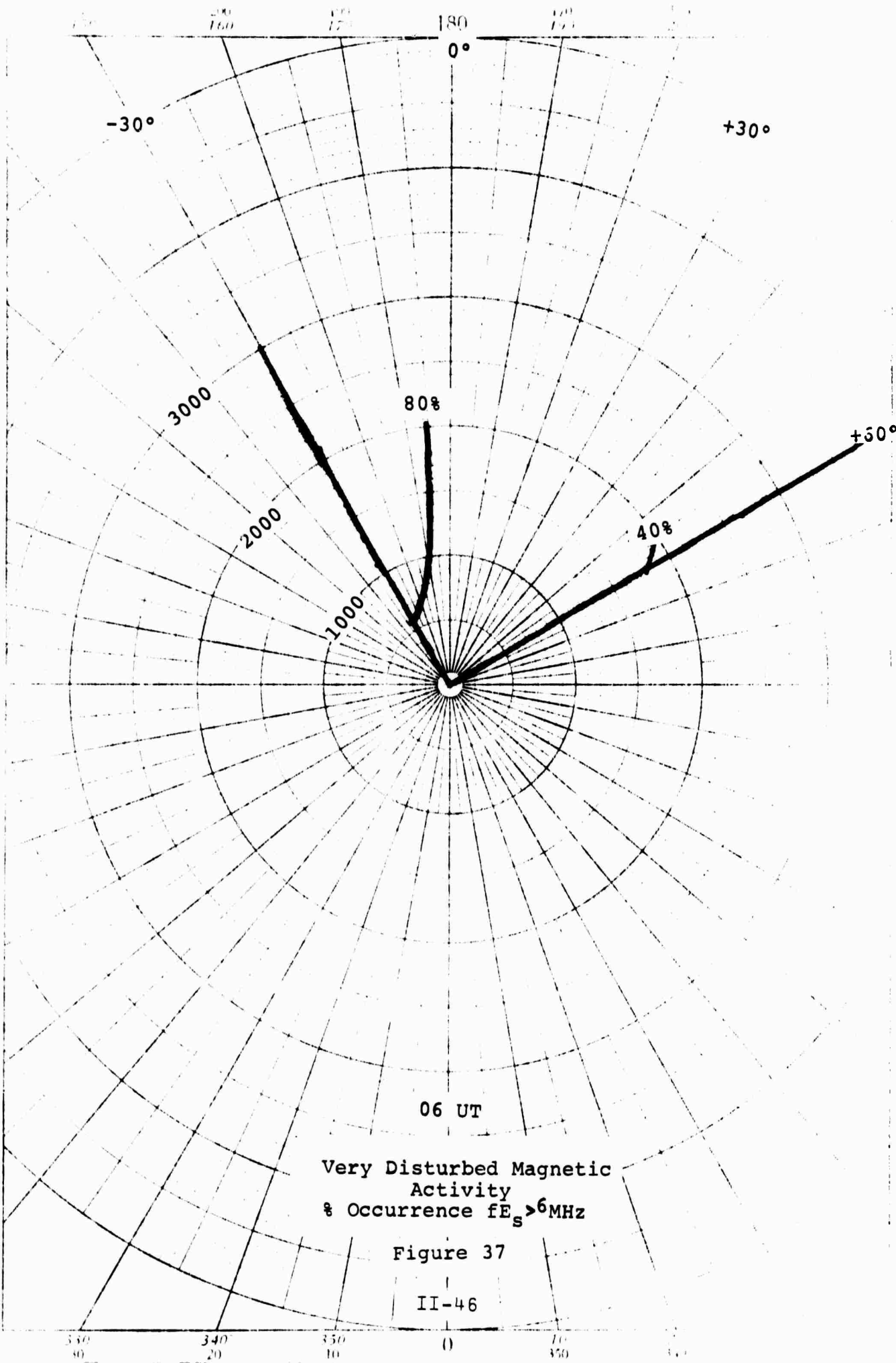
Very Disturbed Magnetic
Activity
& Occurrence > 6MHz

Figure 36

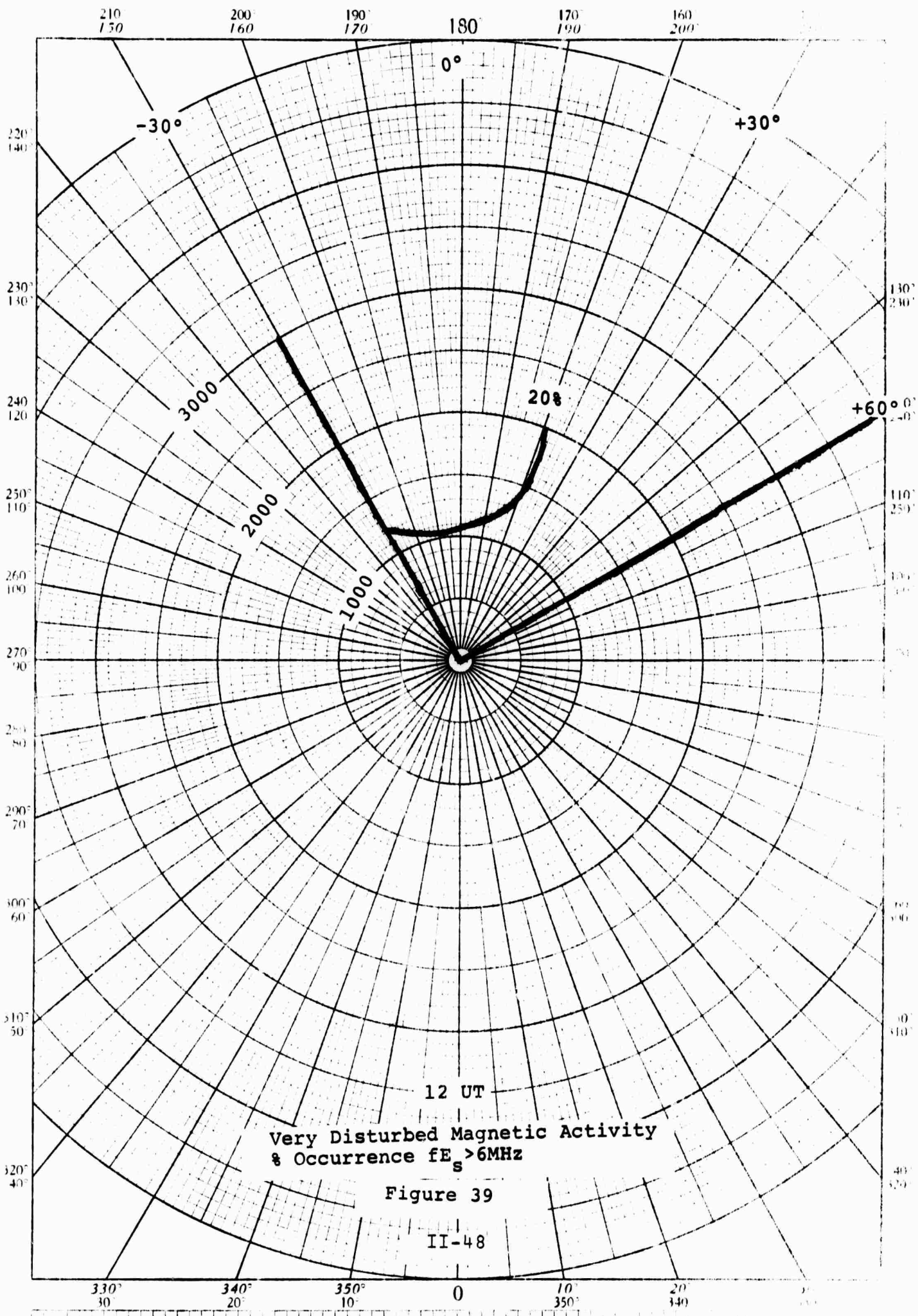
II-45

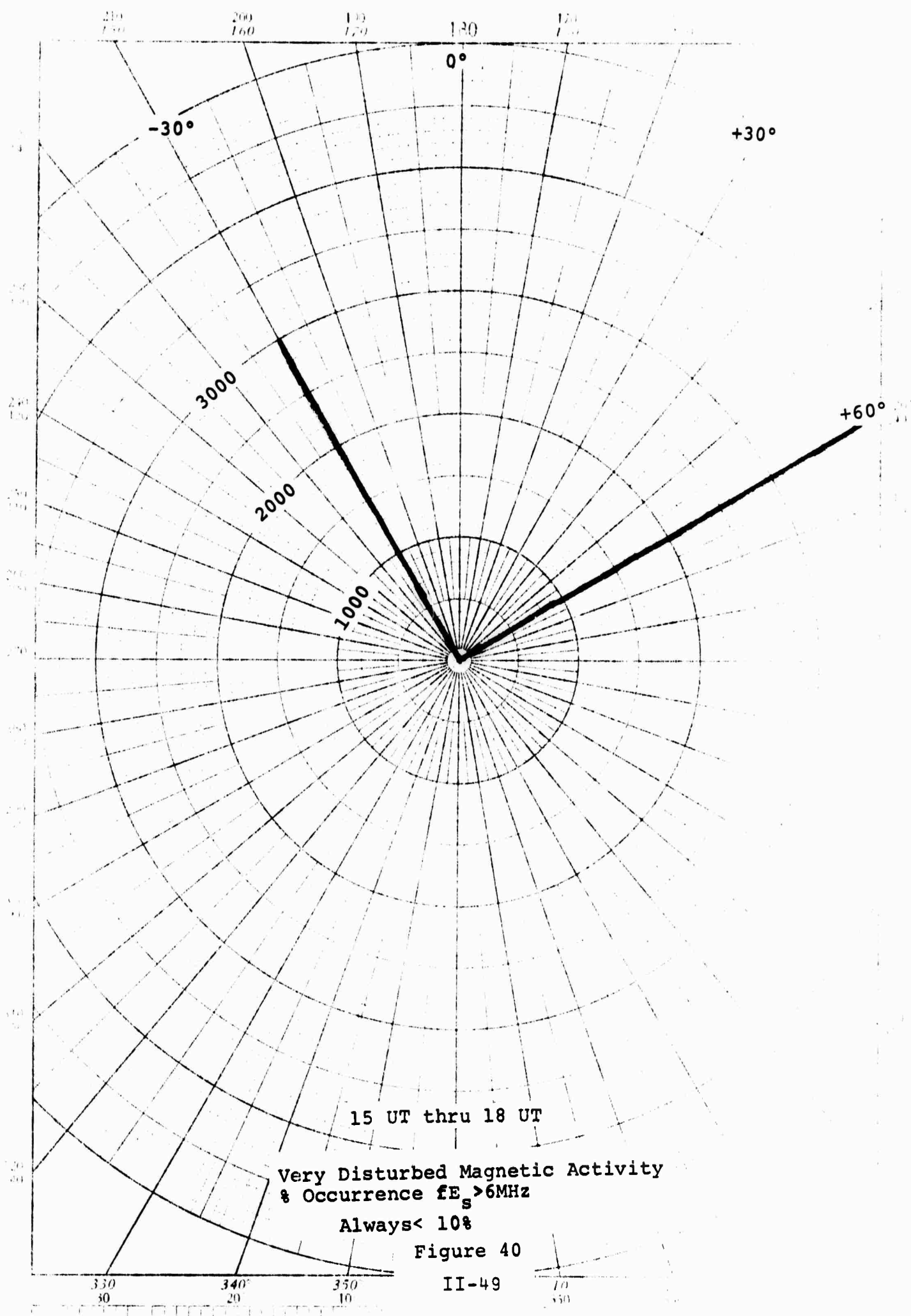
330° 340° 350° 10 20
30° 20° 10° 350° 340°

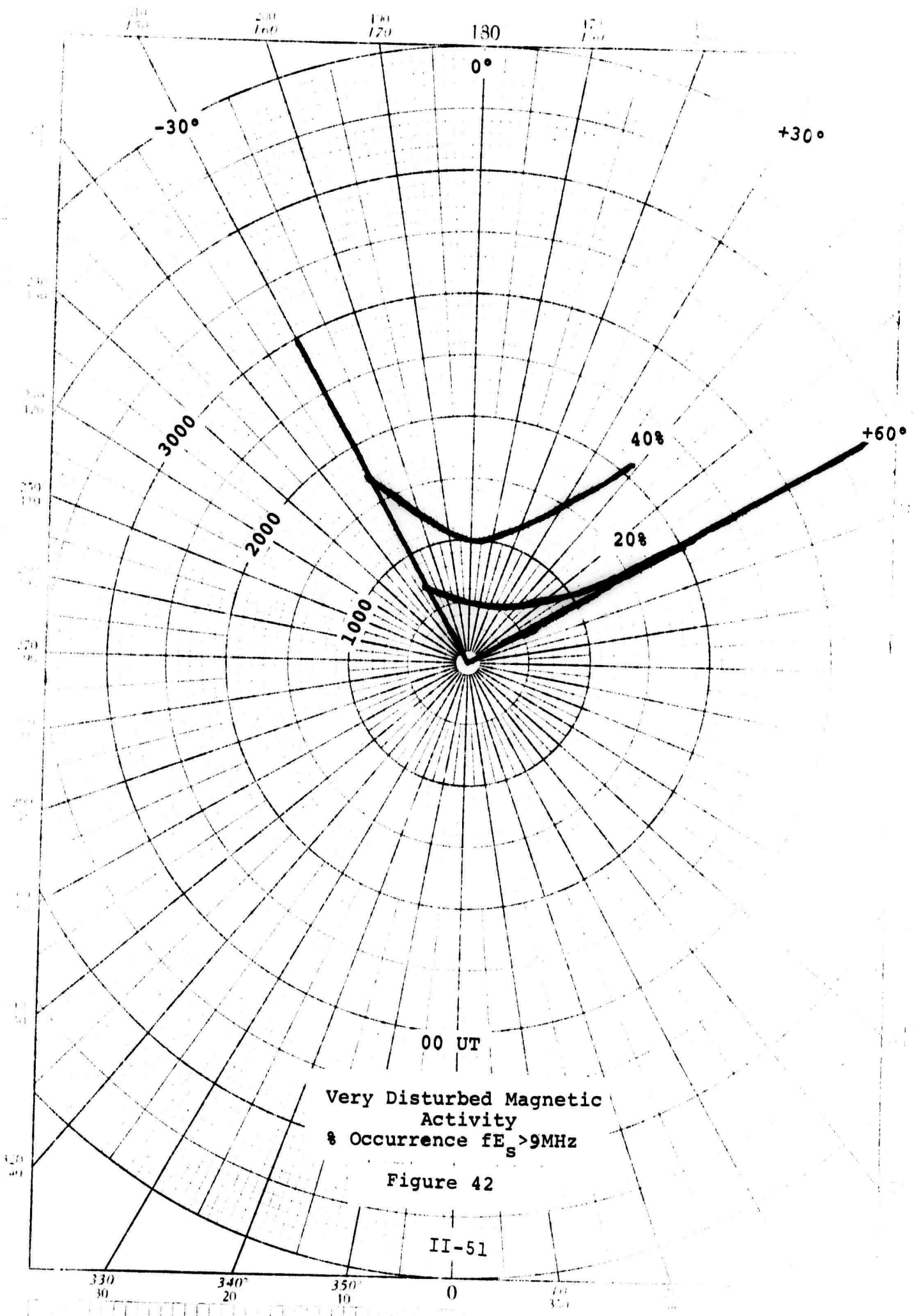
POLAR COORDINATE 46-4412
KEUFFEL & ESSER CO

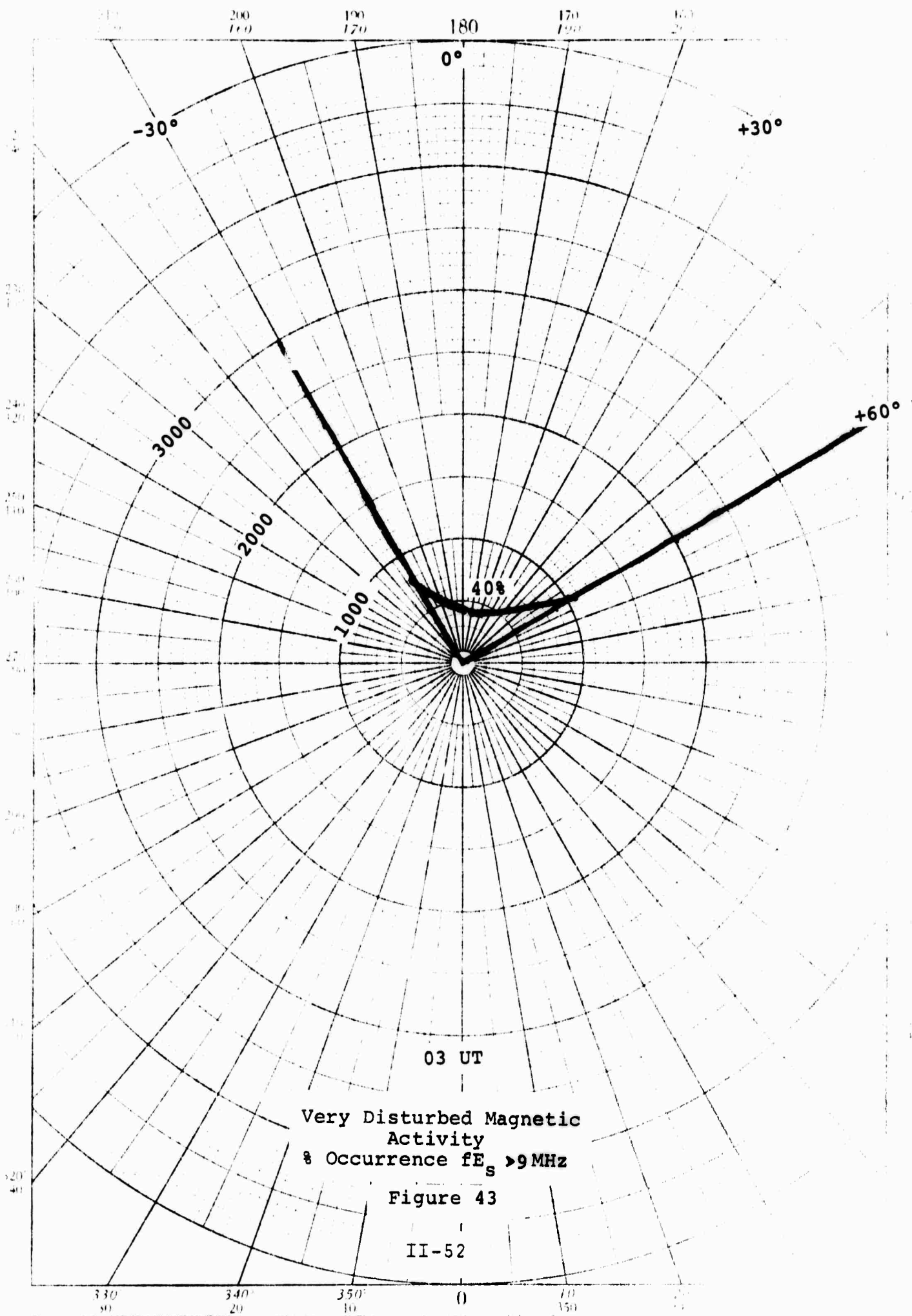


330 340 350 () 350 360

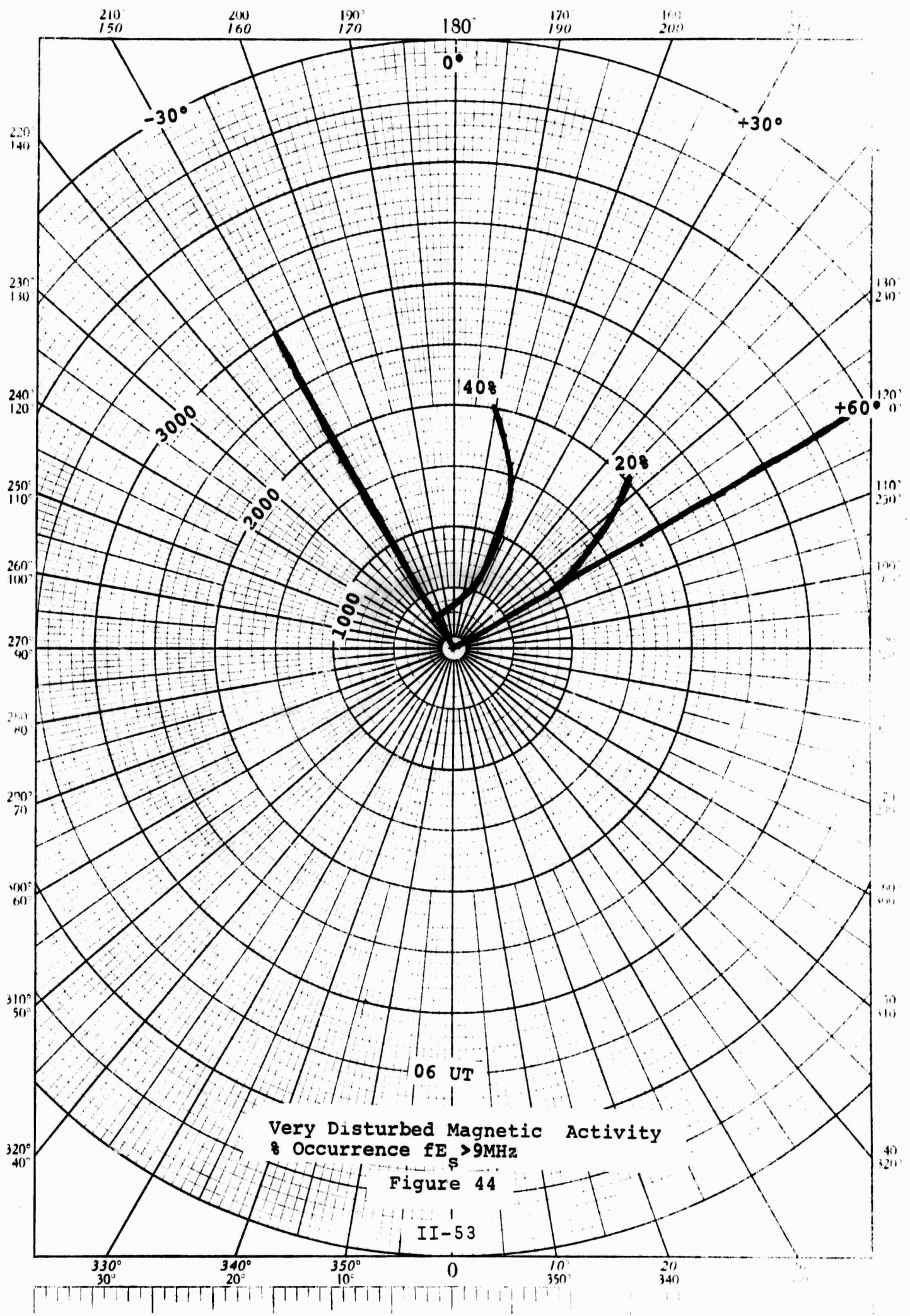


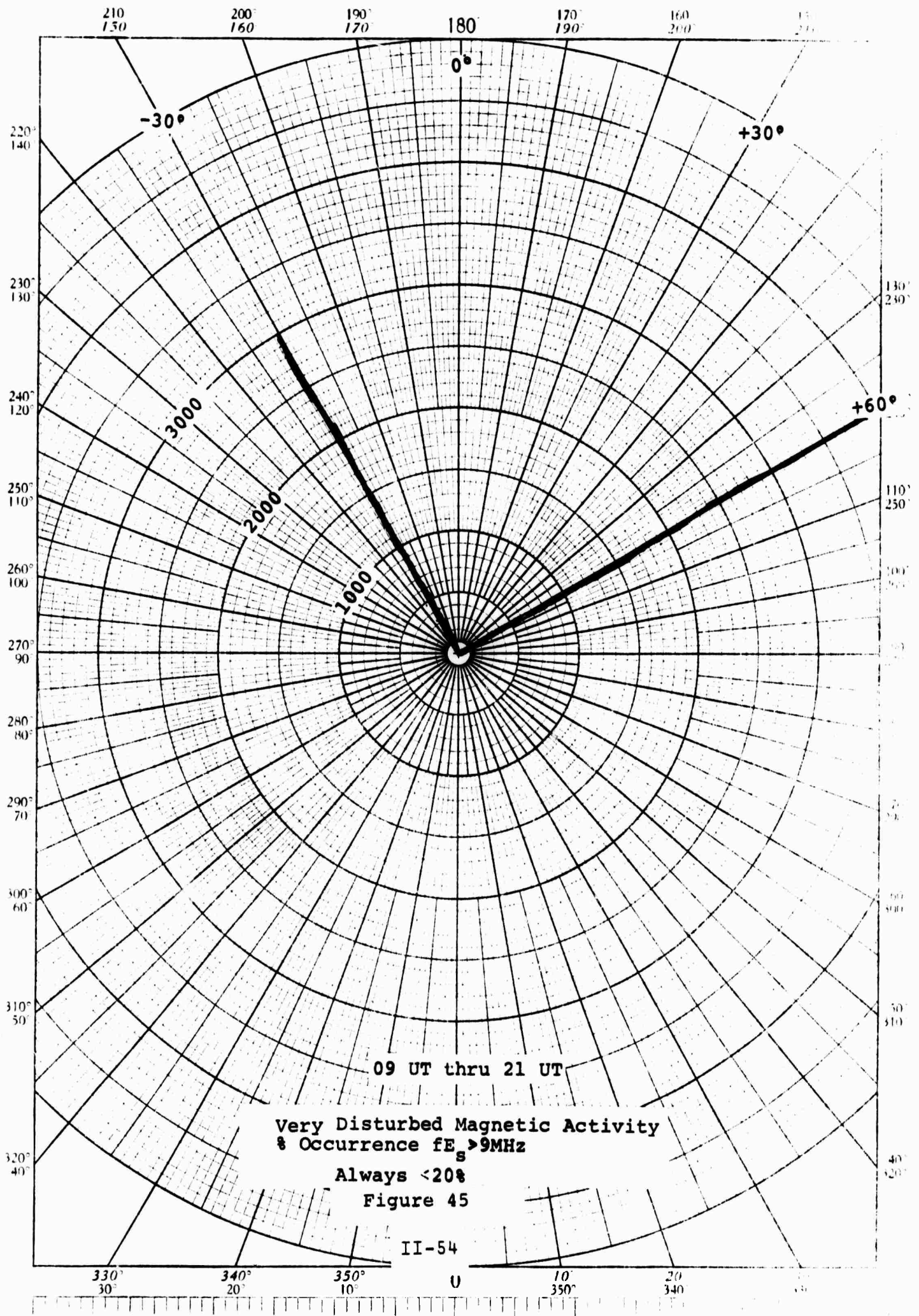






K&E POLAR CO-ORDINATE 46 4412
NEUFFEL & FEUER CO





Analytical Systems CORPORATION 

PART III: AURORAL ABSORPTION

by

R. Vargas-Vila

III-1

1. INTRODUCTION

To describe the auroral absorption of HF radio waves propagating through the polar ionosphere, a series of fan graphs has been generated, showing contours of equal probability of occurrence of various levels of absorption for different frequencies at several times throughout the day. In this report absorption refers to events of auroral absorption only, and precludes such phenomena as sudden cosmic noise absorption and polar cap absorption which have been removed from the data. This absorption is in addition to "normal" D Region nondeviative absorption, however, it is so much stronger than the "normal" absorption, that essentially it is entirely auroral in nature. Auroral absorption is characterized by the irregular variation of the cosmic noise level, it correlates with local magnetic disturbances, visible aurora and particle precipitation of the "drizzle" and splash types as mentioned in Part I of this report.

Originally it was intended to generate these fan graphs of isocontours of probability of auroral absorption manually, however, initial attempts to do so showed that a tremendous amount of labor would have to be expended. It was therefore, deemed necessary to resort to doing the computations by computer. This would have the added advantage that once the data was stored in a computer it would be a simple matter to change the method of computation or the output format for any parameter desirable.

The data used in this report were gathered during a period of approximately two years, from 1959 through 1961. This period is roughly halfway between the maximum and minimum of the solar sunspot cycle, and is therefore, considered to be representative of the period of interest in this study namely, 1971-1972.

2. DATA BASE

The data used in this study consists of maps giving the probability of occurrence of auroral absorption events. Plotting of the maps is done in corrected geomagnetic latitude and corrected geomagnetic time. These maps were generated from observations of chains of riometer stations located along three different longitudes. Specifically the Alaskan data (Hook 1967) shows the percentage time occurrence of auroral absorption of 3 dB or greater, while the Canadian and Norwegian data (Hartz 1963) were used to generate time percentage of occurrence maps of 1 dB or more and 0.425 dB or more auroral absorption respectively. These maps are for vertical absorption at 30 MHz (the Norwegian data was collected at 27.6 MHz and corrected to 30 MHz by $1/f^2$) and are shown in figures 1, 2 and 3. Digitization of these maps was made to enable computer usage. This was accomplished in the following manner, referring to figure 1 for example, radials are chosen at intervals of spacing determined by whether a given probability contour is constant for a given geomagnetic latitude. Therefore, the spacing of radials is not equal but is further apart if the probability contour changes slowly for a given latitude. For example, many more radials are needed in the interval between 18 corrected geomagnetic time (CGT) and 20 CGT than in the interval from 05 CGT to 07 CGT. Enough radials, along which digitization is made, are chosen to preserve the fine detail of the maps. Points between radials are determined by linear interpolation. The maps were extended poleward on a linear scale from the contour of lowest probability to a value of zero at the pole. The data maps were not extended to lower latitudes

From the maps described above a set of cumulative probability distributions was generated showing the percentage of time that the occurrence of auroral absorption exceeded a given level of vertical incidence absorption at 30 MHz. A probability distribution was made for each coordinate of corrected geomagnetic latitude and time of interest, of which Figure 4 is an example. Generation of these cumulative distribution curves was performed in the following manner. For each specified corrected geomagnetic latitude and time, the computer selects one value of probability from each of the probability maps (Figure 1, 2, and 3). Interpolation between the time percentage of occurrence values is made on a logarithmic scale. Interpolation between levels of absorption is made on a linear scale. The result is the tail end of a cumulative probability distribution where the end points are defined by the points extracted from figures 1 and 3. Generally, the cumulative probability runs from maybe one to about 20%. These probability distributions were only used between end points, no attempt was made to extrapolate to mean or median values of absorption. No seasonal nor solar cycle variation was assumed.

All riometers used in the collection of this data were pointing towards the celestial pole. This was done so that the riometers would be observing the same source all day long, and hence avoid any diurnal variation in the measurements. For this reason, it is necessary to multiply every data point by the sine of the geographic latitude in order to transform the data maps into equivalent vertical incidence absorption maps.

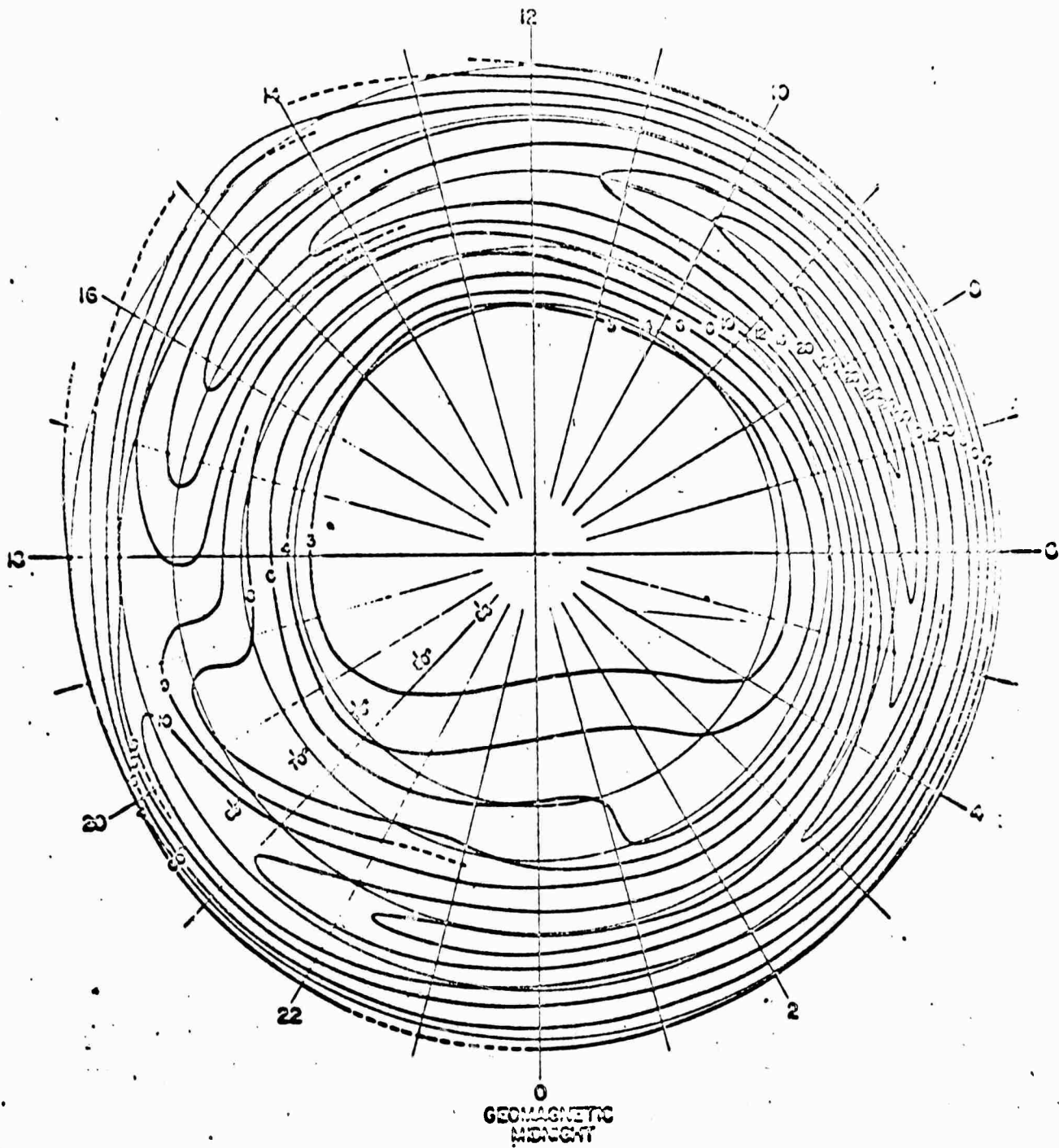


FIGURE 1 CONTOUR PLOT OF PROBABILITY OF OCCURRENCE OF AURORAL ABSORPTION $> 0.42\text{dB}$ IN CORRECTED GEOMAGNETIC COORDINATES.

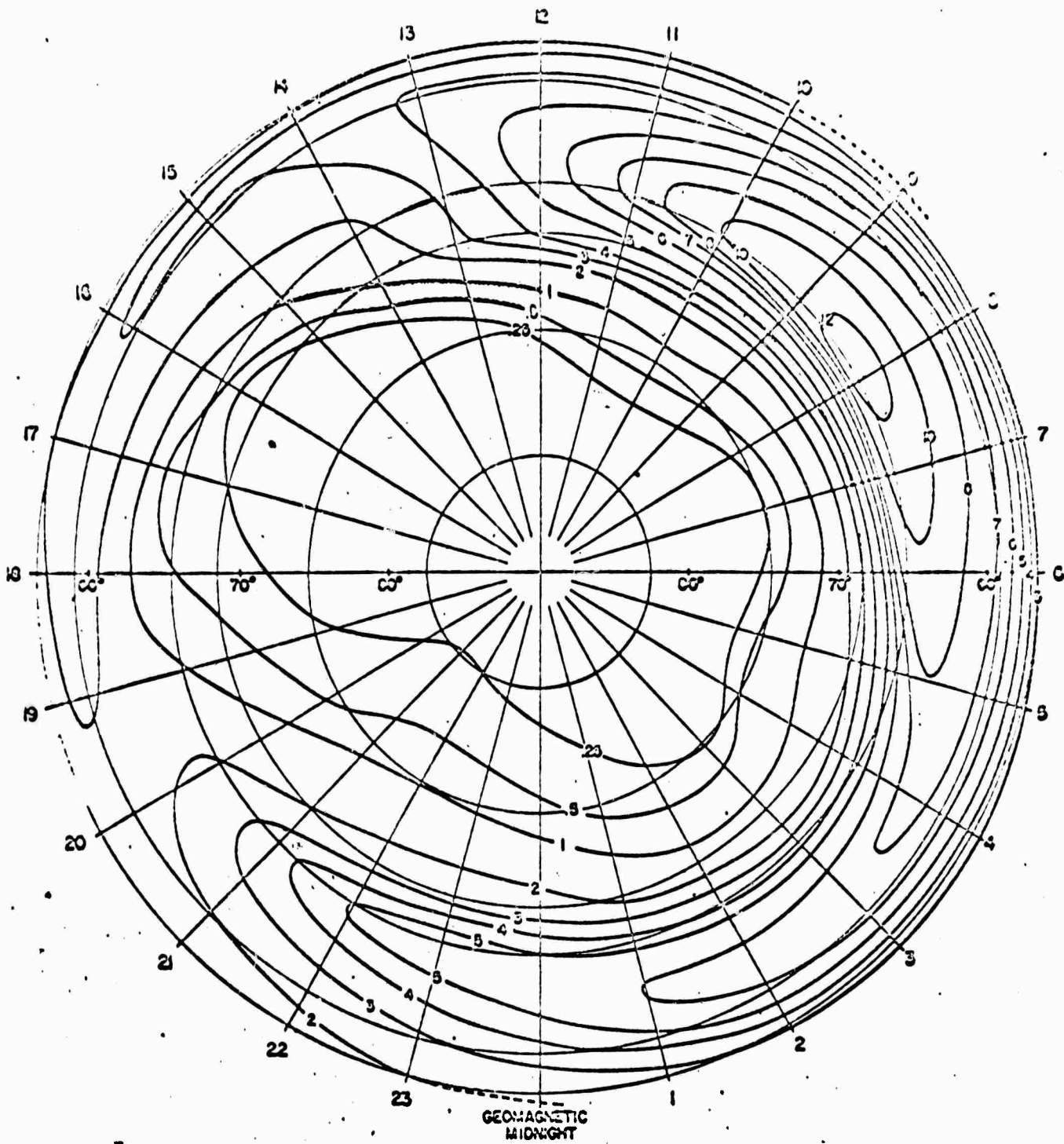


FIGURE 2 CONTOUR PLOT OF PROBABILITY OF OCCURRENCE OF AURORAL ABSORPTION $> 1.0\text{dB}$ IN CORRECTED GEOMAGNETIC COORDINATES.

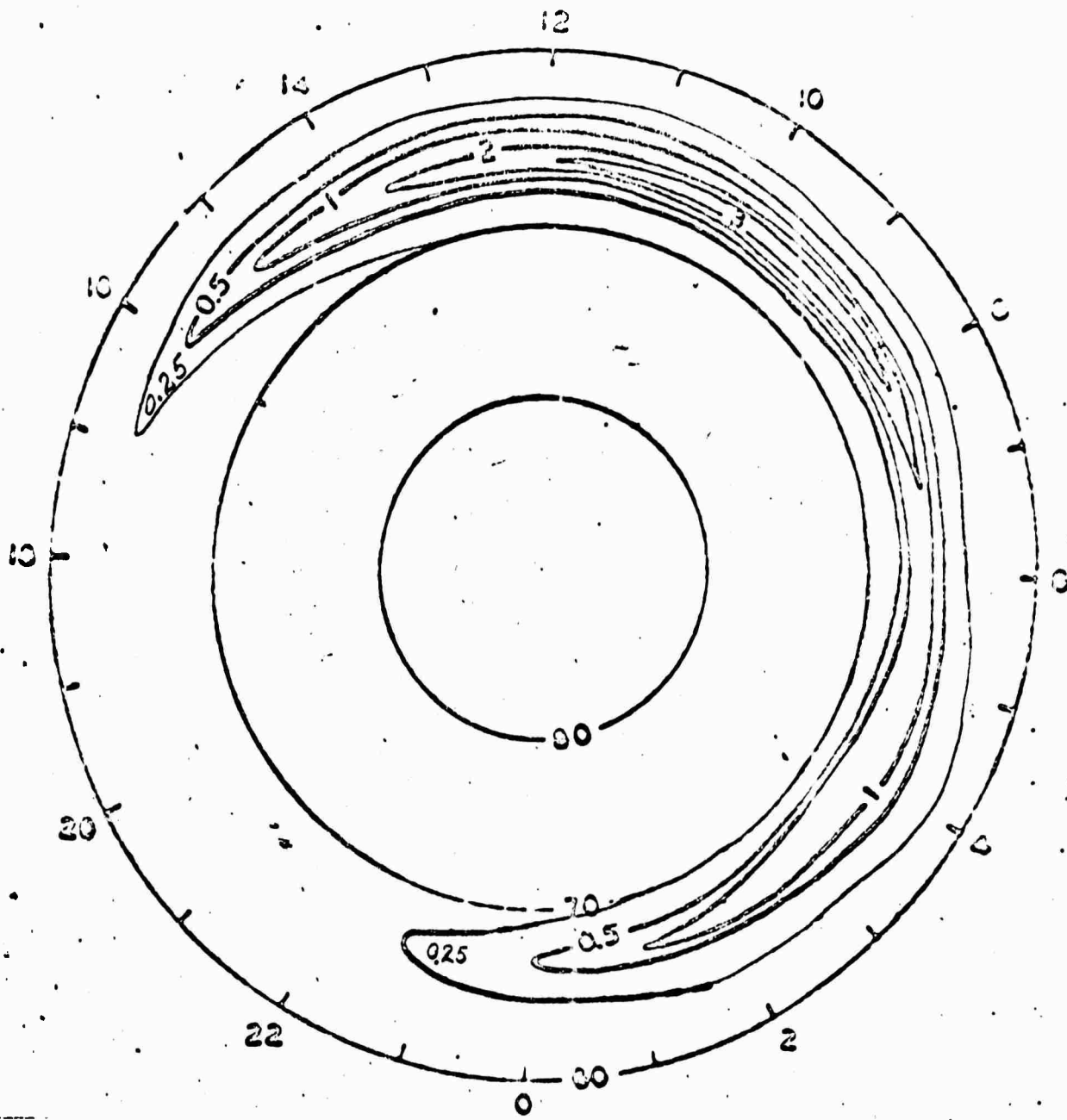


FIGURE 3 CONTOUR PLOT OF PROBABILITY OF OCCURRENCE OF AURORAL ABSORPTION $\geq 3.0\text{dB}$ IN CORRECTED GEOMAGNETIC COORDINATES.

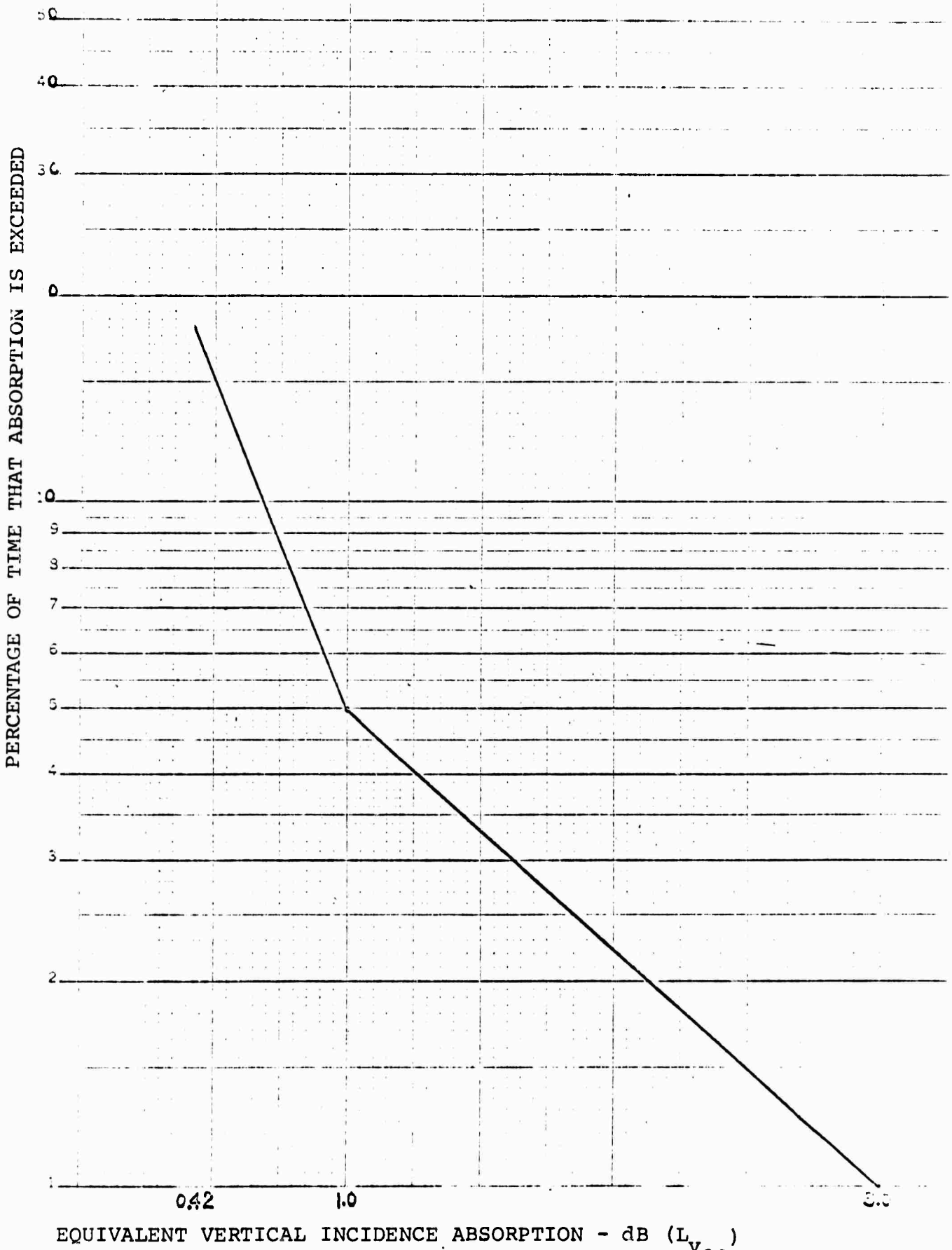


Fig. 4 CUMULATIVE PROBABILITY DISTRIBUTION SHOWING PERCENTAGE OF TIME THAT A GIVEN LEVEL OF ABSORPTION IS EQUALED OR EXCEEDED.

3. METHOD

A "fan" graph such as is shown in Figure 5, is made, the apex of which is located at the transmitter site. Transmission to a given point in that fan graph defines a range and azimuth for the terminal point of the ray path. By assuming a single hop F layer propagation mode over a flat earth with the reflection point at a height of 300 km, two points, A and B are defined, see Figure 6. These points correspond to the areas where the ray passes through the auroral absorption region which in this case is assumed to occur at a height of 100 km. Point A is located at one sixth of the ground range from the transmitter to the terminal point of the ray path; B is situated five sixths of the ground range from the transmitter to the terminal point. Points A and B then each define a range and azimuth. The computer then calculates the corrected geomagnetic latitudes corresponding to these range, azimuth points. Then some time of interest is chosen (in this report a total of three times were chosen 04 UT, 12 UT and 20 UT) from which the corrected geomagnetic time is determined. Once having specified the time, range and azimuth and making the appropriate coordinate transformation, then as previously described, cumulative probability distributions are calculated at each of the corrected geomagnetic coordinates corresponding to these two absorbing regions A and B. For a specified level of absorption the determination of which will be described later, the probability of exceeding that level is calculated and the two probabilities are then averaged. This is felt to be a reasonably good assumption in view of the fact that the range of probabilities is generally less than 20%.

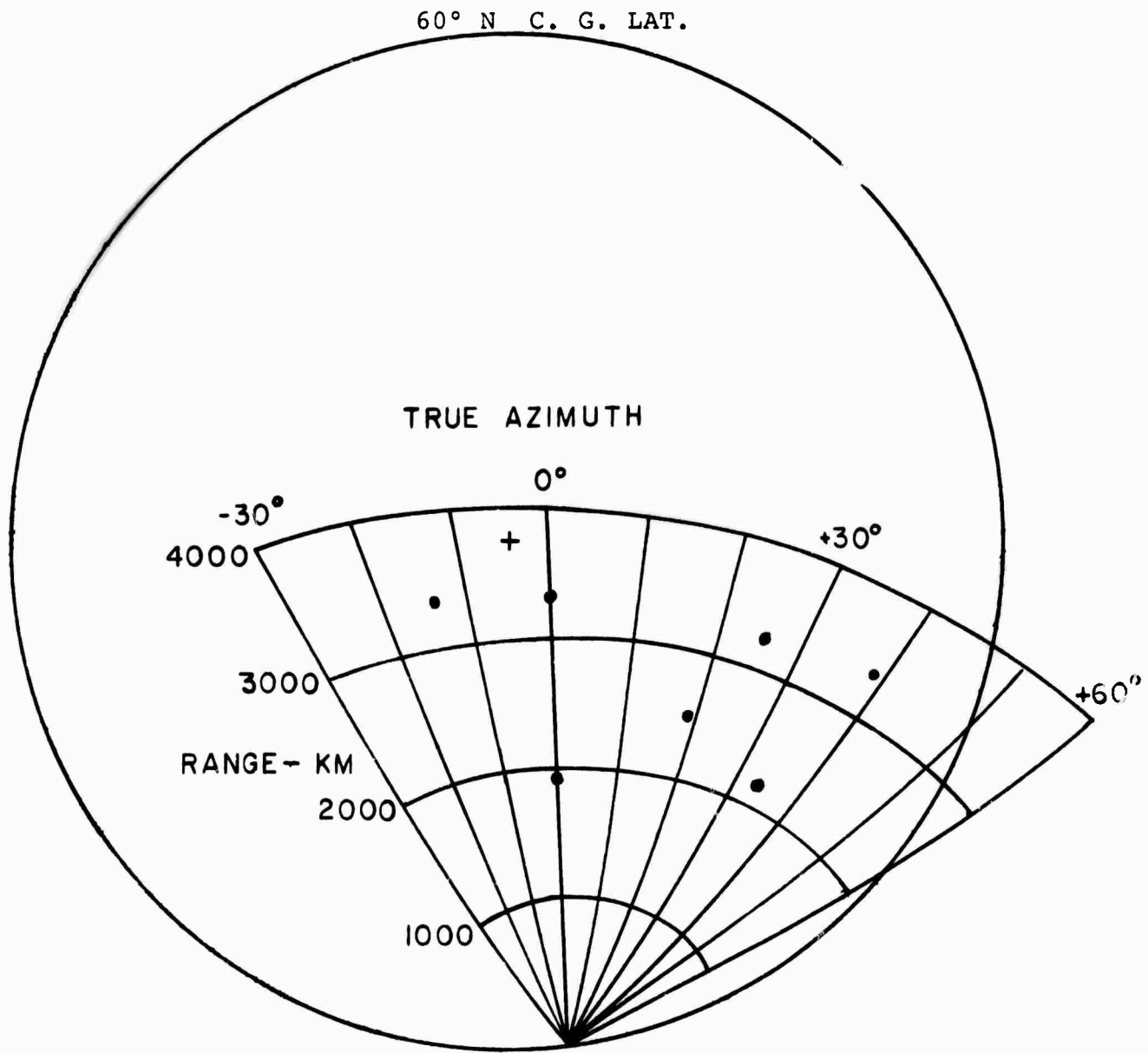
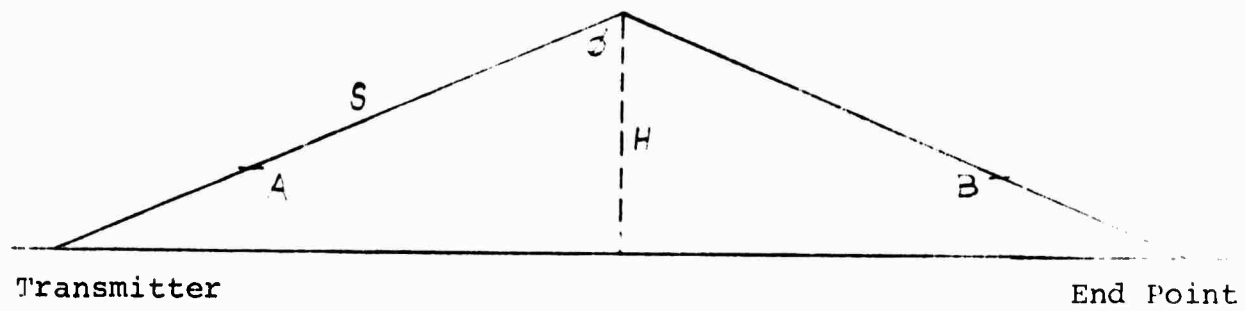


FIGURE 5 RANGE AZIMUTH FAN GRAPH IN CORRECTED GEOMAGNETIC COORDINATES



$$L_{V_{ec}} = \frac{L}{2} \left(\frac{f}{30} \right)^2 \left(\frac{H}{S} \right)$$

FIGURE 6 FLAT EARTH GEOMETRY WITH RELATION BETWEEN PATH LOSS AND EQUIVALENT VERTICAL INCIDENCE ABSORPTION.

In all cases it is assumed that the absorption at A takes place at the same time as it does at B. While the spatial correlation of auroral absorption is not precisely known, this assumption nevertheless, is generally valid especially if A and B are close together in that auroral absorption is a relatively long-lived discrete event, lasting from a few minutes to a few hours. More specifically, the spatial correlation of auroral absorption as a function of latitude is observed by a chain of riometers situated along a given longitude. The spatial correlation of auroral absorption as a function of longitude is established by comparison of three different chains observations taken at three different locations on the earth (Alaska, Canada, and Norway) see Figures 1, 2 and 3. There is, however, a longitudinal time delay in the occurrence of an absorption event between the daytime and nighttime side of the earth which ranges up to an hour. Longitudinal time delays over the ranges of interest in this study may vary from ten to twenty minutes so that for absorption events of a greater duration than this time period there would definitely be simultaneity in occurrence of events between points A and B.

The value for the level of absorption used in determining the probability from the cumulative probability distribution curves is obtained from the following expression:

$$L_{V30} = \left(\frac{f}{30}\right)^2 \left(\frac{H}{S}\right) \left(\frac{L}{2}\right)$$

where L_{V30} = equivalent vertical incidence absorption at 30 MHz in dB

L = total path loss in dB

f = operating frequency in MHz

H = height of reflection point (300 km)

S = distance from transmitter to ionospheric reflection point in km.

A scant relationship is assumed between the vertical and oblique passage through the D Region. An inverse square relationship is used to describe the variation in absorption as a function of frequency. This is a reasonably good approximation for frequencies above 15 MHz. The factor of two enters the relation from the assumption that one half of the absorption takes place at Region A and the second half at Region B. An isocontour map is then computed in the following way: First, a level of absorption L is chosen as well as some specific frequency f . S is then calculated for a given range and azimuth. Then from the expression above the equivalent vertical incidence absorption value L_{V30} is determined which is the same for points A and B. For the range and azimuth in question and for some specified time of day, the corresponding corrected geomagnetic coordinates are determined, as previously explained. Then two cumulative probability distribution curves are generated. Knowing the value of L_{V30} now permits determination of the probability of exceeding the level of

absorption L as mentioned earlier. This percent probability is subtracted from unity and then becomes the percentage of time that the total absorption along the path is less than or equal to some specified level L at a given frequency and time of day. This process is then repeated for a whole spectrum of range and azimuths using the same values of L, F and T. Contours of equal probability are then plotted on a fan type graph. Isocontour maps showing the probability of absorption being equal to or less than a given value were generated for the following conditions:

Frequencies - 15, 20 and 25 MHz

Absorption (one way) - 10, 20, 30 and 40 dB

Time - 4, 12 and 20 UT

For 10 MHz a single hop E mode over a flat earth was assumed, with a reflection height at 100 km. Propagation for this case, therefore extends out to a range of 2000 km. In the expression for L_{v30} , the factor of two disappears since all the absorption takes place in one region. Otherwise, all other parameters remain the same.

It should be noted that the probability of the absorption being less than or equal to some specified level of absorption for transmission in one direction is the same as the probability for twice that level of absorption for transmission in both directions (Radar backscatter), i.e. the probability contour for 30 dB absorption shown on the maps is the same contour for 60 dB radar backscatter absorption.

4. DISCUSSION

Of the three times chosen, 0400 UT (just before midnight geomagnetic time) corresponds to a time of minimum absorption, 1200 UT corresponds to a time near the morning maximum in absorption while 2000 UT is a time of moderate absorption events. The time indicated is the time at the transmitter site which, of course, may differ from the time at any other point in the "fan" plot. Range coverage extends from 1000 km to 4000 km from the transmitter except in the case of the 10 MHz plots, which extend from 1000 km to 2000 km. It should be remembered that the attenuation shown is the component due only to auroral absorption; normal D region absorption as well as $1/R^2$ losses have been omitted.

Some of the gross features of the data are as follows: For any given time of day the probability that the absorption is less than some specified level, is smaller for lower frequencies. For any given frequency the probability that the absorption is less than some specified value is always smaller around 12 UT than it is at 04 UT or 20 UT. This is equivalent to saying that the absorption is greatest at 12 UT, which is the time of the morning maximum. For any given frequency and time the absorption is greater in the northeast sector of the range, azimuth fan, this is so because the ray propagates along the auroral absorption zone. For propagation paths transverse to the auroral absorption zone the attenuation increases going poleward away from the transmitter. Generally speaking, the losses are relatively small for frequencies above 20 MHz propagative via a one hop F-layer mode.

In the case of the 10 MHz probability contours, the features are only visible at the higher absorption levels. This is so because the cumulative probability distribution curves do not extend down to low enough percentages. As was mentioned previously we are working with the tail end of commulative probability distributions. Most of the curves run from not less than 80% to 100%. Generally speaking the losses are high, or expressed in terms of probabilities, the percentage time that a small level of absorption (10 dB) occurs is low. In the computational procedures, if the percentage probability to be calculated is off scale (beyond end points defined by probability distribution) then the end point is used. For this reason some of the contour plots are the same, compare for example the 10 dB and 20 dB maps for 10 MHz at the 12 UT. What this implies is that the absorption is greater than the specified level. More details can be seen upon a closer examination of the plots, which are shown in Figures 7 through 30.

5. SUMMARY

Contour plots showing the probability of occurrence of auroral absorption are useful aids for the design of HF radar and communications circuits in high latitude regions. A method has been described to compute the amount of auroral absorption that would be observed by a high latitude HF radar. It incorporates data from three different riometer networks, which is possible since the observed distribution of absorption events is similar. The probability contour maps generated in this report are projections of expected auroral absorption for the period 1971-1972. Since riometers are relatively insensitive (used only for measuring large absorption events) only the tail end of a probability distribution can be measured. In order to fully benefit from this method it is necessary to extrapolate the distribution up to the median value.

6. REFERENCES

Agy, V., "HF Radar and Auroral Absorption," Radio Science, Vol 5, No. 11, pp 1317-24, November, 1970.

Hargreaves, J. K., "Auroral Absorption of HF Radio Waves In the Ionosphere: A Review of Results from the First Decade of Riometry," Proc. IEEE, Vol. 57, pp. 1348-73, August, 1969.

Hargreaves, J. K., "On the Variation of Auroral Radio Absorption With Geomagnetic Activity," Planetary Space Science, Vol. 14, pp. 991-1006, 1966.

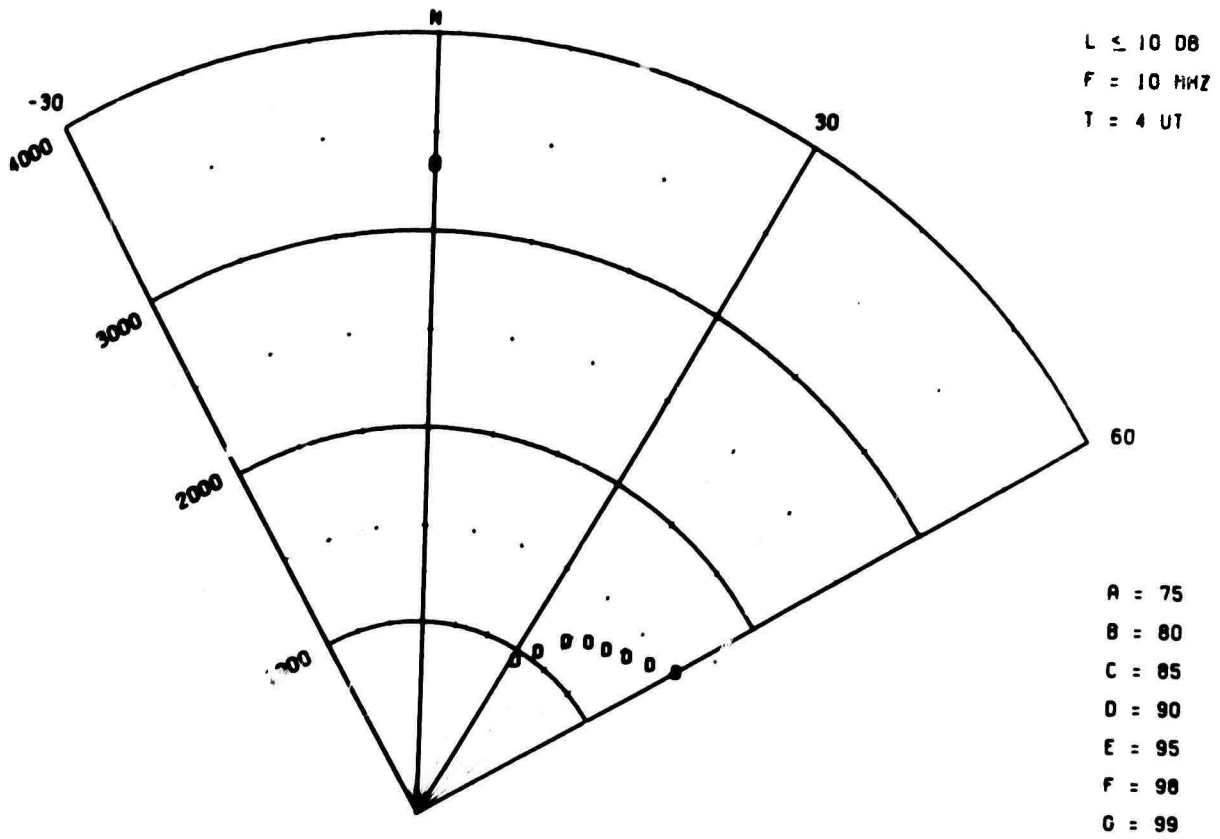
Hargreaves, J. K. and Sharp, R. D., "Electron Precipitation And Ionospheric Radio Absorption In the Auroral Zones," Planetary Space Science, Vol. 13, pp. 1171-83, 1965.

Hartz, T.R., "Multi-Station Riometer Observations," Radio Astronomical And Satellite Studies of the Atmosphere, pp 220-37, 1963.

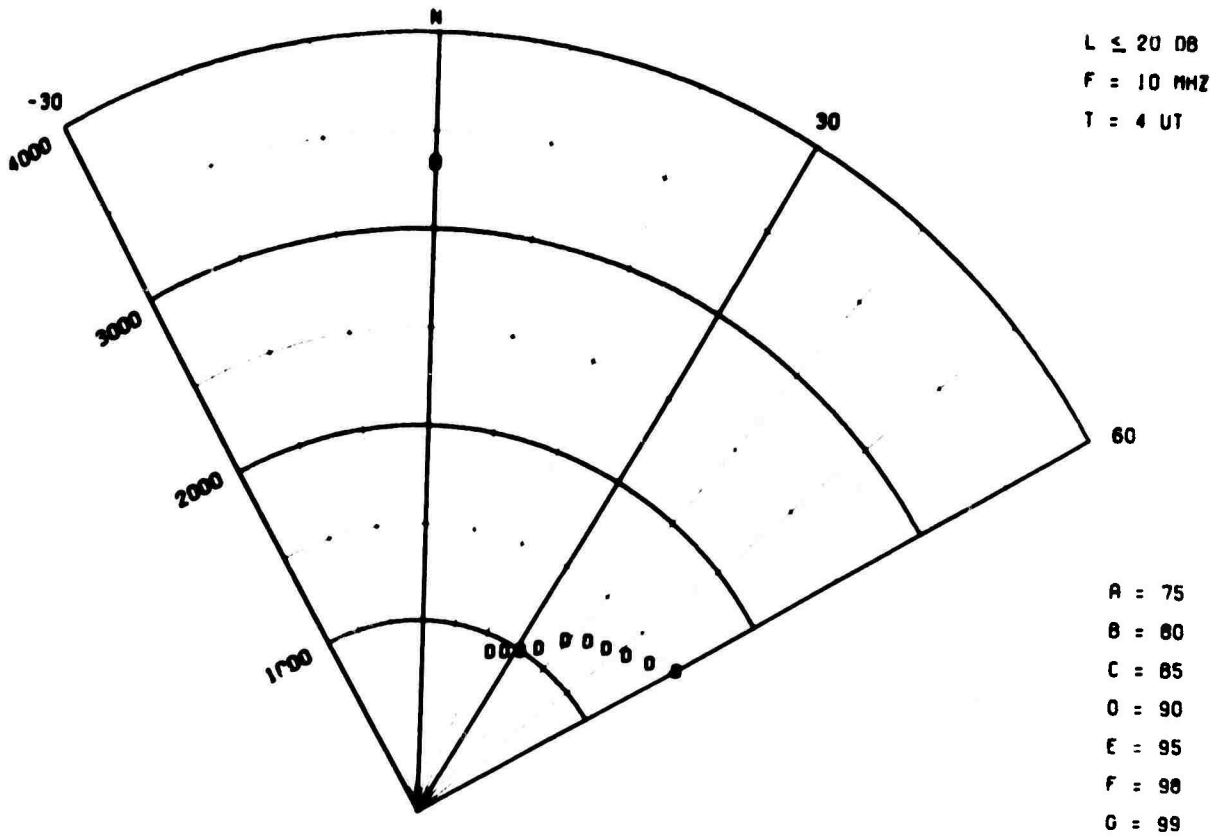
Hook, J. L., "Morphology of Auroral Zone Radiowave Absorption In the Alaska Sector," JATP Vol. 30, pp 1341-51, 1968.

Penndorf, R., "High Latitude Propagation Study," Final Report Con. No. F30602-69-C-0201, September, 1970.

AURORAL ABSORPTION



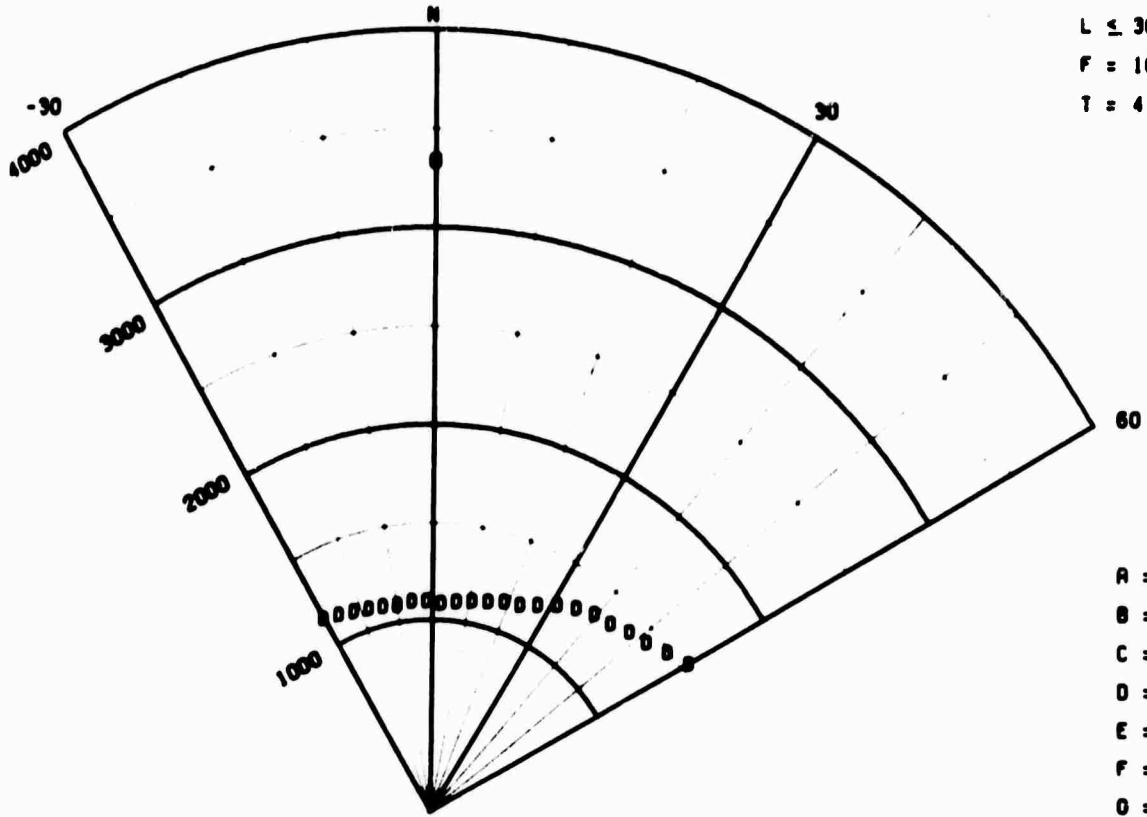
AURORAL ABSORPTION



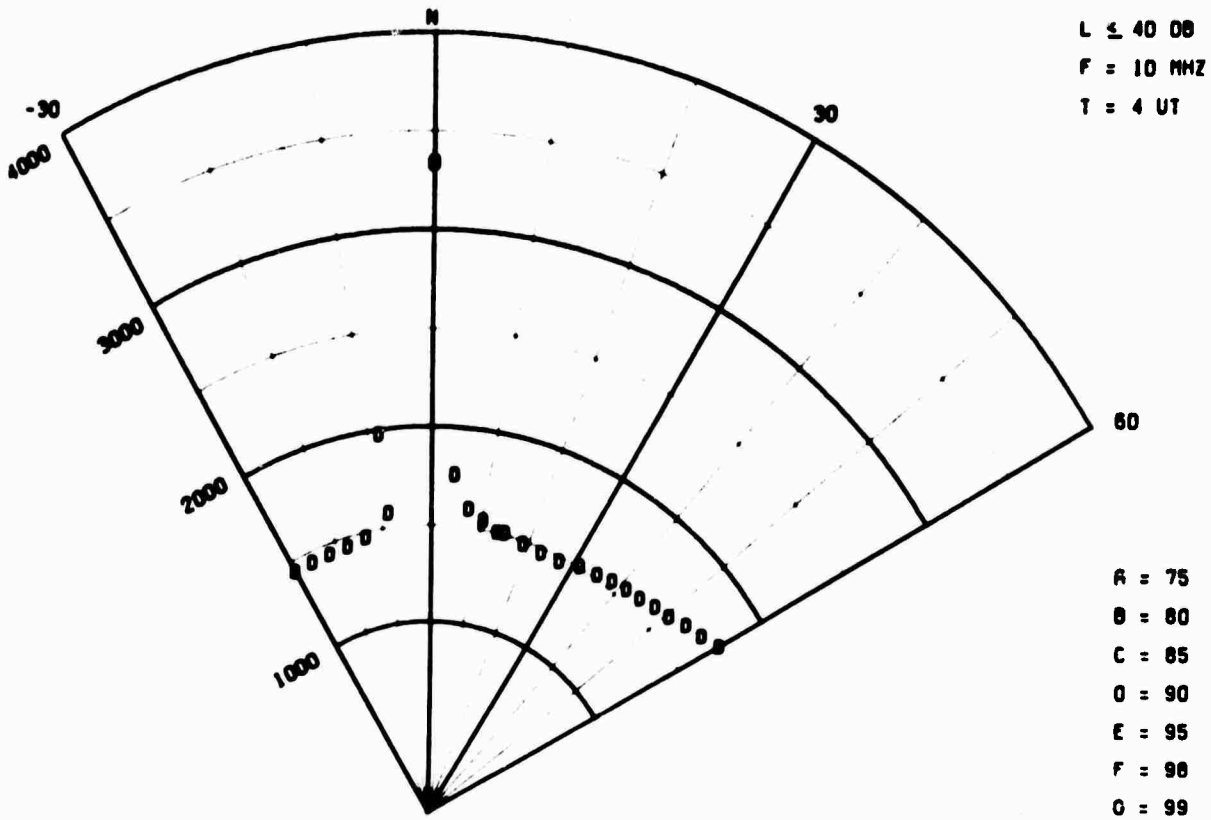
III-19

Figure 7

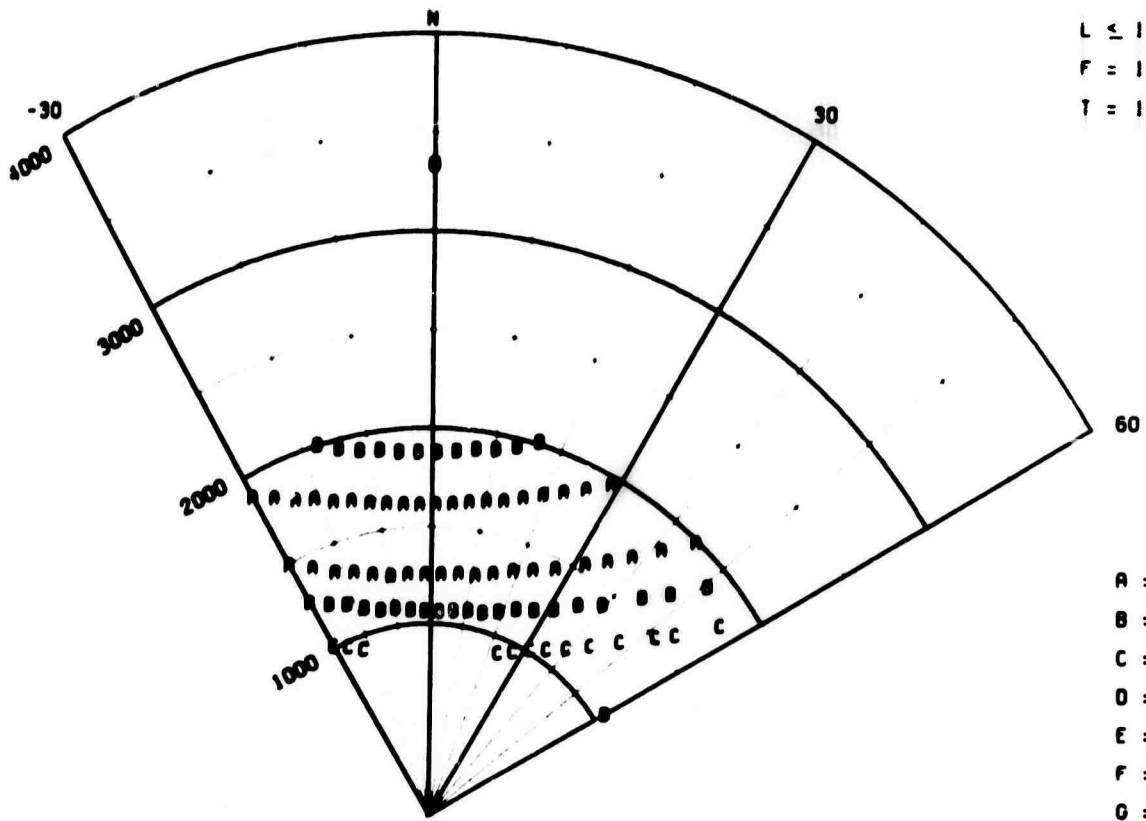
AURORAL ABSORPTION



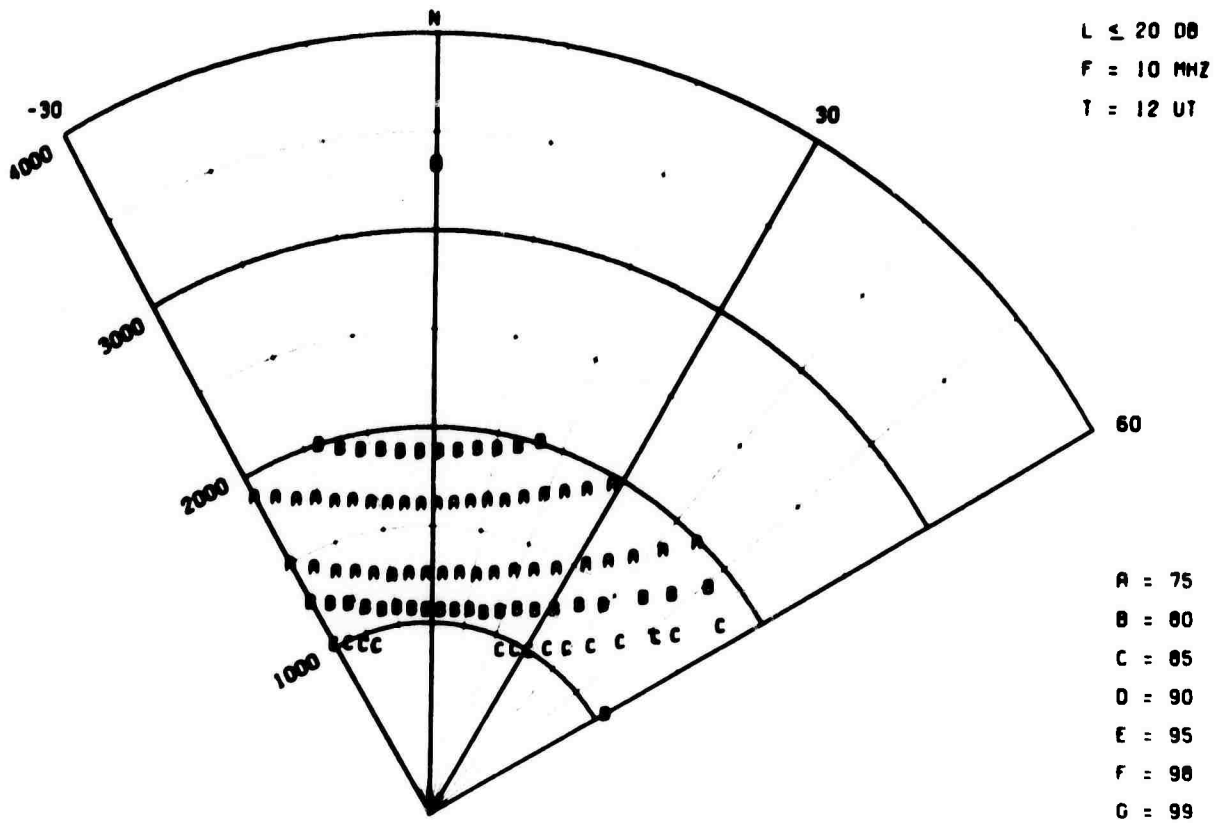
AURORAL ABSORPTION



AURORAL ABSORPTION



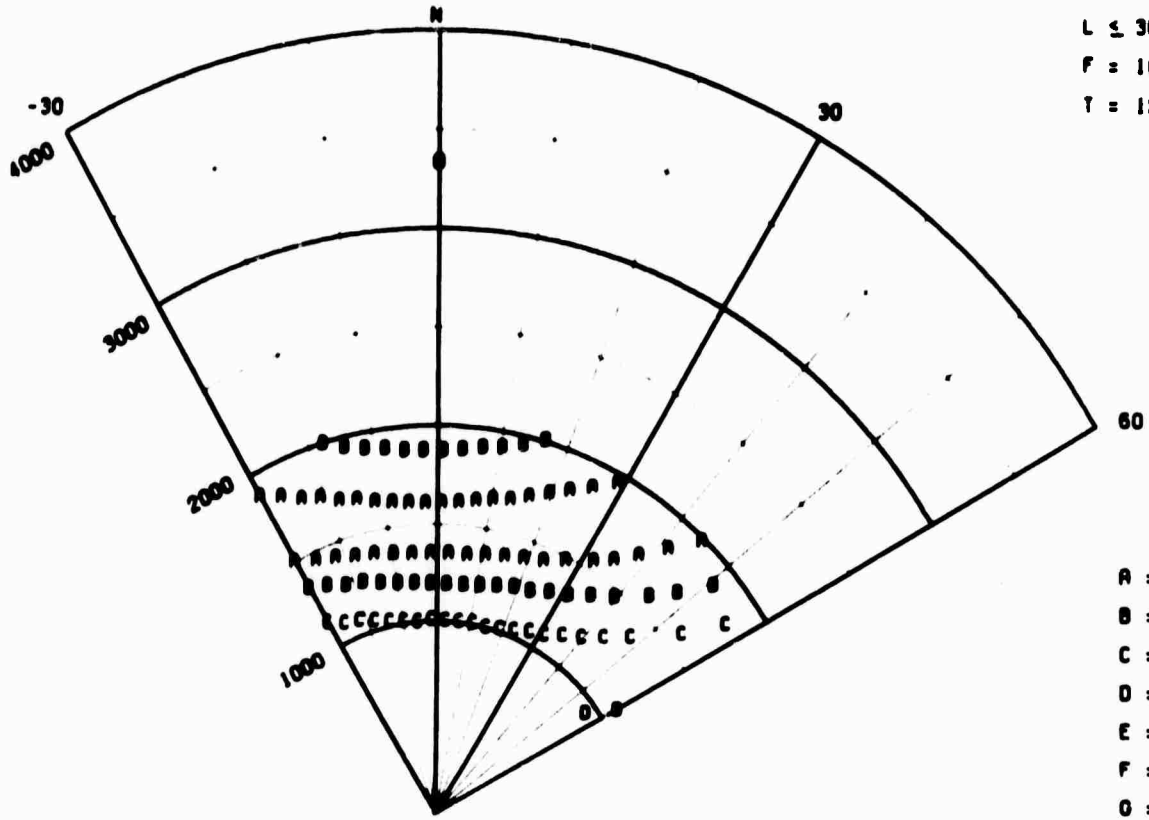
AURORAL ABSORPTION



III-21

Figure 9

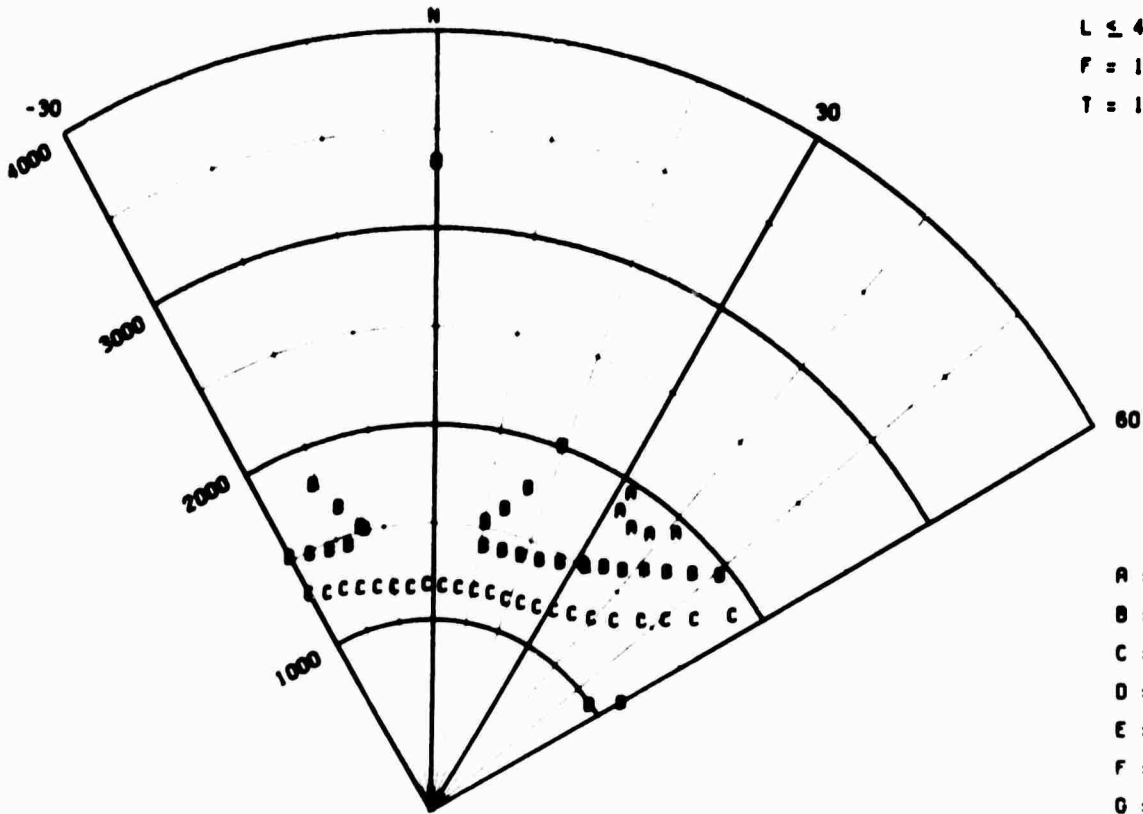
AURORAL ABSORPTION



L ≤ 30 00
 F = 10 MHz
 T = 12 UT

A = 75
 B = 80
 C = 85
 D = 90
 E = 95
 F = 98
 G = 99

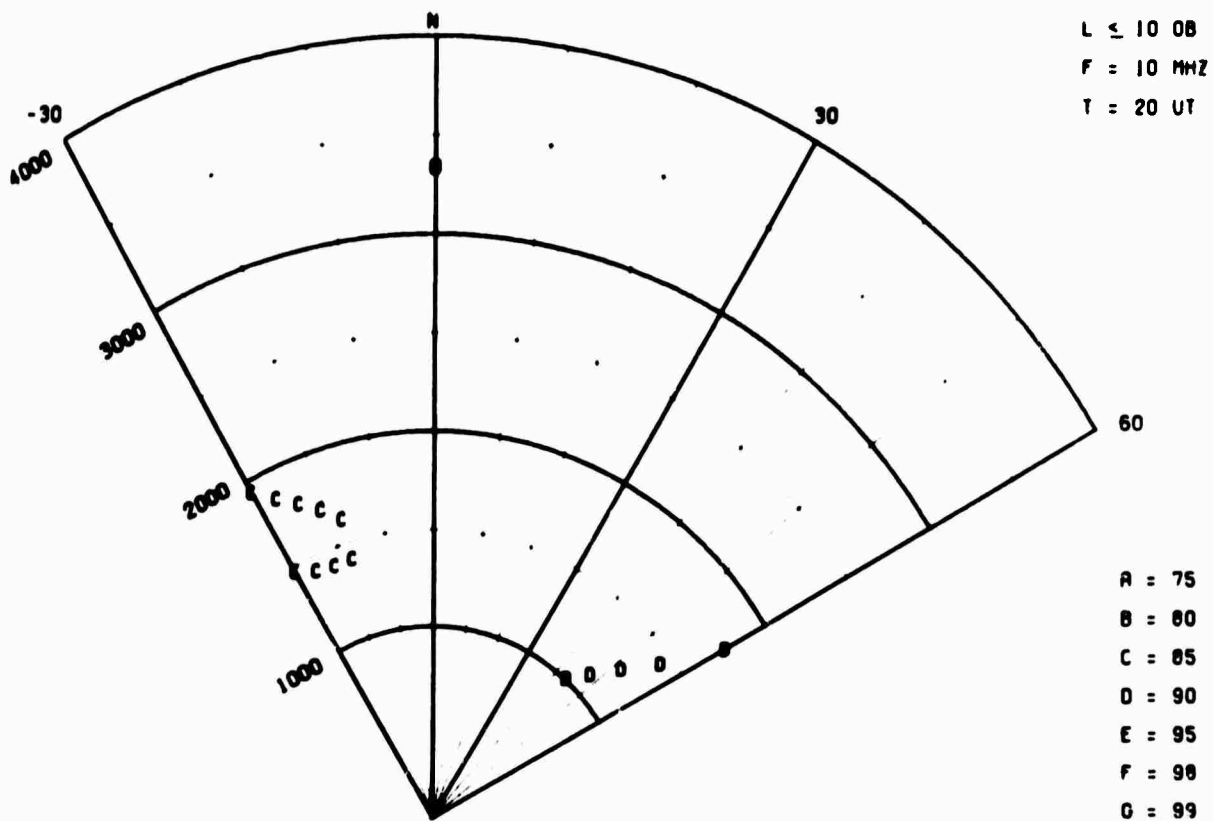
AURORAL ABSORPTION



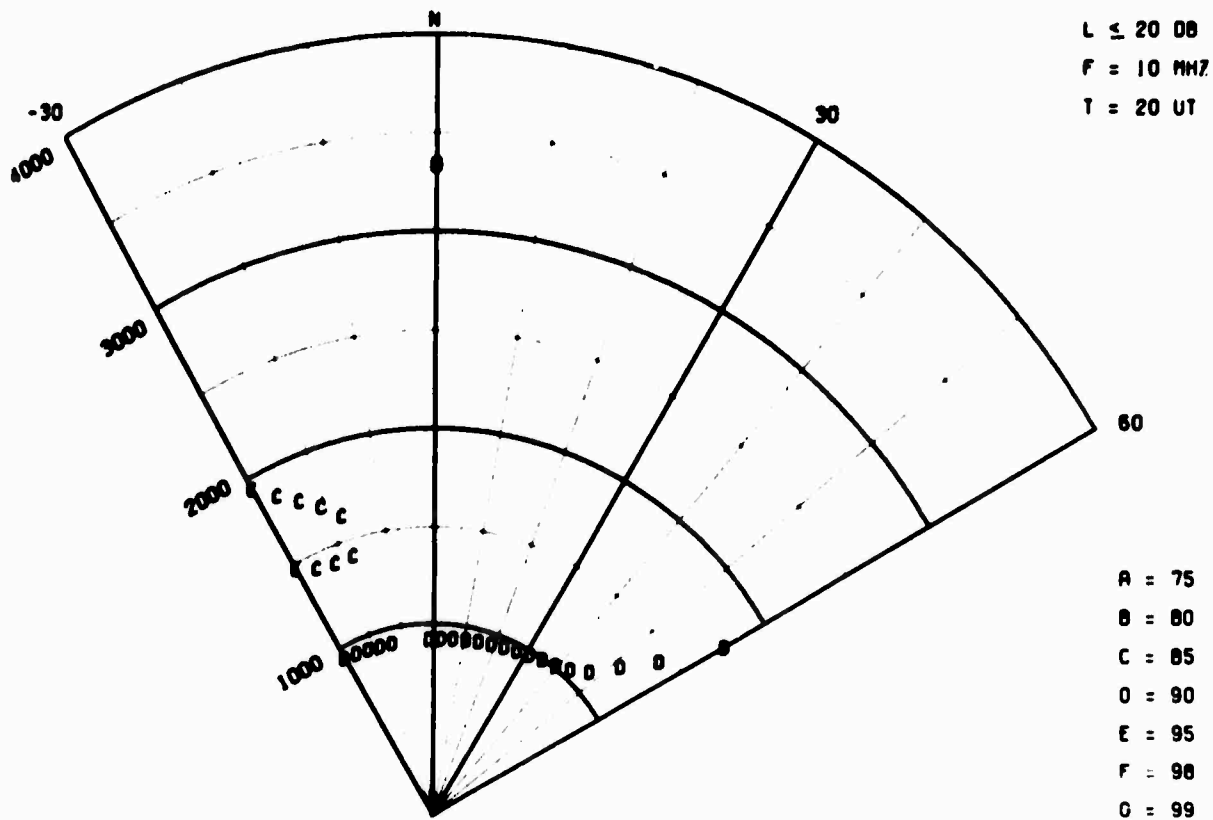
L ≤ 40 00
 F = 10 MHz
 T = 12 UT

A = 75
 B = 80
 C = 85
 D = 90
 E = 95
 F = 98
 G = 99

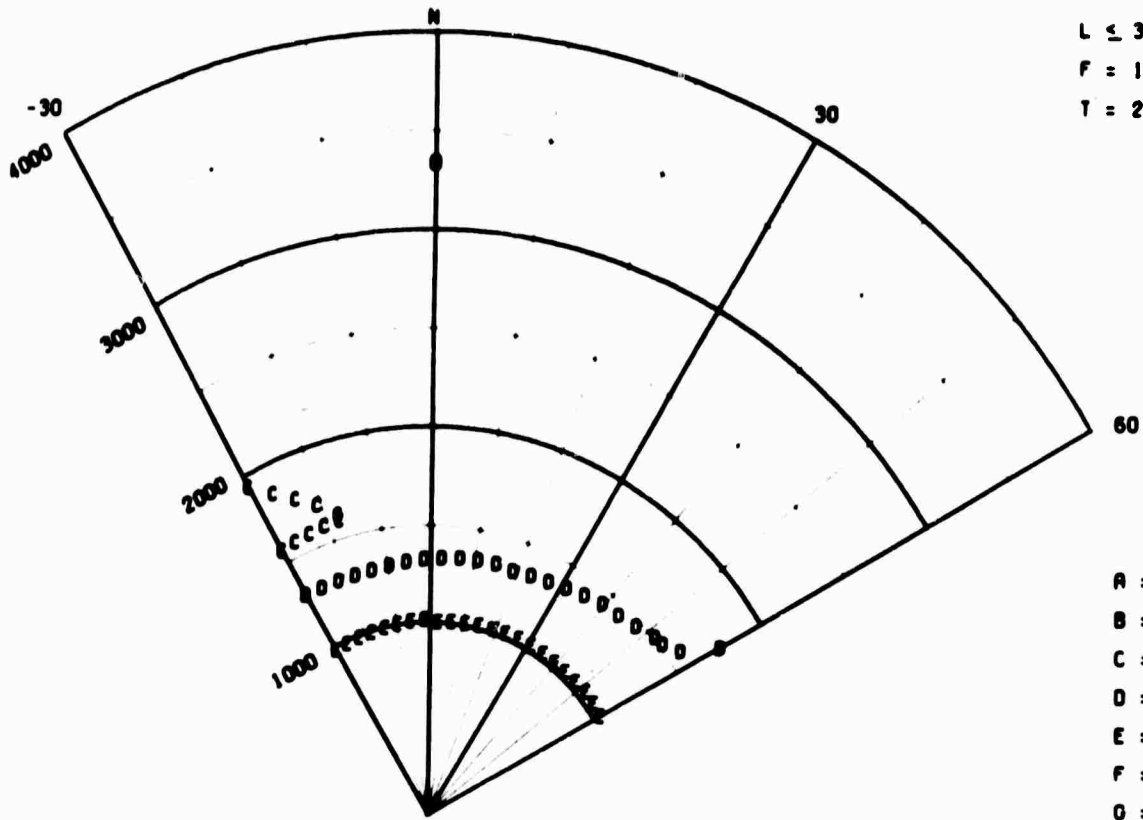
AURORAL ABSORPTION



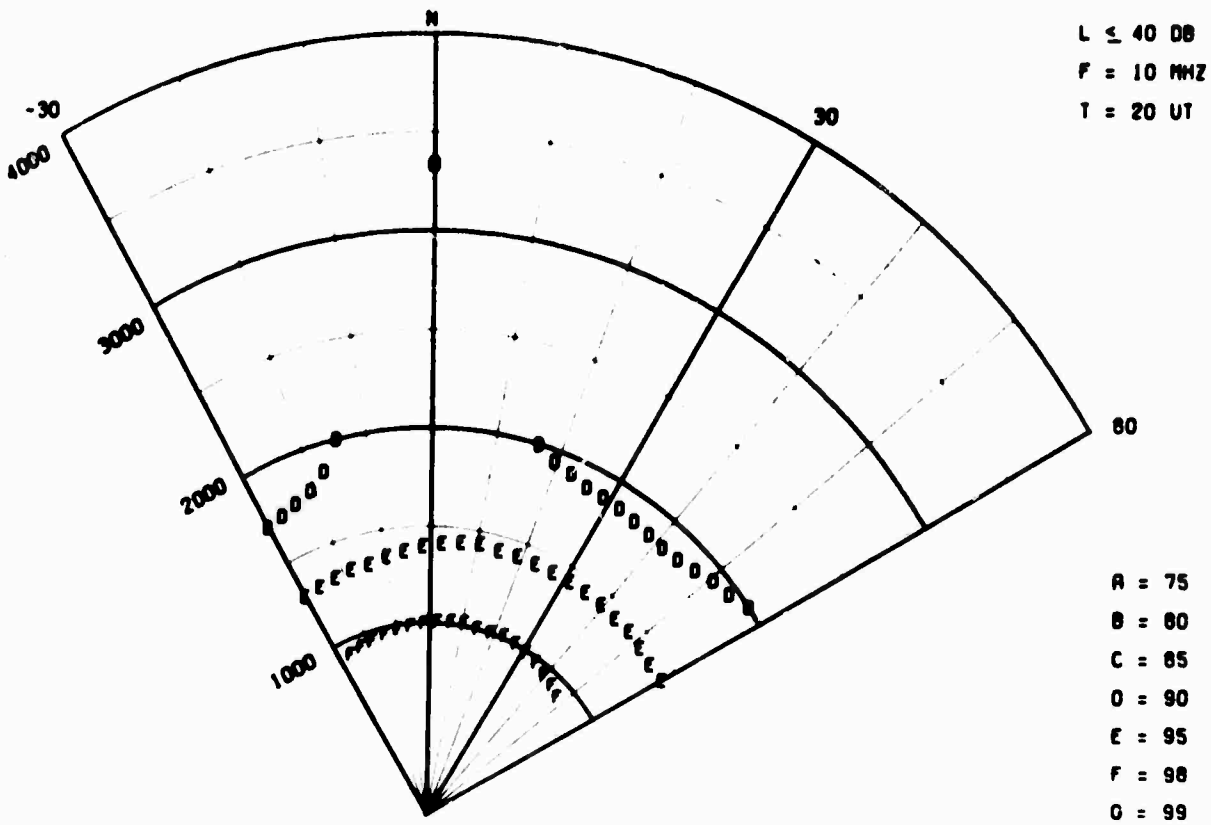
AURORAL ABSORPTION



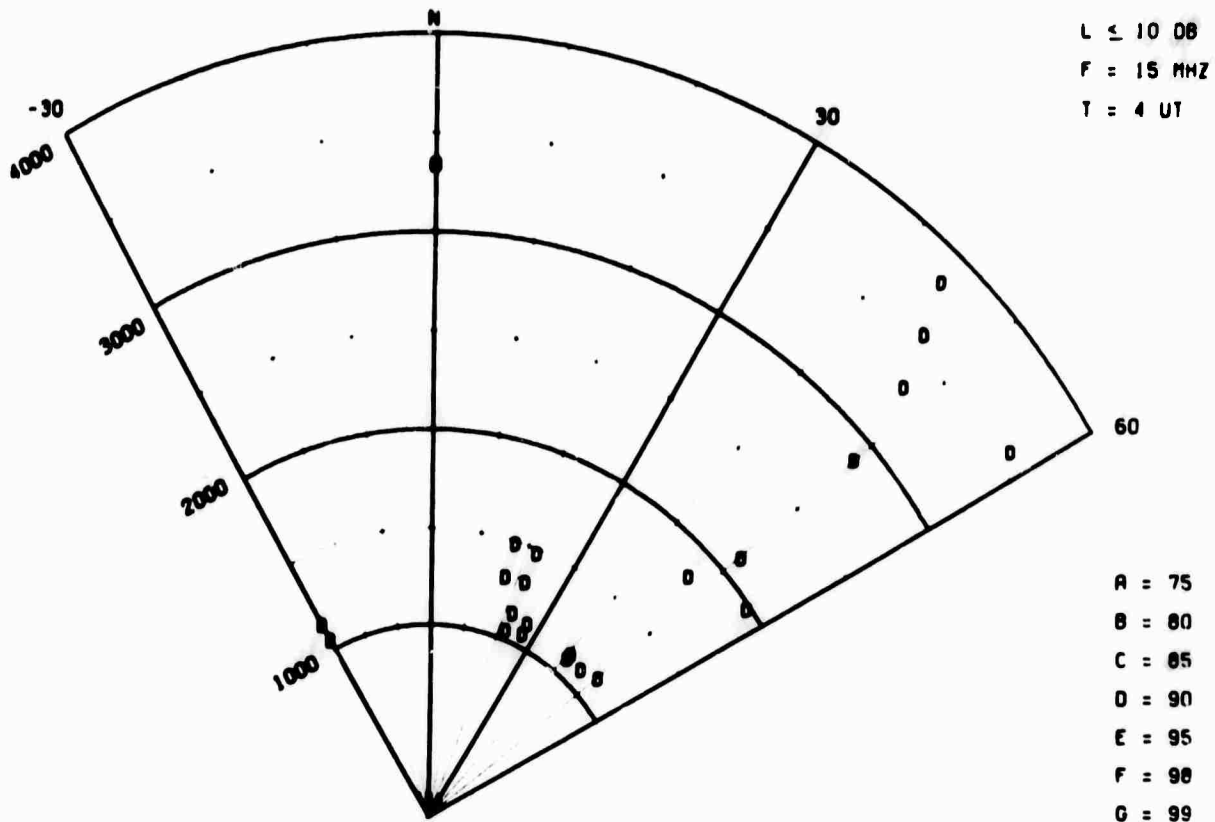
AURORAL ABSORPTION



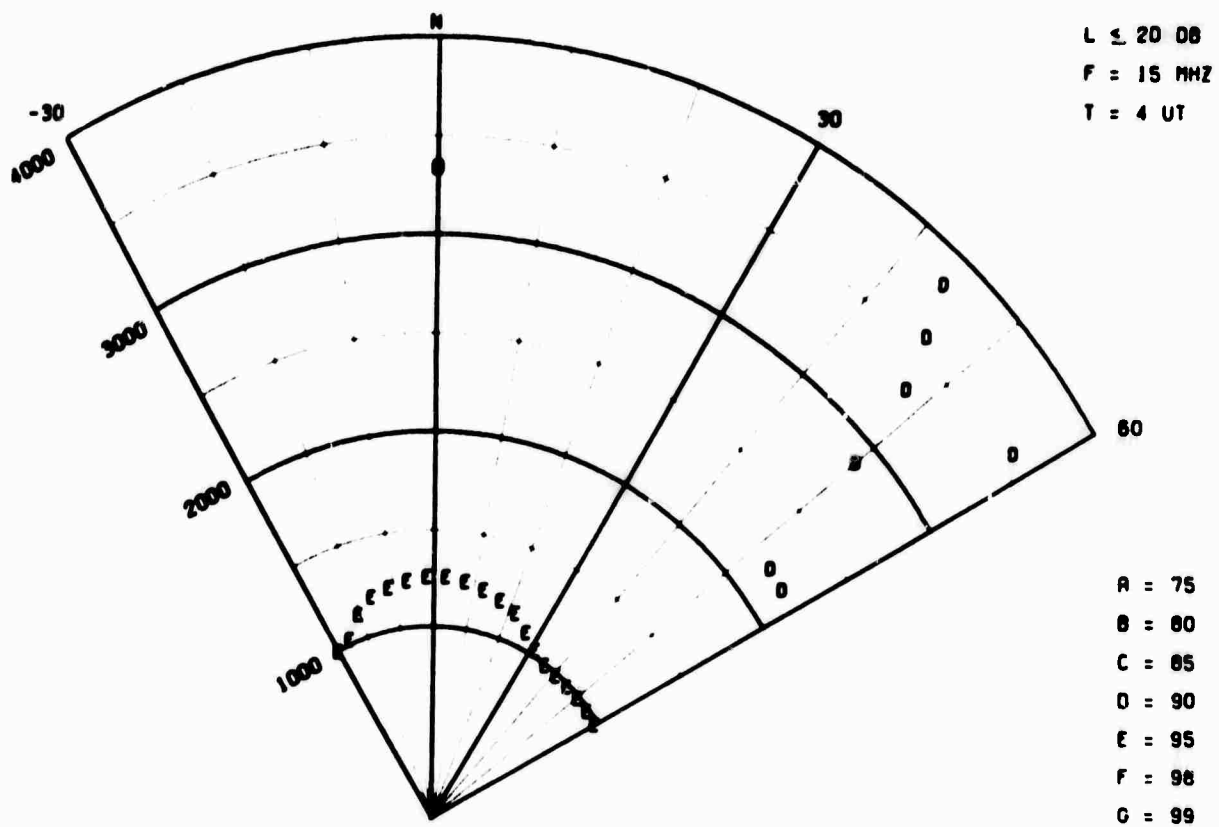
AURORAL ABSORPTION



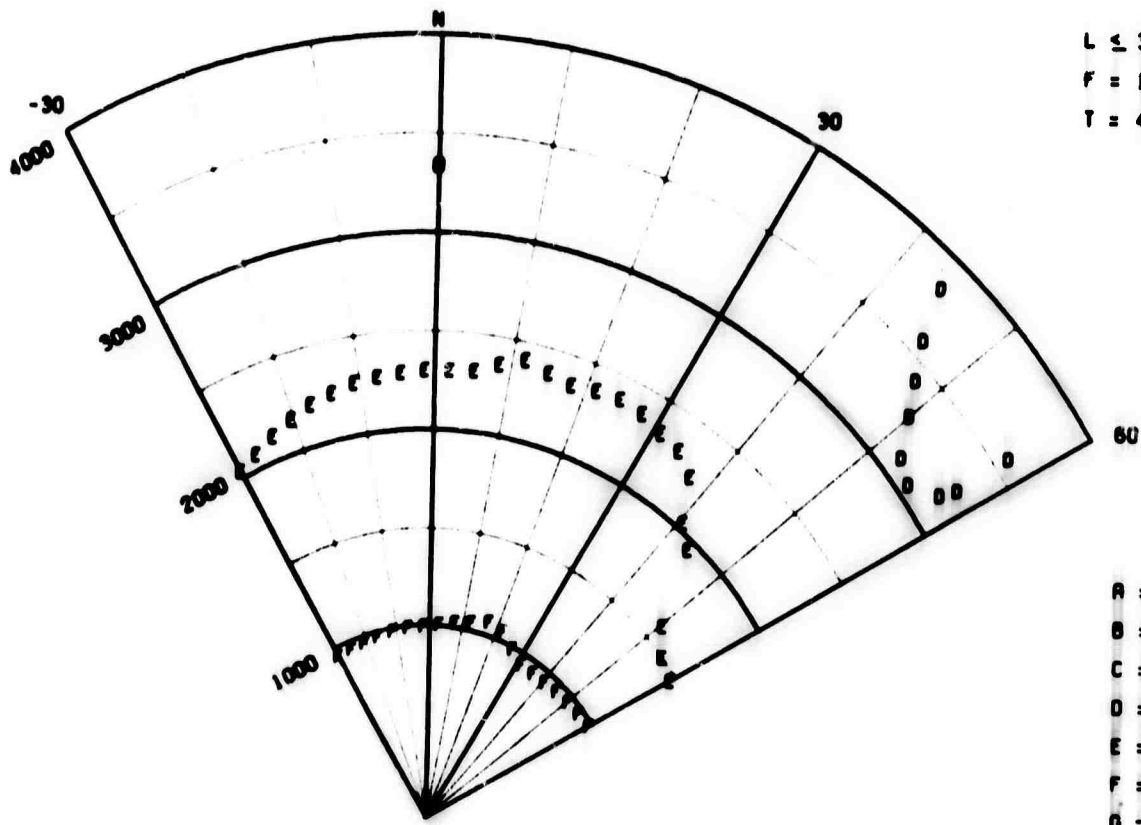
AURORAL ABSORPTION



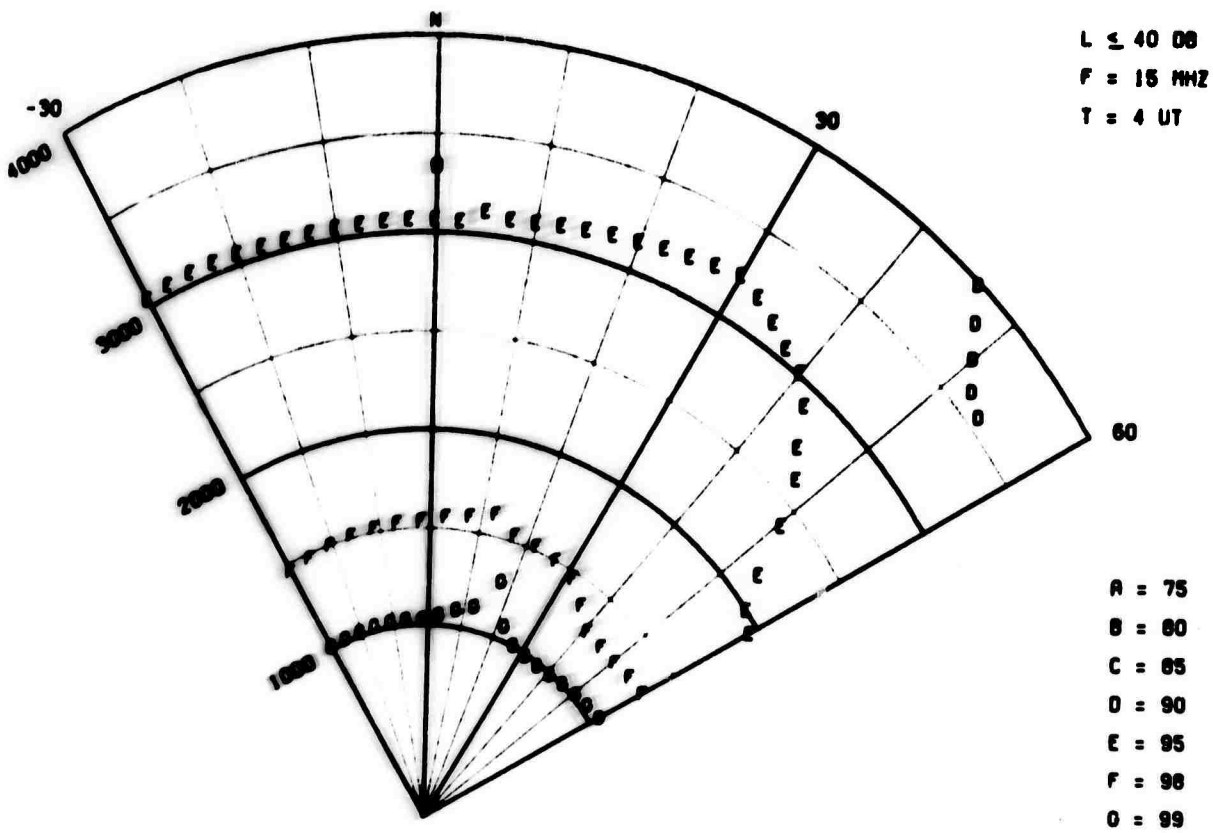
AURORAL ABSORPTION



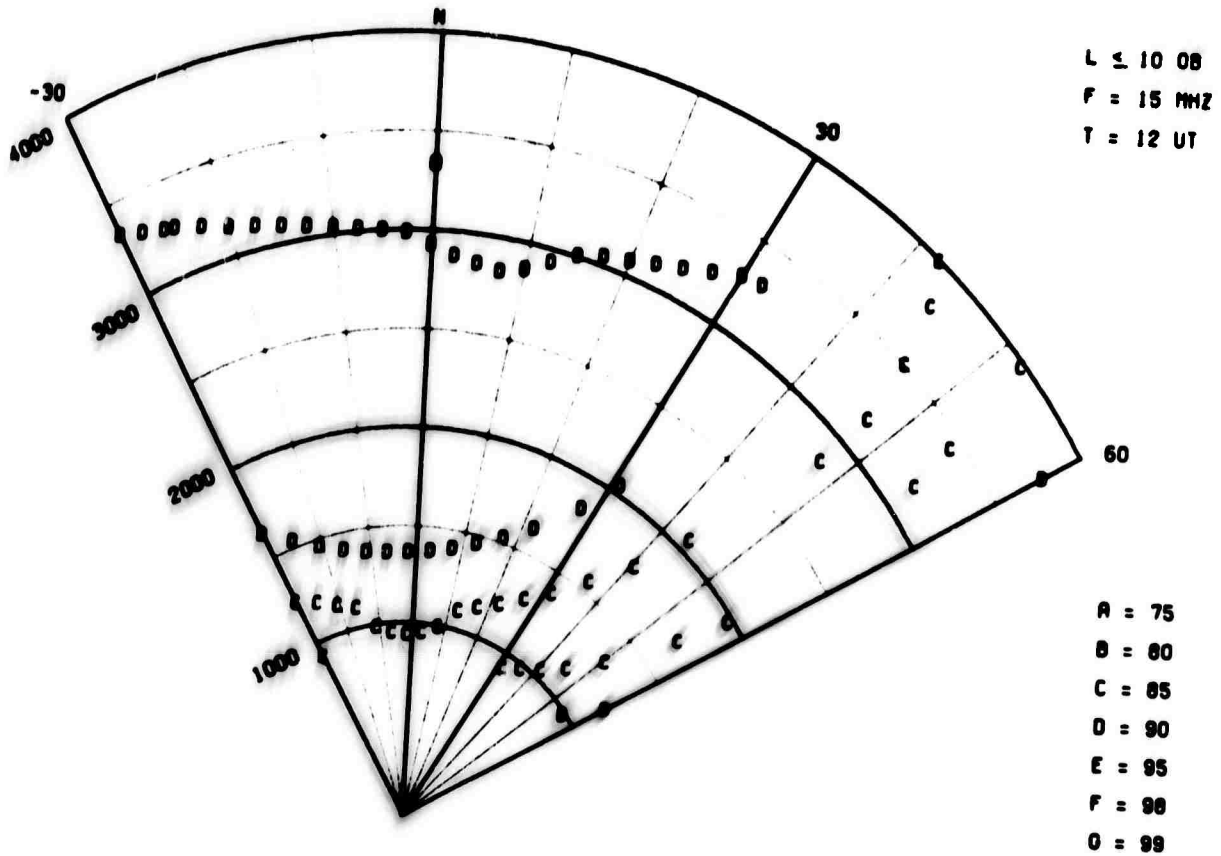
AURORAL ABSORPTION



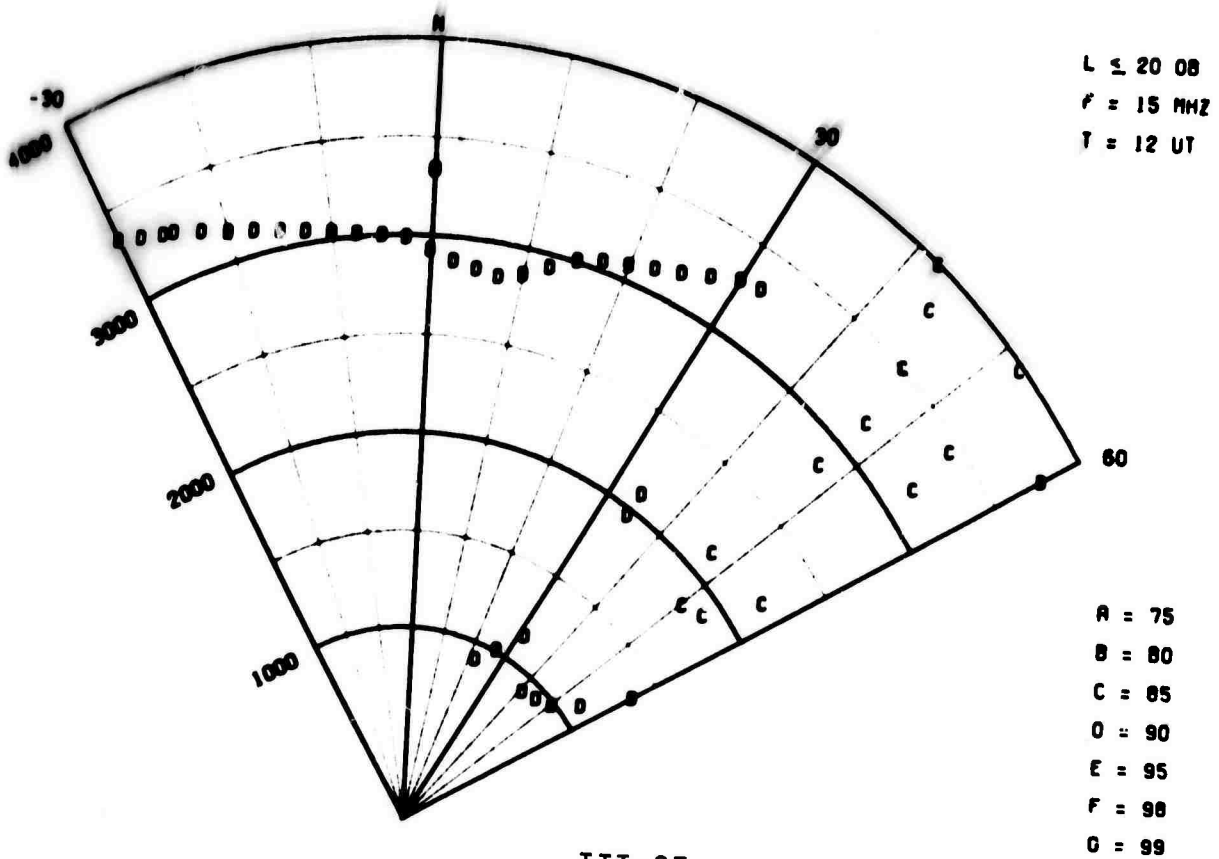
AURORAL ABSORPTION



AURORAL ABSORPTION



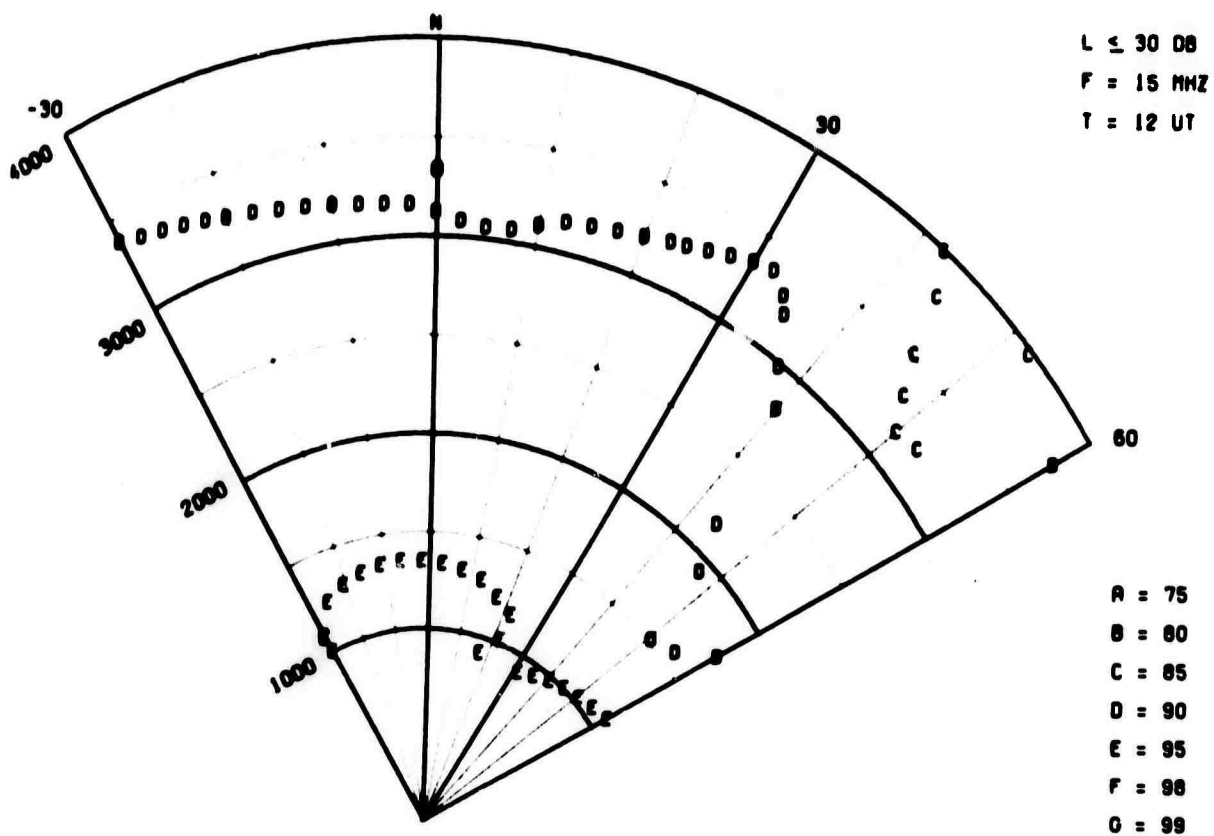
AURORAL ABSORPTION



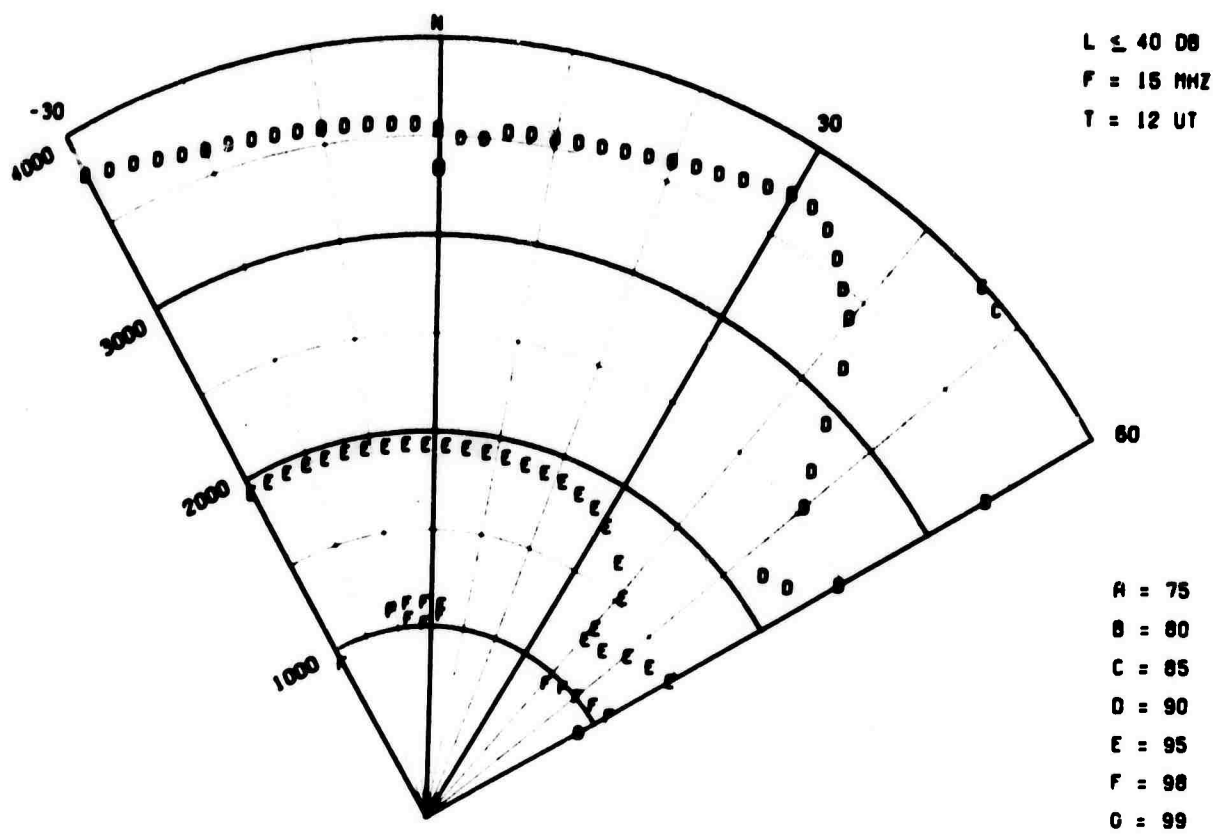
III-27

Figure 15

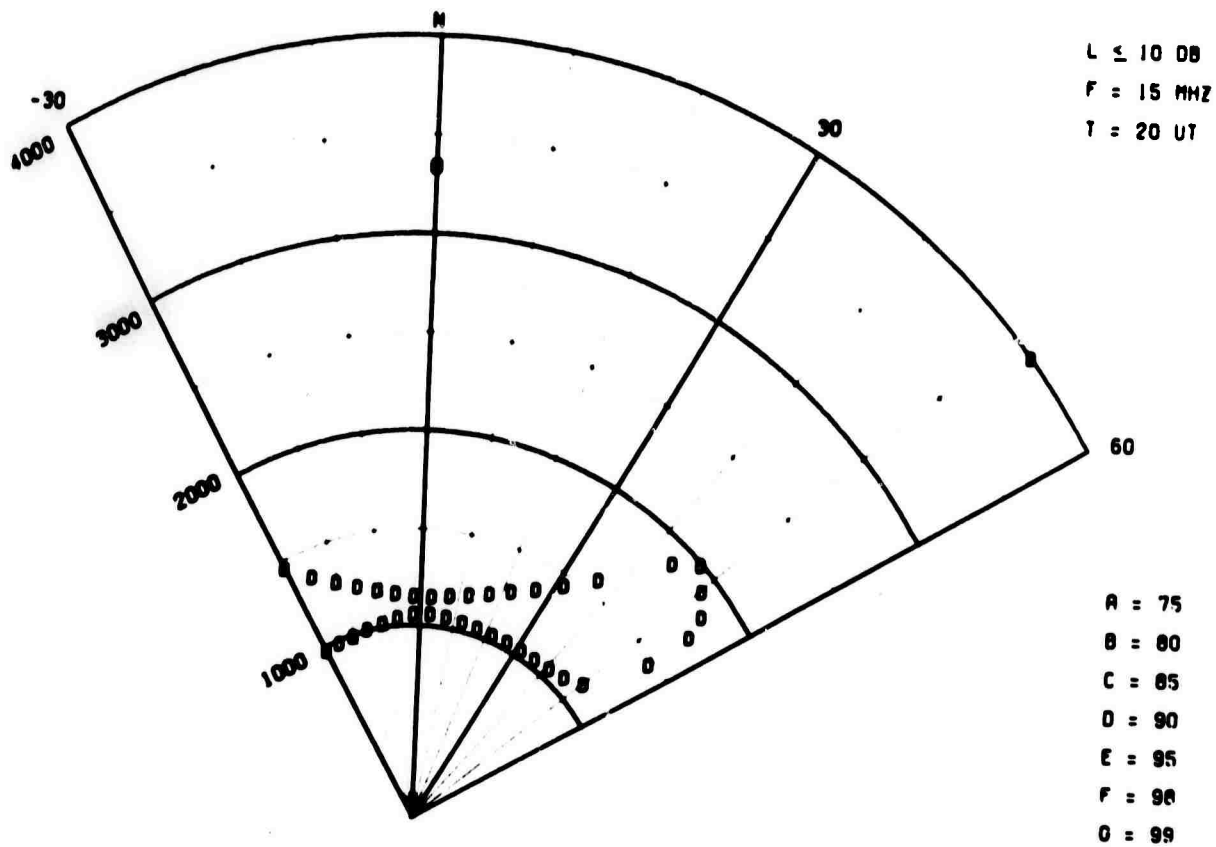
AURORAL ABSORPTION



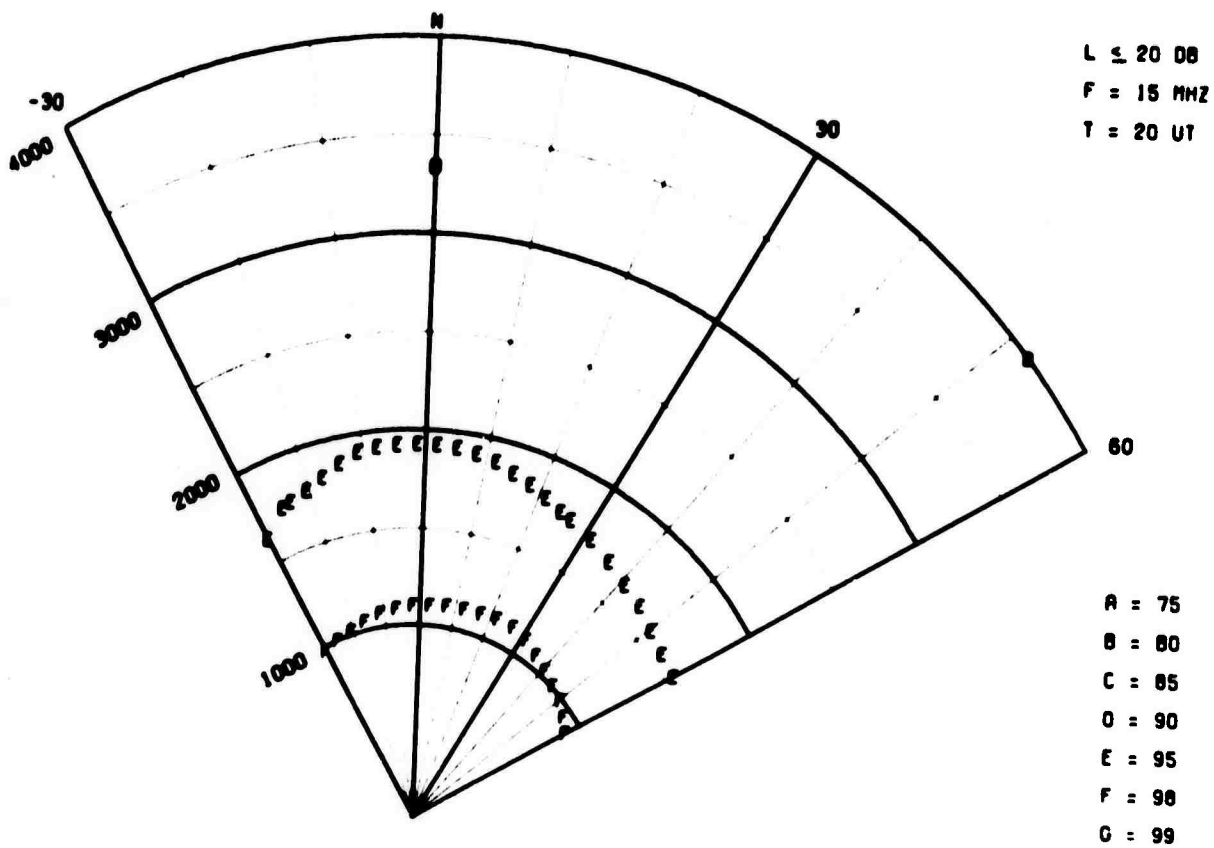
AURORAL ABSORPTION



AURORAL ABSORPTION



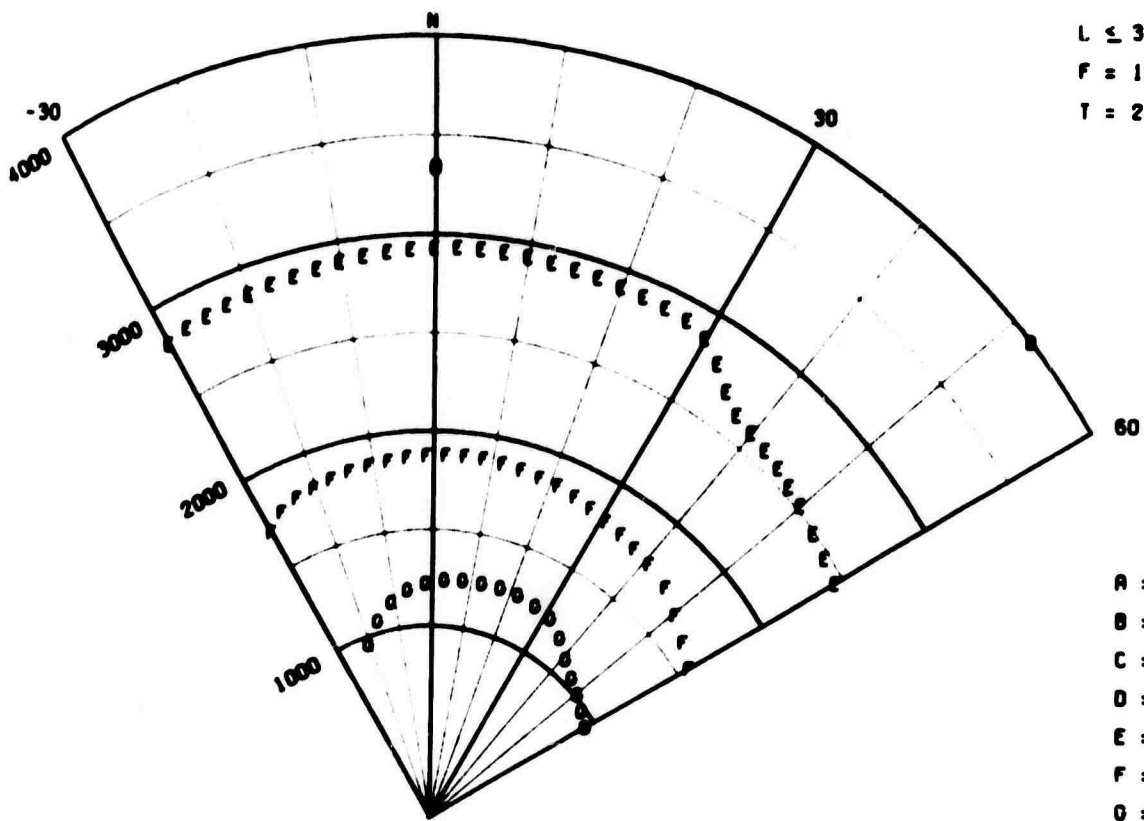
AURORAL ABSORPTION



III-29

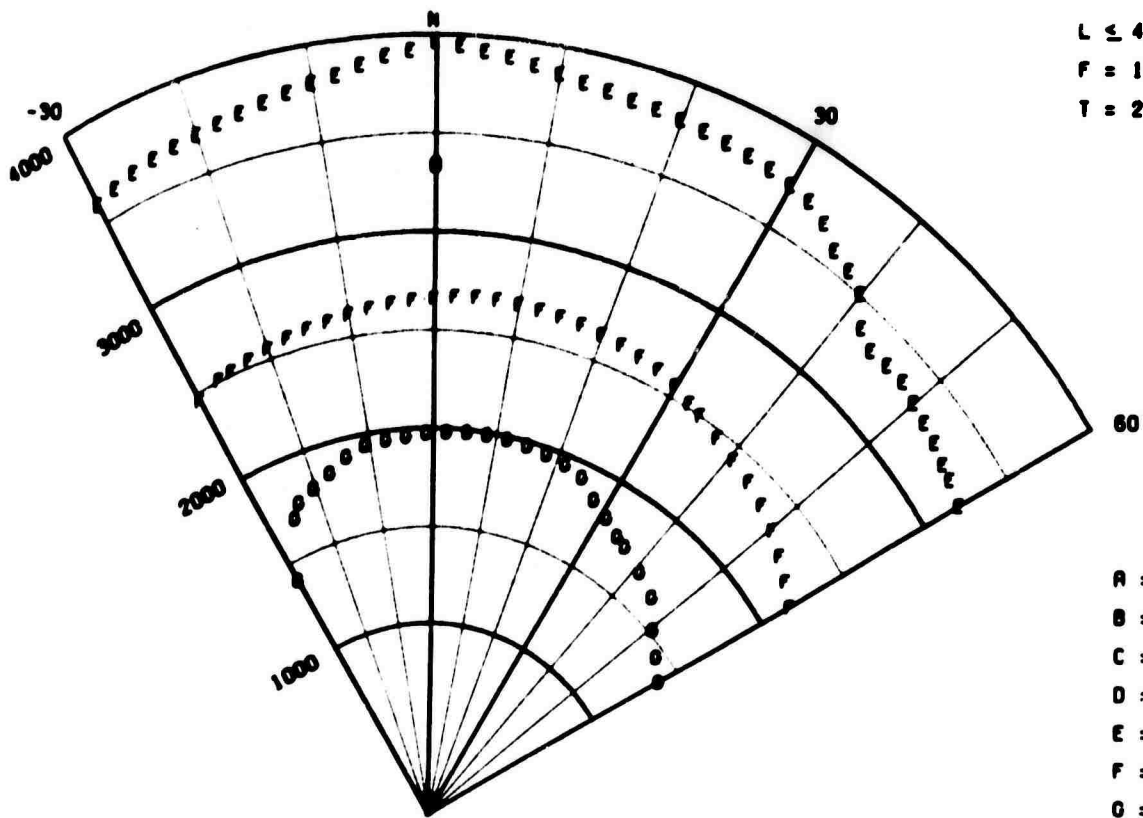
Figure 17

AURORAL ABSORPTION



- A = 75
- B = 80
- C = 85
- D = 90
- E = 95
- F = 98
- G = 99

AURORAL ABSORPTION

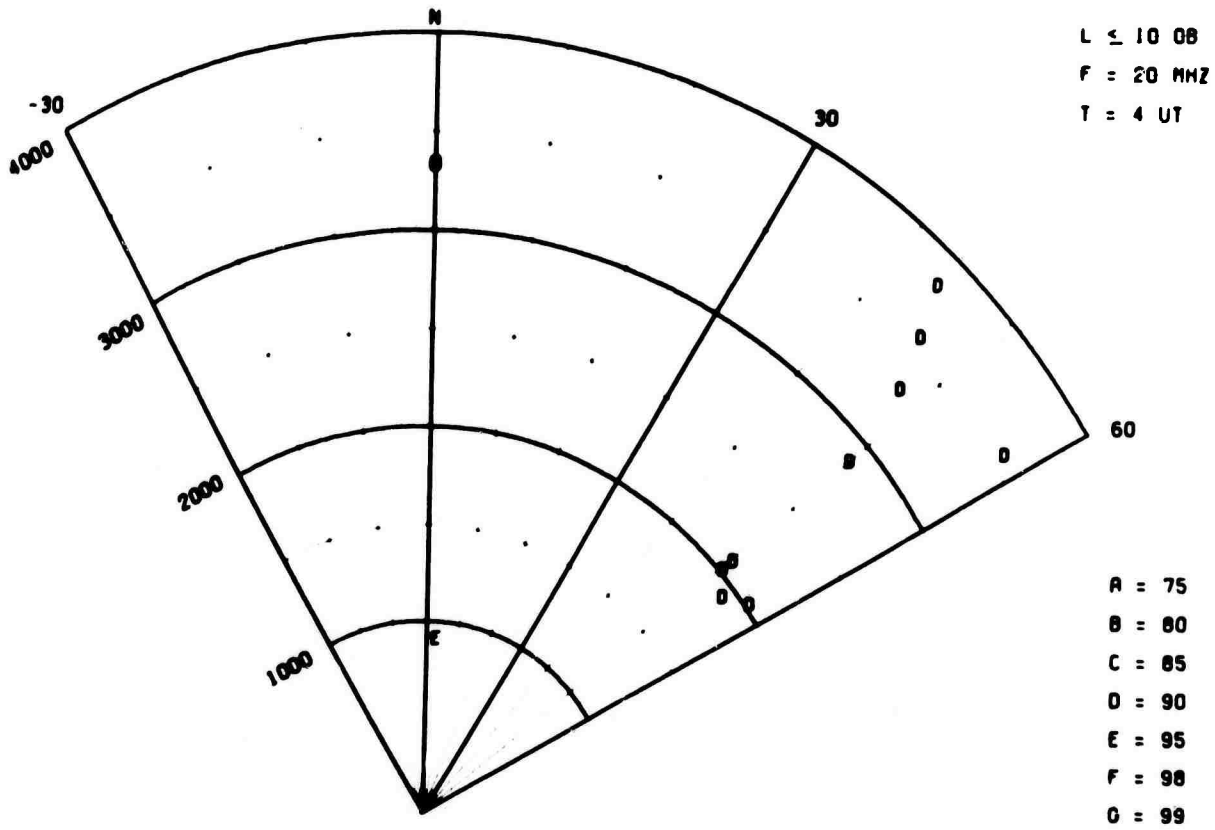


- A = 75
- B = 80
- C = 85
- D = 90
- E = 95
- F = 98
- G = 99

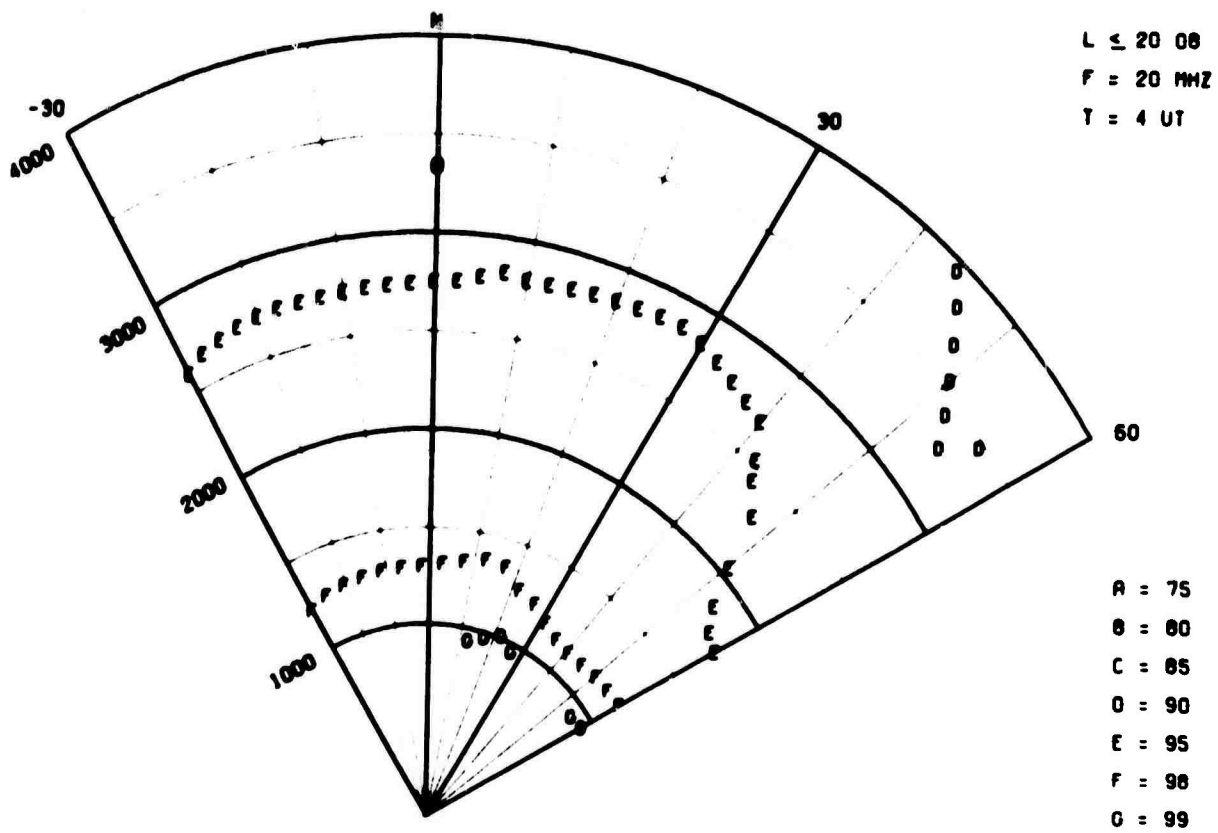
III-310

Figure 18

AURORAL ABSORPTION



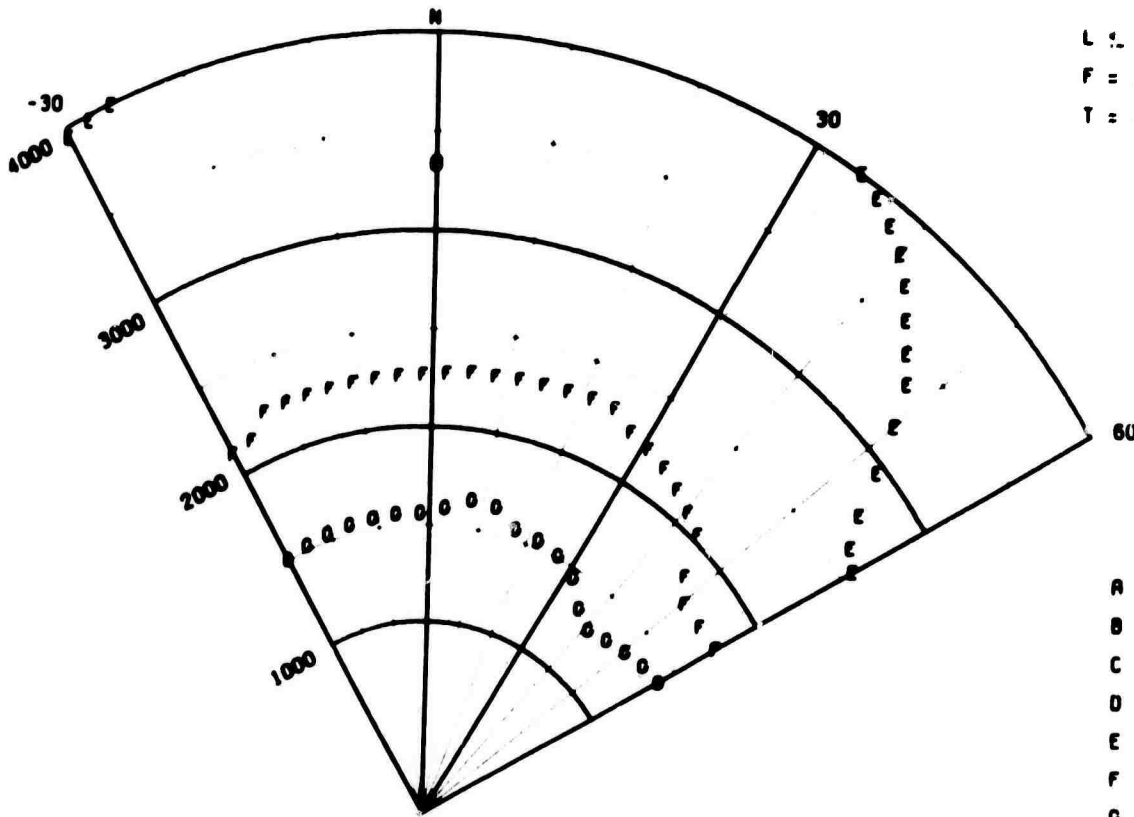
AURORAL ABSORPTION



III-31

Figure 19

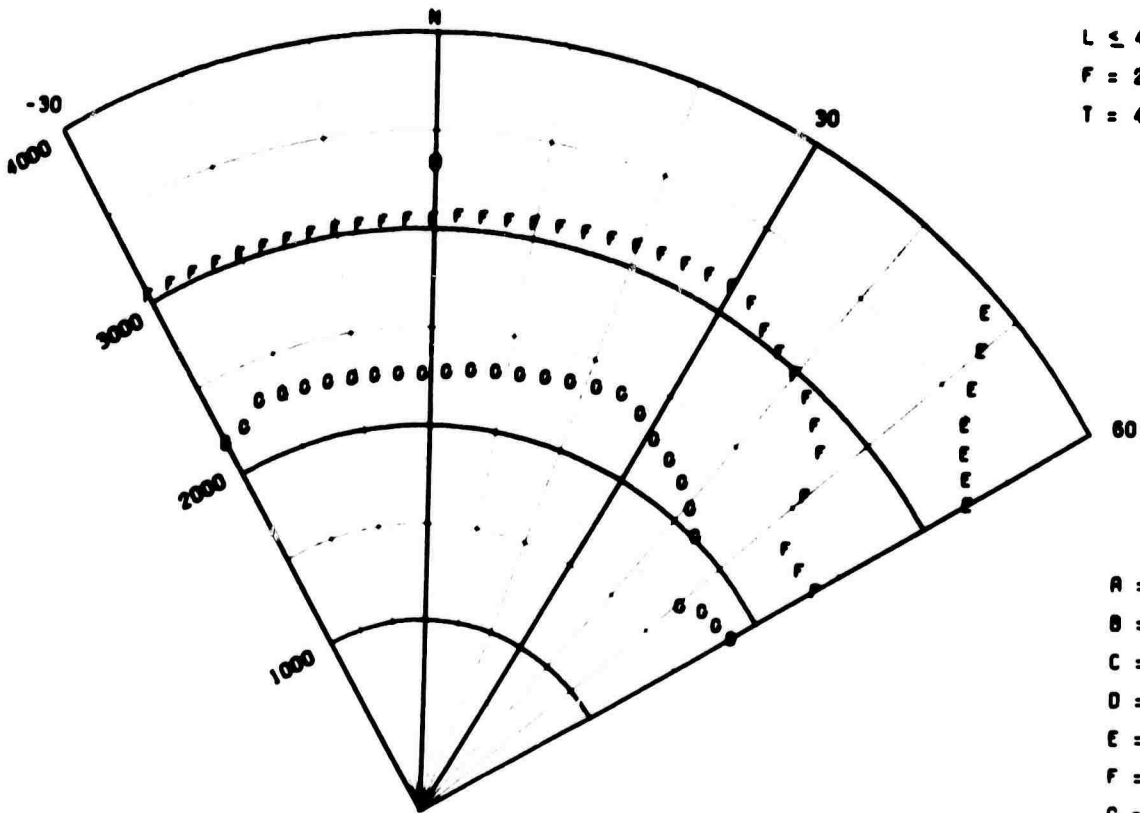
AURORAL ABSORPTION



L = 30 OB
 F = 20 MHZ
 T = 4 UT

A = 75
 B = 80
 C = 85
 D = 90
 E = 95
 F = 98
 G = 99

AURORAL ABSORPTION



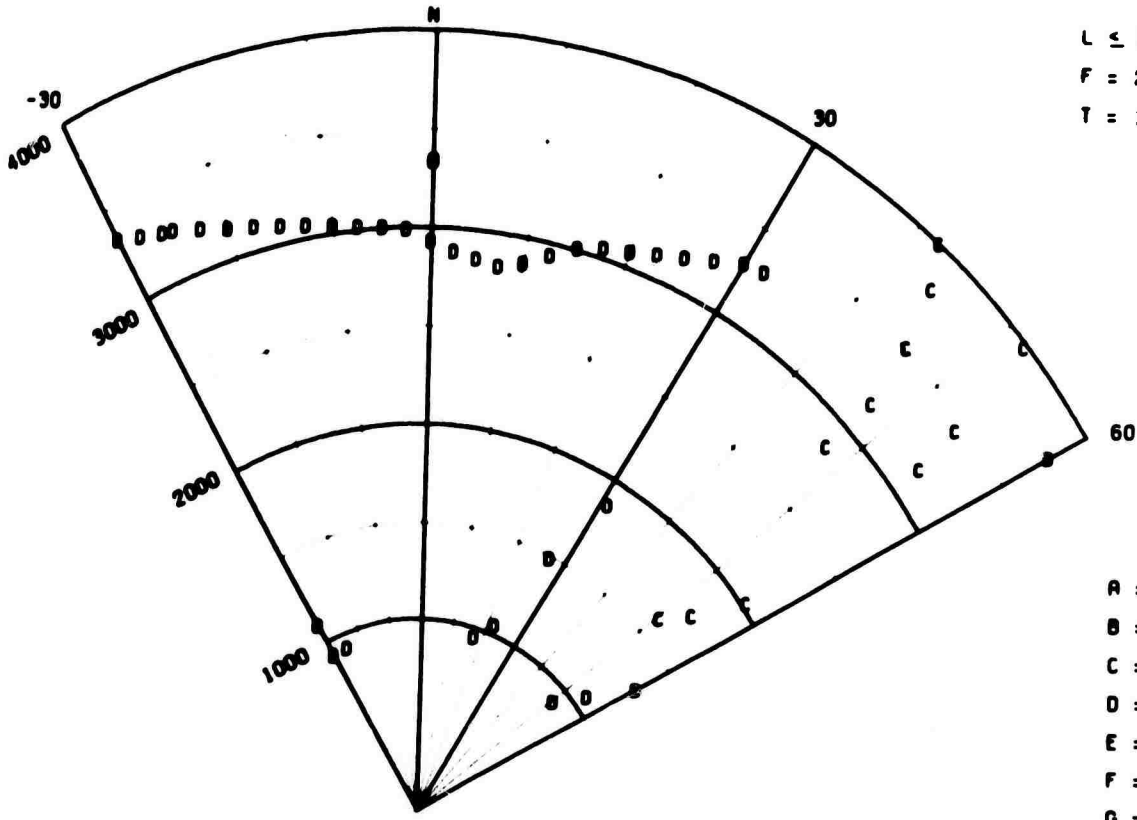
L = 40 OB
 F = 20 MHZ
 T = 4 UT

A = 75
 B = 80
 C = 85
 D = 90
 E = 95
 F = 98
 G = 99

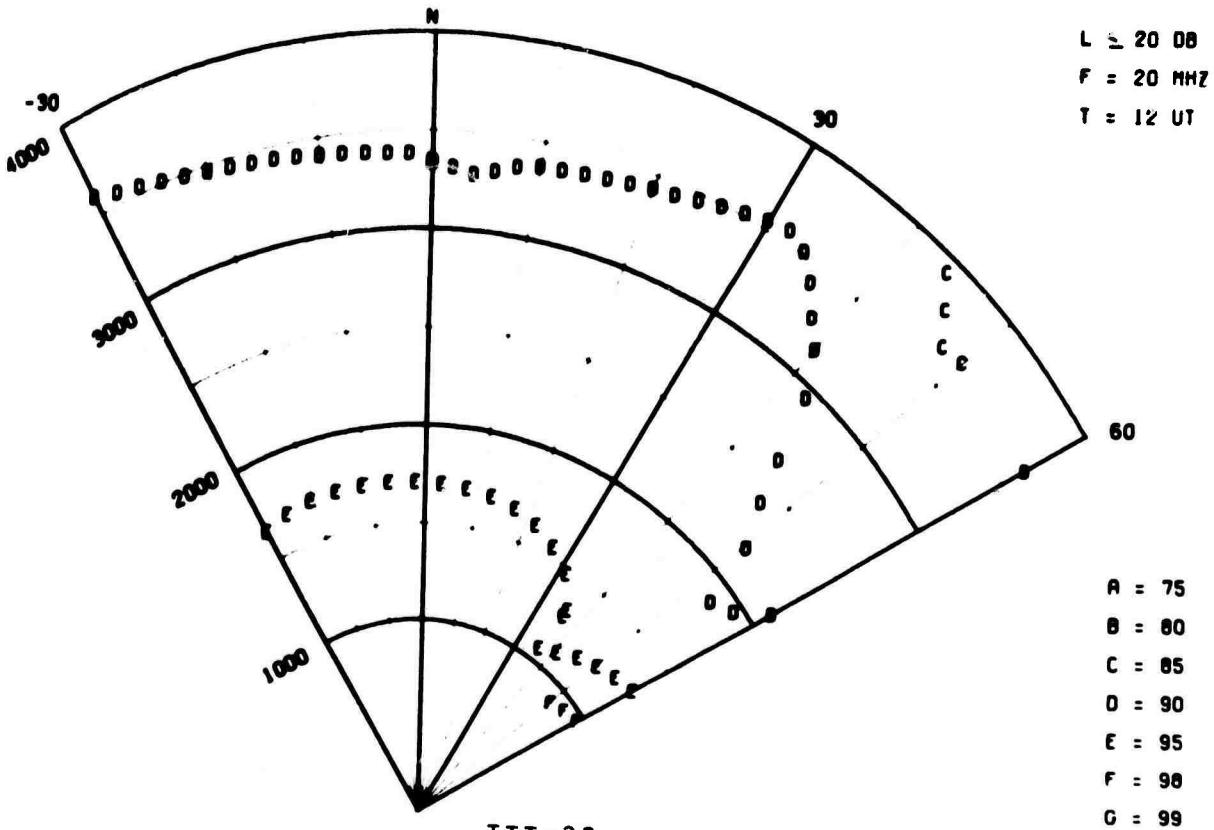
III-32

Figure 20

AURORAL ABSORPTION



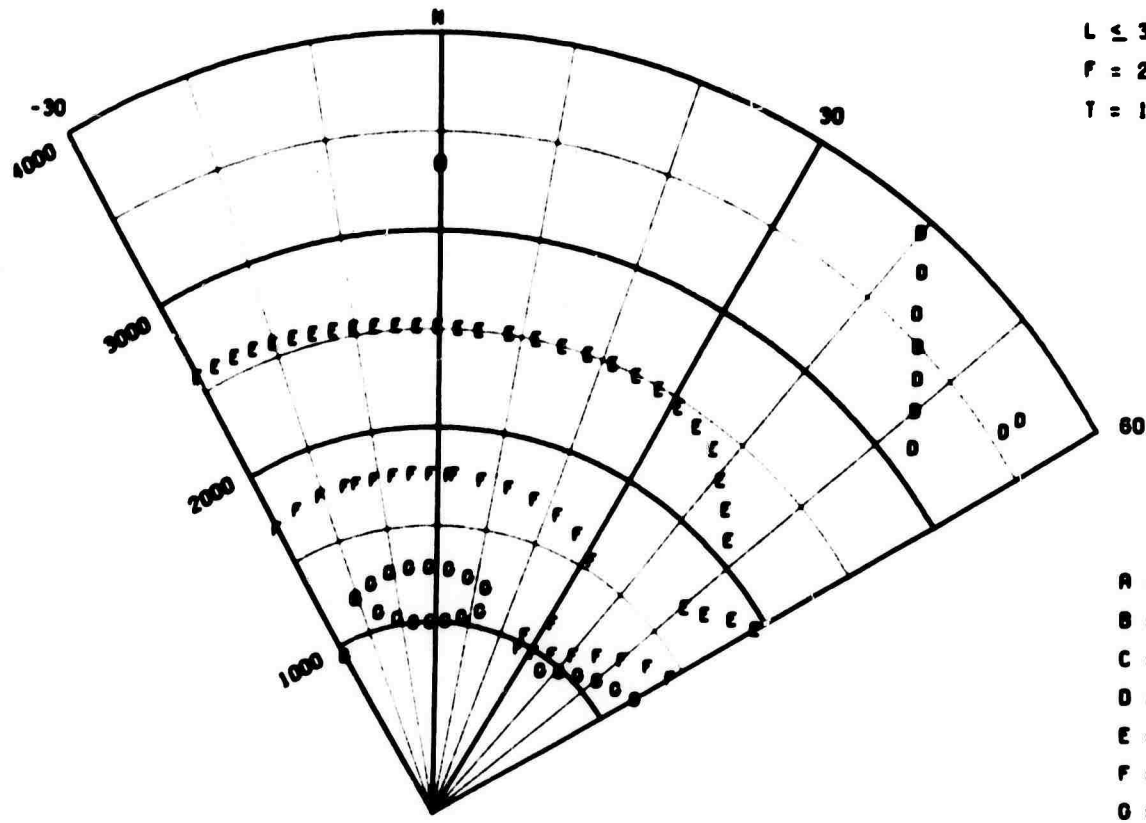
AURORAL ABSORPTION



III-33

Figure 21

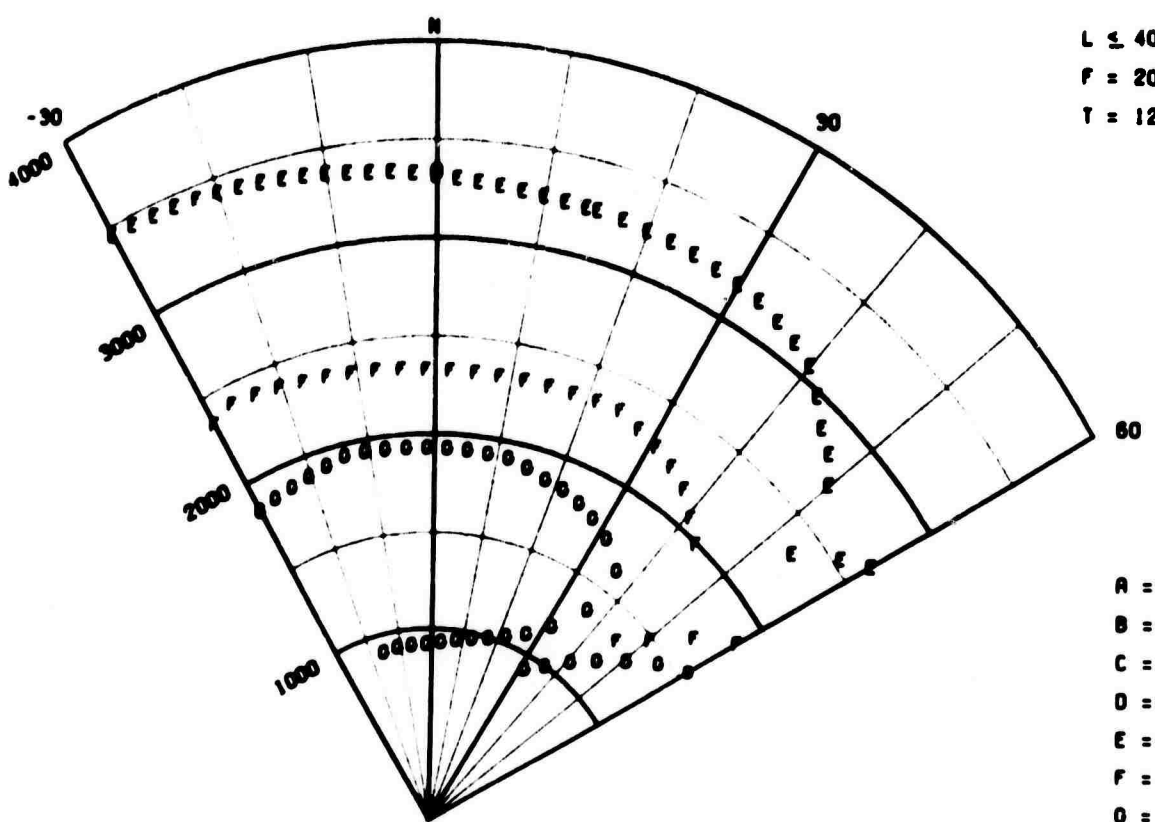
AURORAL ABSORPTION



L ≤ 30 DB
 F = 20 MHz
 T = 12 UT

A = 75
 B = 80
 C = 85
 D = 90
 E = 95
 F = 98
 O = 99

AURORAL ABSORPTION



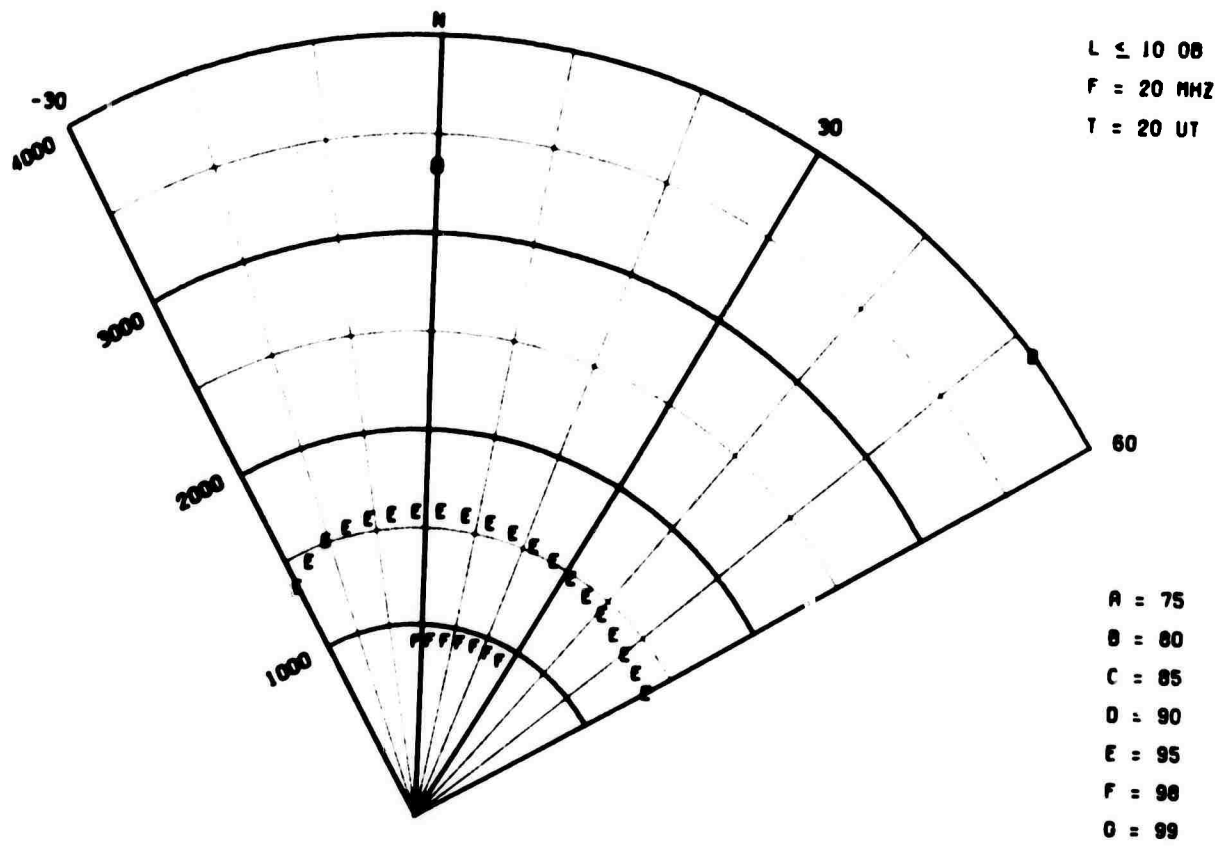
L ≤ 40 DB
 F = 20 MHz
 T = 12 UT

A = 75
 B = 80
 C = 85
 D = 90
 E = 95
 F = 98
 O = 99

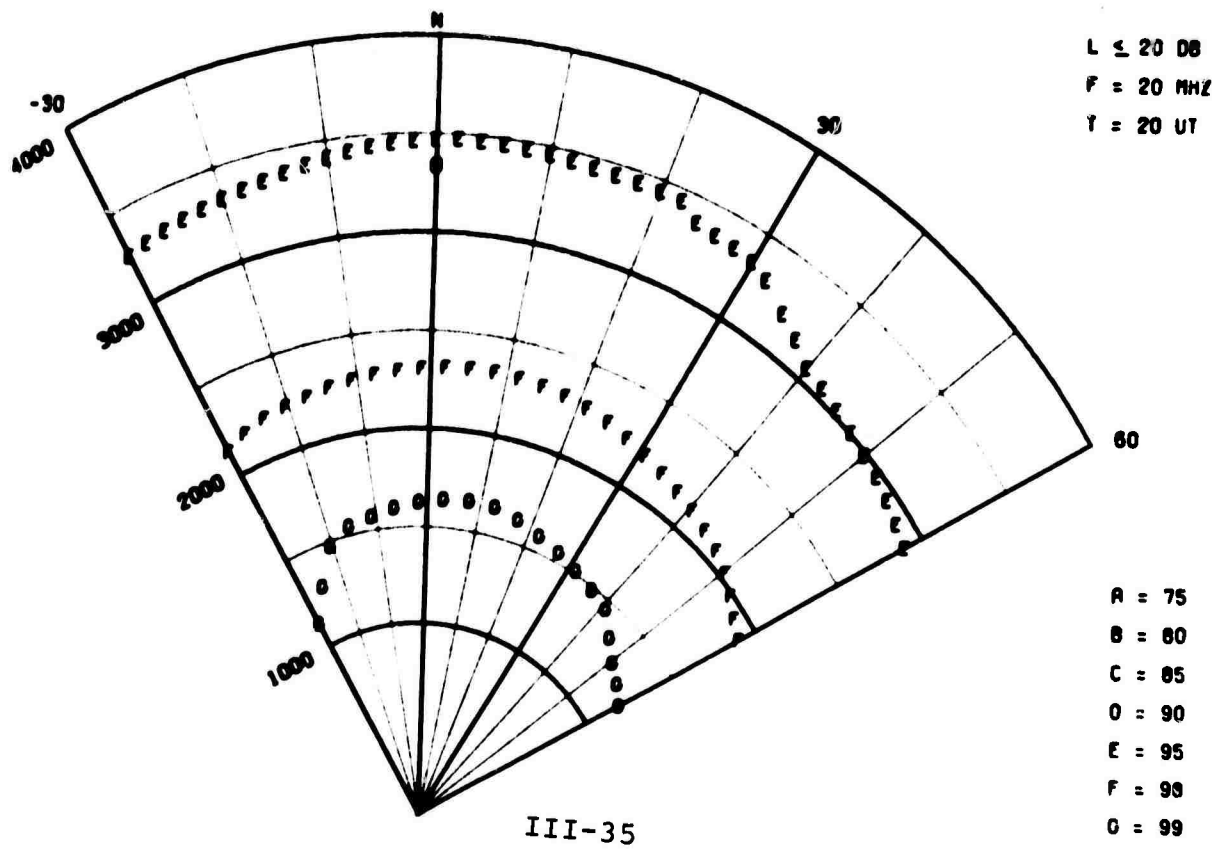
III-34

Figure 22

AURORAL ABSORPTION



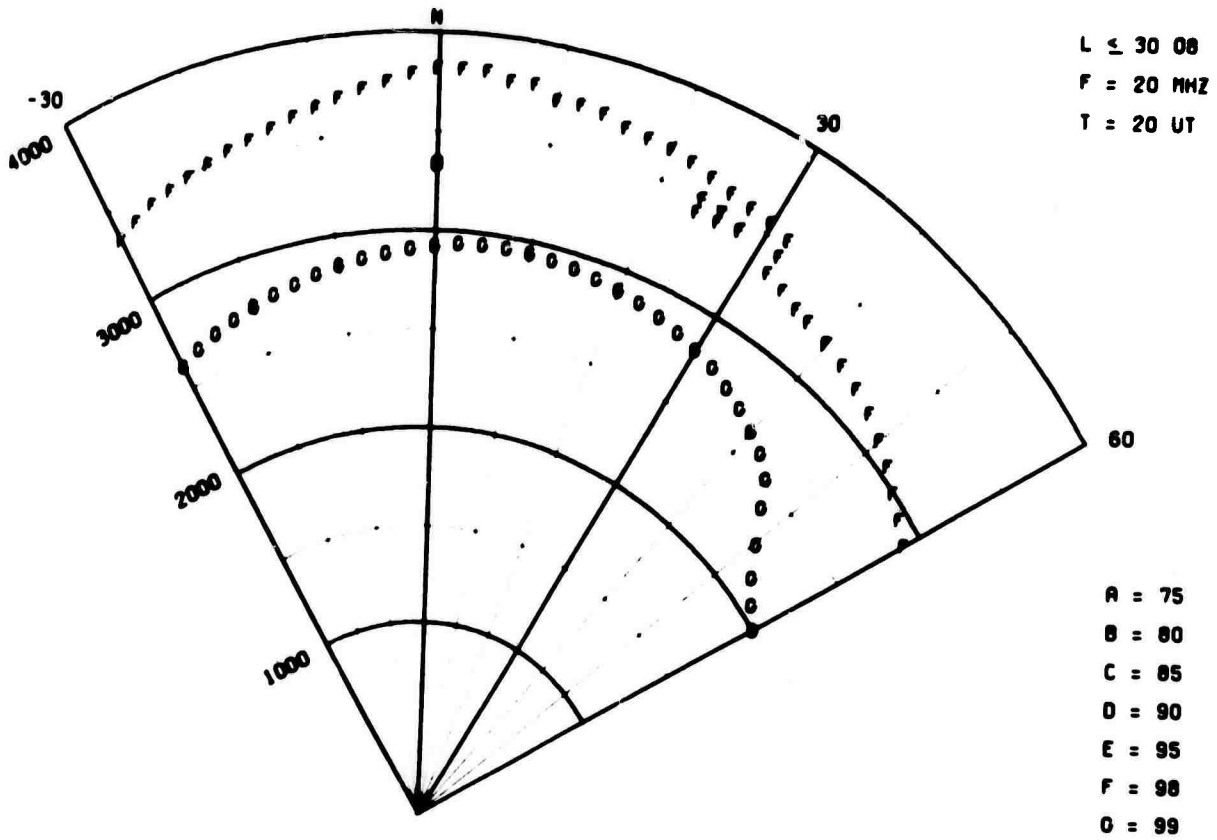
AURORAL ABSORPTION



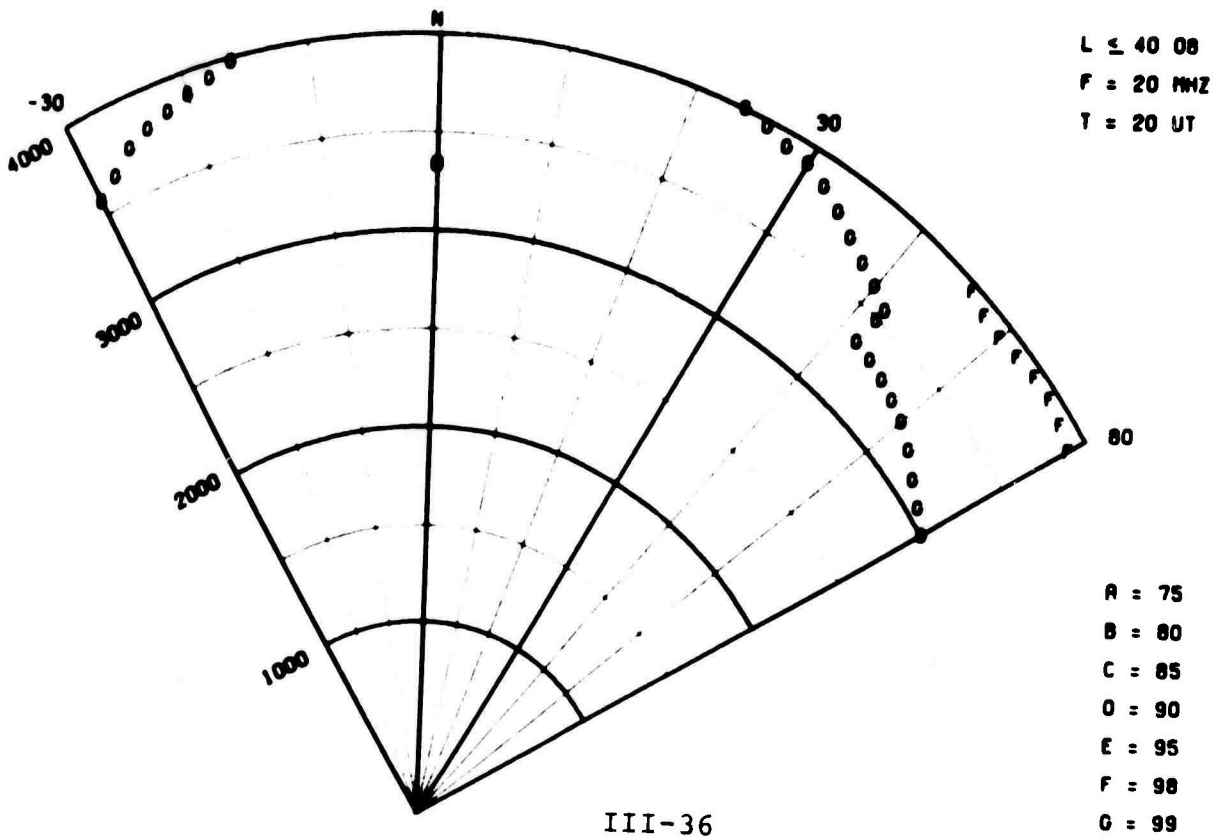
III-35

Figure 23

AURORAL ABSORPTION



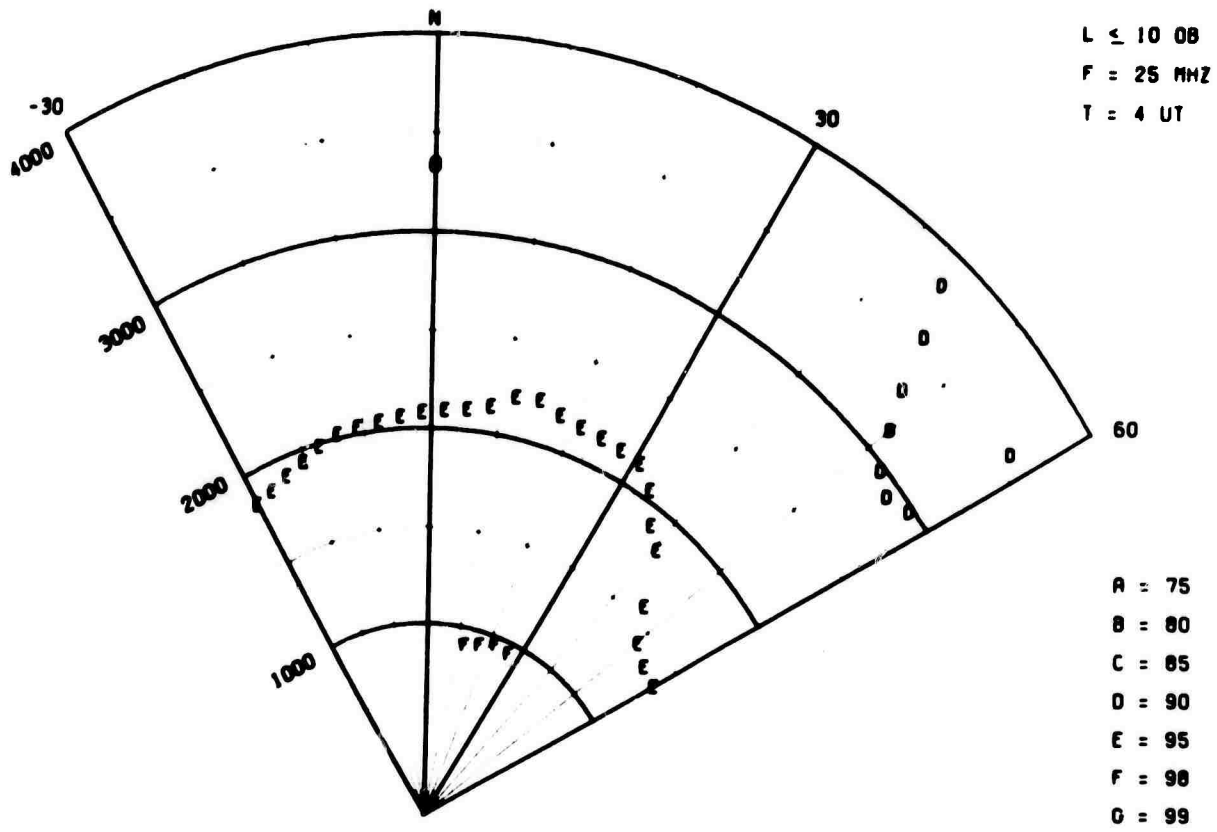
AURORAL ABSORPTION



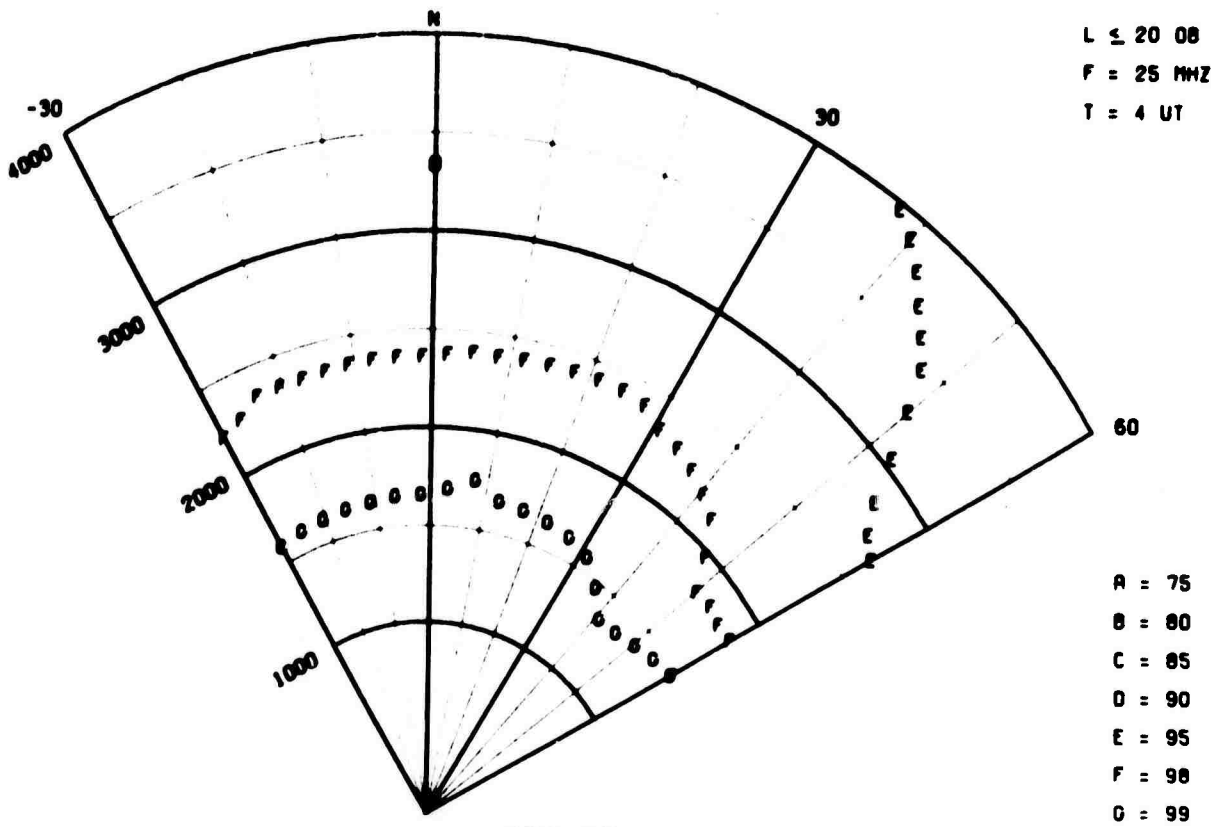
III-36

Figure 24

AURORAL ABSORPTION



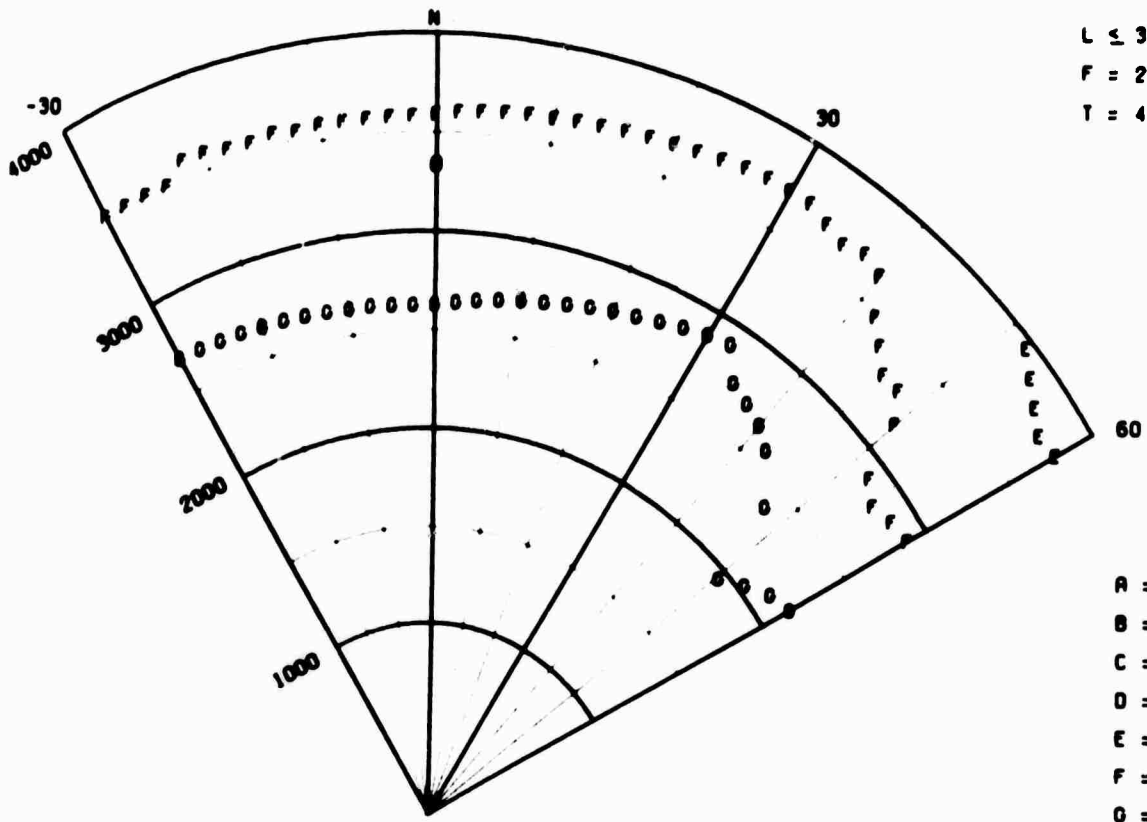
AURORAL ABSORPTION



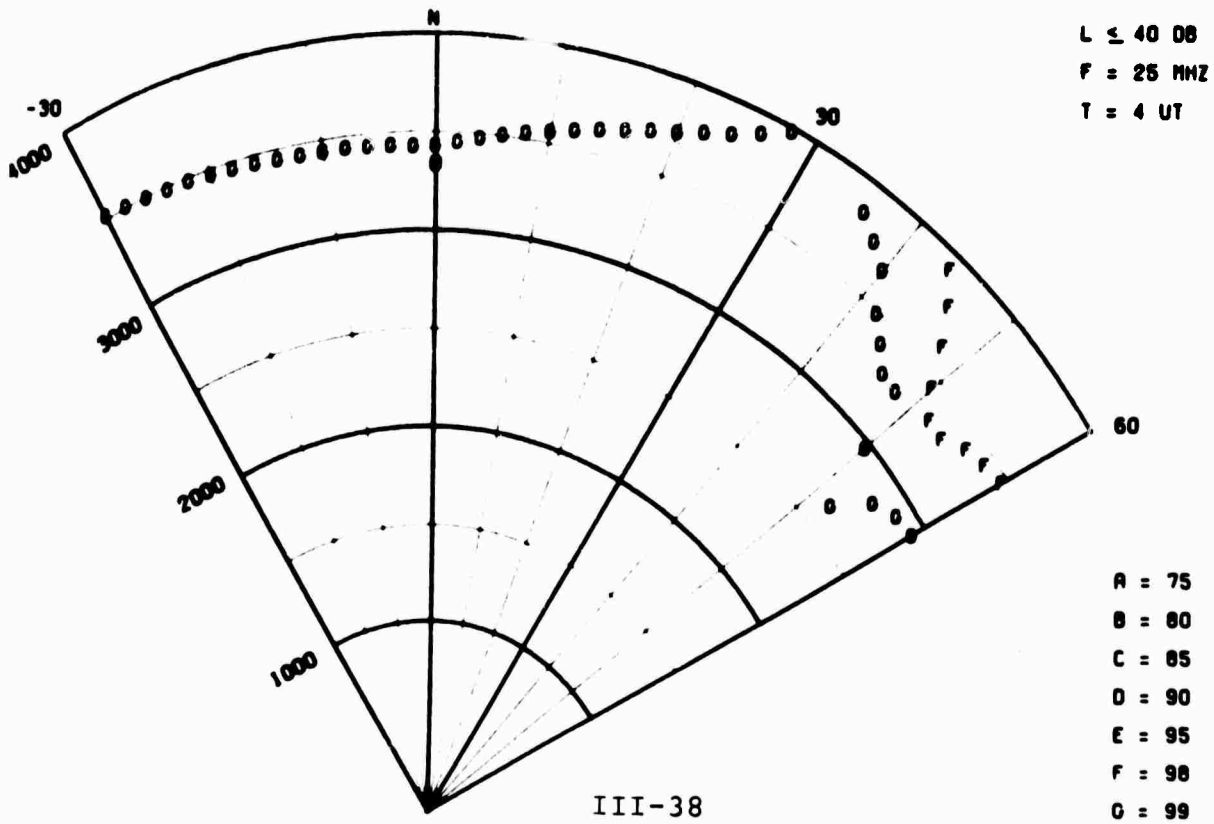
III-37

Figure 25

AURORAL ABSORPTION



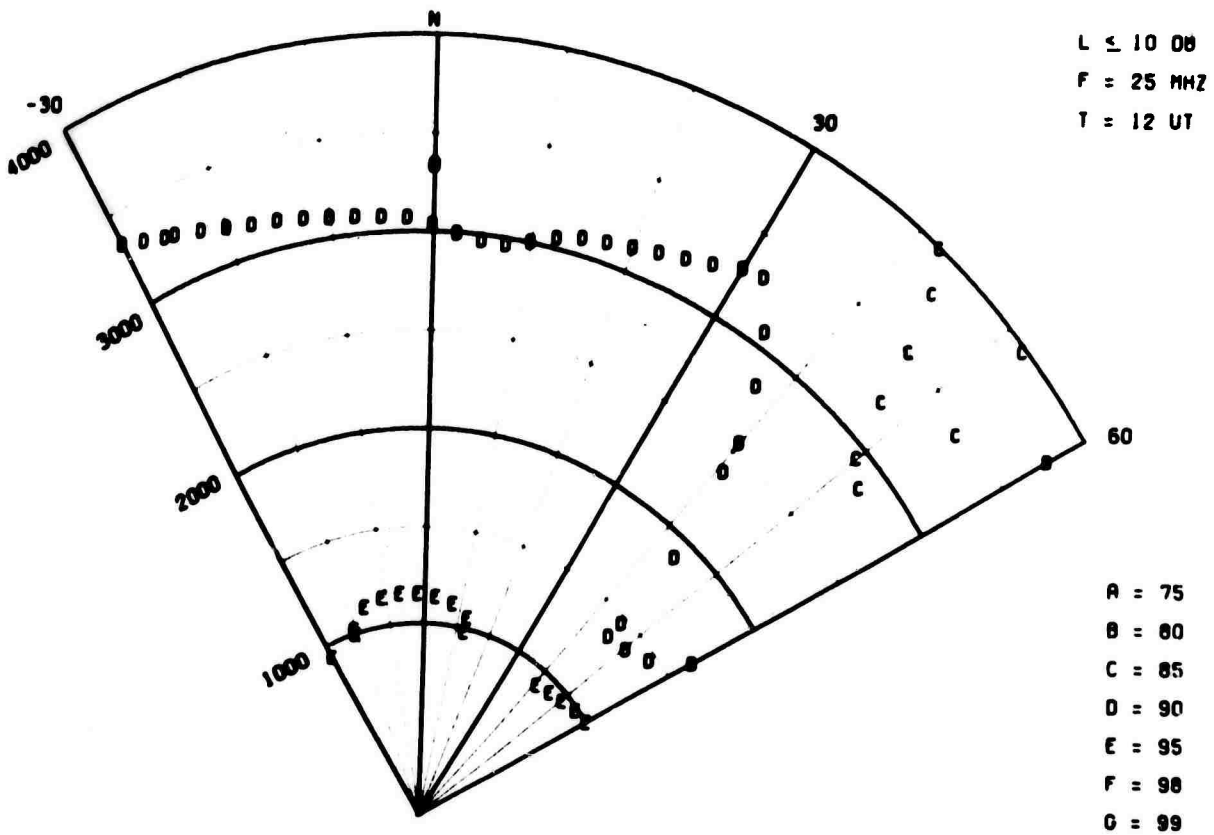
AURORAL ABSORPTION



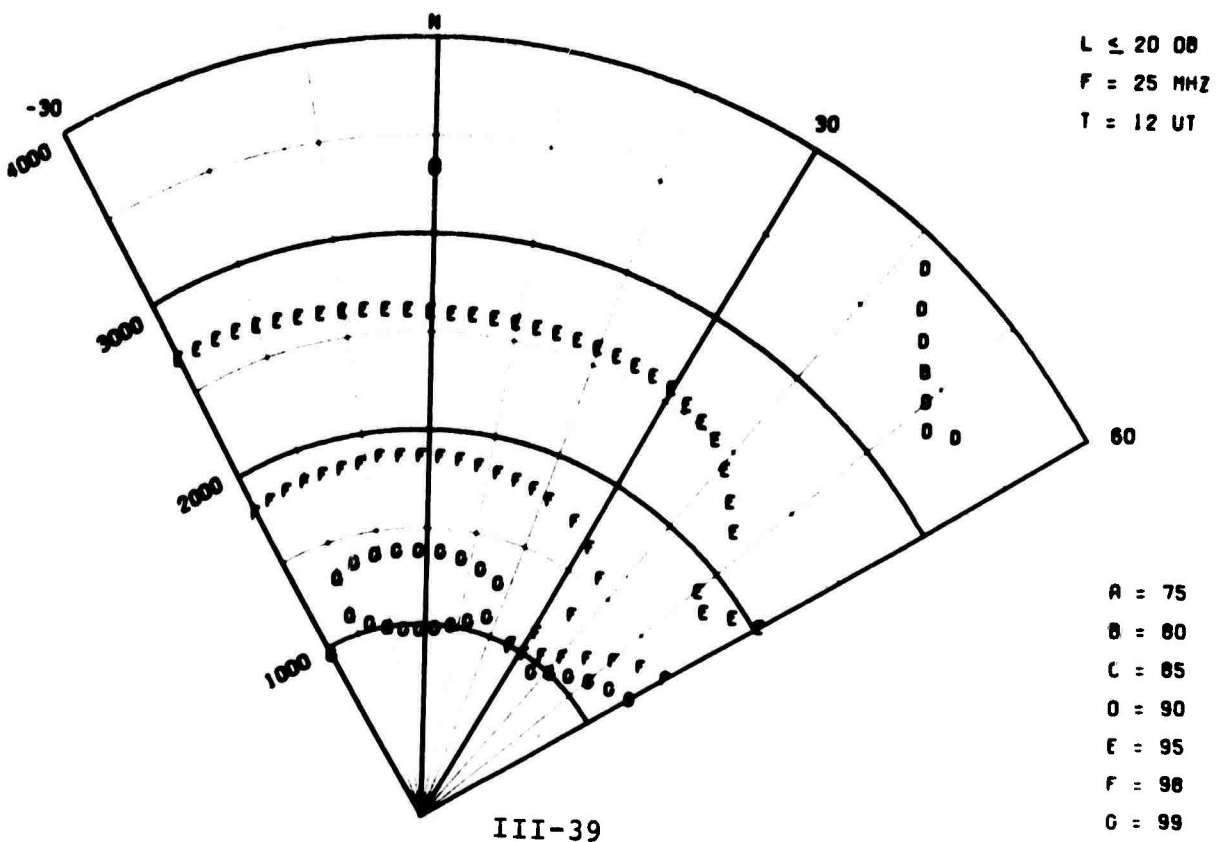
III-38

Figure 26

AURORAL ABSORPTION



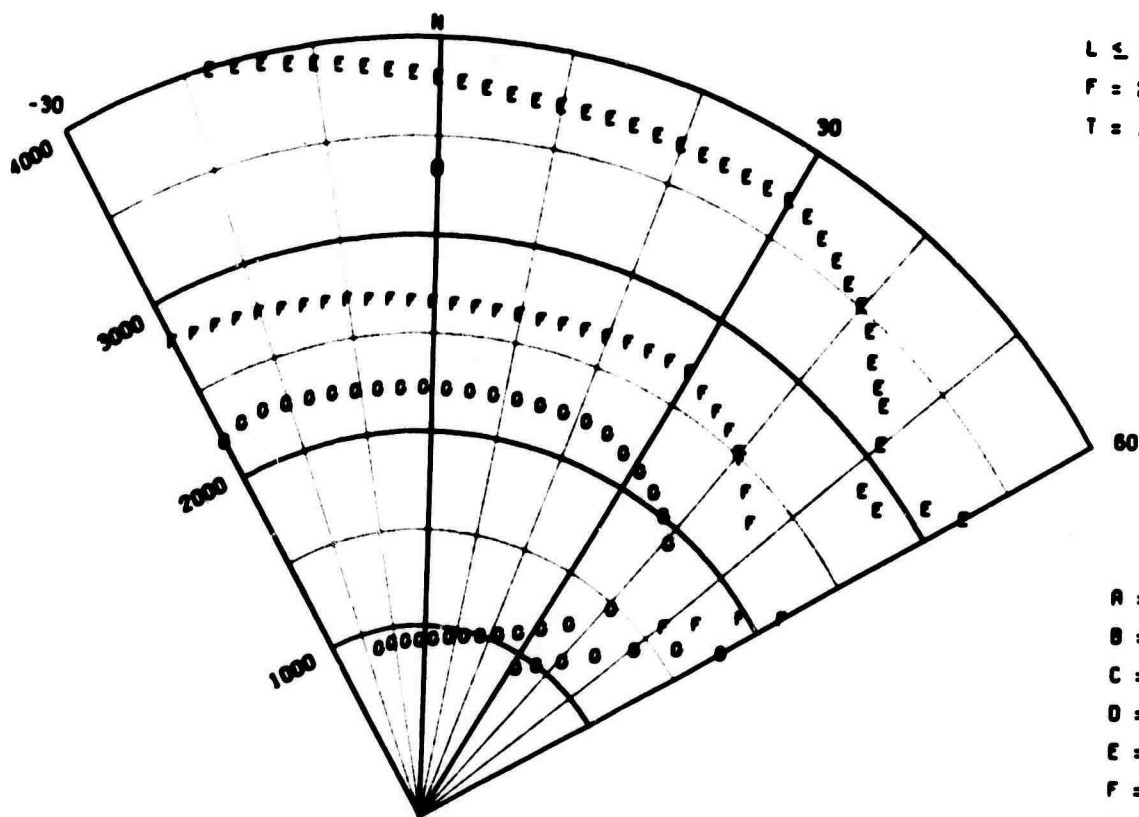
AURORAL ABSORPTION



III-39

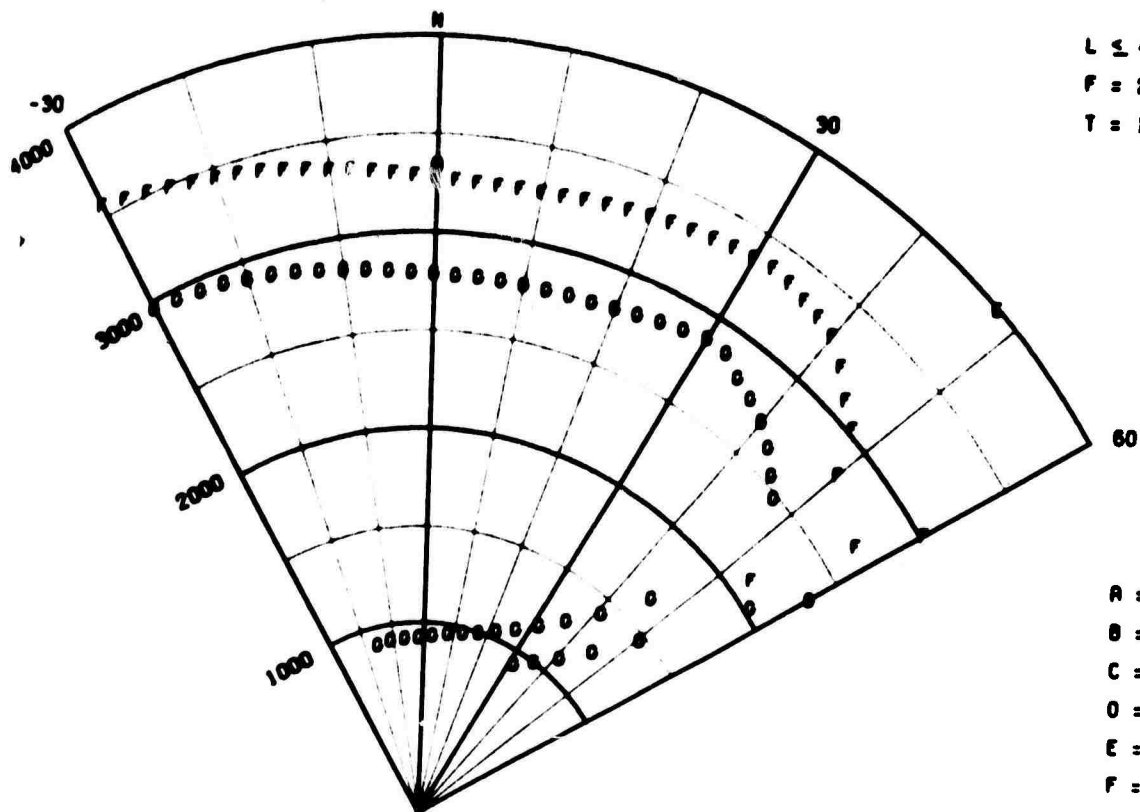
Figure 27

AURORAL ABSORPTION



A = 75
 B = 80
 C = 85
 D = 90
 E = 95
 F = 98
 U = 99

AURORAL ABSORPTION

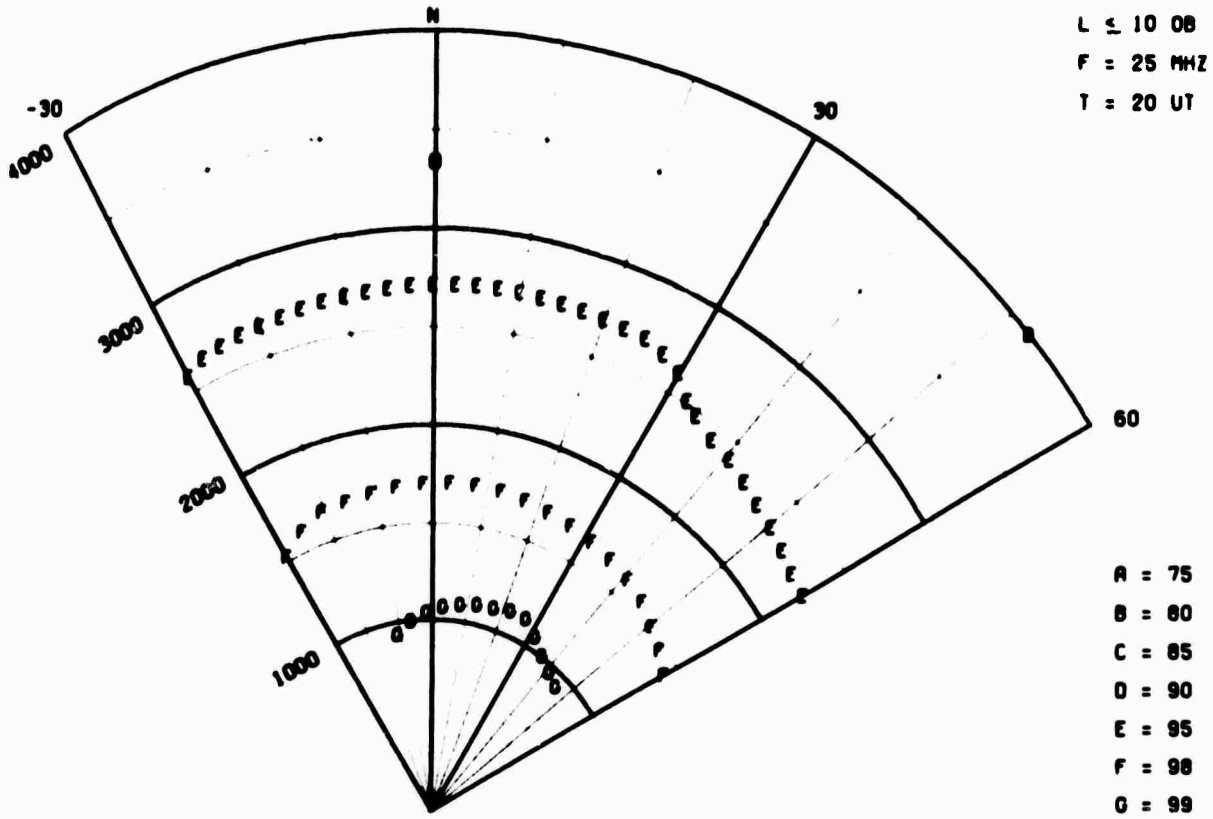


A = 75
 B = 80
 C = 85
 D = 90
 E = 95
 F = 98
 U = 99

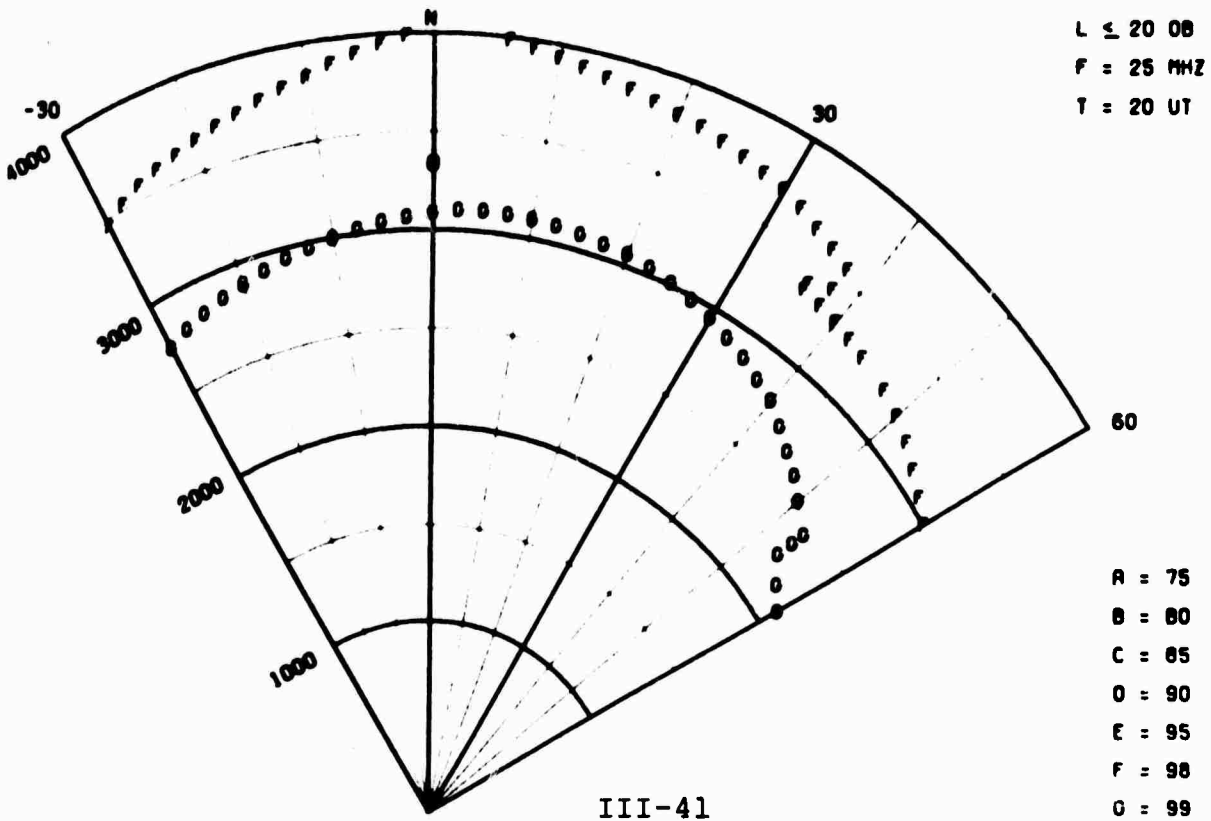
III-40

Figure 28

AURORAL ABSORPTION



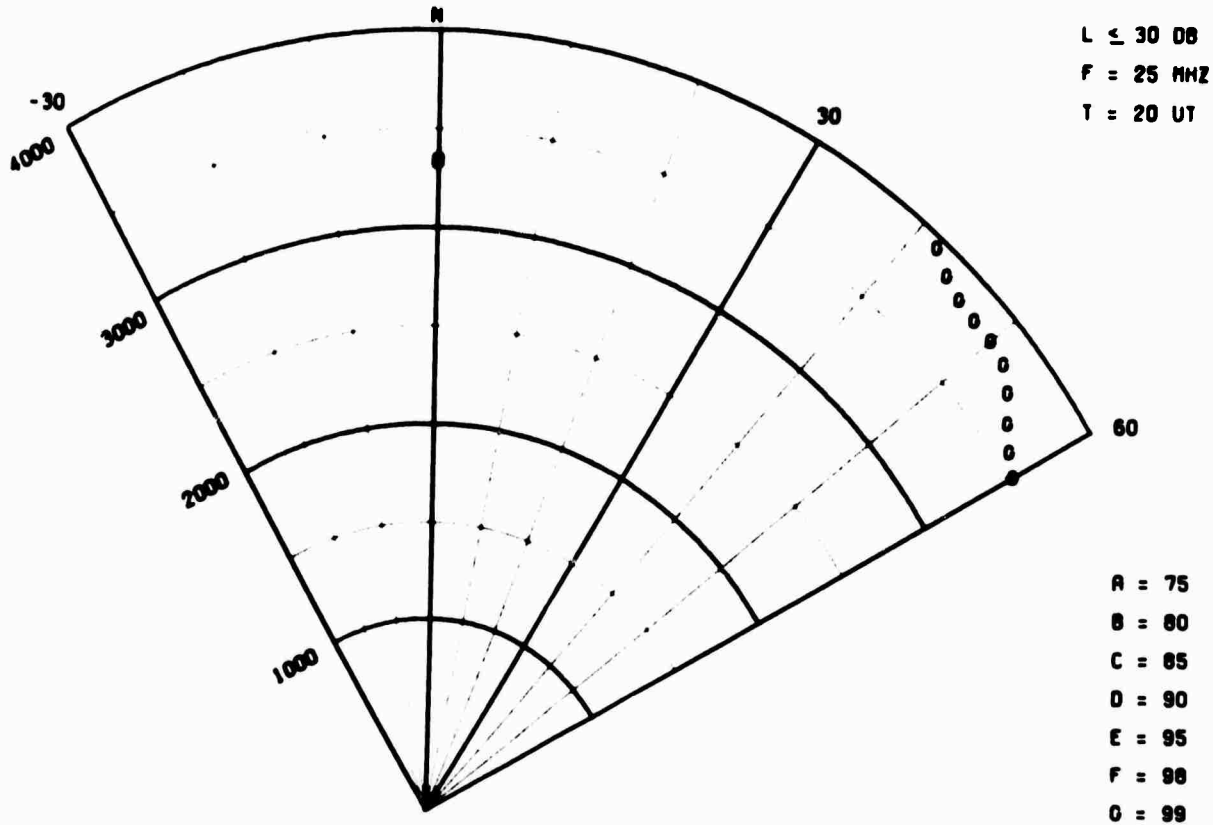
AURORAL ABSORPTION



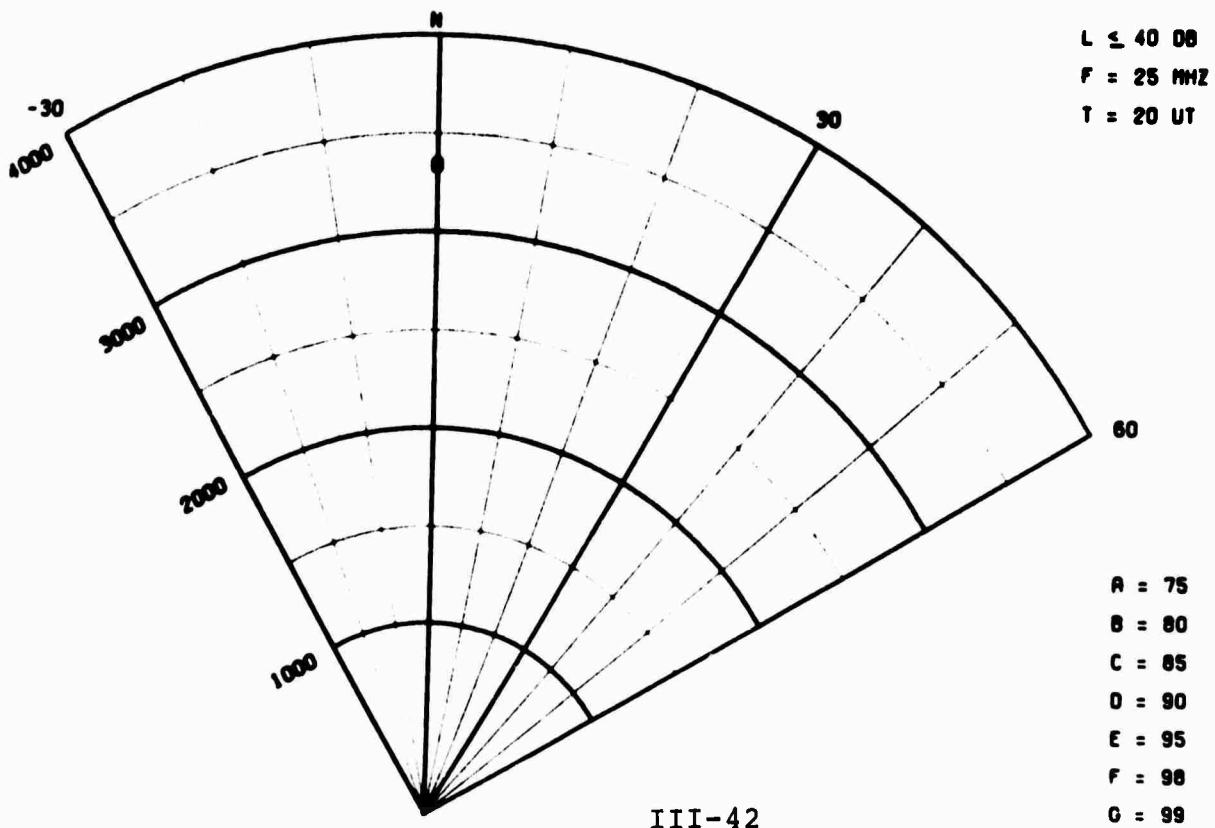
III-41

Figure 29

AURORAL ABSORPTION



AURORAL ABSORPTION



III-42

Figure 30

Analytical Systems CORPORATION 

PART IV: HIGH LATITUDE IONOSPHERIC TROUGHS

by

John R. Herman

IV-1

1.0 INTRODUCTION

A basic feature of the high latitude ionosphere identified only within the past decade by topside sounding techniques (King, et al, 1964; Muldrew, 1965) may have significant impact on the prediction of radiowave propagation in polar regions. This feature, referred to by Muldrew (1965) as the "mid-latitude trough" is a latitudinally-narrow, deep depression in ionospheric electron density compared to the ambient density outside the trough, and it therefore, has steep horizontal gradients near its northern and southern boundaries. With such gradients present, the actual ray/trajectory of a HF radiowave may suffer significant lateral and vertical displacements from the ray path predicted with a smooth model ionosphere without horizontal gradients.

These potentially major discrepancies between actual and predicted ray paths can lead to large errors in locating a backscatter source when interpreting experimental data from Polar Fox II observations. The purpose of this part of our final report, therefore, is to summarize the characteristics of ionospheric troughs in the geographic areas of interest and to make a preliminary assessment of the impact they may have on ray tracing predictions.

A historical perspective of ionospheric trough knowledge is treated in Section 2 to establish the phenomenon as a truly basic feature. The characteristics of the trough are dealt with in Section 3, and their importance in ray-trace calculations for propagation prediction is examined in Section 4.

2.0 HISTORICAL BACKGROUND

Recognition of the existence of a deep narrow trough in ionization density at 1000 km altitude was first made by King, et al (1964) on the basis of early Alouette 1 measurements. Utilizing topside soundings provided by the Alouette 1 sweep frequency ionosonde, Muldrew (1965), showed that the electron density depression extends down to at least the peak of the F layer, established some of the time and space characteristics of the main trough and also showed that additional troughs sometimes occur poleward of the main trough. Measurements made with an ion trap aboard an eccentric-orbit satellite enabled Sharp (1966) to demonstrate that the trough extends below the peak of the F layer, and it exists in the south polar region as well as over Canada.

Further work by Liszka (1967) using Faraday rotation of S66 satellite signals showed that the trough is quite apparent in total electron content and therefore, is not simply the result of a redistribution of ionization below 1000 km.

With a new perspective thus established for certain electron density depressions within the F layer it became possible to reinterpret ground-based ionosonde observations which earlier had been viewed as a "replacement layer phenomenon" (Bellchambers, et al, 1962) "extra traces" (Agy, 1950, unpublished) or moving ionospheric disturbances" (Ansari, 1963). In particular, Stanley (1966) inferred that oblique echoes observed on vertical incidence ionograms taken at polar stations (Bellchambers, et al 1962; Ansari 1963; Herman 1966b) were in fact reflections from the poleward side of the trough as it moved toward the station.

Bowman (1969) compared southern hemisphere ionosonde data with a conjugate projection of Muldrew's (1965) results to verify that the bottomside and topside observations are manifestations of the same phenomenon - an electron density trough extending all the way through the F layer.

Further, Bowman (1969) utilized true height analysis to obtain two dimensional electron density distributions (in altitude and transverse horizontal displacement across the trough) at times when the trough was in the neighborhood of Ellsworth, Antarctica. These distributions indicate that the decreased electron density within the trough extends at least down to the bottom of the F layer and according to Bowman, probably into the E layer.

Subsequent study of Explorer 22 Langmuir probe data (Miller, 1970) has shown that the mean position of the main trough is independent of the solar cycle (at least in Winter for the years 1964 to 1967). The minimum electron density in the trough center is about a factor of 3 higher near solar max than min, but since the F region electron density is generally much higher in maximum years, it appears that the relative depth of the trough may not be significantly changed. Miller's (1970) results indicate that high latitude troughs poleward of the main trough are much more variable in occurrence both temporally and spatially in solar maximum years.

Rycroft and Thomas (1970) have drawn upon the results of these earlier works to establish that statistically the main trough center is along the same L shell as the plasmopause

identified by Carpenter (1963;1966) and thereby, provided insight into the trough's relationship with the magnetosphere.

The culmination of the discovery and definition of the main trough as directly related to the Polar Fox II interests is given by the ray trace results of Thompson (1970), who showed that refraction effects leading to pronounced azimuthal and vertical deviations may be expected on HF (6 MHz) ray trajectories when the trough center is situated 100 km from the transmitter site.

Since the main trough seems to be irrefutably established as a more or less permanent feature of the ionosphere in the general vicinity of 60° geomagnetic latitude, and since significant HF propagation effects have been demonstrated under certain conditions, it is apparent that the phenomenon should be examined in detail.

3.0 TROUGH CHARACTERISTICS

3.1 GENERAL FEATURES

The midlatitude trough identified by Muldrew (1965) is most pronounced in Winter on the night side. In this report it is referred to as the main trough. It first becomes evident nominally at about 1400 LT at a latitude corresponding to an L shell of approximately 10, gradually shifts equatorward to about L=4 near local midnight and poleward again after midnight to L \approx 5 where it disappears around 0700 LT. The latitudinal width of this main trough is typically about 6°, and it is aligned approximately magnetically east-west. The background-to-trough electron density ratio is generally greater than 4 to 1. With increasing magnetic activity the trough position moves equatorward about 3.5° per unit increase in K_p . Poleward of the main trough so-called "high latitude" troughs are often seen (Muldrew, 1965), but their appearance is sporadic with respect to both time and position.

3.2 DIURNAL AND LATITUDINAL VARIATIONS

An example of the latitudinal variation in f_xF_2 (extraordinary wave critical frequency at F peak) for a nearly constant local time is illustrated in Figure 1 (reproduced from Muldrew, 1965). Contours of constant f_xF_2 (roughly proportional to the square root of the peak electron density) have been constructed from consecutive Alouette 1 crossings from 16 UT Oct. 30, to 05 UT, Oct. 31, 1962, and displayed in geographic coordinates. Due to the satellite precession, these UT times all correspond to about 1800 LT at the subsatellite point. Note that f_xF_2 is about 2.4 MHz in the center

of the main trough and 5 MHz at its equatorward edge (this is roughly a factor of 4 difference in peak density).

Geographically, the trough center latitude decreases from about 60°N at 25°W to 52°N at 65°W and then increases again to 70°N at 145°W. In geomagnetic coordinates these latitudes are all approximately equal to 65°N. Thus, there appears to be no dependence of the latitudinal position on longitude, at least at 1800 LT.

Jelly and Petrie (1969) and Bowman (1969) have extended this coordinate conversion to all local times of the day with additional data appropriate for $K_p = 2$ in Winter and expressed the results in geomagnetic latitude/local time (G/T) space. Their findings are replotted in Fig. 2 (heavy line) wherein it is readily seen that when the main trough first appears at about 1400 LT it is at a geomagnetic latitude of 74° ($L \approx 10$); by midnight it has moved southward to 59° ($L \approx 4$). If there are no longitudinal complications, and there seem to be none, then the main trough position in G/T space can be considered as fixed with reference to the sun while the Earth rotates beneath it once per day. With the aid of an overlay in range/azimuth (R/A) space as described in part 1 of this report, this sun-oriented pattern can be described in terms of the experimental configuration as a function of UT. The mean positions for very quiet ($K_p=0$) and disturbed ($K_p=4$) magnetic conditions as deduced from Muldrew's (1965) scaling factor are illustrated as dashed lines in Fig. 2.

3.3 SEASONAL AND SOLAR CYCLE VARIATIONS

Muldrew (1965) has observed that the main trough persists for a longer period of the day in Winter compared to Summer. In Winter (November to March) it develops at about 1400 LT (Muldrew 1965), but in Summer (April to August) the main trough becomes evident at about 2000 LT (Rycroft and Burnell, 1970). The mean latitudinal position appears to be insensitive to season.

The occurrence frequency of a well-defined main trough appears to be about 60% between 2000 and 0700 LT in April to August (Rycroft and Burnell, 1970), and in Winter it is evident nearly every night over Canada (Muldrew, 1965). If it is assumed that observations of "extra traces" or "moving ionospheric reflections" can be interpreted as HF echoes from the edge of the trough (see Section 2), then early unpublished work by Agy, in 1950 (discussed by Herman, 1966b) indicates that the trough is also a nightly occurrence in Winter over Alaska.

Solar cycle variations deduced by Miller (1970) for 1000 km density indicate that the mean trough position does not change, but the minimum electron density at the trough center is a factor of about 3 higher in high - compared to low - sunspot years. Based on ground-based ionosonde data, Stanley (1966) has speculated that the trough may exist only in low-sunspot years; however, Bowman's (1969) analysis based on 1958 (IGY) ionograms from Antarctic stations reveals very pronounced trough occurrence at and below the F-layer peak in sunspot maximum years. There is little question that the main trough will be a major feature of the polar ionosphere to be reckoned with in mid-solar cycle

years (1971-1972). As mentioned in Section 2, there are additional steep troughs poleward of the main trough in both high sunspot years (Miller, 1970) and low years (Muldrew, 1965), but since their occurrence is random it is difficult to make average predictions. Their effect on HF propagation though, is expected to be similar to that due to the main trough; this fact should be considered in interpretations of oblique-incidence experimental data.

3.4 TROUGH STRUCTURE

For application to ray tracing the foregoing gross statistical properties of the main trough are insufficient; also required are the structural characteristics including latitudinal width, maximum depth of the trough relative to the ambient ionization density gradient across the boundary, and hopefully, the electron density distribution at and below the F-layer peak throughout the trough region. In this section a preliminary assessment is made of the structural properties. Additional results are expected as a result of ongoing work.

A typical example of trough structure at the F peak observed on a single pass of Alouette 1 over Canada is given in Fig. 3 (reproduced from Muldrew, 1965). Attention is drawn to the main trough centered at about 45°N (57°N geomagnetic), where the minimum plasma frequency is about 2 MHz compared to 6 or 7 MHz south of the trough. The background-to-trough electron density ratio (where $N = 1.24 \times 10^4 \times f_p^2$ with f_p in MHz) is thus about 10:1. A trough passage over Ellsworth as analyzed by Bowman (1969) and reproduced in Fig. 4, reveals a ratio of about 11:1 (f_p ratio of 5:15) on both equatorward and poleward sides of the center when the maximum f_p of 10 MHz in the Antarctic bulge (Rourke, 1966) is ignored. The ratio of 10:1 is therefore, considered to be typical.

Using Calvert's (1966) definition of "logarithmic density gradient" as dN/Ndx , the fractional change in electron density per unit horizontal distance, we find a gradient of $6.2 \times 10^{-2} \text{ km}^{-1}$ across the lower boundary of the main trough in Fig. 3. Other observations of the electron density variations in this area in different years with different techniques reduce to essentially the same gradient, i.e. $6 \times 10^{-2} \text{ km}^{-1}$ (Calvert, 1966; Sharp, 1966; Ulwick, et al, 1964). This typical magnitude is a factor of about 600 greater than horizontal gradients observed in a quiet midlatitude ionosphere (Herman, 1967). Gradients associated with high latitude troughs are typically .01 to .05 km^{-1} .

Main trough latitudinal halfwidths range from about 2° to 5° (Muldrew, 1965; Calvert, 1966), but on occasion seem to range up to 15° latitude (Sharp, 1966). For the present we follow Jelly and Petrie (1969) and consider Sharp's (1966) wide troughs to be atypical, and restrict our upper limit to 5° . The particular main trough example in Fig. 3 is illustrative of a 5° halfwidth. The high latitude troughs are 1° to 3° typically. The main trough example in Fig. 4 has a halfwidth of about 3° (325 km).

Bowman (1969) performed true height analysis on a sequence of ionograms taken during a main trough passage over Ellsworth to obtain plasma frequency vertical profiles. Knowing the relative speed of the trough as it passed over the station, he was able to relate the time sequence to appropriate horizontal ranges for placement of the vertical profiles. Contouring of constant f_p in height and range then yielded the distribution of ionization reproduced here in Fig. 4. Worthy of note is the

considerable rise in layer base true height along with the decrease in plasma frequency. Further note that poleward (to the right) of the trough the ambient layer is somewhat thicker, has a higher peak height and lower peak density than the layer well equatorward of the trough. Since the speed of the passage depicted in Fig. 4 was 111 m/sec, just the average speed of an average trough found by Bowman in a number of cases (see Section 3.4 above) it is tentatively concluded that the electron density distribution in Figure 4 can be considered to be a typical of main troughs.

Possible variations in the above typical values of the structural parameters with season, magnetic activity and other factors have not been investigated yet, but will be addressed in ongoing work.

4.0 APPLICATION TO RAY TRACING

In investigating ionospheric trough effects on HF ray path trajectories, no ray tracing has been attempted under the study phase being reported here. The present assessment is made solely on the basis of calculations performed by Thompson (1970).

For a trough input model, Thompson utilized essentially the same information discussed in the previous section (3.6) to derive the version reproduced here in Fig. 5. For simplicity, however, he ignored differences in ambient ionization north and south of the trough and made it symmetric about the center.

Ray tracing was accomplished with a version of the ESSA (Jones 1966) three-dimensional ray tracing program adapted to a Boeing computer. The trough model was introduced as a perturbation on the normal ionosphere. Besides determining three-dimensional ray paths, Thompson (1970) also computed radiowave absorption, doppler shift and wave focusing and defocusing associated with the trough model. Rather than reiterate details here, the reader is referred to the cited Thompson report.

In summary, however, Thompson found that "ray path trajectories are significantly affected in the vicinity of the trough; the rays whose wave reversals occur near the trough center are the most severely affected."

Also, certain high angle ($>60^\circ$) waves obliquely incident on the trough may actually be reflected back to the transmitter, which is in agreement with the "extra traces" and oblique echoes observed on ionograms (Section 3). Typical doppler shifts associated with reported trough velocities are on the order of ± 2 Hz. In general, rays reflected from near the center of the trough are focused while those from near the edges are defocused. The major finding in the absorption phase of Thompson's (1970) study is that "the signal strength is in general maximized when the trough is near the point at which the ray enters or exists (sic) the ionosphere."

Two projections of ray path trajectories on the surface of the earth were computed. Both assumed a signal frequency of 6 MHz and a ground transmitter location 100 km poleward of the trough center (this situation may be encountered at night in Polar Fox II when $K_p \approx 2$; c.f. Fig. 2). The results are reproduced in this report as Fig. 6 (assumed elevation angle was 60°) and Fig. 7 (for 30° elevation).

In general it was found that the lateral (or azimuthal) deviations were greatest when the wave was launched parallel to the orientation of the trough and least when perpendicular to it. In Fig. 6, it can be seen that bearing errors of up to 40° can be introduced in signals propagating in the neighborhood of the trough. With a smaller take-off angle of 30° the amount of

lateral bending (and bearing error) appears to be smaller (Fig. 7) under the same conditions.

Thompson's (1970) results are important to the present effort in that they show that significant HF propagation effects due to the ionospheric trough may be expected under certain conditions. The significance of these effects suggest that additional ray tracing with more realistic trough models and geometries (take off angles, location of transmitter relative to trough) more appropriate to Polar Fox II experiments should be performed.

5.0 SUMMARY

The possible importance of ionospheric troughs to Polar Fox II experiments has been examined and found to be sufficiently significant to warrant further investigation.

The existence of the main trough as a basic and permanent feature of the polar ionosphere is established through a historical survey of its discovery and subsequent study by topside sounding techniques and reinterpretation of conventional (bottomside) sounder observations of some years standing.

The main trough is identified as a deep narrow depression in electron density, oriented approximately magnetic east-west along a shell of 7 in the afternoon and 3.5 at night under average magnetic conditions ($K_p \approx 2$). It is typically a few degrees of latitude wide and its electron density is 10x lower than background. With increasing magnetic activity the trough migrates southward. Its mean position and its typical width and density characteristics appear not to change with the solar cycle.

Under some conditions when an oblique incidence transmitter is in the neighborhood of the main trough, there can be significant deviations in the ray path trajectories computed by ray tracing techniques. At fairly high elevation angles on 6 MHz, azimuthal deviations leading to serious bearing errors of up to 40° are found. It is recommended that additional ray tracing be performed.

6.0 REFERENCES

- Ansari, Z.A., 1963, J. Atmos Terr. Phys., 25, p. 210
- Bellchambers, W. H., et al, 1962, R. Soc. IGY Expedition Halley Bay, D. Brient Ed, p. 179
- Bowman, G.G., 1969, Planet. Space Sci., 17
p. 777.
- Calvert, W., 1966, J. Geophys., Res., 71 p. 3665.
- Carpenter, D. L., 1963, J. Geophys, Res., 68
p. 1675.
- Carpenter, D.L., 1966, J. Geophys. Res., 71
p. 693.
- Gassmann, G.J., 1971, Paper presented at ARPA/
Air Force Review Meeting, Washington, D.C., March.
- Herman, John R., 1964, Research on Spread F studies
AVCO Corp, Report No. RAD-TR-64-9.
- Herman, John R., 1966b, Rev. Geophys., 4, p. 255.
- Herman, John R., 1967, GCA Corp., Rpt. No. GCA-TR-
671.
- Jelly, D. H. and L. E. Petrie, 1969, Proc. IEEE,
57, p. 1005.
- Jones, R. M., 1966, ESSA Tech Rpt. IER 17-ITSA 17.
- King, J. W., et al, 1964, in Electron Density Distribu-
tions in Ionosphere and Exosphere, E. Thrane, Ed., North-
Holland Publ. Co., p. 322.
- Liszka. L., 1967, J. Atmos. Terr. Phys., 29, p. 1243.
- Miller, N. J., 1970, J. Geophys., Res., 75, p. 7175.
- Mirkotan, S.F., 1962, Geomag. Aeronomy English Transl.
2, p. 578.
- Muldrew, D.B., 1965, J. Geophys. Res. 70, p. 2635.
- Rourke, G.F., 1966, AVCO Corp., Rpt. No. RAD-TR-66-11.

Rycroft, M. H., and S. J. Burnell, 1970, J. Geophys. Res.,
75, p. 5600.

Rycroft, M. H., and J. O. Thomas, 1970, Planet. Space Sci.,
18, p. 65.

Sharp, G.W , 1966, J. Geophys. Res., 71, p. 1345.

Stanley, G. M., 1966, J. Geophys. Res. 71, p. 5067.

Thompson, A. D., 1970, Boeing Company Report No. D5-
25385, Renton, Washington.

Ulwick, J. C., et al, 1964, AFCRL Rpt. No. 64-1021
(Environmental Research Paper No. 74).

Whalen, J. A., 1970, AFCRL Rpt. AFCRL-70-0422.

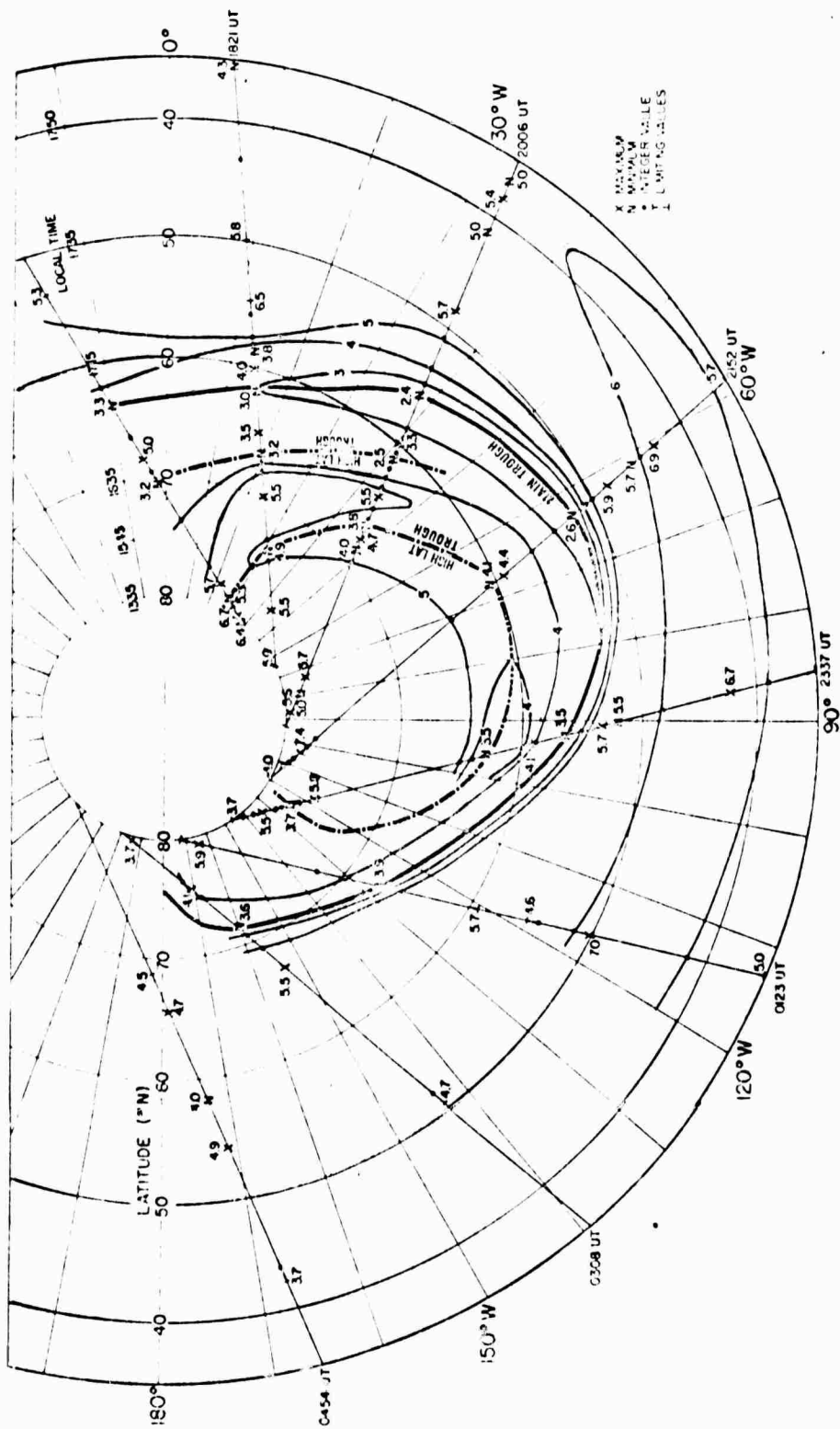


FIG. 1 Contour map of $f_x f_2$ observed by Alouette 1 on consecutive passes spanning 16 UT Oct. 30 to 05 UT Oct. 31 1962, presented in geographic coordinates and approximately constant local time (reproduced from Muldrew, 1965)....4-18

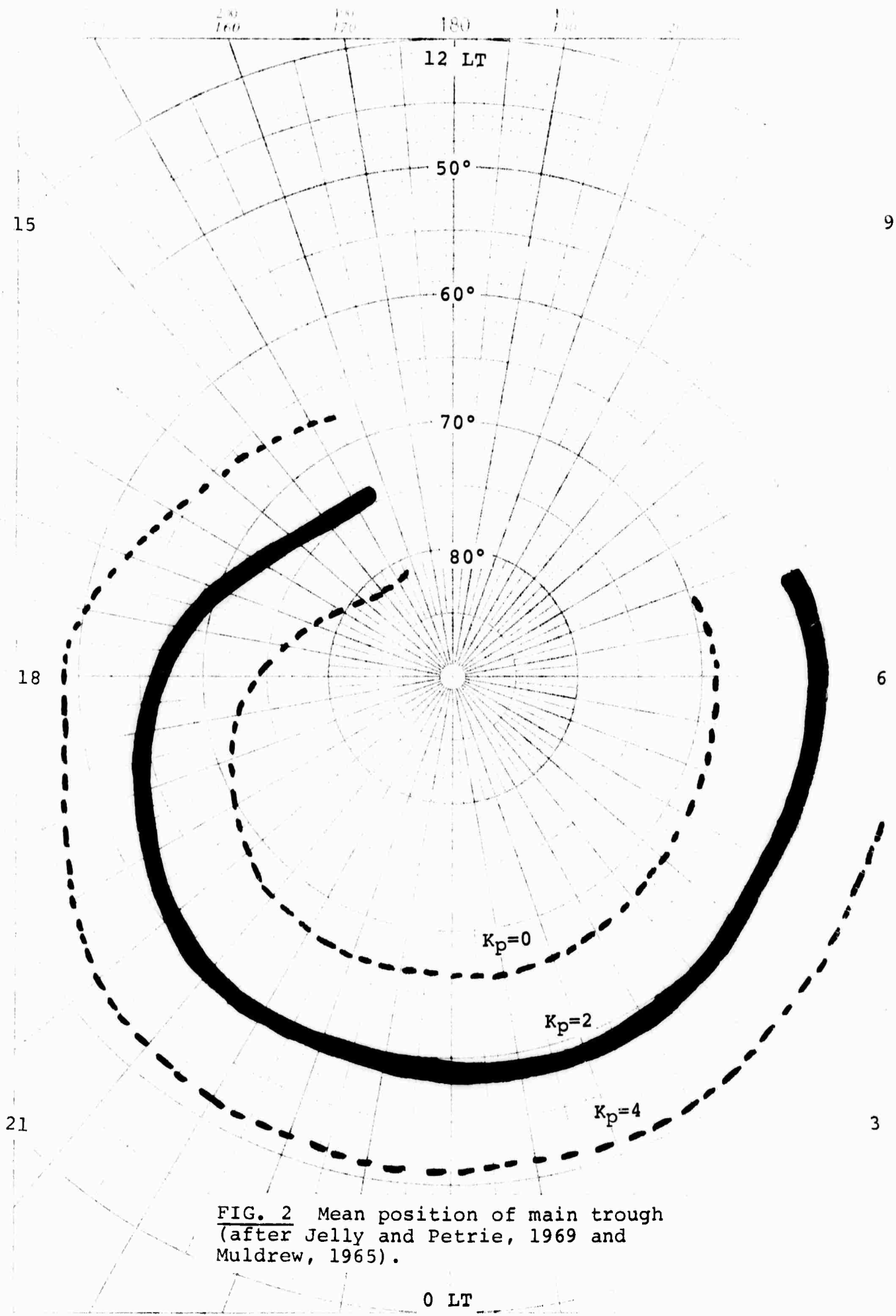


FIG. 2 Mean position of main trough
 (after Jelly and Petrie, 1969 and
 Muldrew, 1965).

0 LT

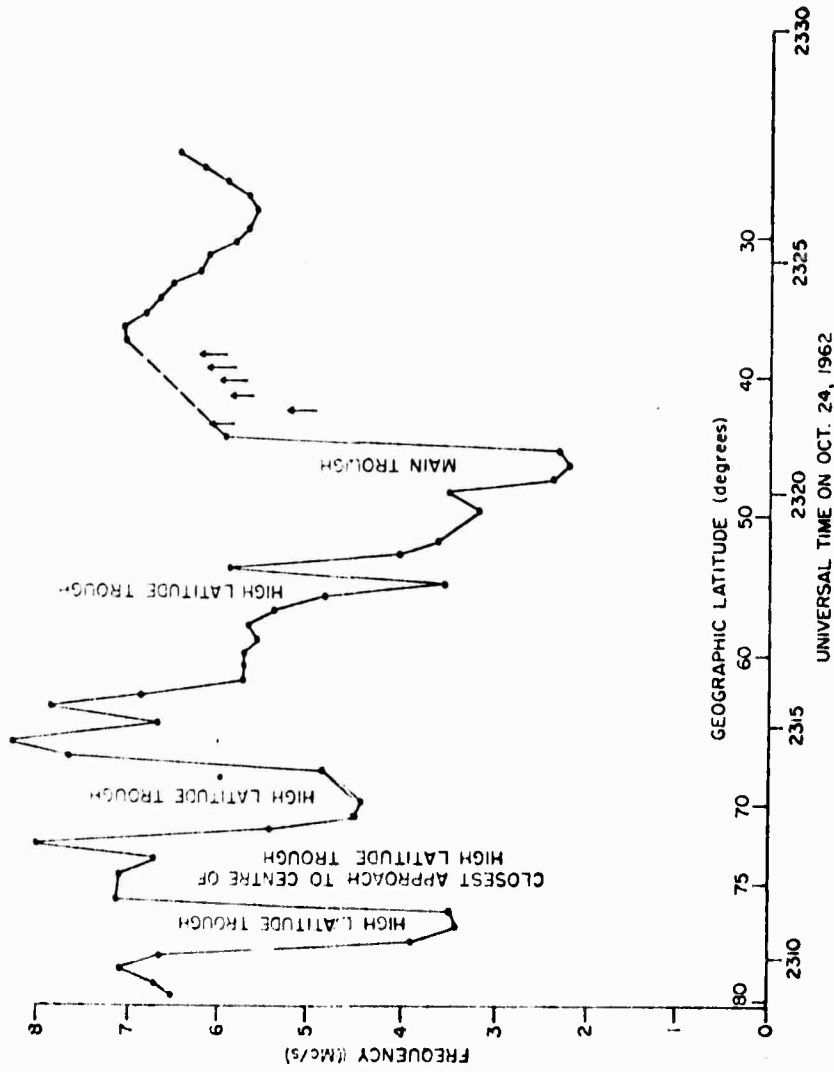


FIG. 3 Variation in peak electron density (plasma frequency) with latitude showing main trough and high latitude troughs (Muldrew, 1965)

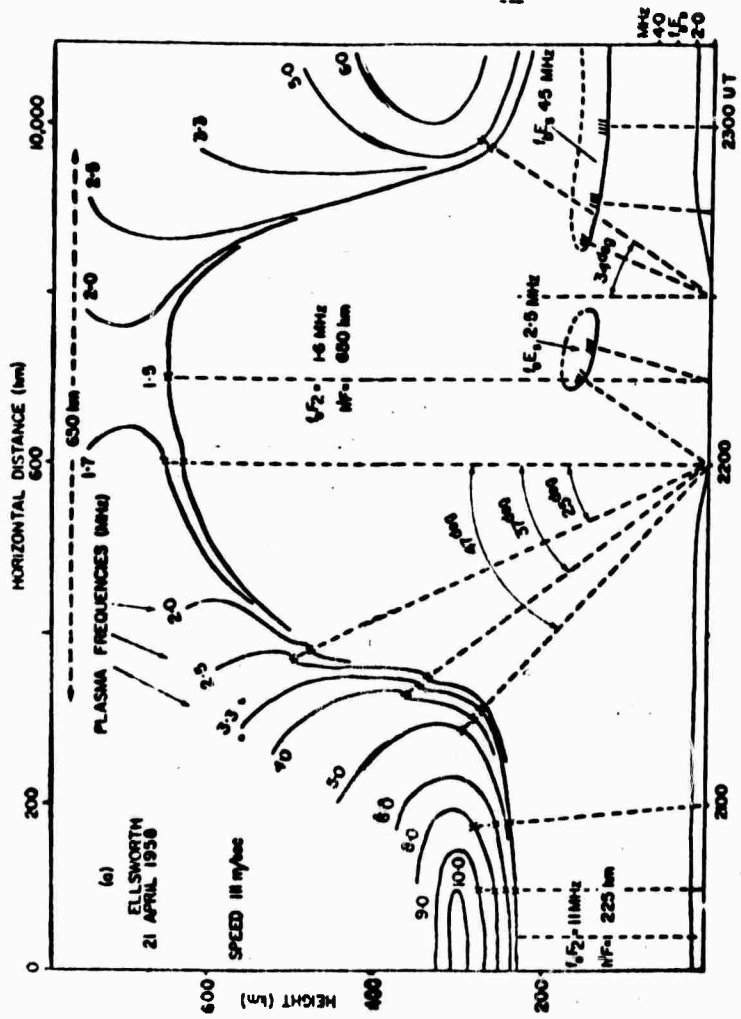


FIG. 4 Observed distribution of electron density (plasma frequency) in a bottomside trough deduced by Bowman (1969).

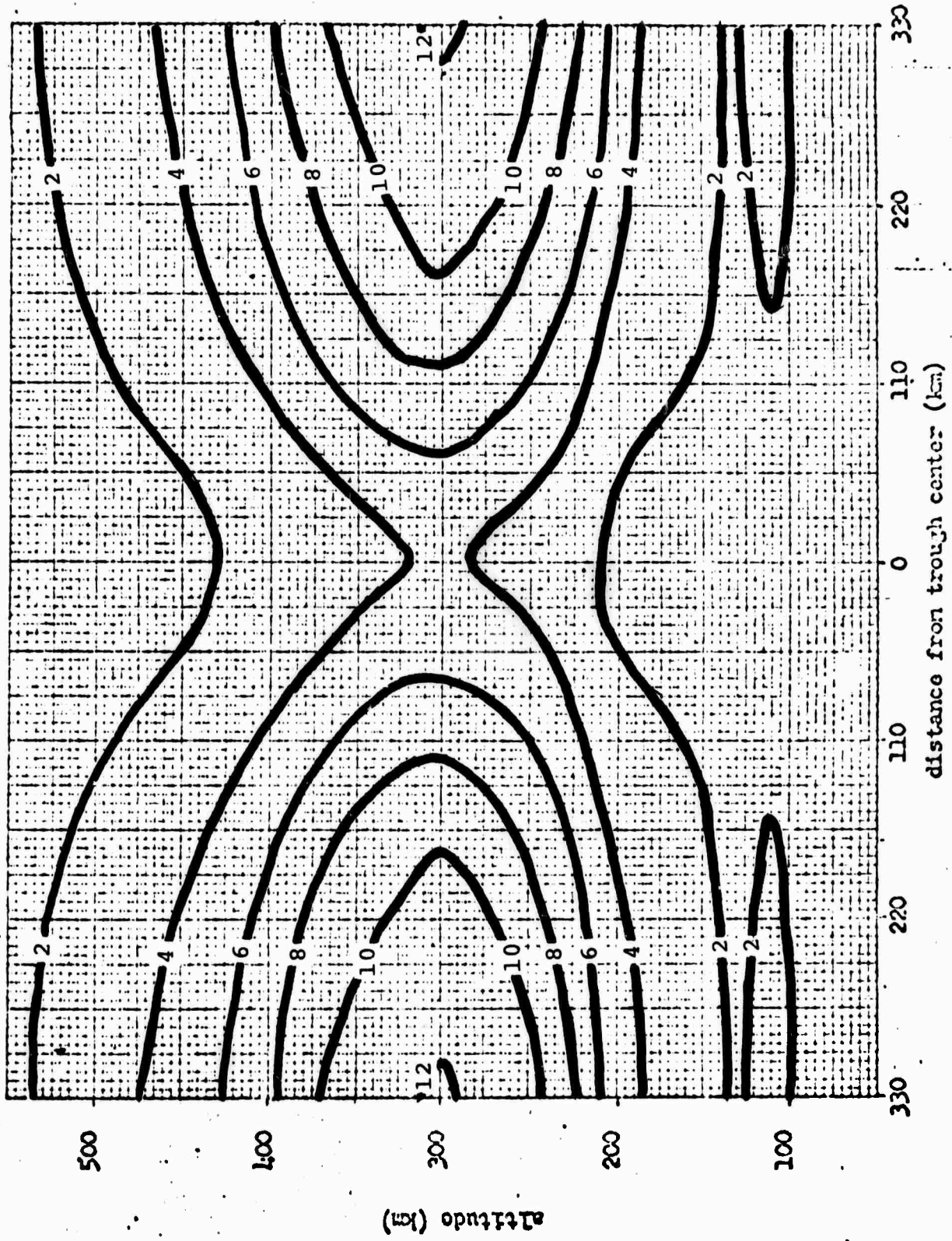


FIG. 5 Model of main trough (electron density expressed as plasma frequency contours) utilized by Thompson (1970).

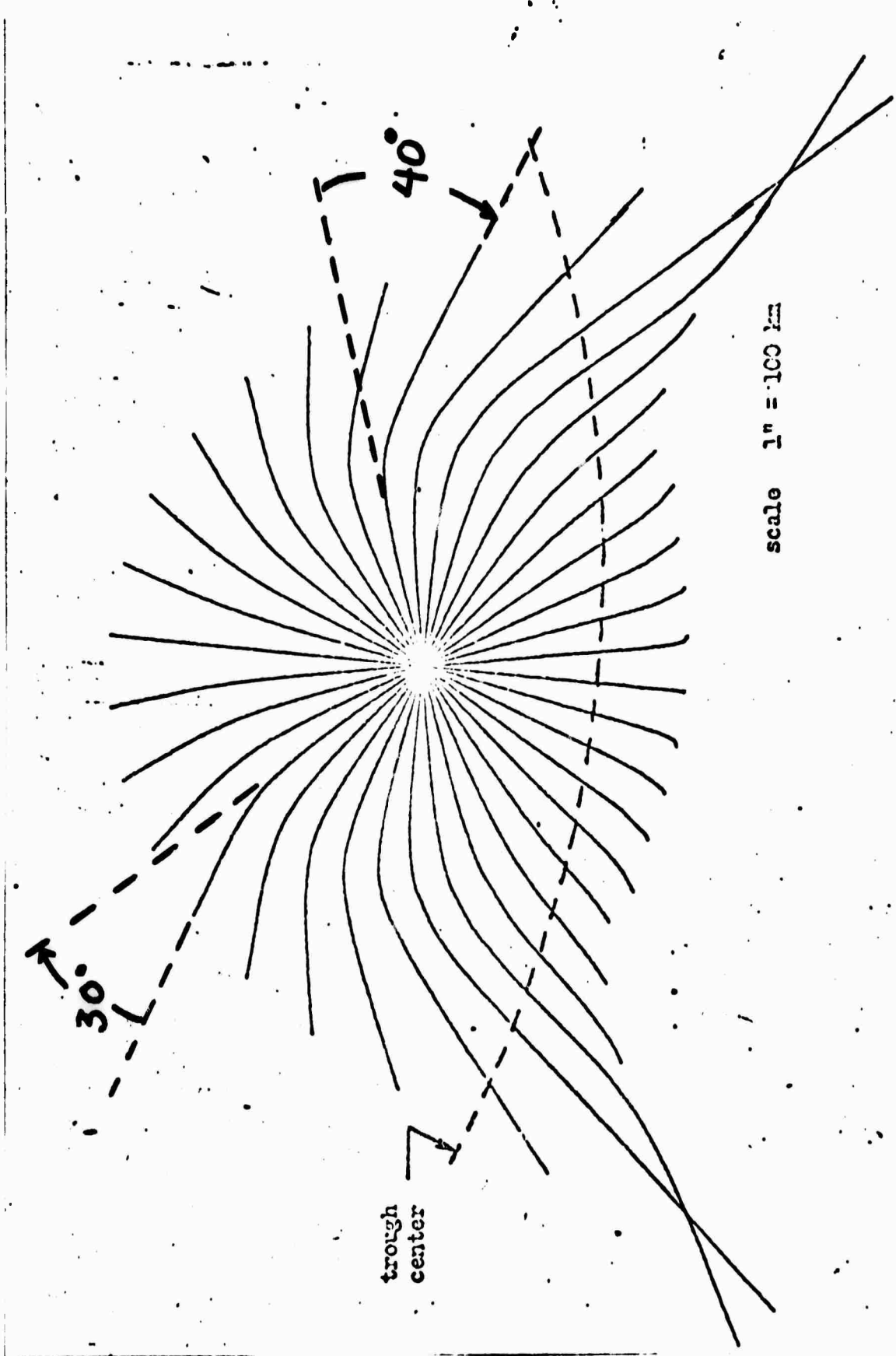


FIG. 6 Ray path projections on Earth's surface showing lateral deviations of 6 MHz rays through main trough with elevation angle of 60° (after Thompson, 1970).

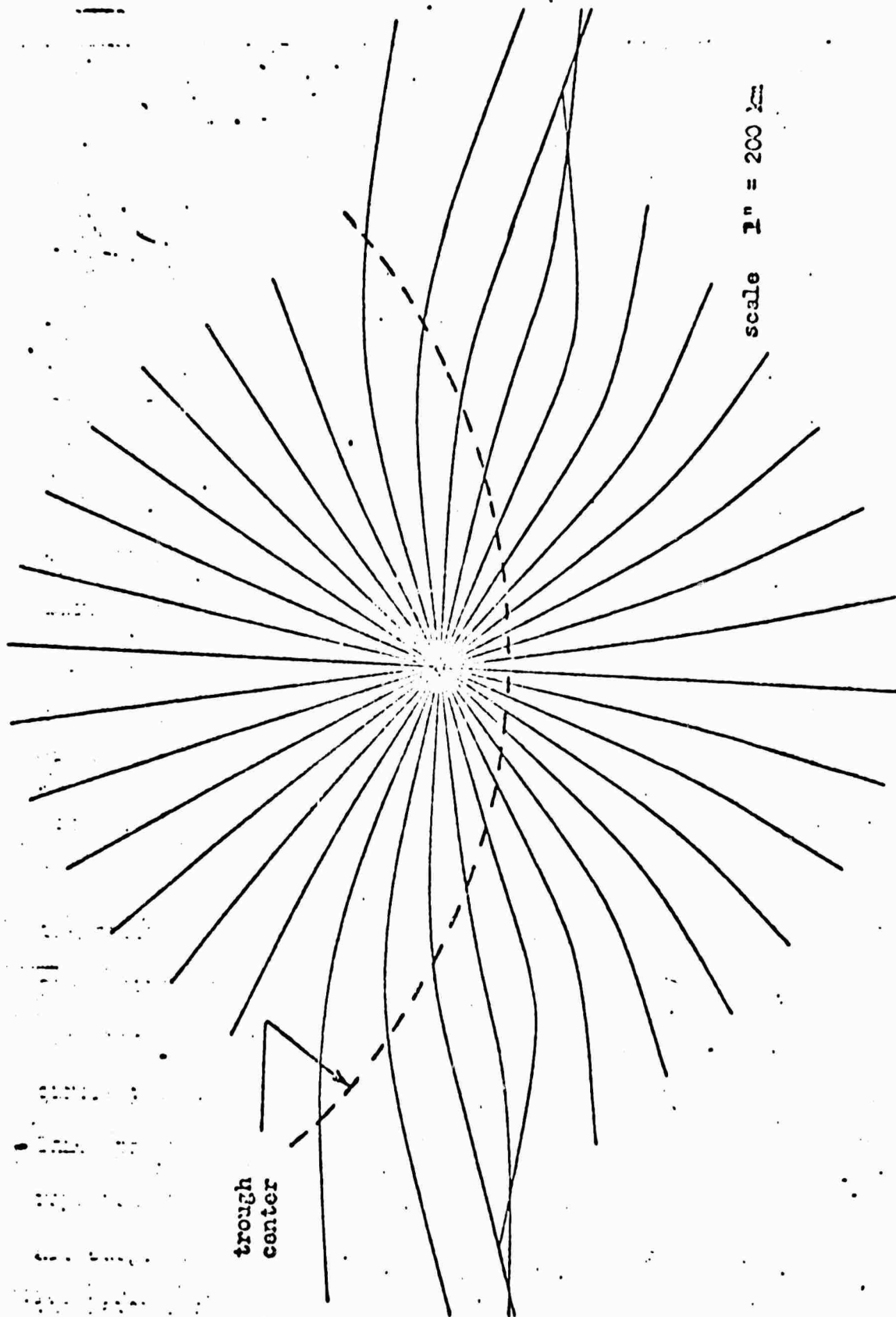


FIG. 7 Ray path projections on Earth's surface showing lateral deviations of 6MHz rays through main trough with elevation angle of 30° (after Thompson, 1970).

At this time (Fig. 10) the sun is at approximately 255°E geomagnetic longitude and the 80% contour in the auroral oval component is on the night side between about 80°E and 125°E centered on 70°N. The secondary maximum region (60%) centered at 80°N in the longitudinal sector 310°E is the dip pole component maximum. The 40% contour surrounding the DPC maximum is somewhat distorted due to the presence of the AOC. The two maximums are well separated at this time.

As the day proceeds, the sun position rotates clockwise with respect to the maps, approximately 45° for each 3-hour change and the occurrence patterns change in accordance with the diurnal variations of the DPC and the rotation of the auroral oval component. At 03 UT, July 1971/72, for example (Fig. 11), it is evident that the area covered by the 60% DPC contour has expanded and the AOC maximum has moved westward along 70°N geomagnetic latitude. Pattern variations through the rest of the day are evident in Fig. 12 through 17. The remaining maps in the July series are self-explanatory. It is of interest to note, however, that even when the dip pole is on the night side, the projected DPC and AOC maximum areas are so far separated that it was felt inadvisable to construct a single 80% contour covering the whole region.

The spread F occurrence frequency projections for Equinox (September 1971/72) are presented in Figs. 18 through 25. There are substantial differences between these maps and those just presented for Summer (July). Of particular note is the single very large area encompassed by the 80% contour level during

nighttime on the dip pole side of the earth (03 UT to 12 UT). The AOC and DPC maximum areas are separate at 1500 UT and later hours, and in these maps (Fig. 23, 24 and 25) the auroral oval component clearly covers a much larger area than it does in Summer. For example, the 80% AOC region extends from about 65° N to 80° N compared to the 3° latitudinal width of its summer counterpart. Also noteworthy is the larger area within the 20% contour level in equinox compared to Summer.

For Winter time, insufficient base data were available at the time of the analysis to make the same interpolative projection to mid-solar cycle as was made for Summer and Autumn. Therefore, correction factors to modify July conditions to Winter as determined by Penndorf (1960) were utilized to correct our July projections to predict Winter patterns in a middling sunspot year. These factors, reproduced in Fig. 26 are plotted as a function of geographic latitude versus magnetic dip latitude, where the indicated percentage is that to be added to (or subtracted from) the occurrence frequency in Summer. At high geographic latitudes in the neighborhood of the dip pole the largest correction factors are found, but of course, the total of July-plus-factor cannot exceed 100%. Results of this conversion are given in Figs. 27 through 34

Comparison between the gross features of the projected Winter and Summer maps indicates trends similar to those in cursory comparisons between Summer and Winter in sunspot maximum years and sunspot minimum years (Tao, 1965; Singleton,

1960, 1968). In comparing projected Winter to projected Autumn results as given here, however, it appears that the 20% Winter contour may be about 3° too far north. The higher core maximum of 100% occurrence frequency in both DPC and AOC found in Winter (Figs.28-30) are believed to be real, but it is questionable whether or not the two should be merged to form a single 100% occurrence region on the night side. It is noteworthy that even in daytime on the dip pole side of the earth, the occurrence frequency in the DPC is never less than 80%; this agrees with Tao's (1965) results for both solar minimum and maximum years in the permanent maximum region, and is therefore, considered to be real.

Because of the manner in which the Winter maps have been derived, however, there is in general a greater uncertainty in their reliability compared to the projected Summer and Autumn maps.

With projections for overhead spread-F occurrence probability now in hand, it is of interest to apply these to oblique-incidence paths radiating northward from a fixed observing point.

3.4 APPLICATION TO OBLIQUE INCIDENCE RAY PATHS

To convert the vertical incidence spread F occurrence frequency projections to oblique paths, it is assumed for simplicity that 1-hop F-layer propagation obtains, with reflection at the path midpoint. The probability of spread F occurrence viewed vertically at midpoint is assumed to be representative of the occurrence frequency to be expected on the corresponding oblique path. Such factors as the horizontal distance over which the ray path is within the F-region (and subject to irregularity effects), the height distributions of irregularities and possible variations with observing frequency are ignored for the present. Off-path reflections and two-hop propagation are likewise ignored.

With the aid of a range- azimuth overlay whose 0° azimuth is directed toward true north, spread F percentage occurrence at the midpoint of a path with range R ($1000 \leq R \leq 4000$ km in 500 km steps) and azimuth A ($-30^\circ \leq A \leq 60^\circ$ in 10° steps) was determined for one-hop propagation in Summer and Equinox. For the Winter map conversion to oblique incidence, the azimuthal width of the overlay was expanded to encompass -50° to $+70^\circ$. The percentage values so determined were then plotted in a range/azimuth (R/A) display of the type illustrated in Fig. 35 and isolines of constant occurrence percentage were constructed. For convenience in orientation, a selection of ionospheric ground stations as located in the R/A space whose apex is at 60°N , 7.8°E geomagnetic (47°N , 68°W geographic) is given in Fig. 35.

In plotting the points, it is important to note that the occurrence percentage at the midpoint of a propagation path described by R and A is plotted at the endpoint of the path in the antenna fan (R/A space). This method of presentation allows ready determination of the fraction of time that a signal passing through the F region may encounter spread F, that is, ionospheric irregularities, and presumably suffer spectral spreading. The results of this application to oblique incidence are given in Figs. 36-43 for Summer 1971/72, Figs. 44-51 for Equinox and Figs. 52-59 for Winter.

The diurnal variation of occurrence frequency in the field of view for a given season is readily apparent in these maps. For example, beginning at 00 UT in Summer (Fig. 36) one sees nearly the entire fan covered by at least 20% probability, with the magnitude gradually increasing to about 50% beyond 3500 km in the central azimuthal portion. (It will be recalled that the 50% occurrence plotted at say, 4000 km, derives from the vertical incidence at a range of 2000 km along the appropriate azimuth from the station).

Going further into the night side (Fig. 37) the occurrence frequency intensifies over the whole R/A sector, and the maximum core of the auroral oval component is just entering the field of view at about 4000 km/30°. Three hours later (Fig. 38), the probability of spread F occurring at 06 UT ranges from 30% at the far eastern tip of the fan to 80% or more in the central portion. The pattern gradually moves westward and outward in range (Figs. 39 and 40) until on the dayside (Figs. 41 and 42) only low probabilities

associated with lower edge of the receding oval component and the southern extremity of the dip pole component can be seen in the western section of the fan at ranges of 2500 km or greater. As local evening approaches (Fig. 43) the fan begins to fill up again.

Quite similar diurnal variations are evident in the Equinox and Winter R/A maps, except that in general there is greater occurrence probability for a given time in these seasons compared to Summer and the maximum percentage in local day is always 50% or greater compared to 30% in Summer.

Diurnal variations on particular paths are easily extracted from the R/A maps. For example, noting that the R/A coordinates for Keflavik (Fig. 35) are 3350 km/39°, the Summer variation ranges from less than 20% probability in the hours 12-21 UT (Fig. 40-43) to about 65% at 03 UT (Fig. 37). It is remembered, of course, that these percentages are predicted only for one-hop propagation and are subject to the additional limiting assumptions set forth in the first paragraph of this section.

3.5 REFERENCES FOR SECTION 3

- Aarons, J., et al, 1971, Proc. IEEE, 59, p. 159.
- Au, W. L., and G. L. Hower, 1970, J. Atmos. Terr. Phys., 32, p. 1577.
- Baggaley, W. H., 1970, J. Geophys. Res., 75, p. 152.
- Bates, H. F., and P. R. Albee, 1969, J. Geophys., Res., 74, p. 1164.
- Bates, H. F., and P. R. Albee, 1970, J. Geophys., Res., 75, p. 165.
- Dyson, P. L., 1969, J. Geophys, Res., 74, p. 6291 .
- Hakura, Y., 1965, Rpt. Ionosphere Space Res. Japan, 19, p. 121.
- Herman, John R., 1966b, Rev. Geophys., 4, p. 255.
- Hower, G. L. et al, 1966, J. Geophys, Res, 71, p. 3215.
- Hunsucker, R., and H. F. Bates, 1969, Radio Science, 4, p. 347.
- Jones, J. E., 1970, ESSA Tech. Report, ERL 153-SDL 12.
- Penndorf, R., 1960, AVCO Tech Rpt., RAD-TR-61-1.
- Penndorf, R., 1962, J. Geophys, Res., 67, p. 2779.
- Penndorf, R., 1966, Spread F and its Effects Upon Radiowave Propagation and Communication, P. Newman, Ed., Technavision Press., p. 137.
- Petrie, L., 1966, Spread F and its Effects Upon Radiowave Propagation and Communications, P. Newman, Ed., Technavision Press, p. 67.
- Shimazaki, T., 1959, J. Radio Res. Lab. Japan, 6, p. 669.
- Shimazaki, T., 1962, J. Geophys. Res., 67, p. 4617.
- Singleton, D. G., 1960, J. Geophys. Res., 65, p. 3615.
- Singleton, D. G., 1968, J. Geophys. Res., 73, p. 295.
- Tao, K., 1965, J. Radio Res. Lab Japan, 12, p. 317.

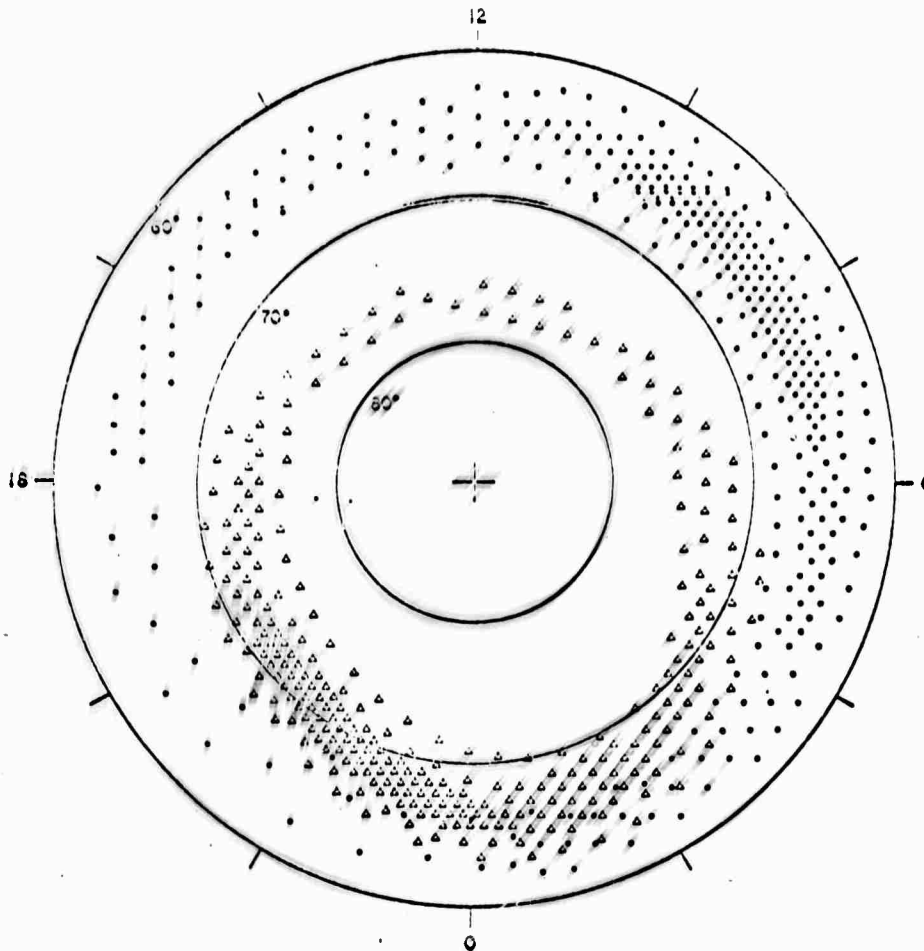


FIG. 1 Hartz and Brice (1967) zones of auroral particle precipitation in geomagnetic latitude and time. Dots are diffuse events and drizzle precipitation and triangles are discrete events and associated splash-type precipitation.

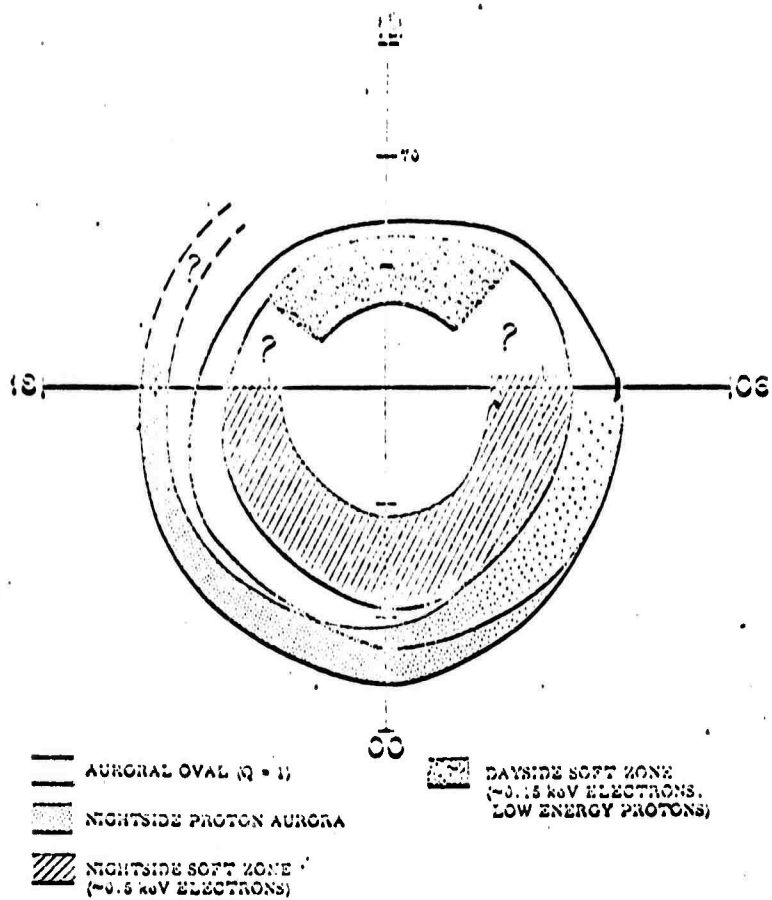
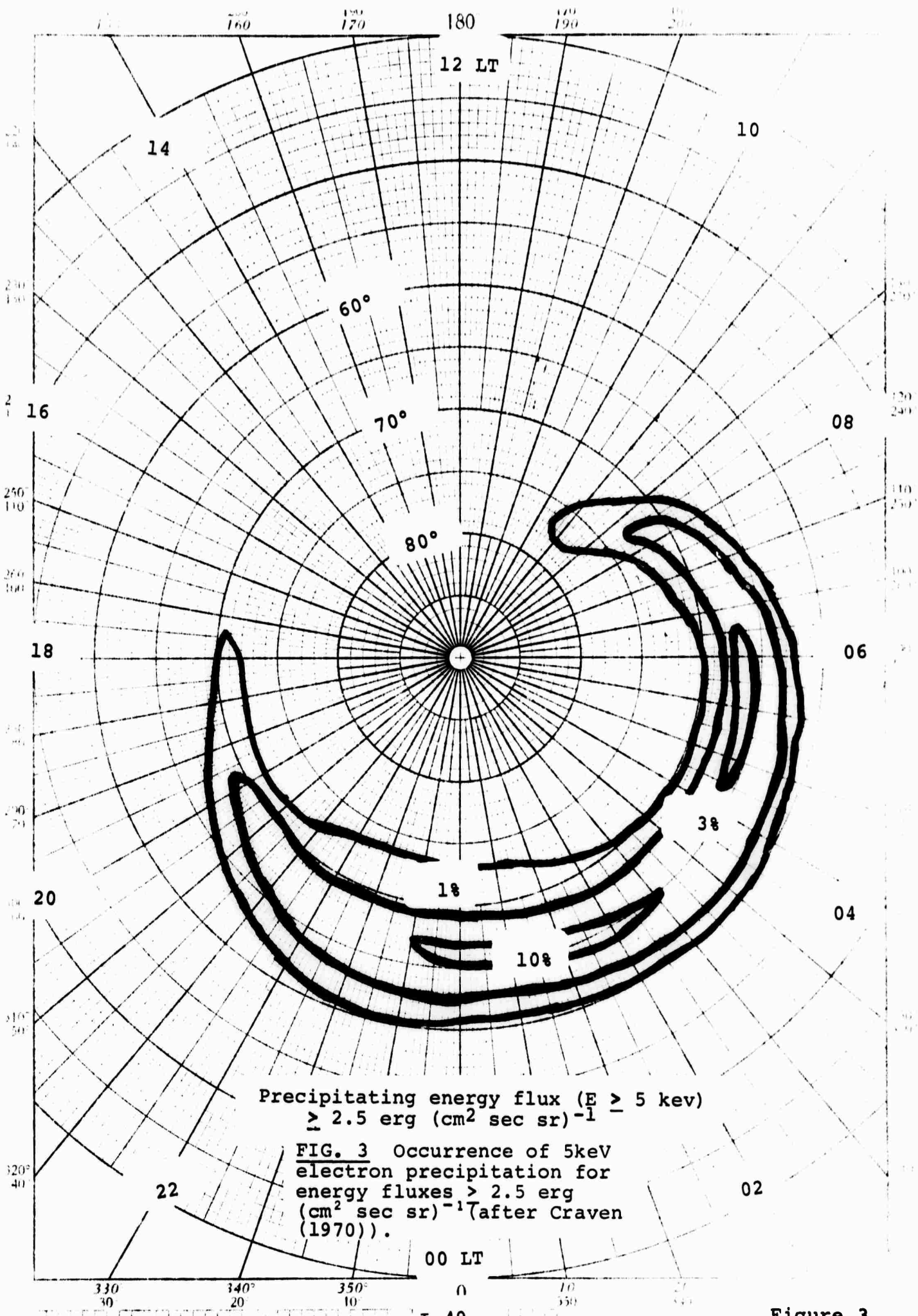


FIG. 2 Various zones of auroral particle precipitation as deduced by Eather and Mende (1971).



Precipitating energy flux ($E \geq 5 \text{ keV}$)
 $\geq 2.5 \text{ erg (cm}^2 \text{ sec sr)}^{-1}$

FIG. 3 Occurrence of 5keV
 electron precipitation for
 energy fluxes $> 2.5 \text{ erg}$
 $(\text{cm}^2 \text{ sec sr)}^{-1}$ (after Craven
 (1970)).

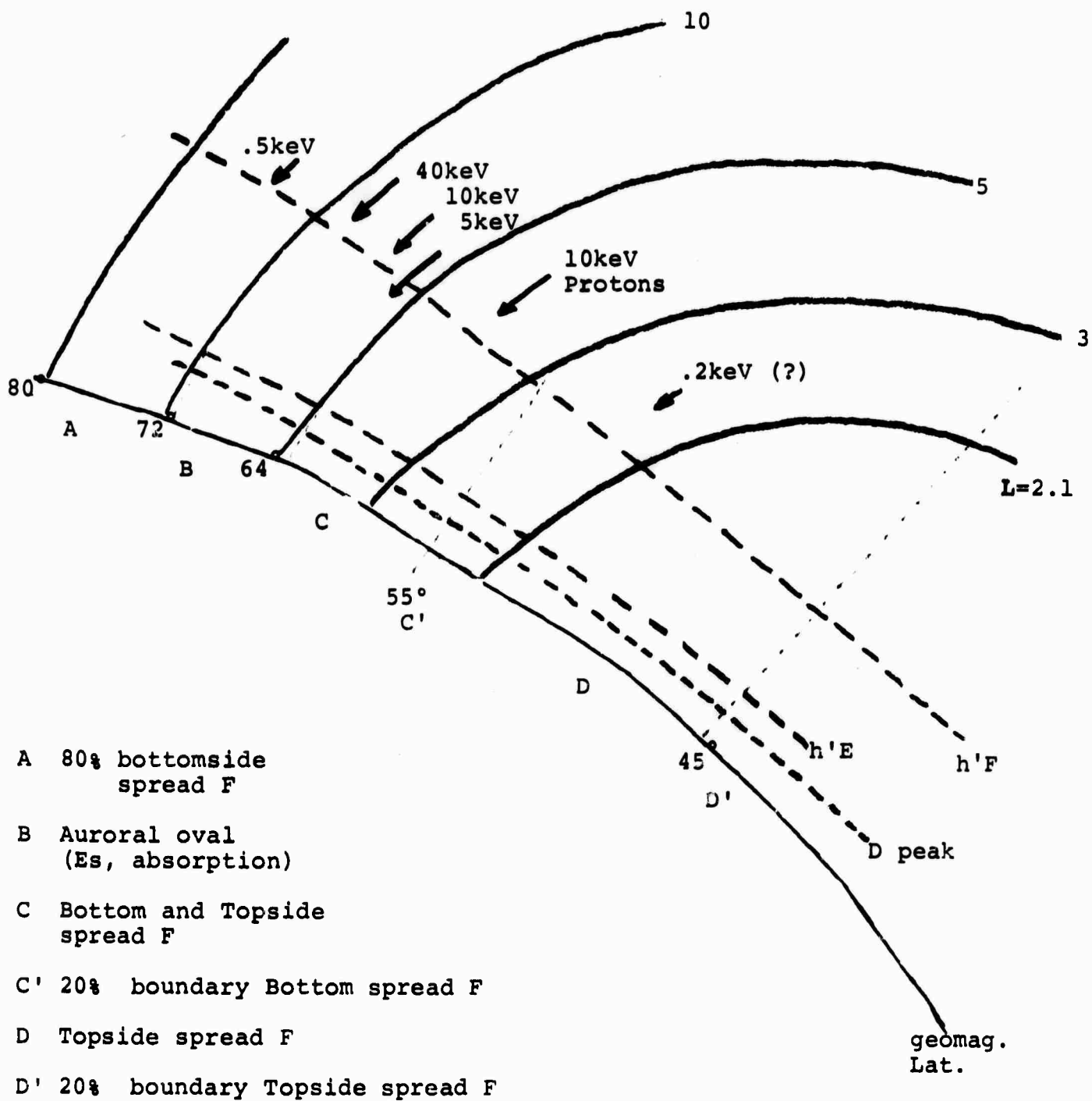
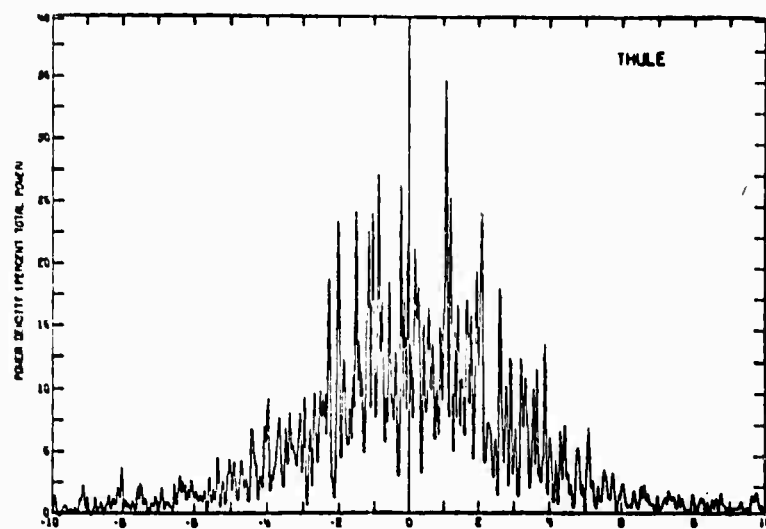
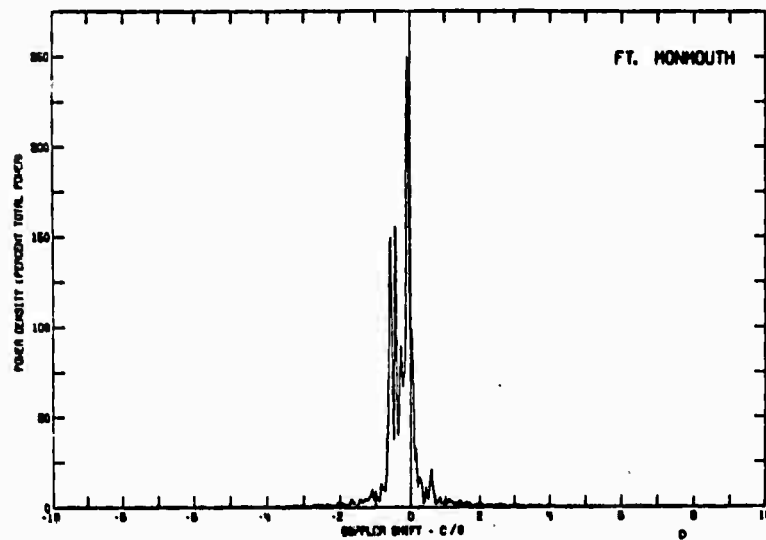


FIG. 4 Meridional model of precipitating particles and associated ionospheric phenomena for typical night time along 75° W longitude.

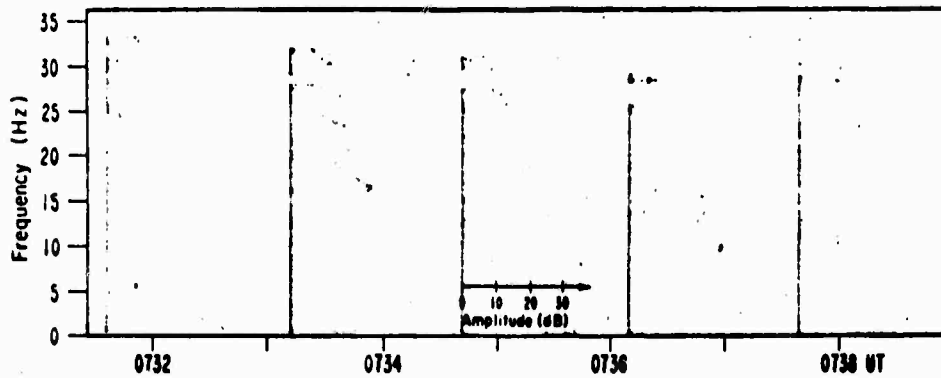


POLAR PATH

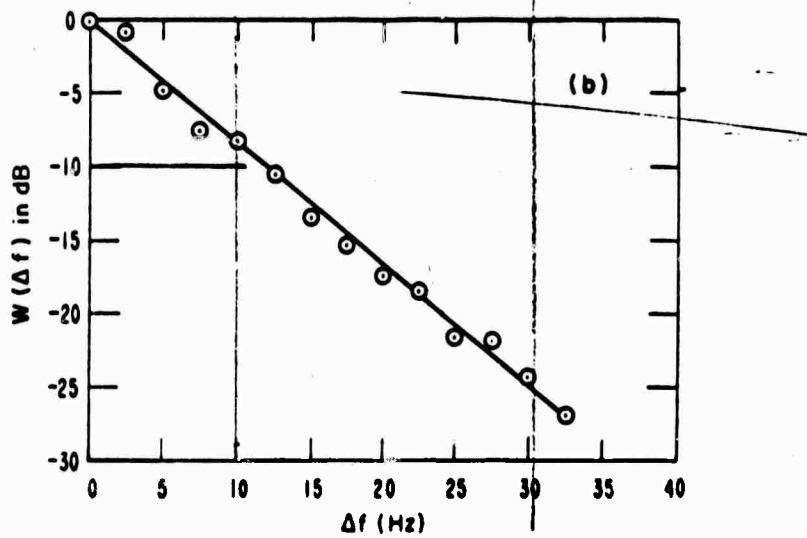


MID LATITUDE PATH

Typical spectral spread on a polar path compared to a mid-latitude path (reproduced from Hunsucker and Bates, 1969)

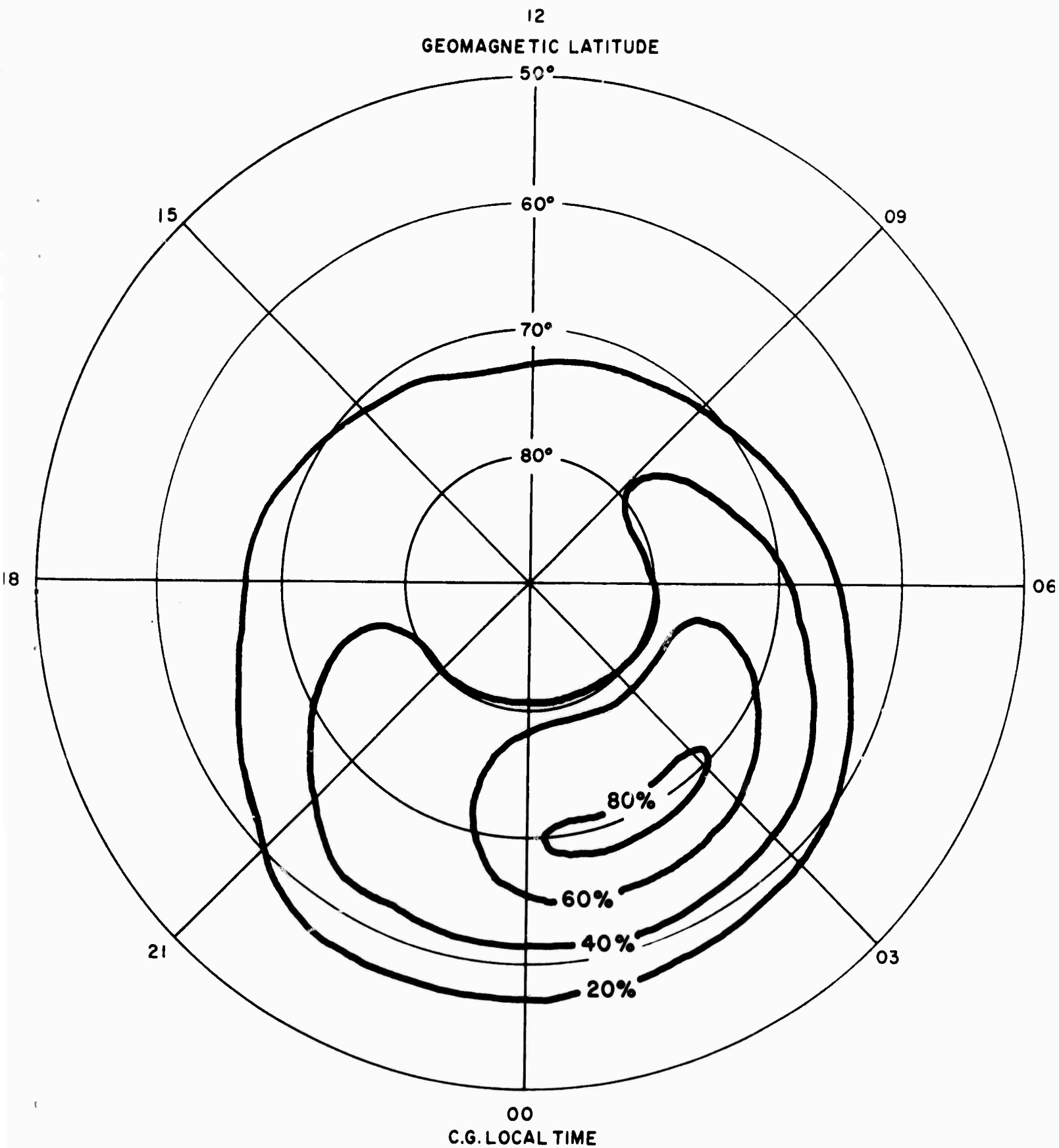


Amplitude spectral density:
6.0 MHz, 1 May 1968



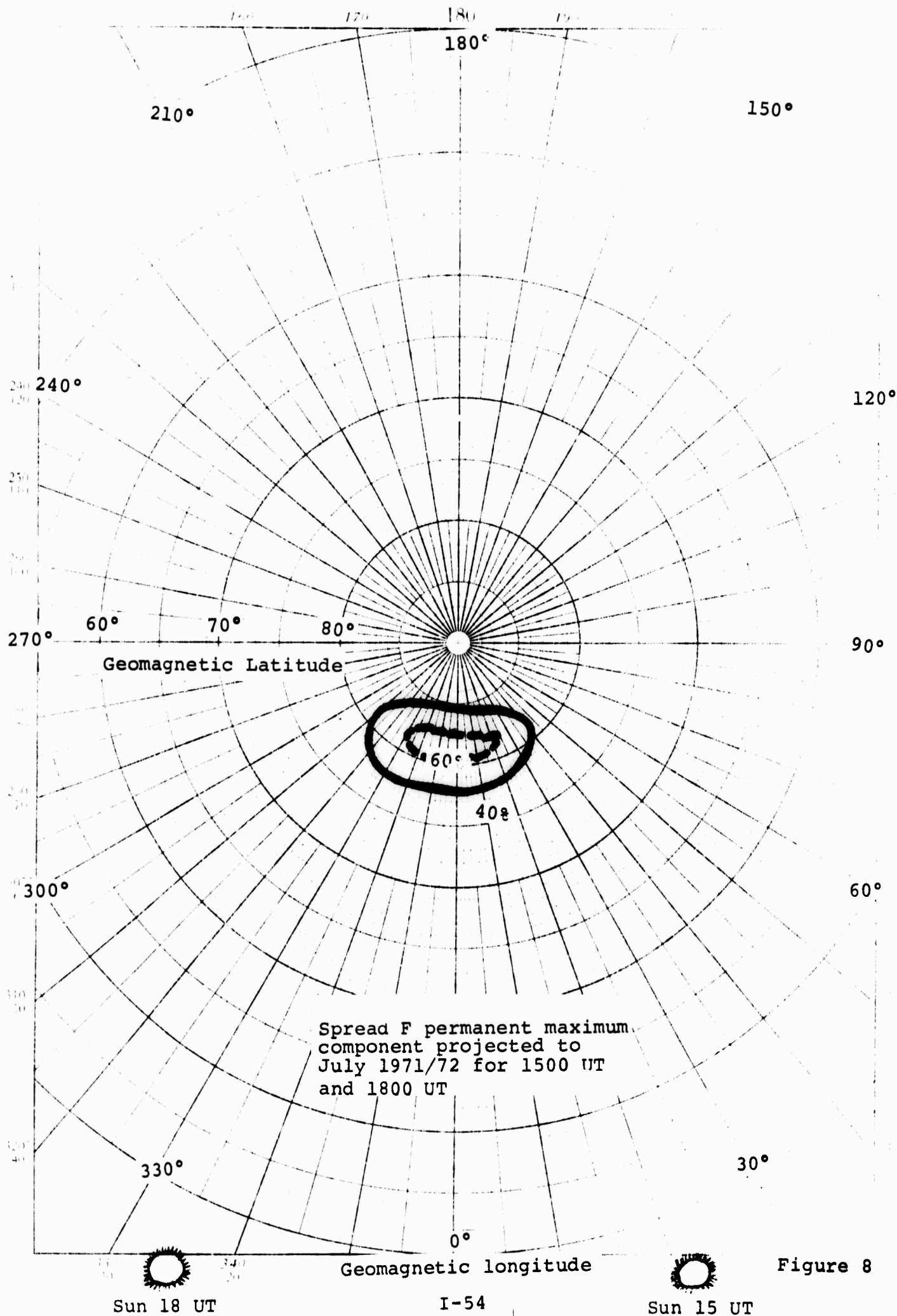
Average power spectra
of above records.

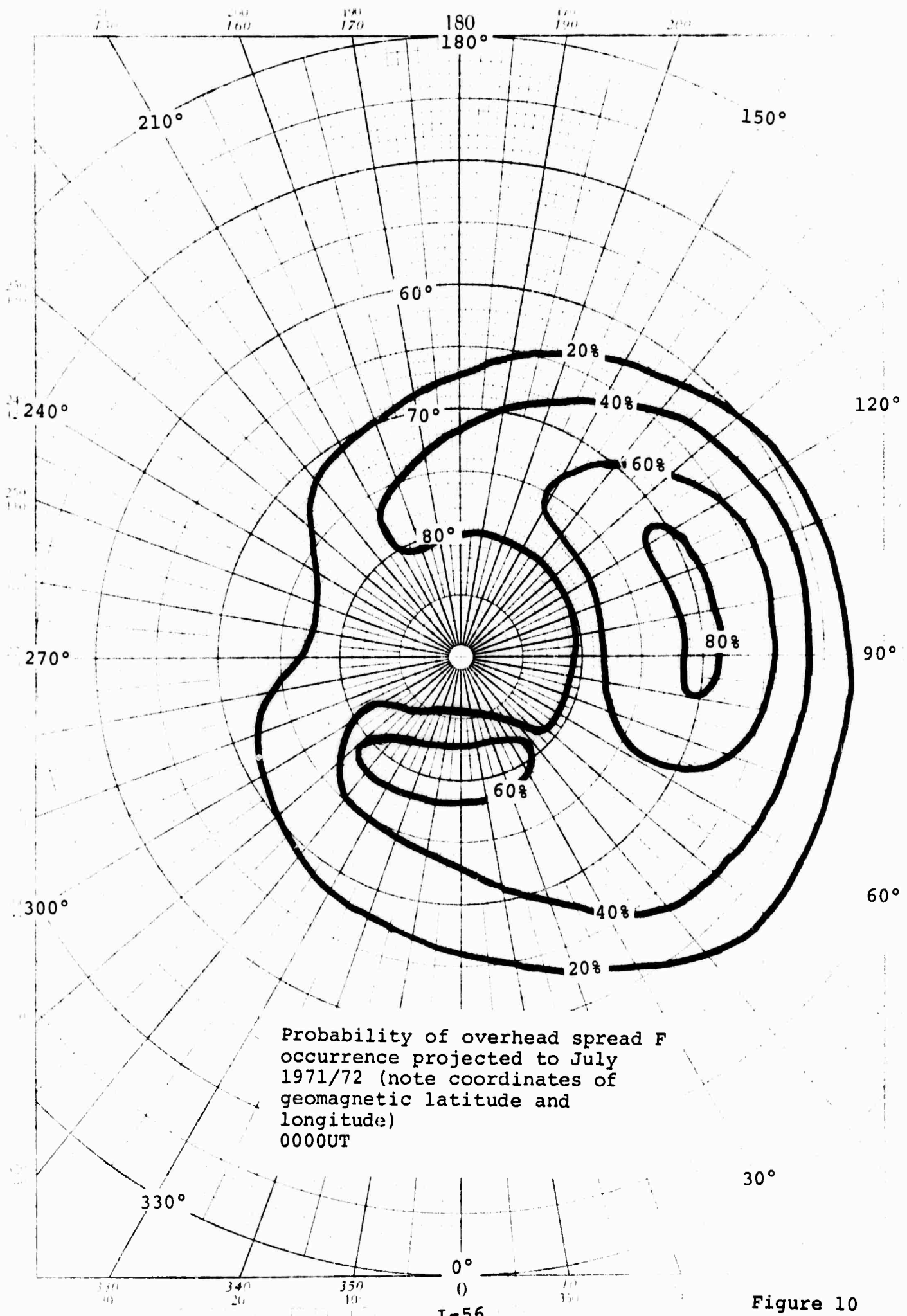
Spectral spread on an Antarctic path (South Pole to McMurdo) with spread F at path midpoint (after Jones, 1970).



Auroral oval component of spread F occurrence interpolated to mid solar cycle for July presented in geomagnetic latitude/local time coordinates.

Figure 7





Probability of overhead spread F
 occurrence projected to July
 1971/72 (note coordinates of
 geomagnetic latitude and
 longitude)
 0000UT

Figure 10

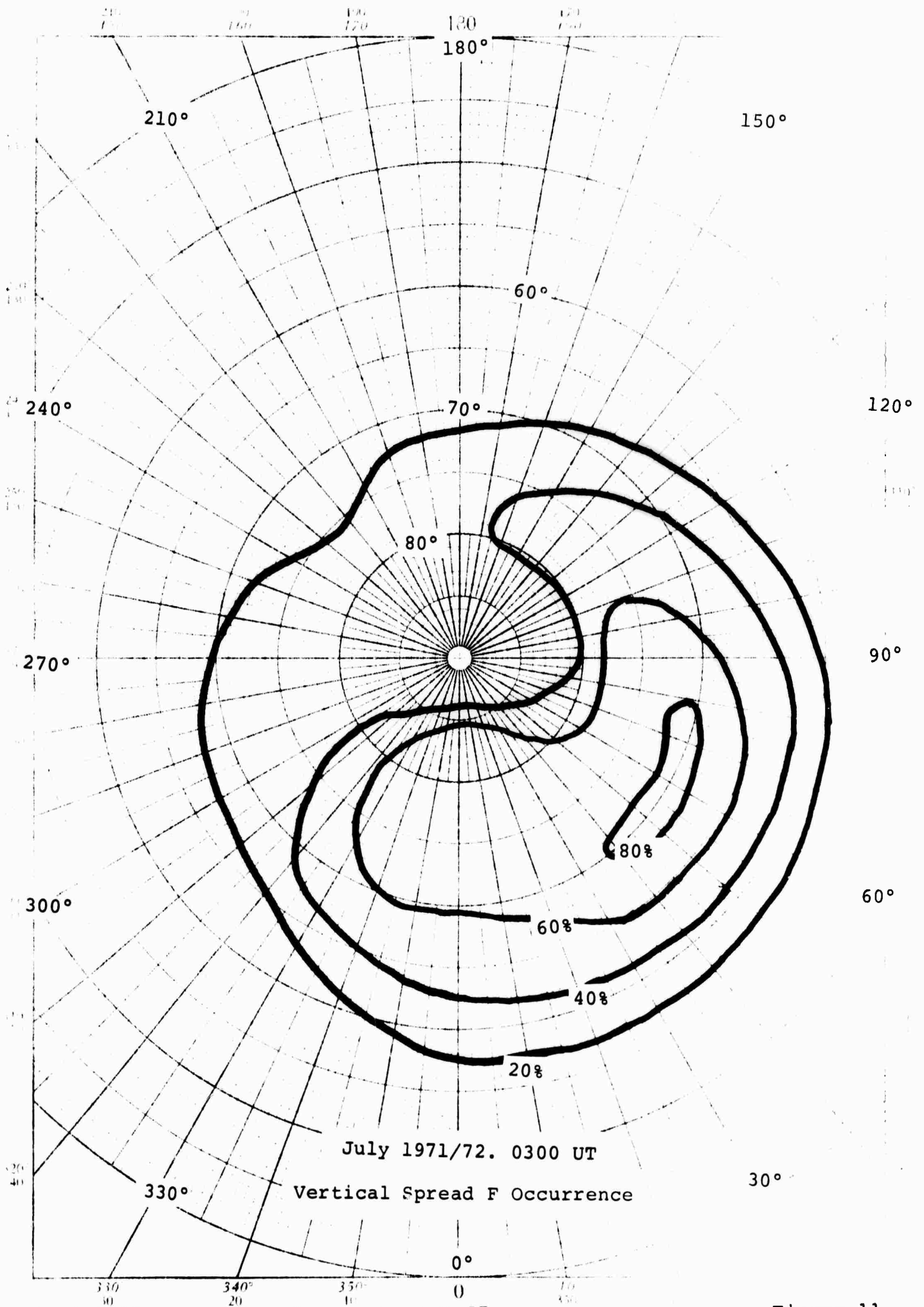


Figure 11

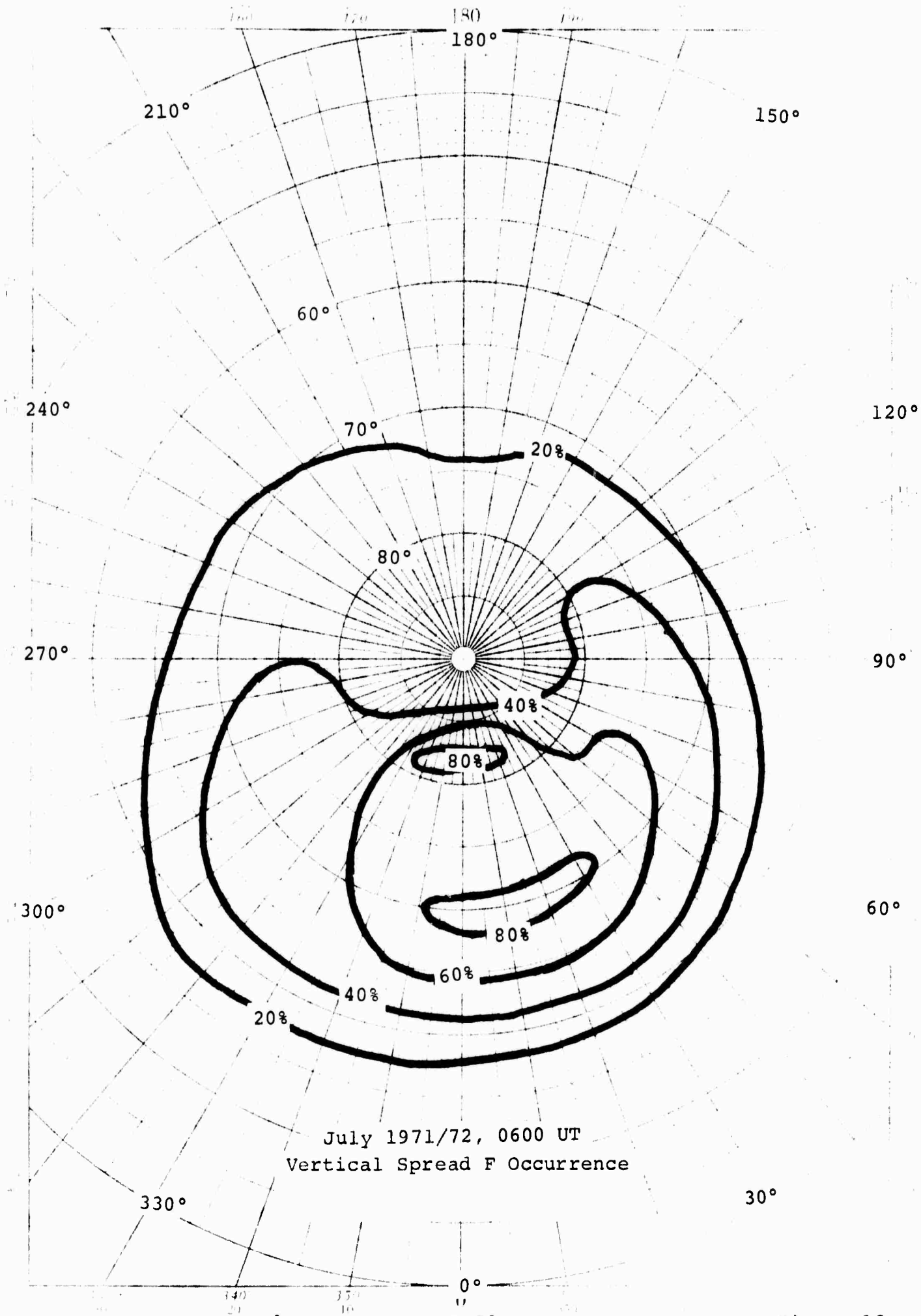
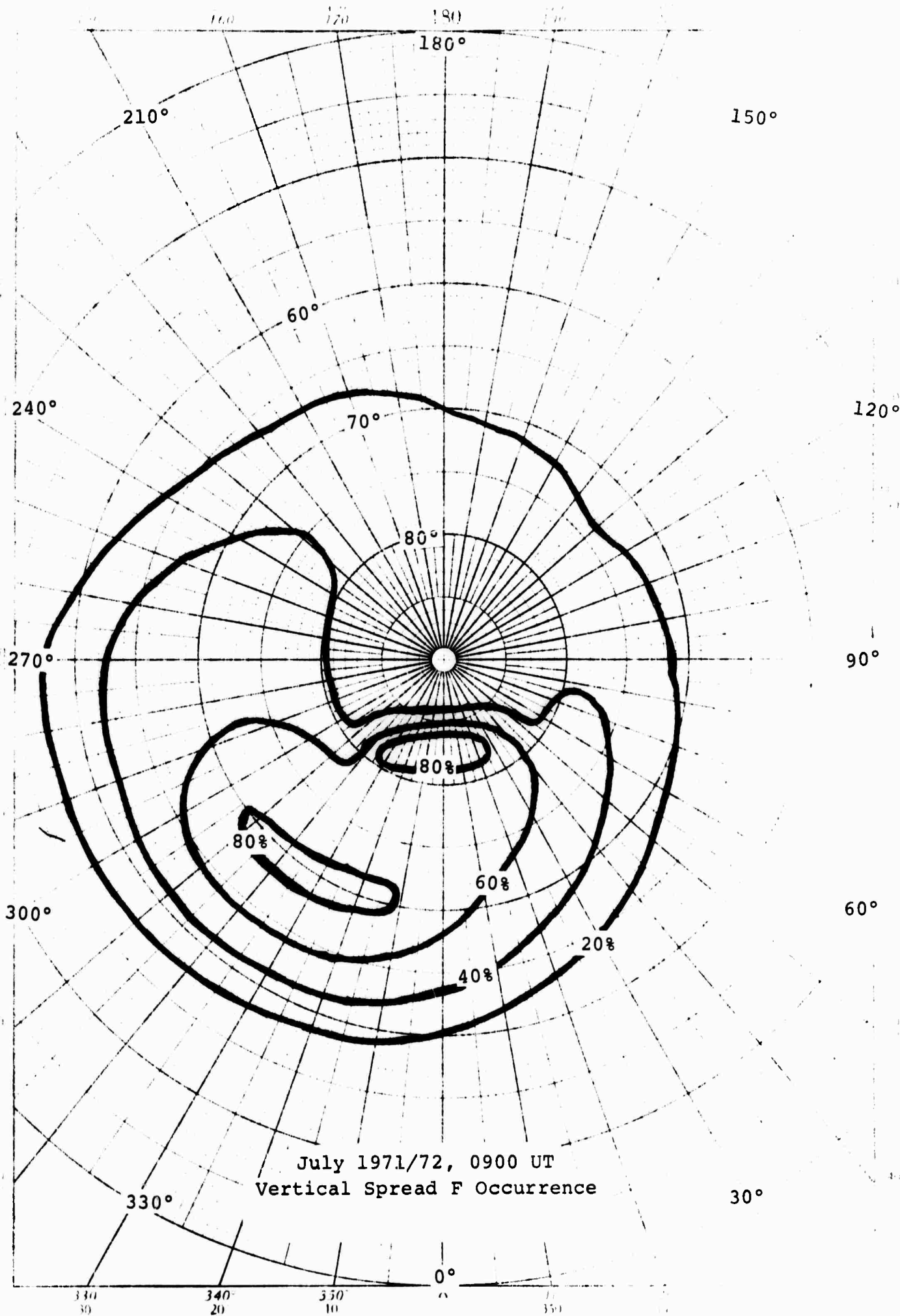
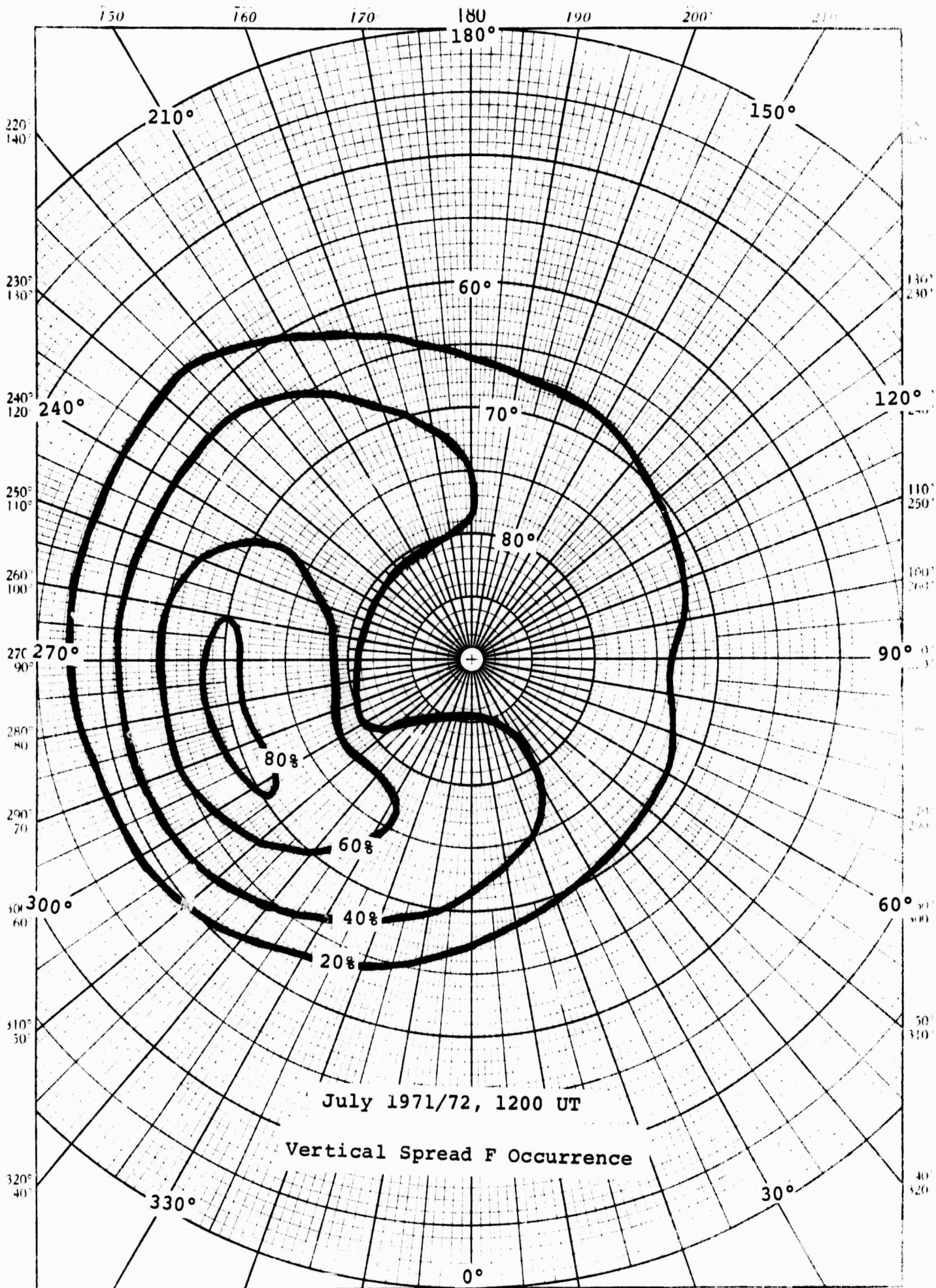


Figure 12



July 1971/72, 0900 UT
Vertical Spread F Occurrence

Figure 13

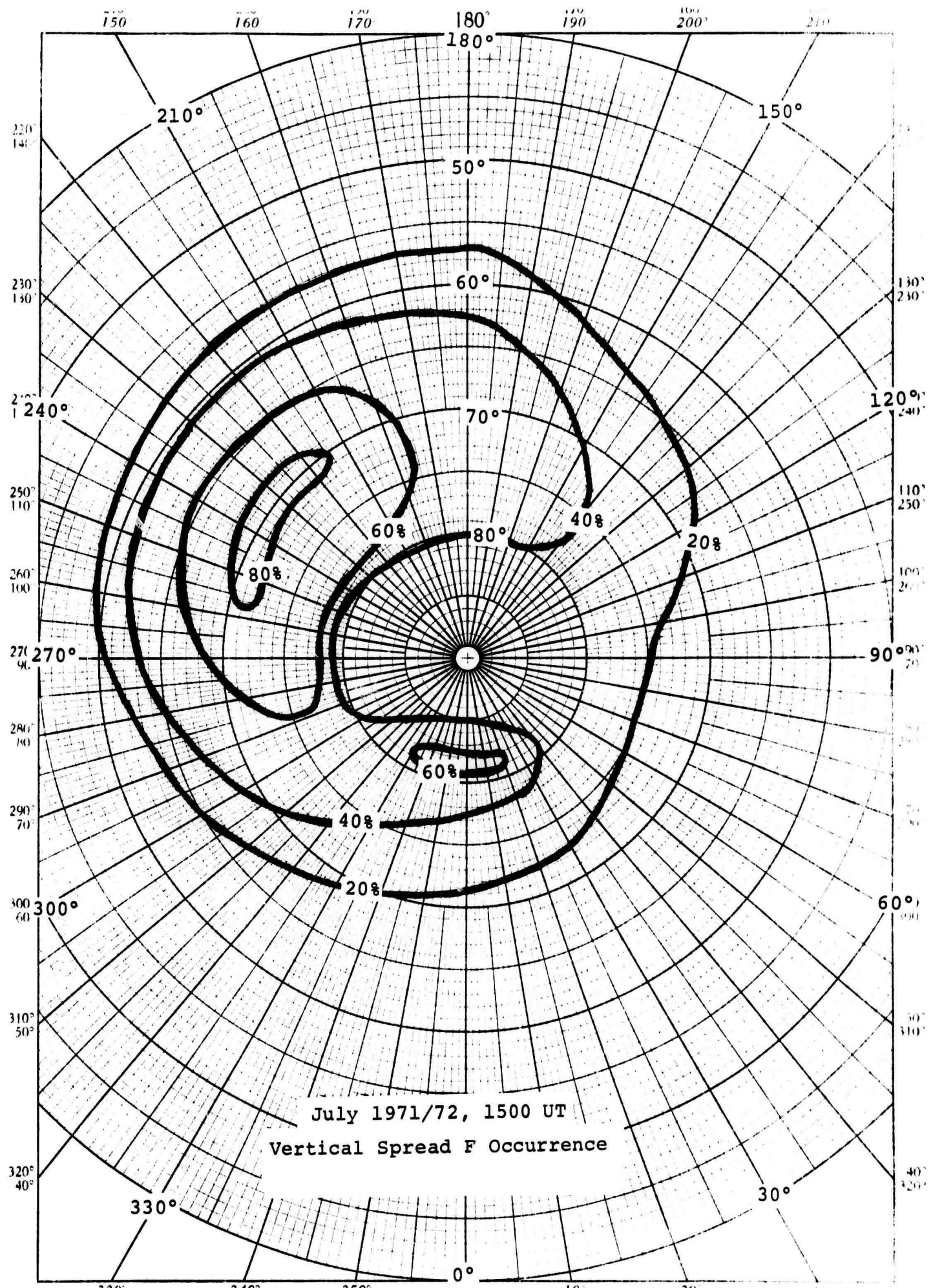


July 1971/72, 1200 UT

Vertical Spread F Occurrence

Figure 14

30° POLAR COORDINATE 48 4514



I-61

Figure 15

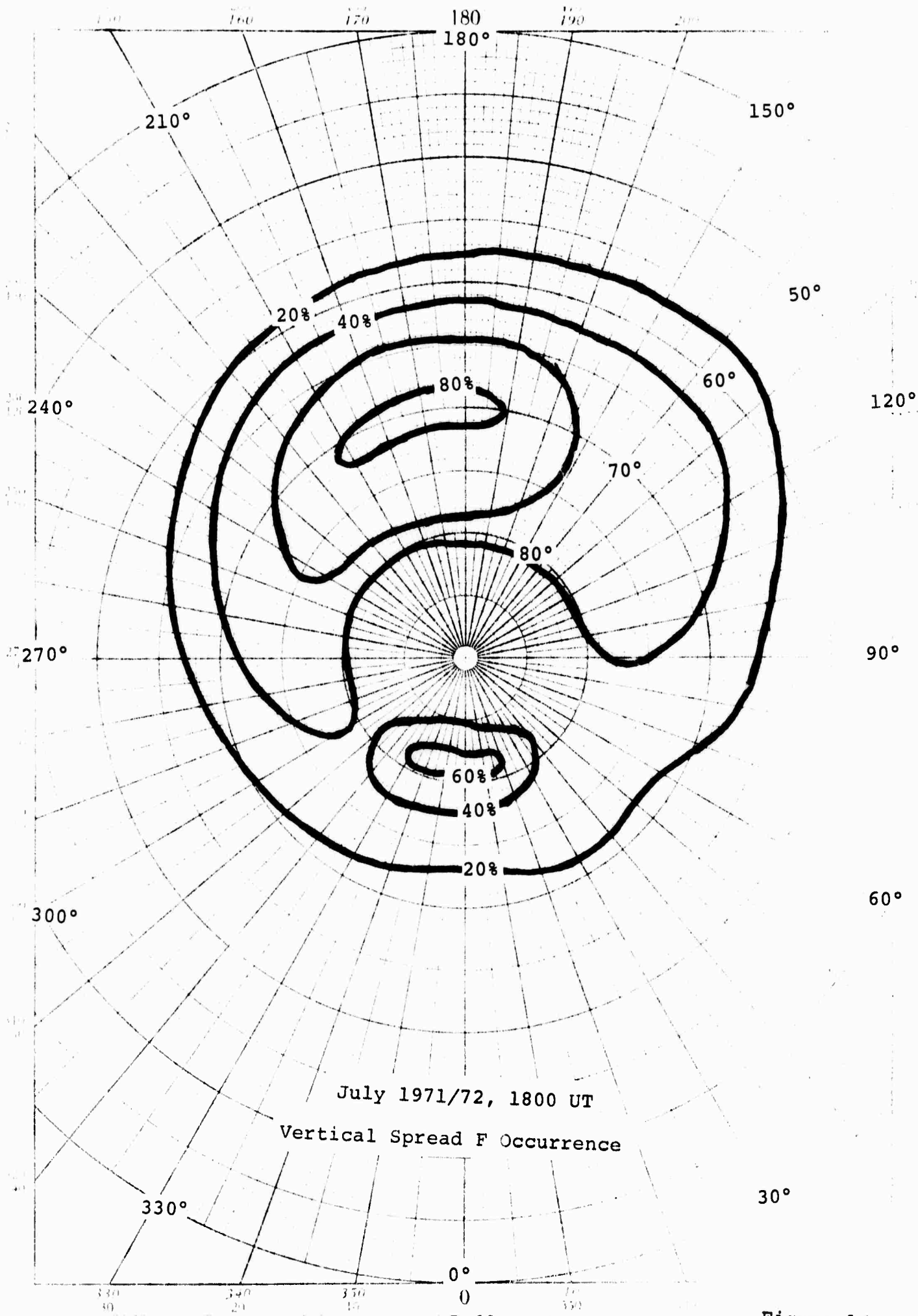


Figure 16

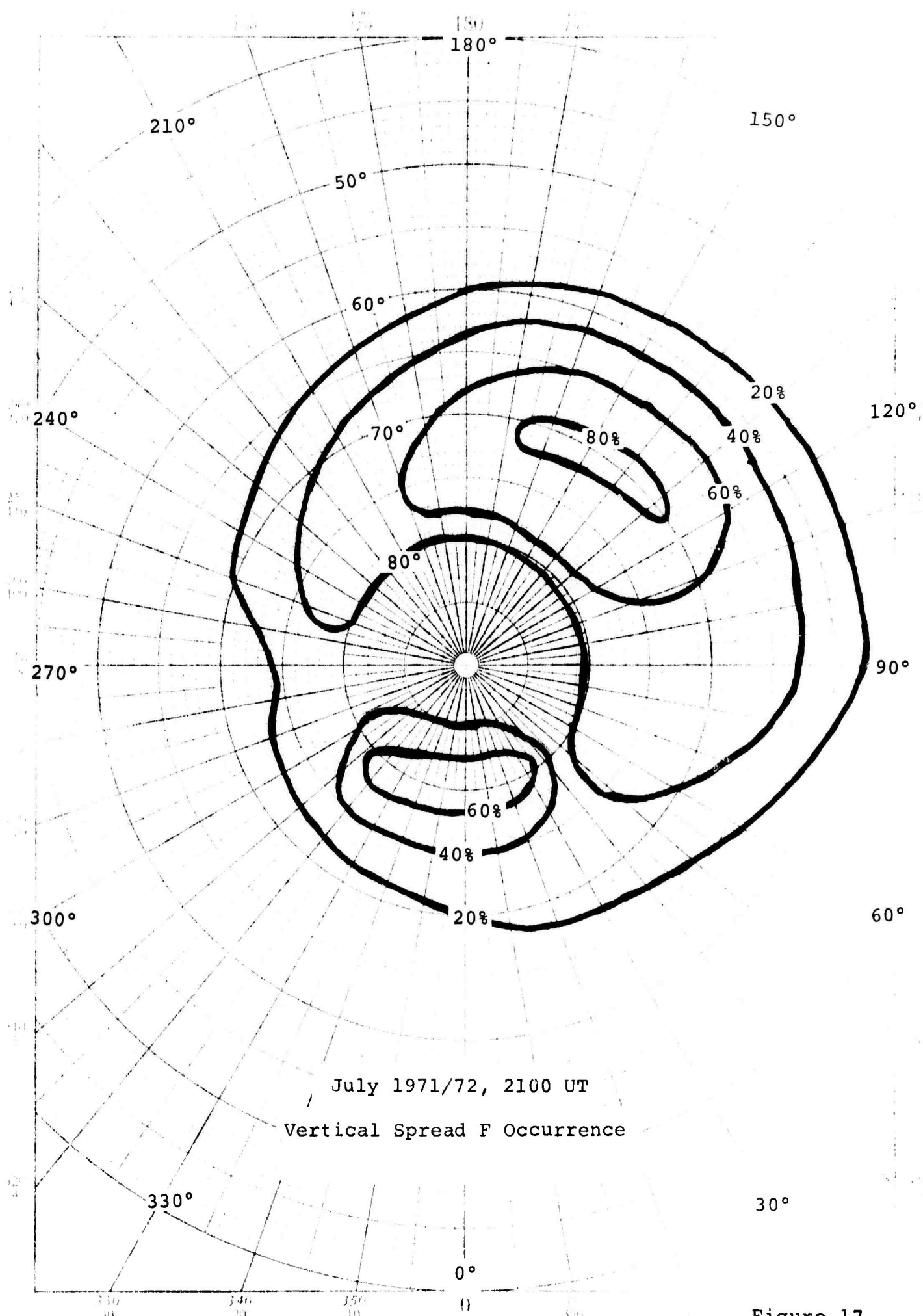


Figure 17

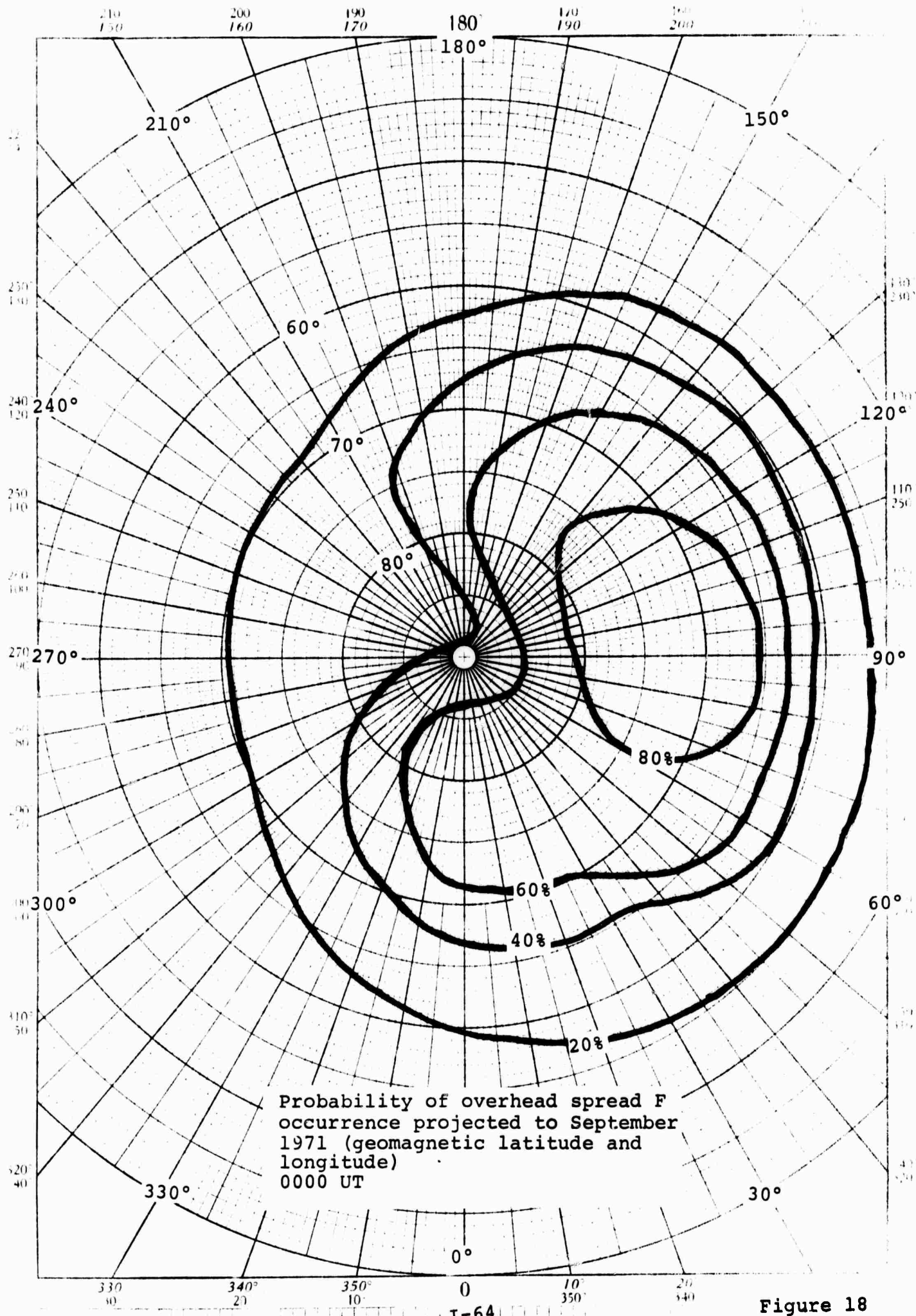


Figure 18

K&E POLAR CO-ORDINATE 46 4412
SCUFFEL & TAYLOR CO

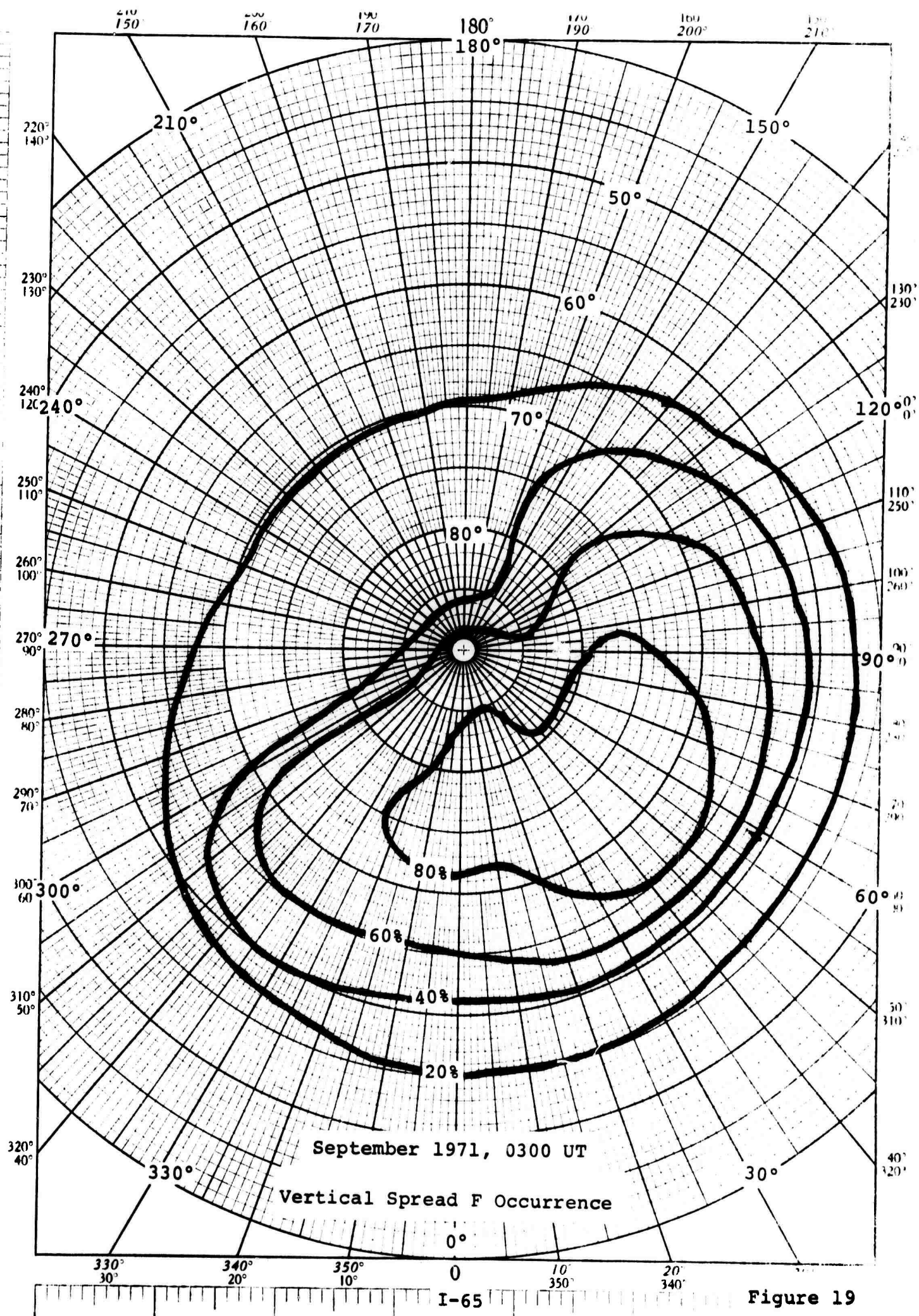


Figure 19

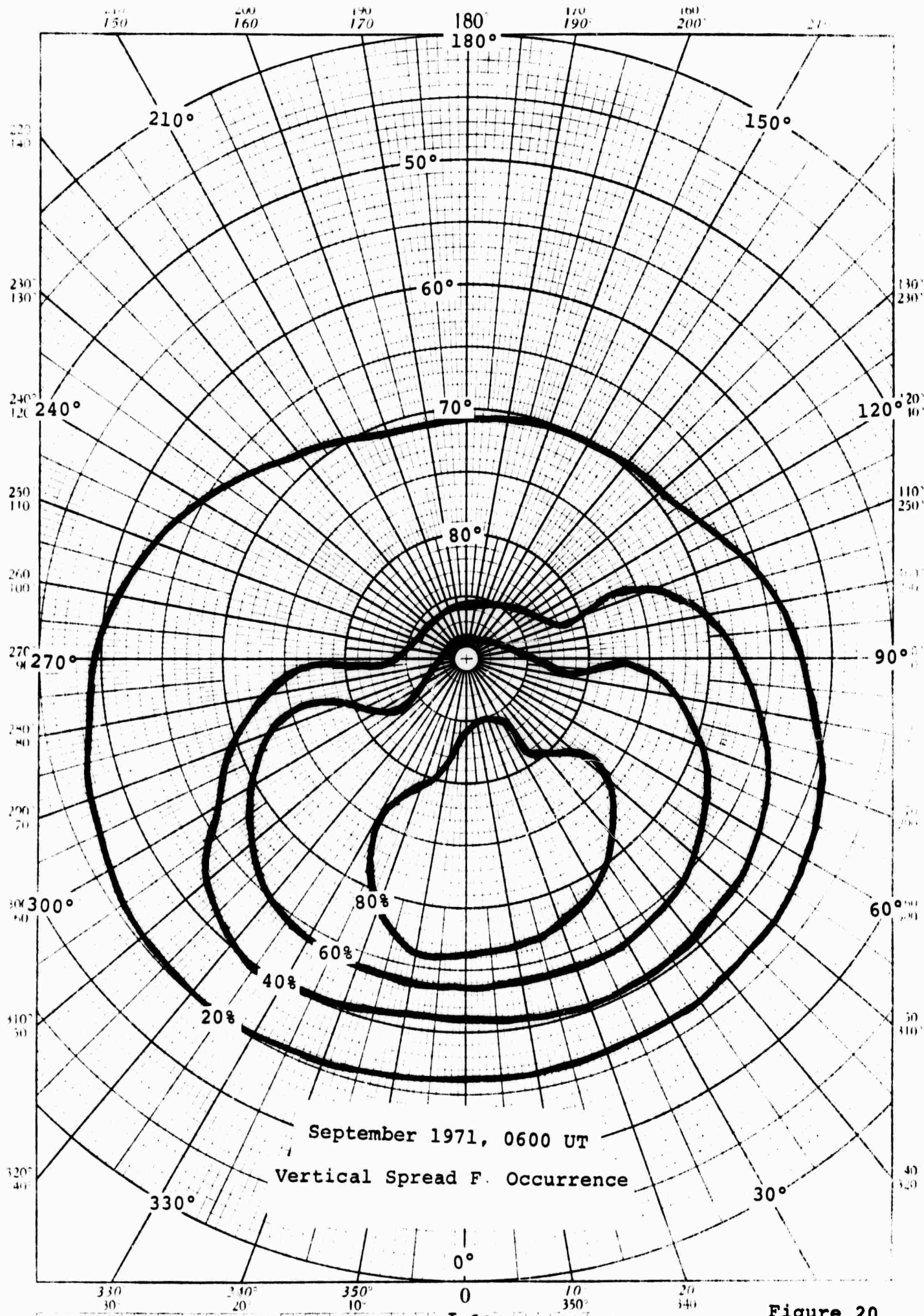


Figure 20

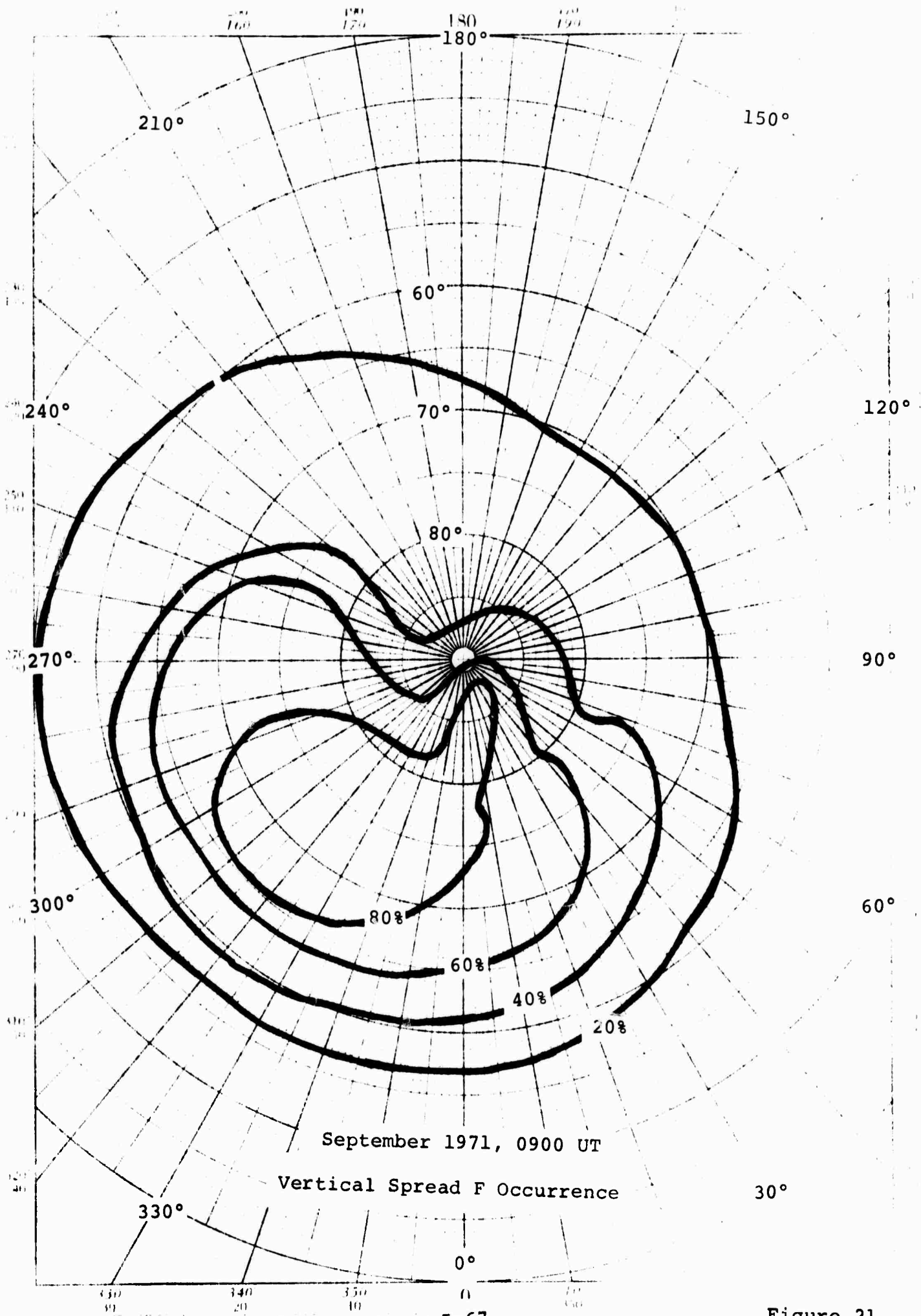


Figure 21

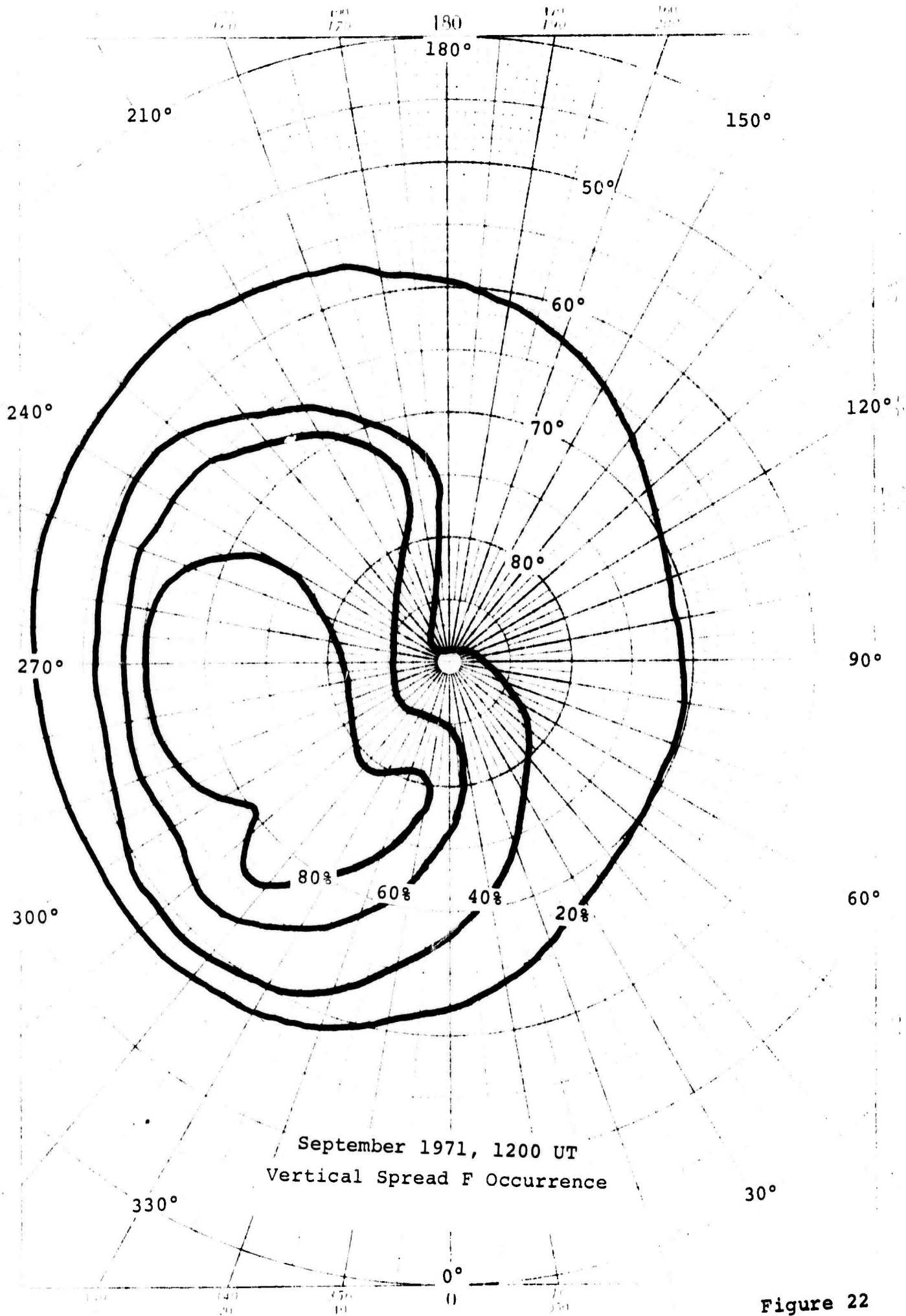


Figure 22

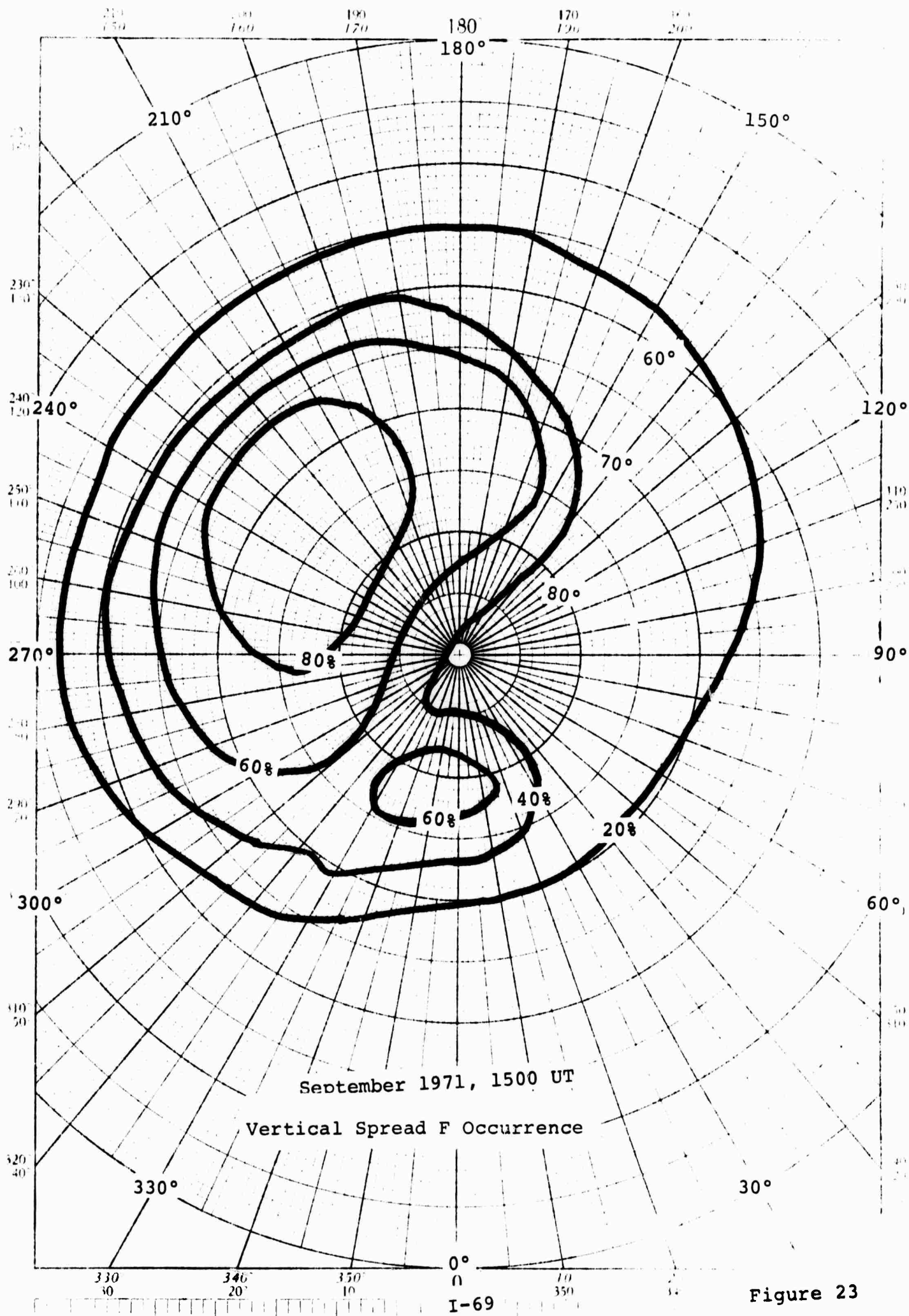
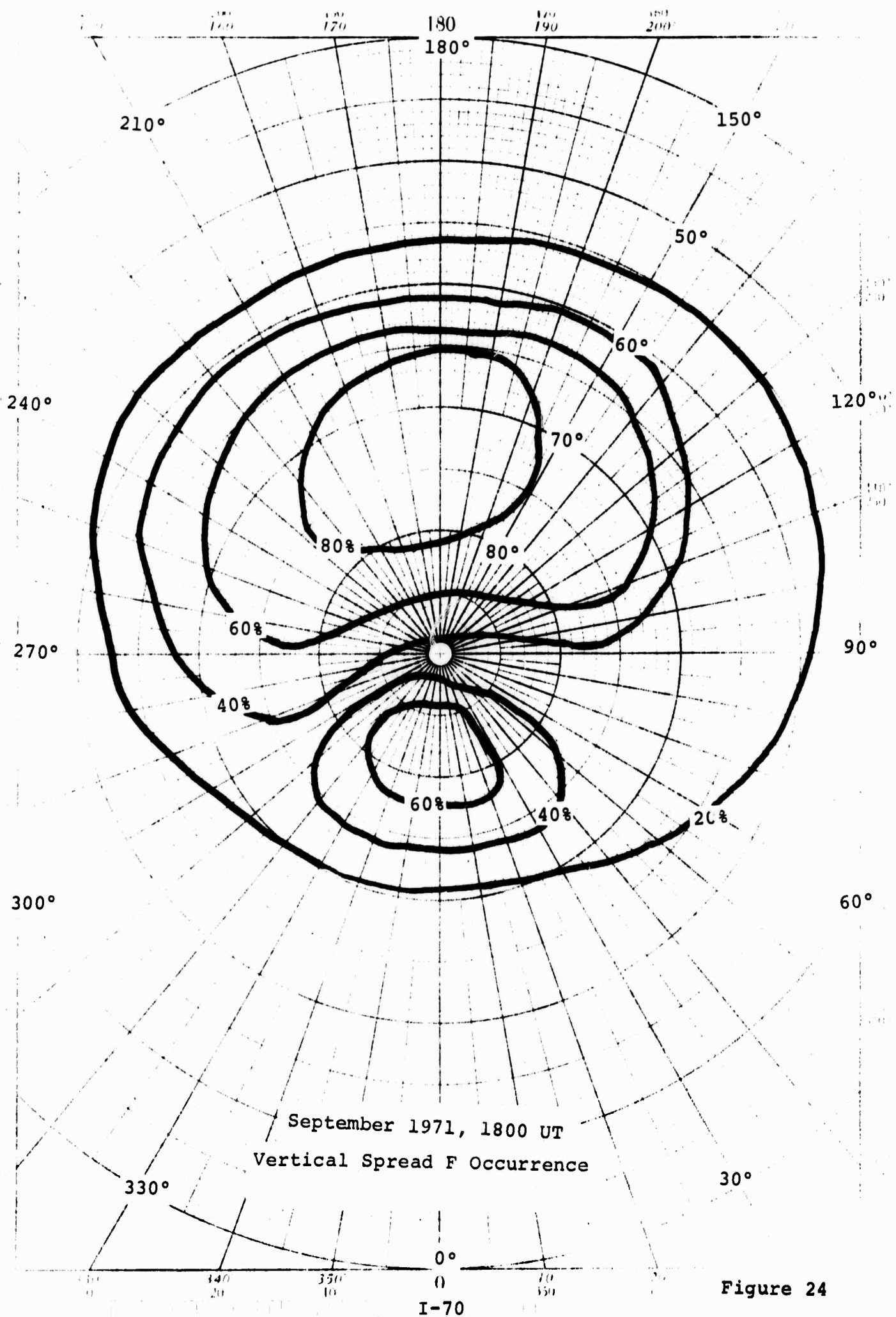
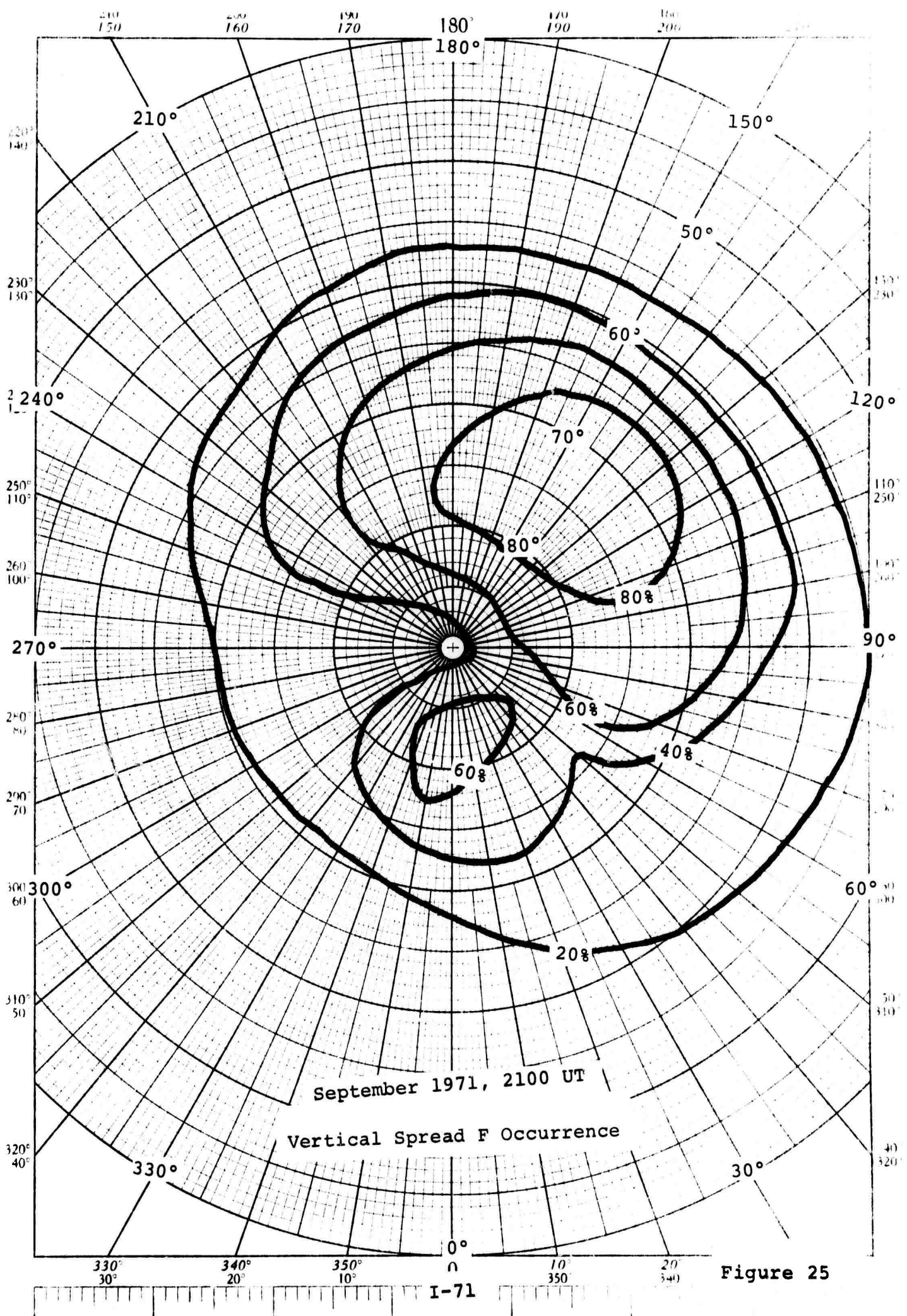


Figure 23



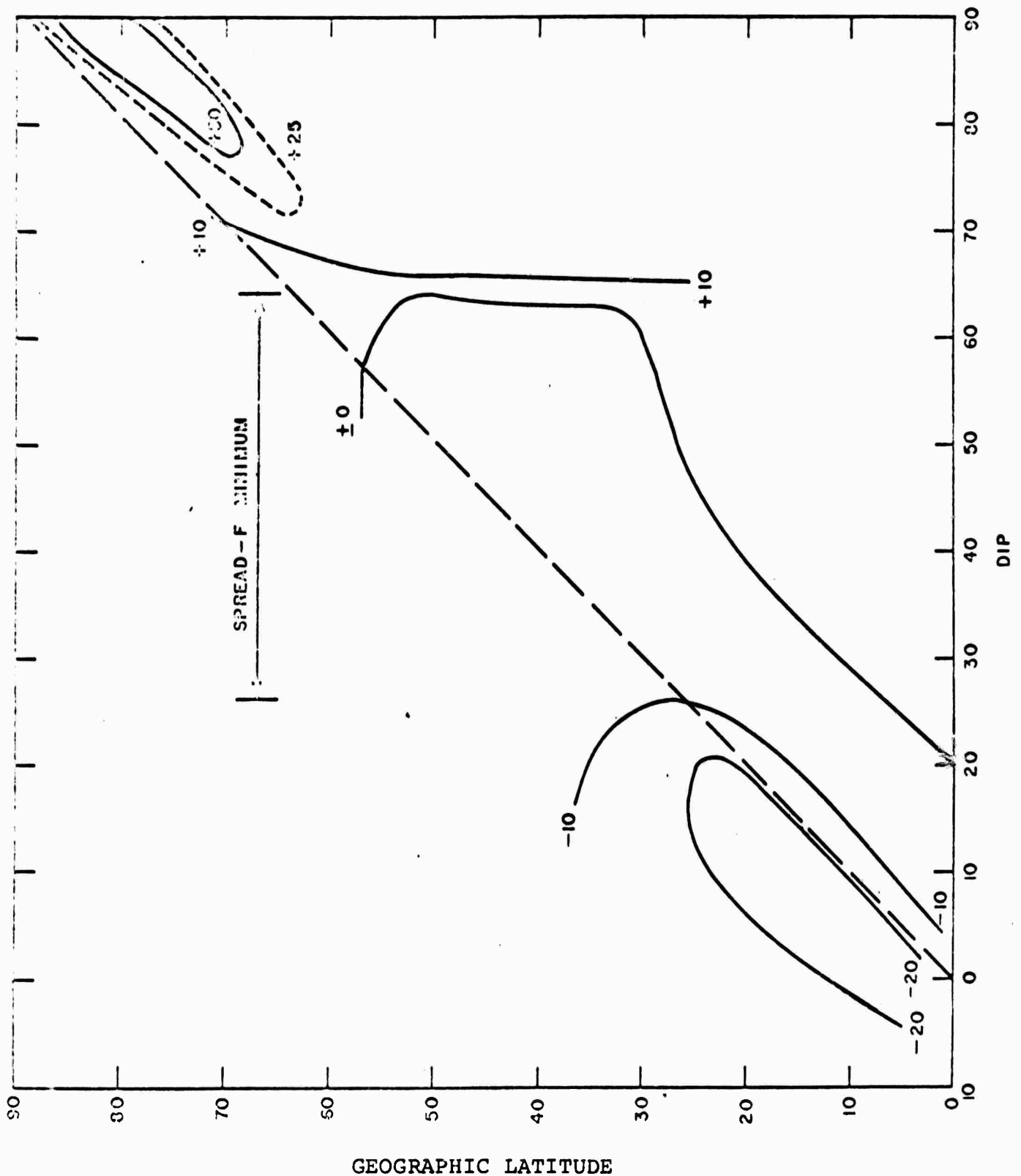
POLAR OCCURRENCE 48 4-12
REF: 1-1-10



September 1971, 2100 UT

Vertical Spread F Occurrence

Figure 25



Factors to convert July spread F occurrence percentages to Winter conditions (reproduced from Penndorf, 1960).

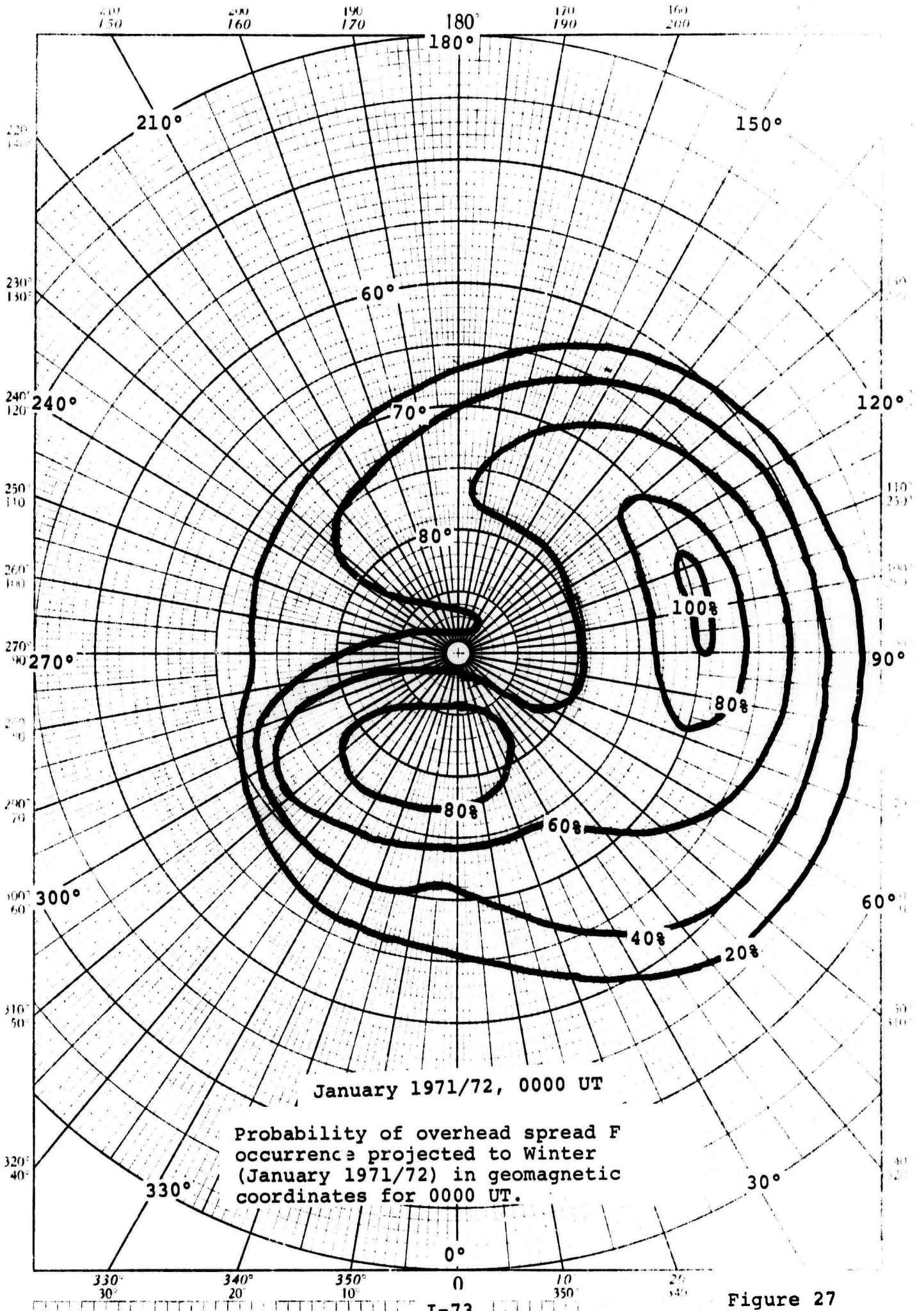
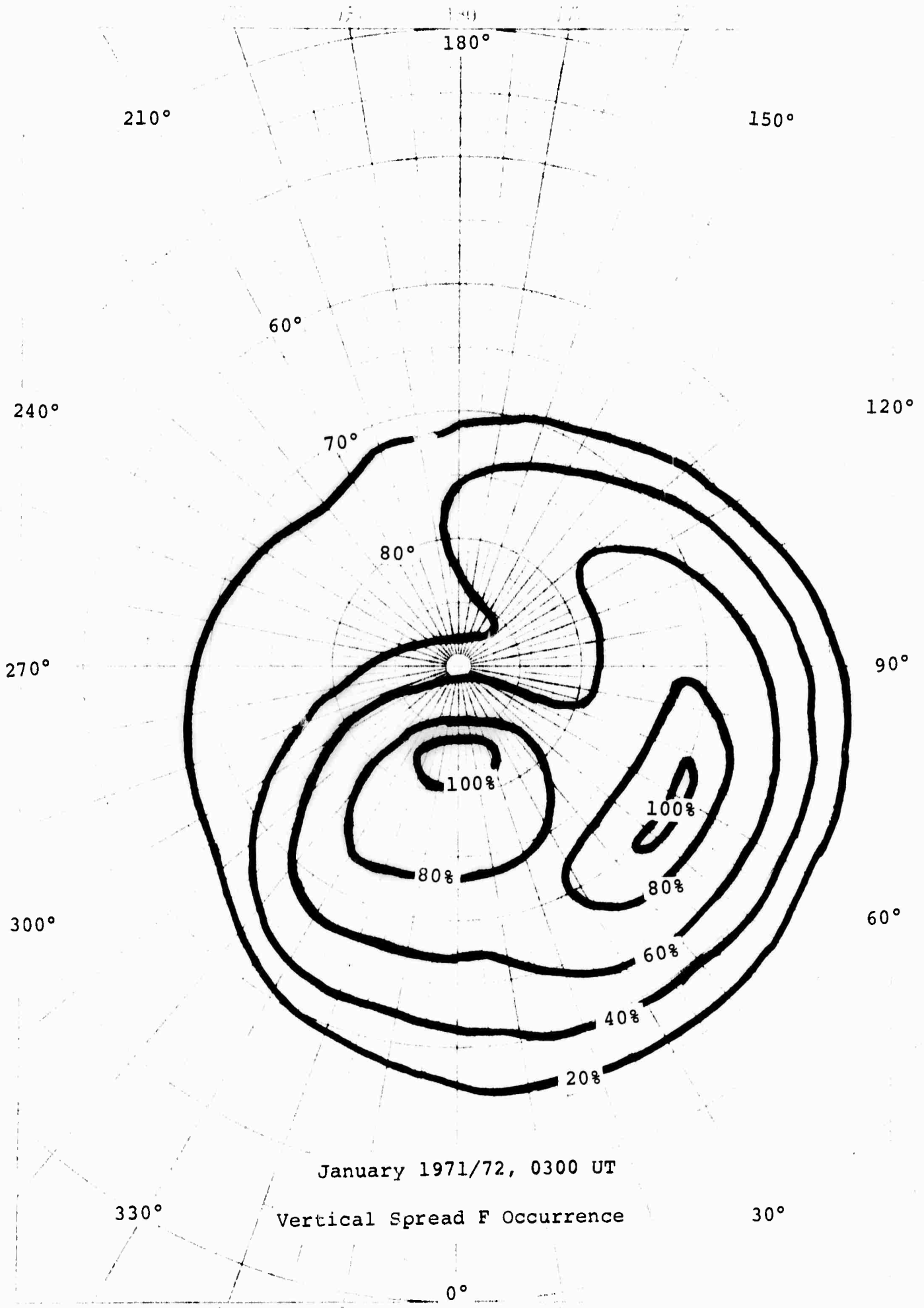


Figure 27



January 1971/72, 0300 UT

Vertical Spread F Occurrence

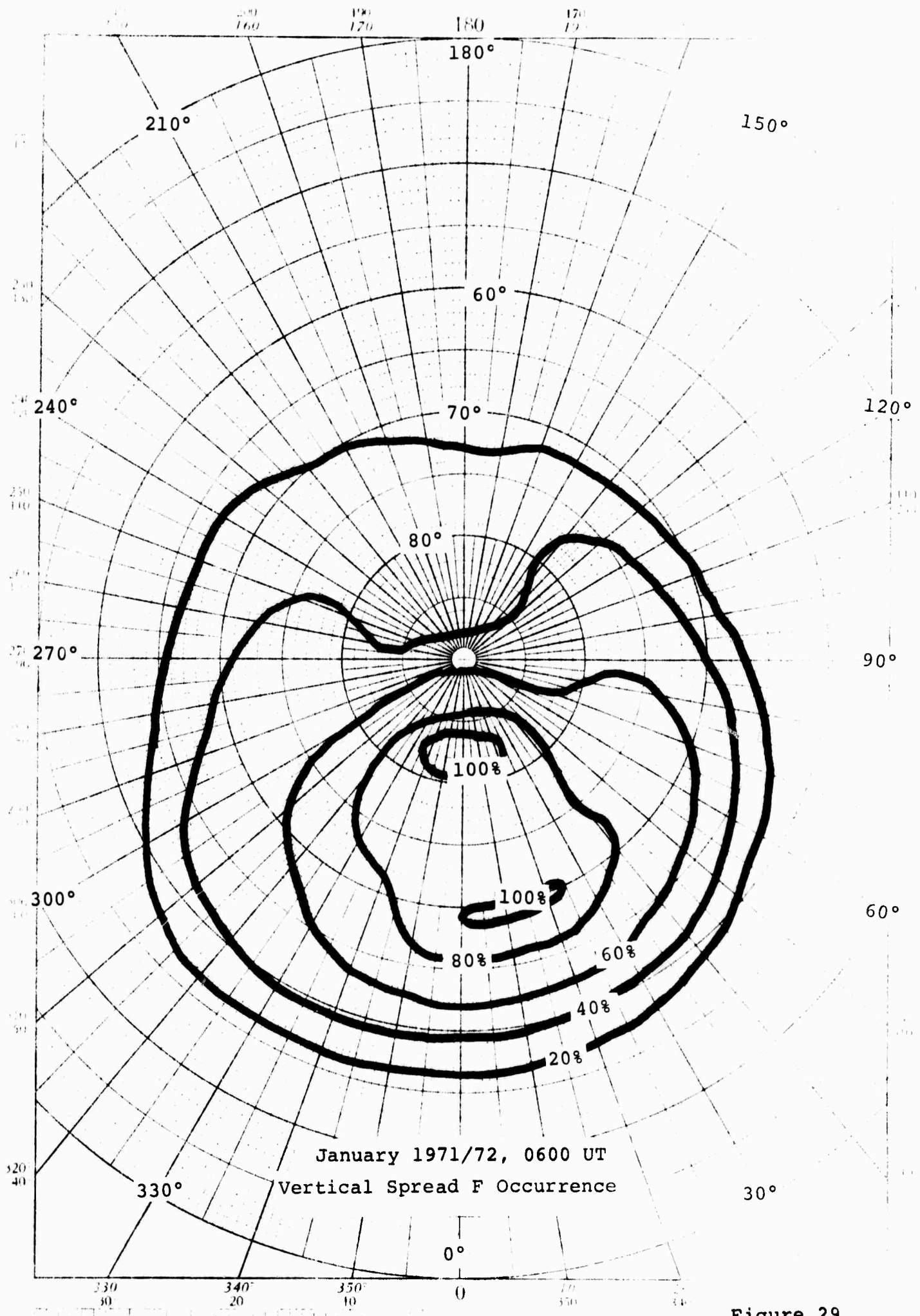
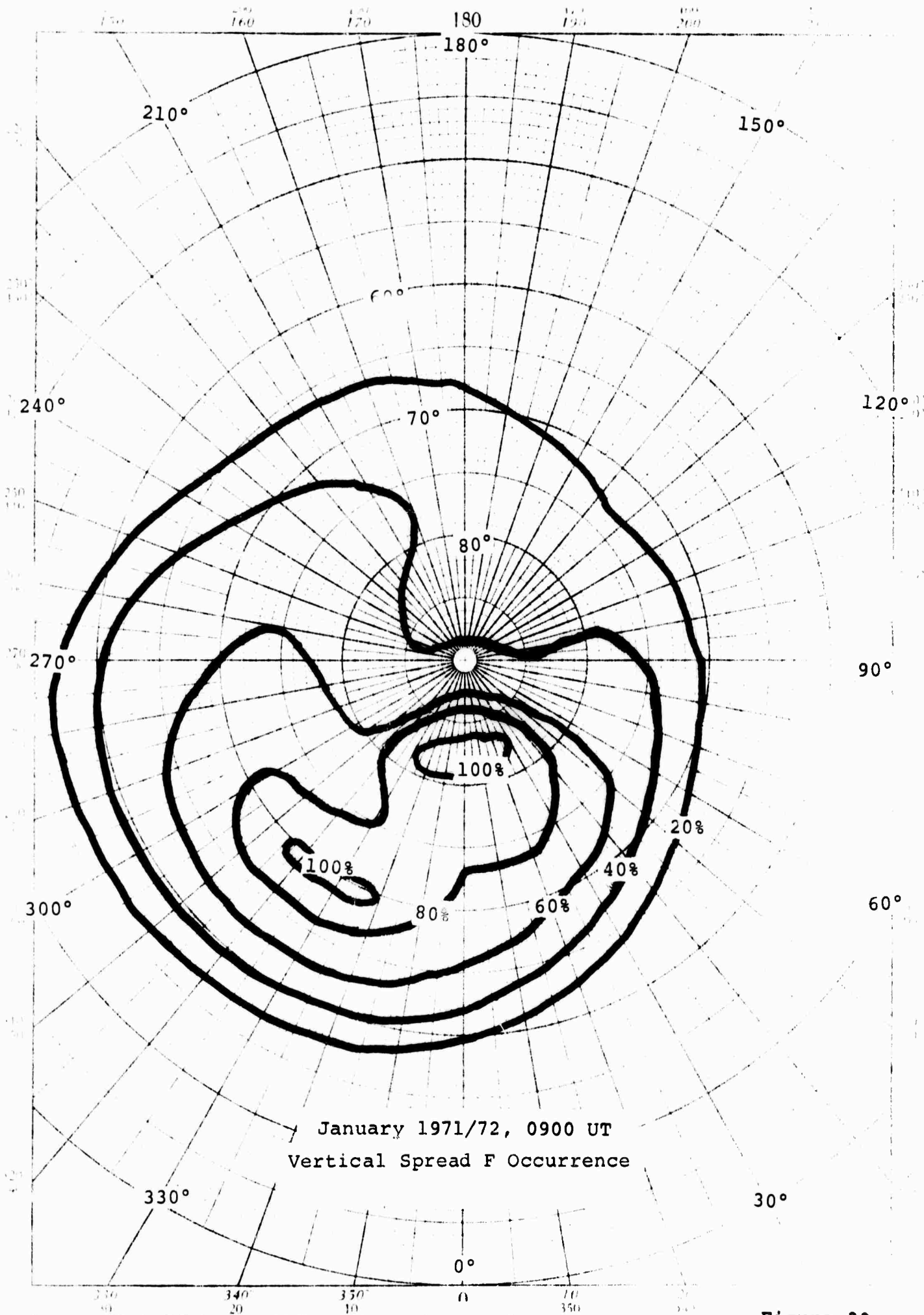
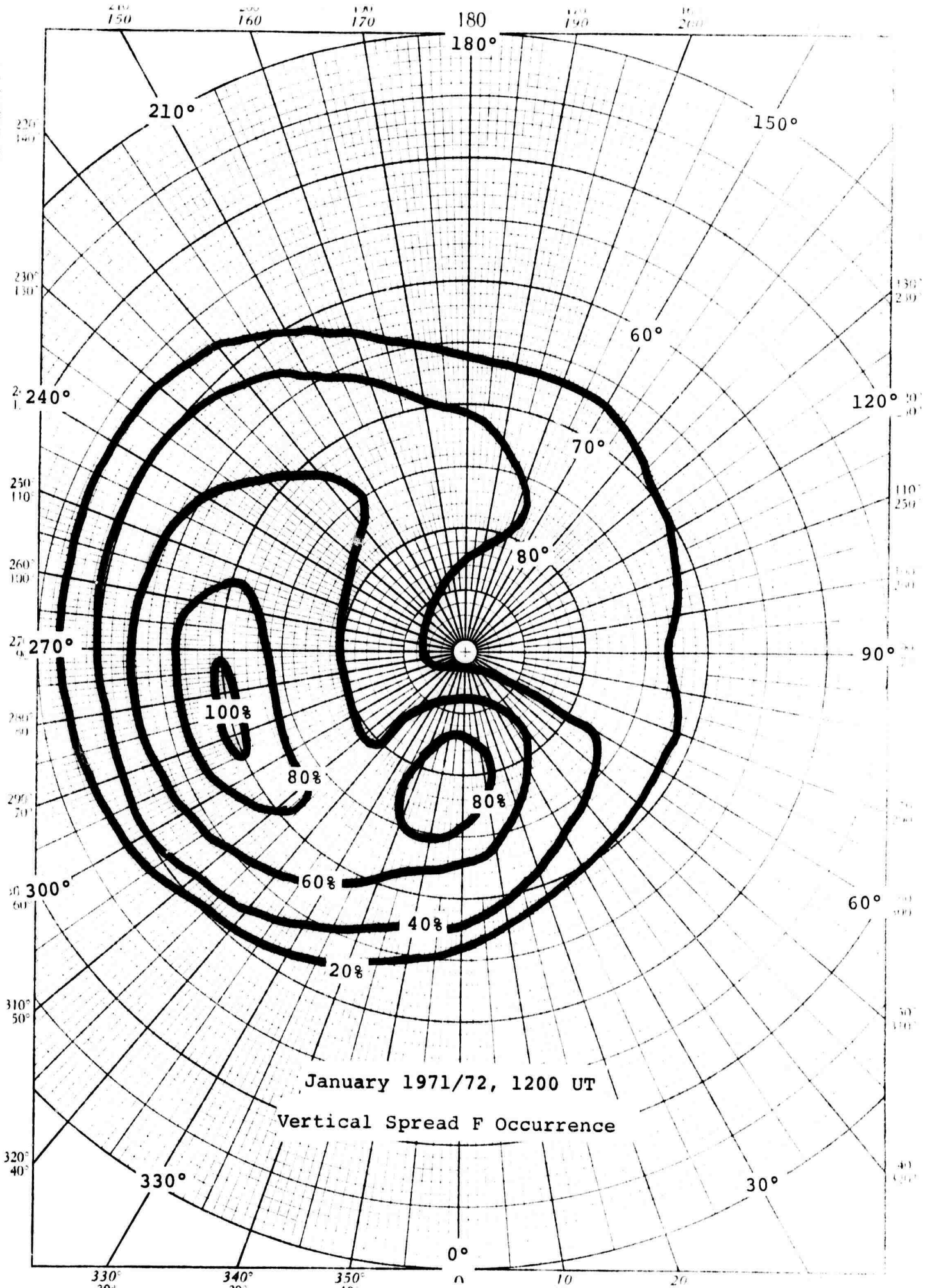


Figure 29

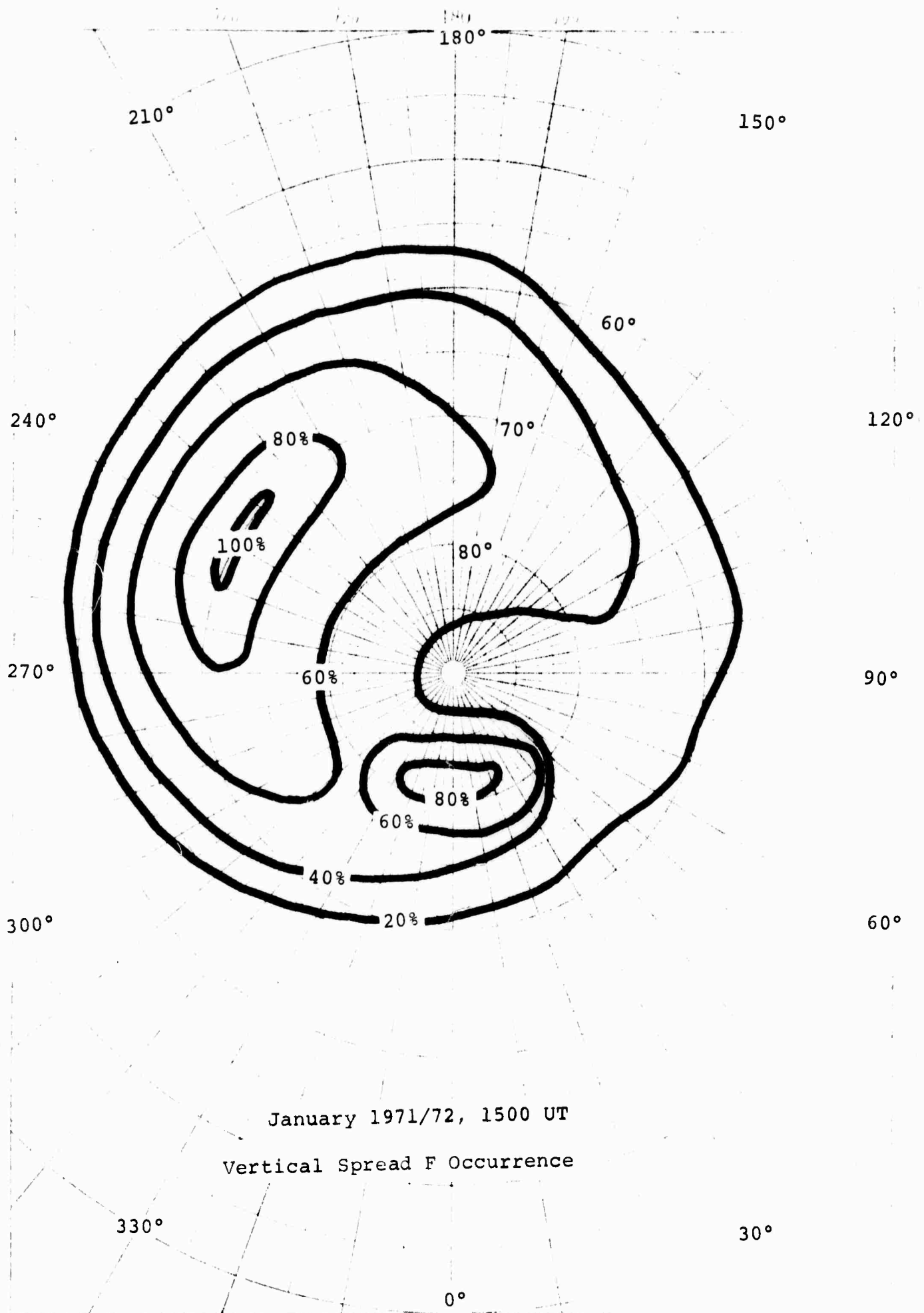


POLAR COORDINATE



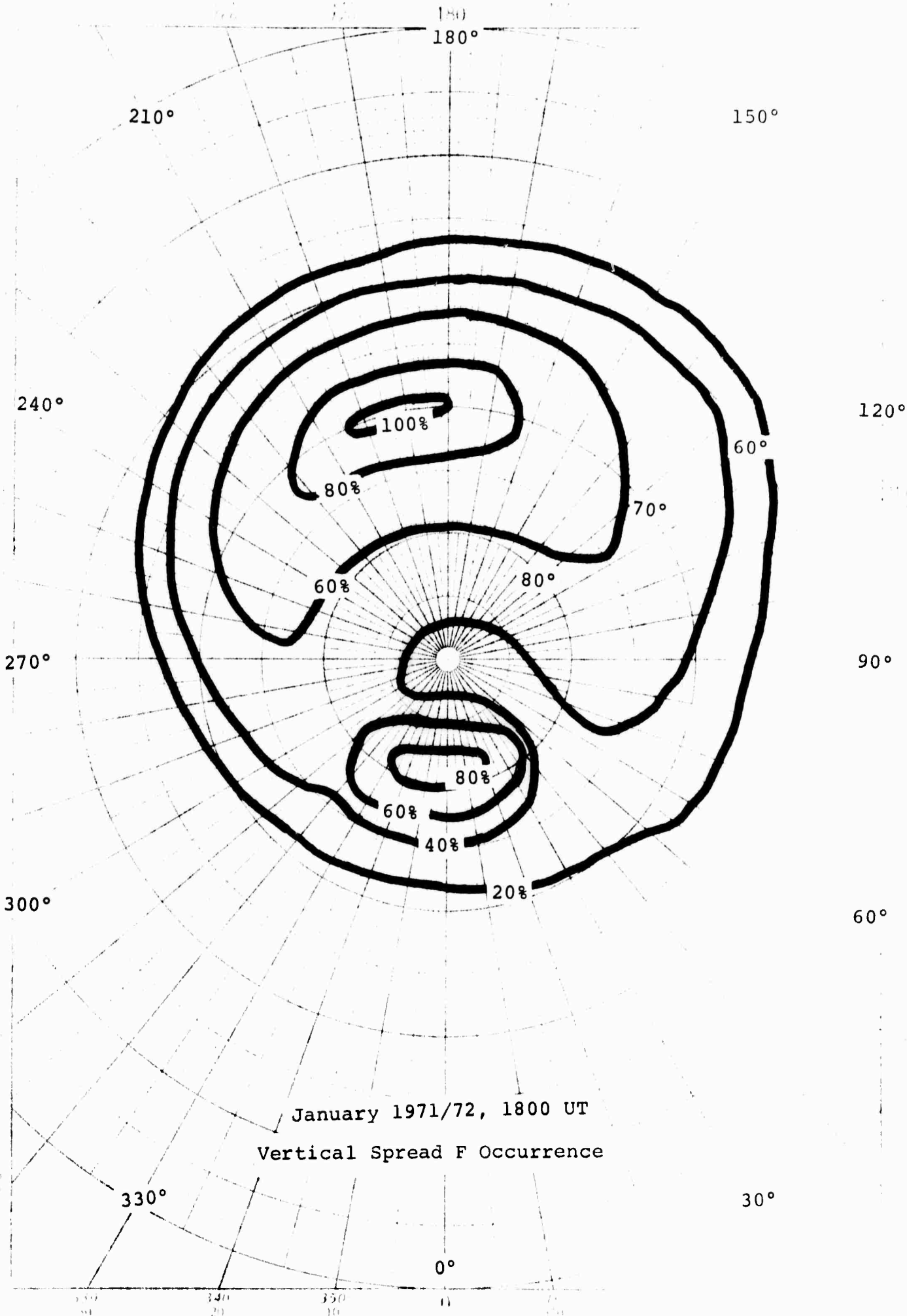
January 1971/72, 1200 UT
Vertical Spread F Occurrence

Figure 31



January 1971/72, 1500 UT
 Vertical Spread F Occurrence

Figure 32



January 1971/72, 1800 UT
 Vertical Spread F Occurrence

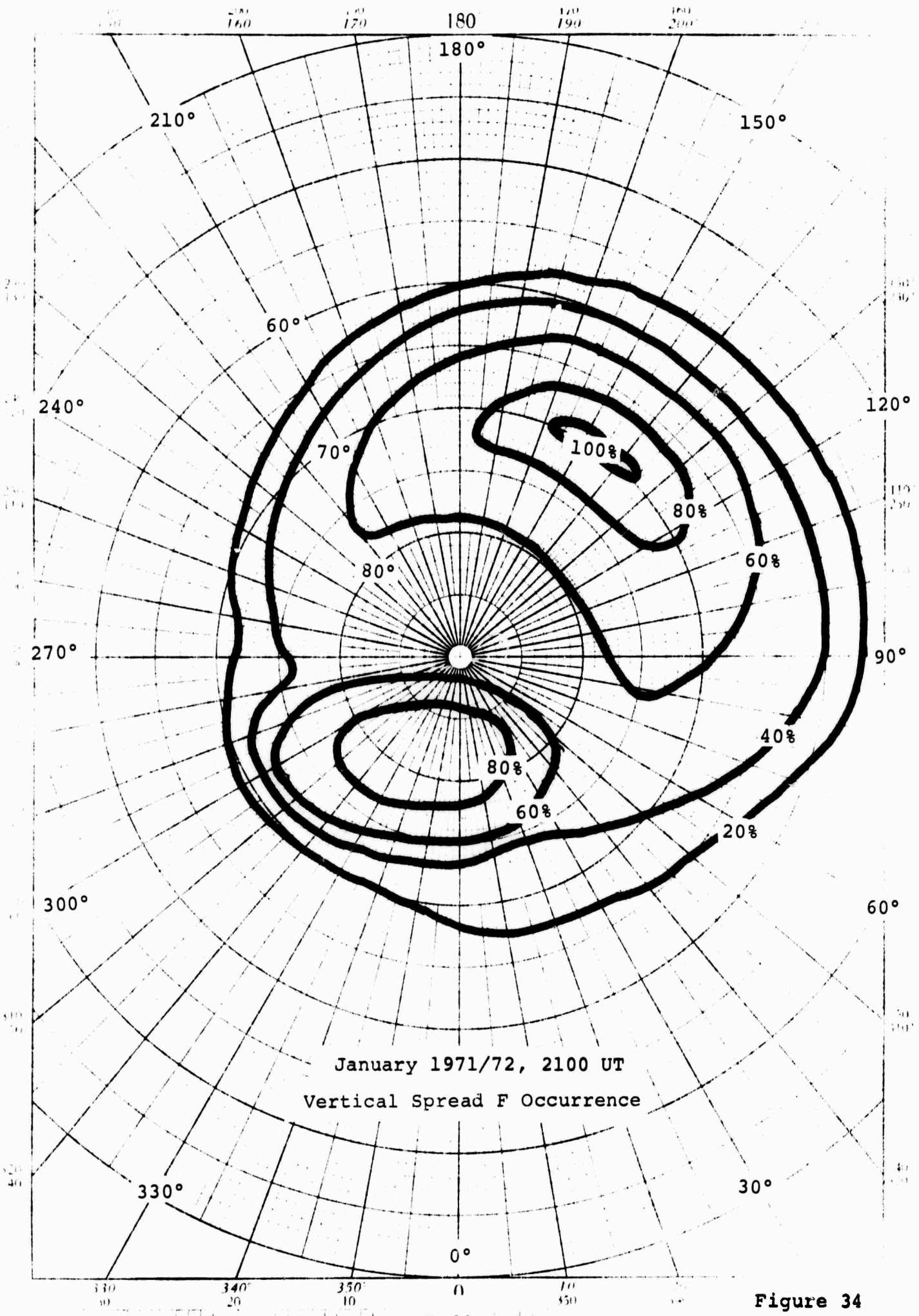
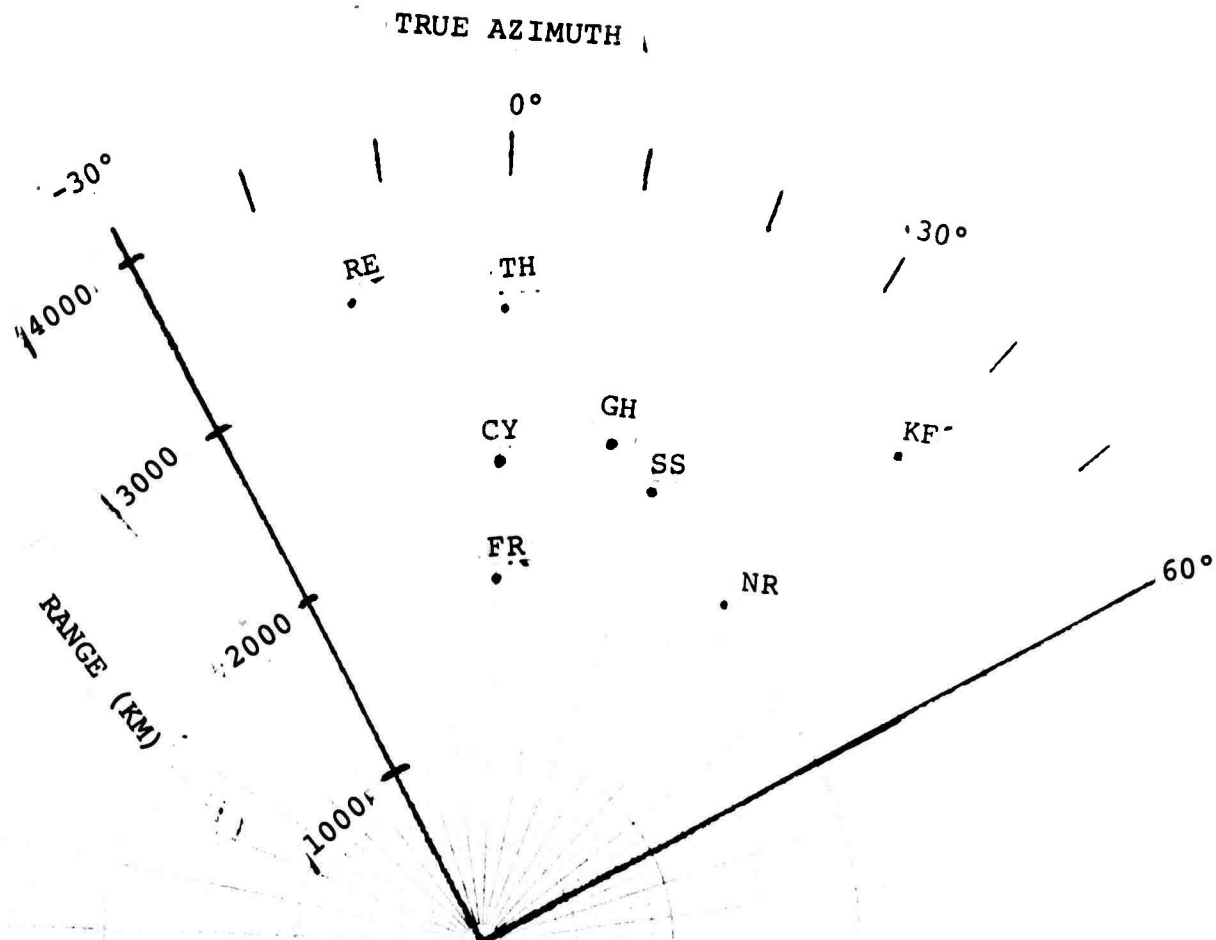
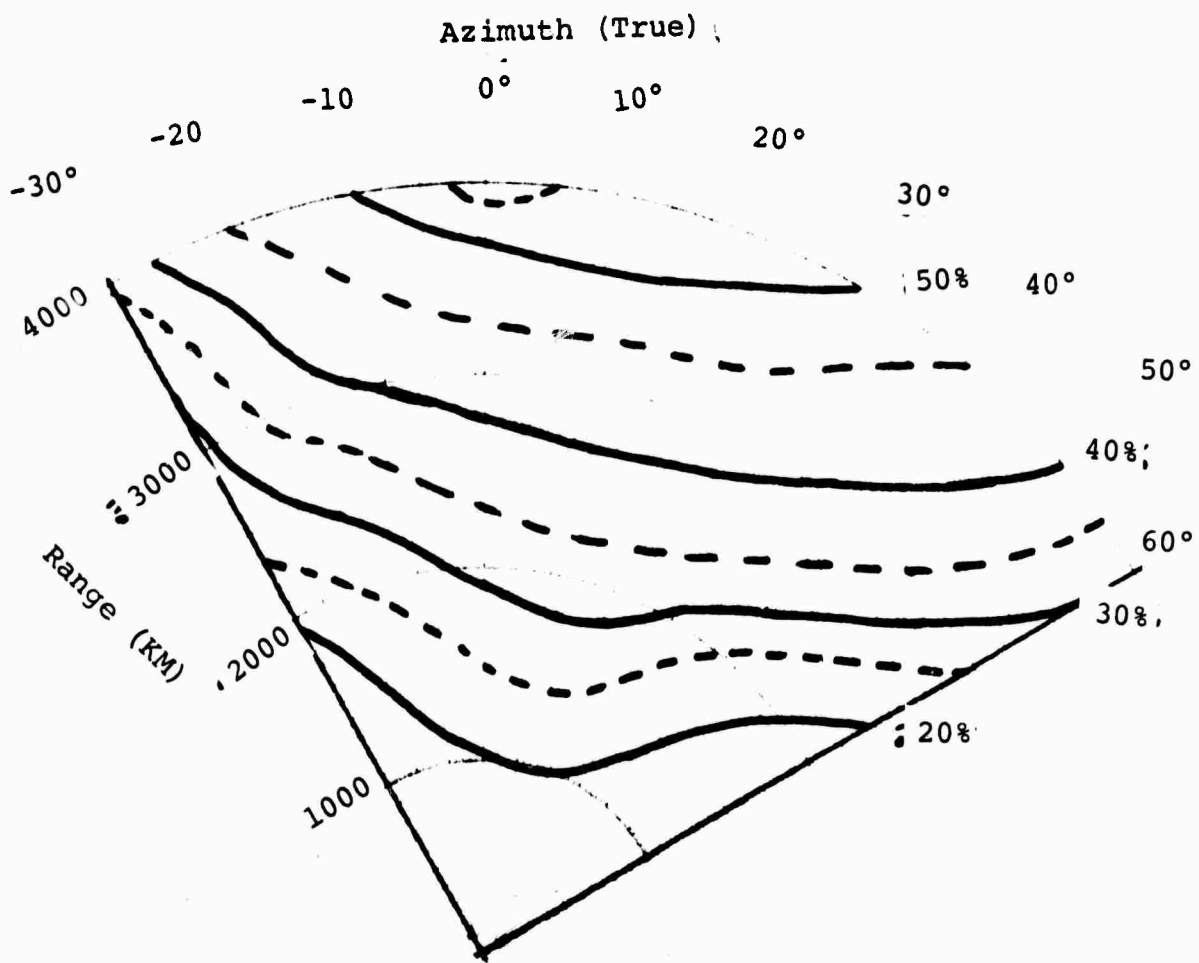


Figure 34



Range/Azimuth grid with origin at 46° 56' N, 68° 0' W (geographic coordinates), showing relative locations of geophysical ground station

- Key:
- RE Resolute Bay
 - TH Thule
 - FR Frobisher Bay
 - SS Sondes Strom
 - NR Narssarssuag
 - KF Keflavik
 - GH Godhavn
 - CY Clyde Riv.



Spread F occurrence probability at midpoint of path terminating at indicated range and azimuth: projected to July 1971/72 at 0000 UT.

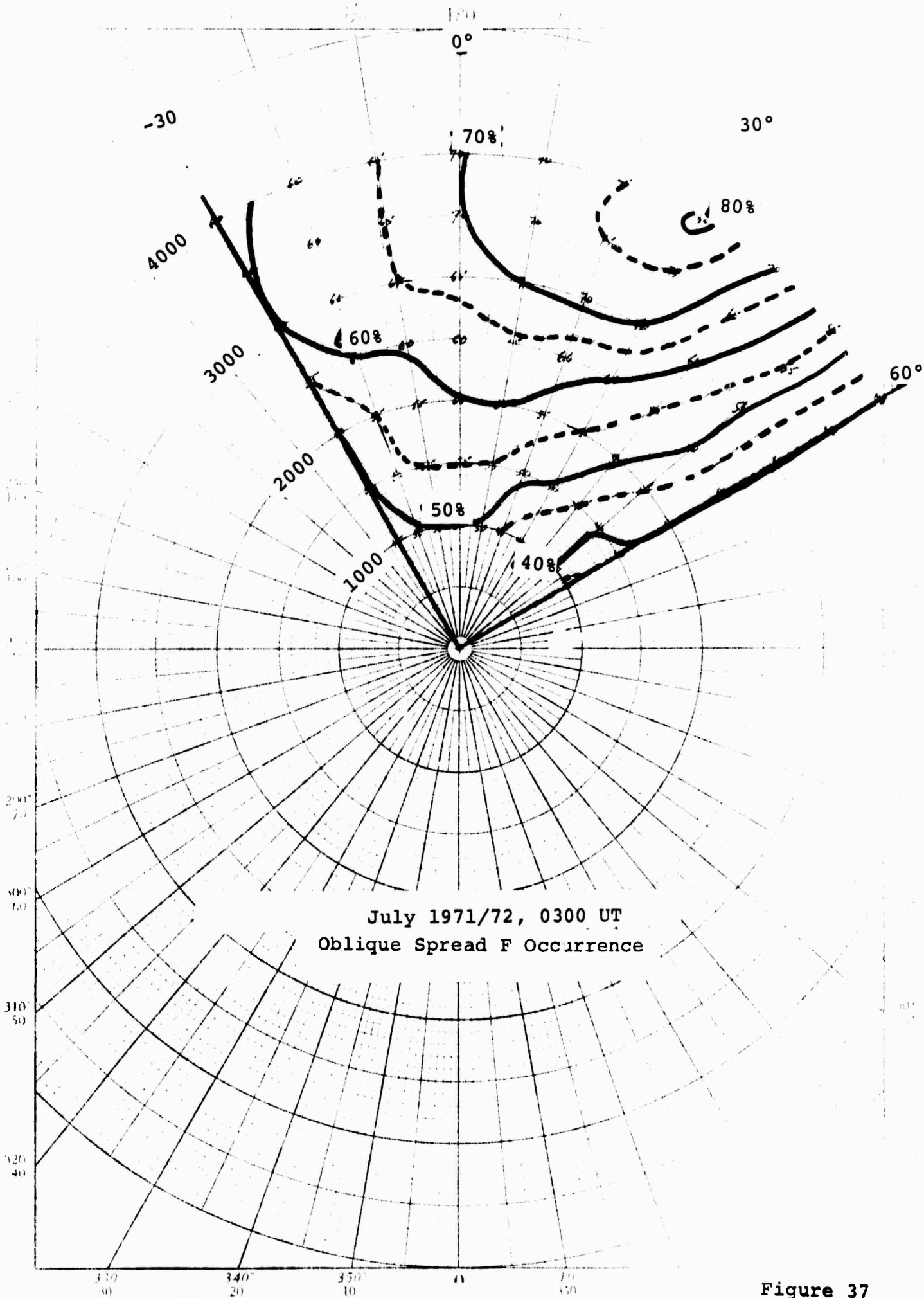


Figure 37

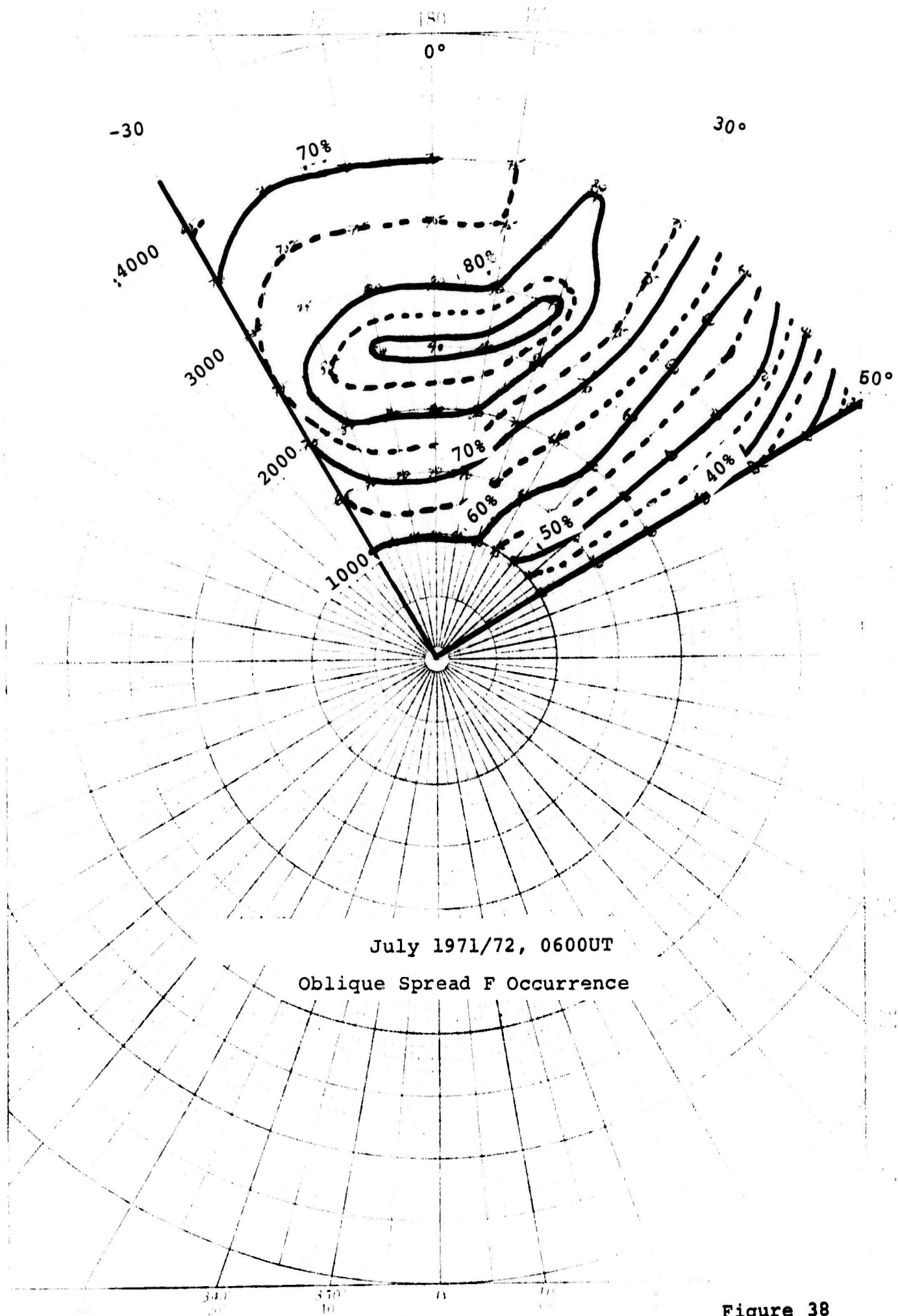
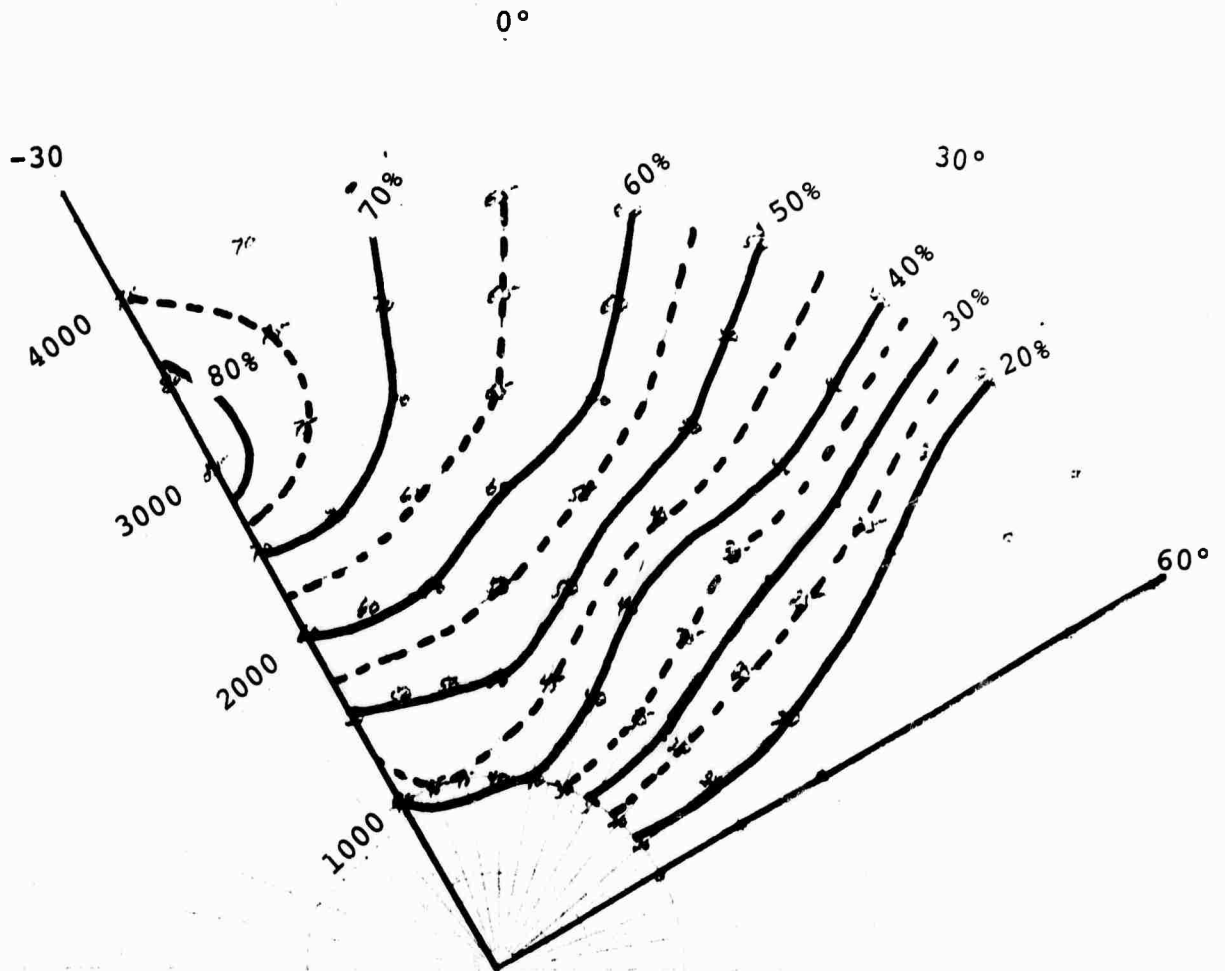
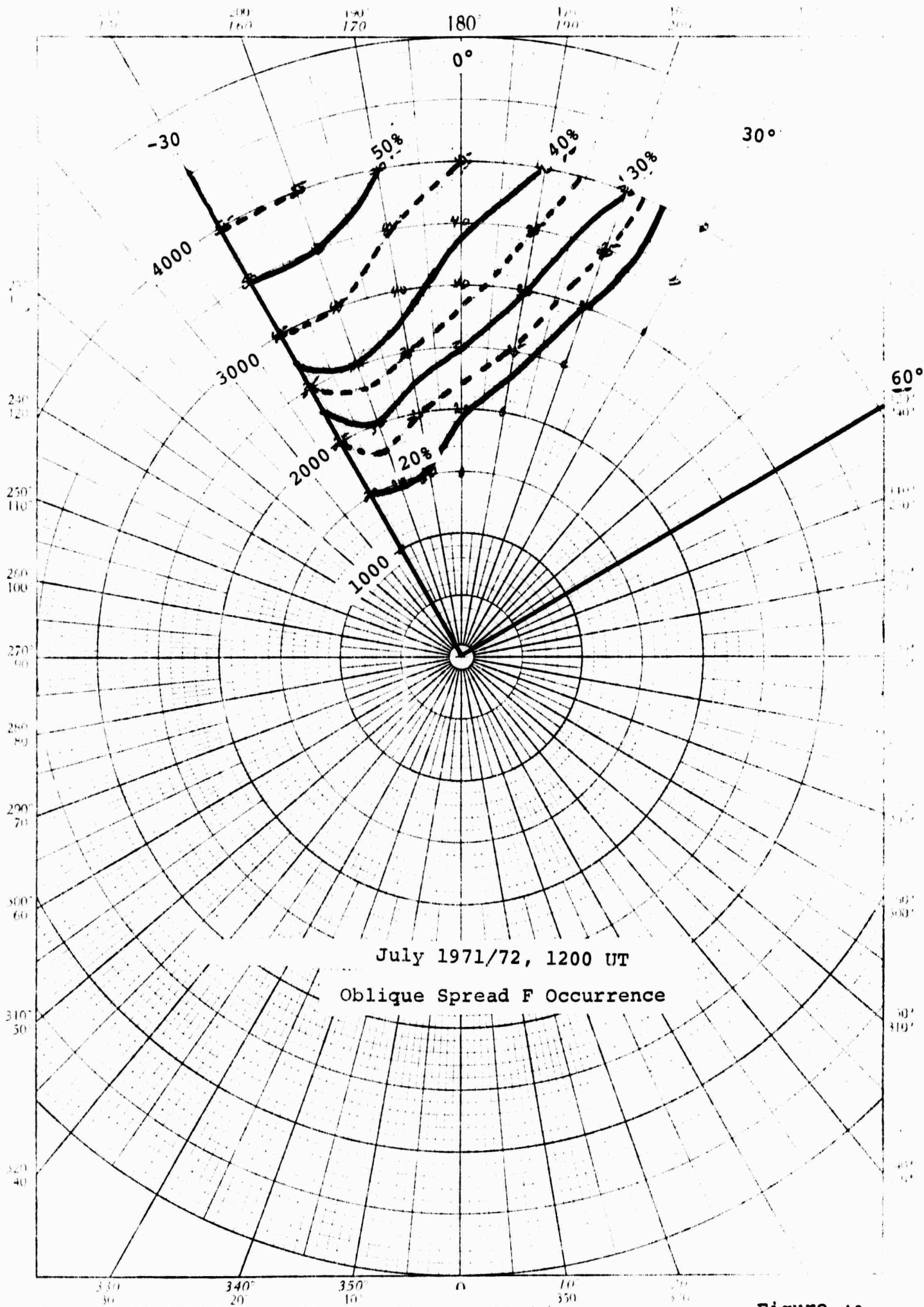


Figure 38

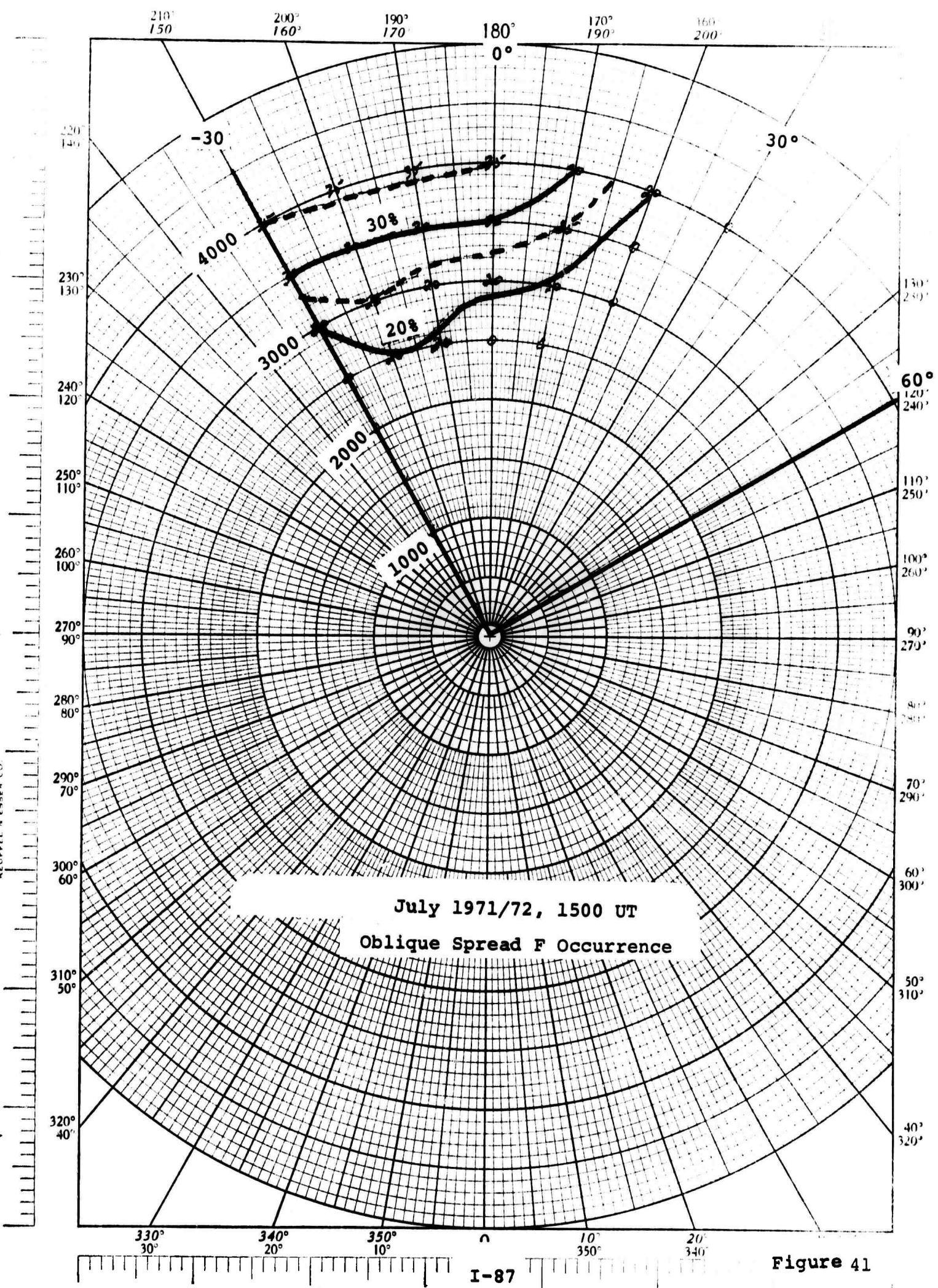


July 1971/72, 0900 UT
 Oblique Spread F Occurrence

Figure 39



K&E POLAR COORDINATE 46-4412
KEUFFEL & ESSER CO.



July 1971/72, 1500 UT
Oblique Spread F Occurrence

Figure 41

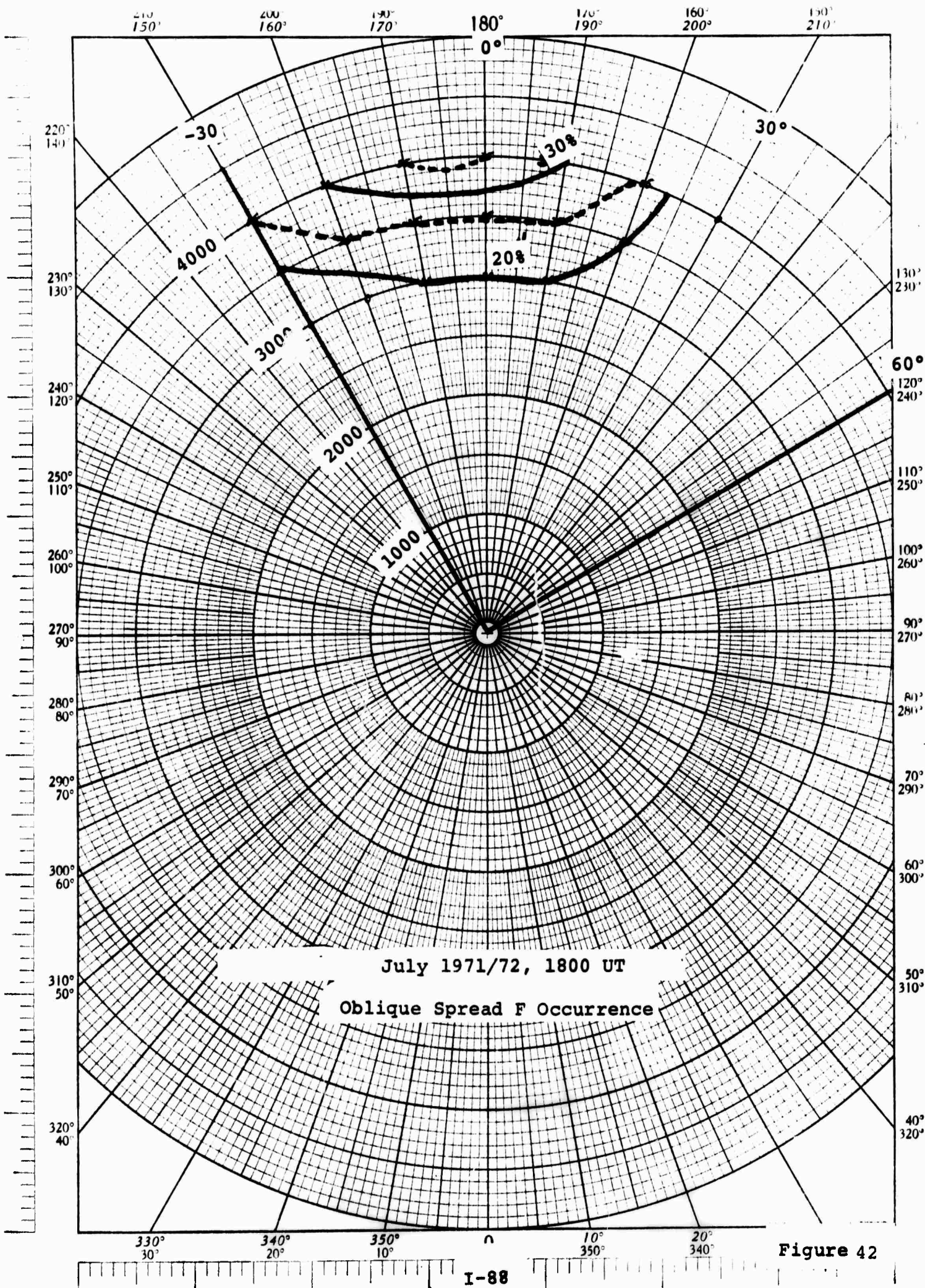
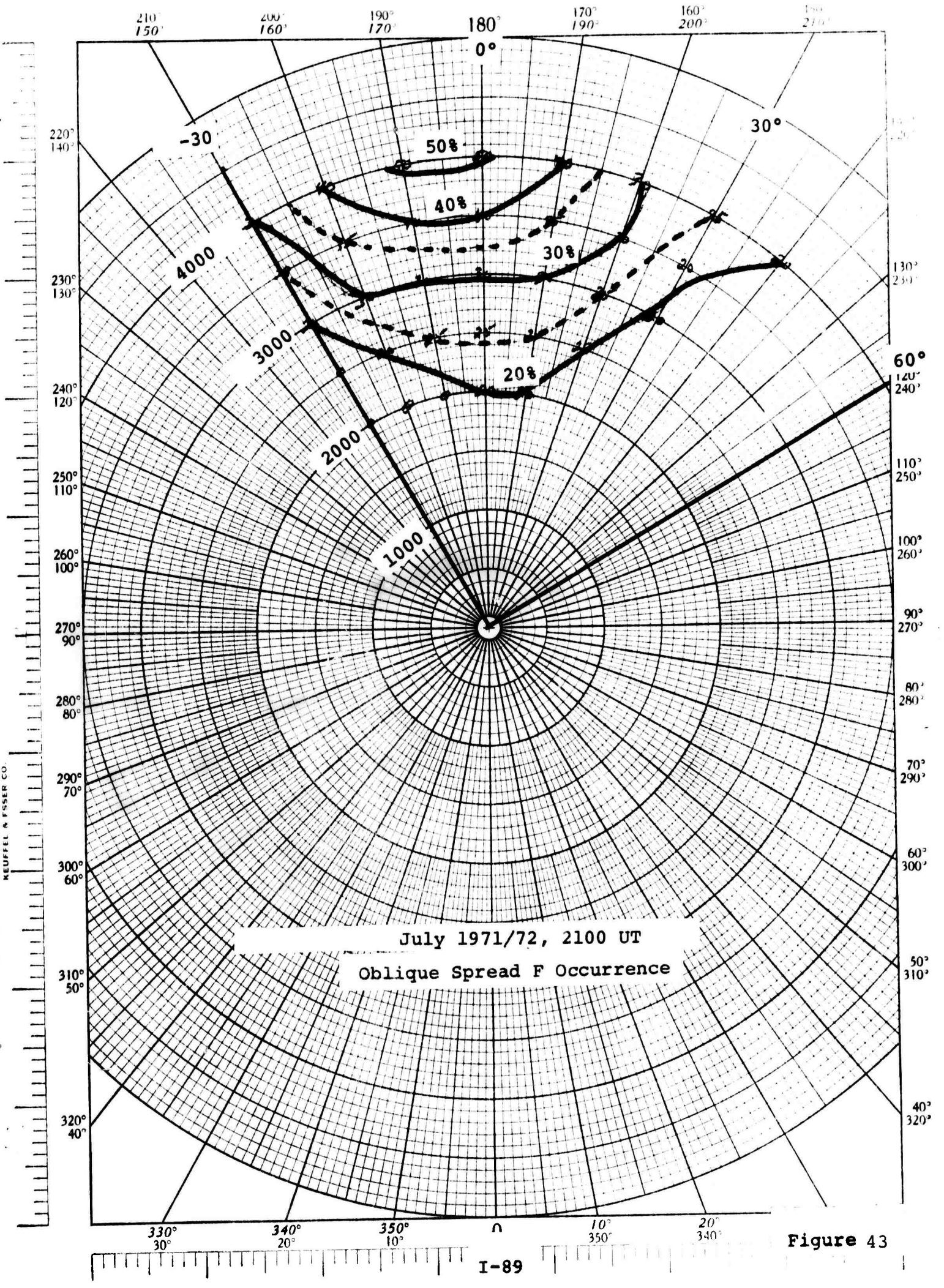
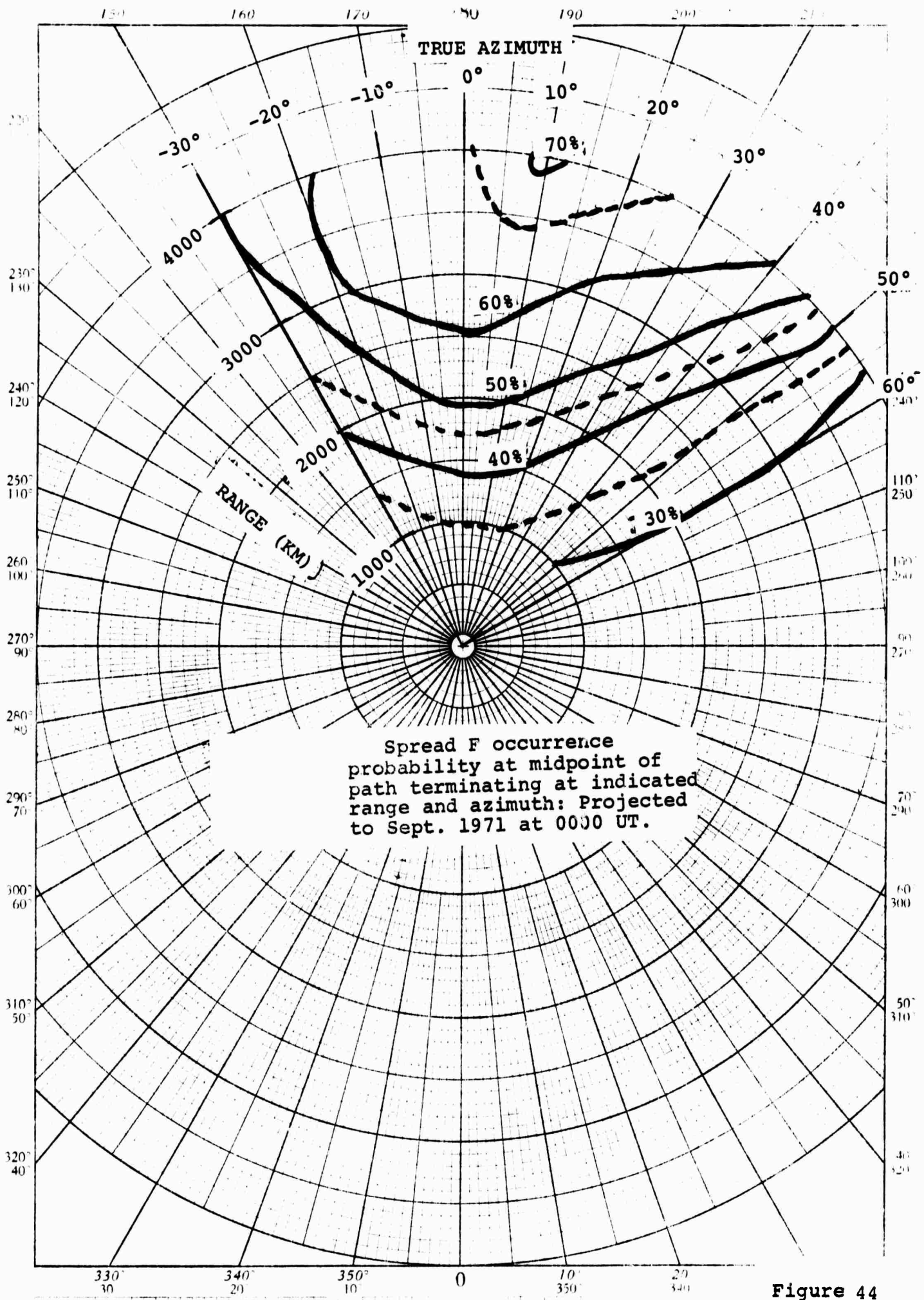


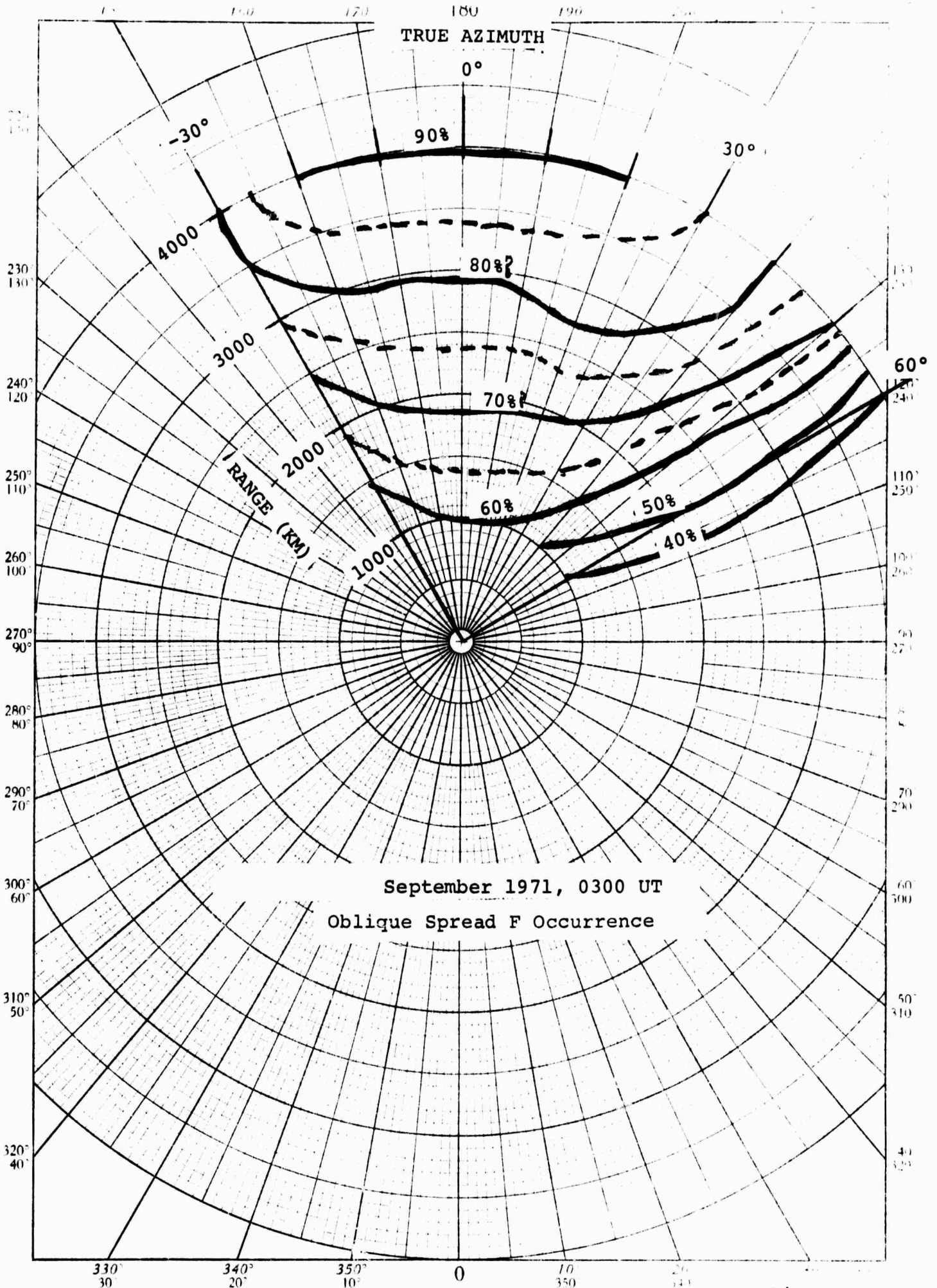
Figure 42



July 1971/72, 2100 UT
Oblique Spread F Occurrence

Figure 43





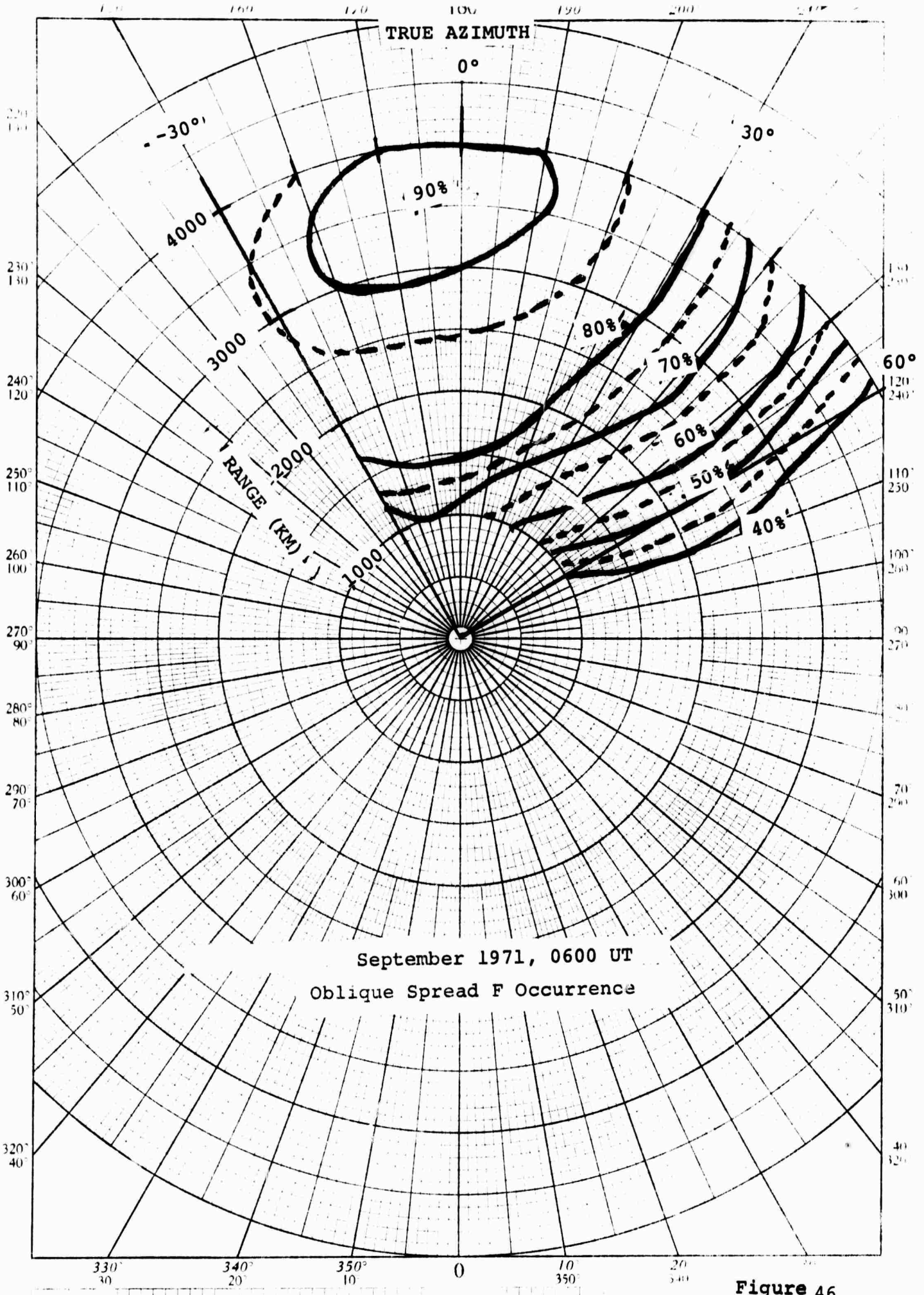


Figure 46

K&E POLAR COORDINATE 45 4412
REVISED EDITION

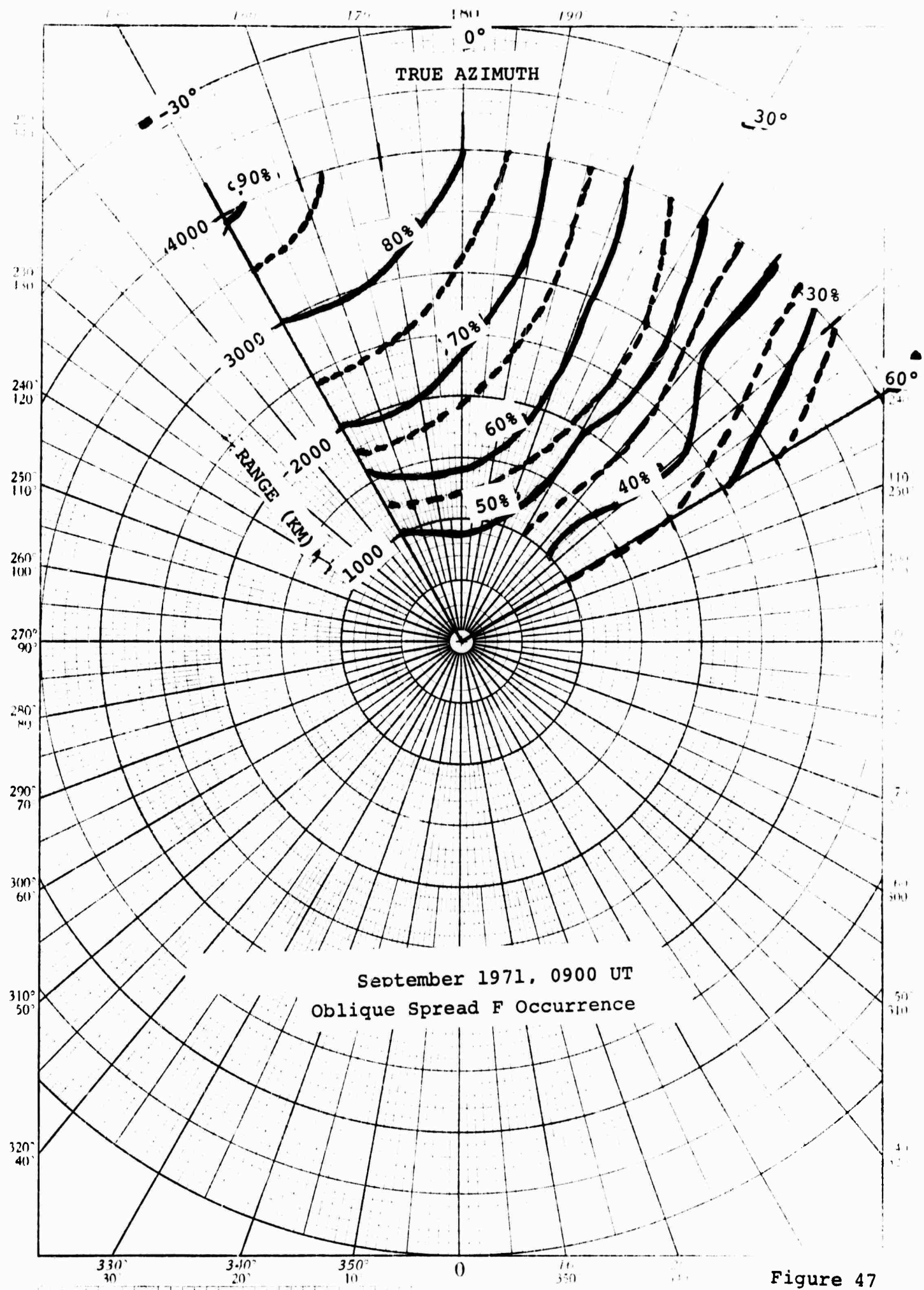
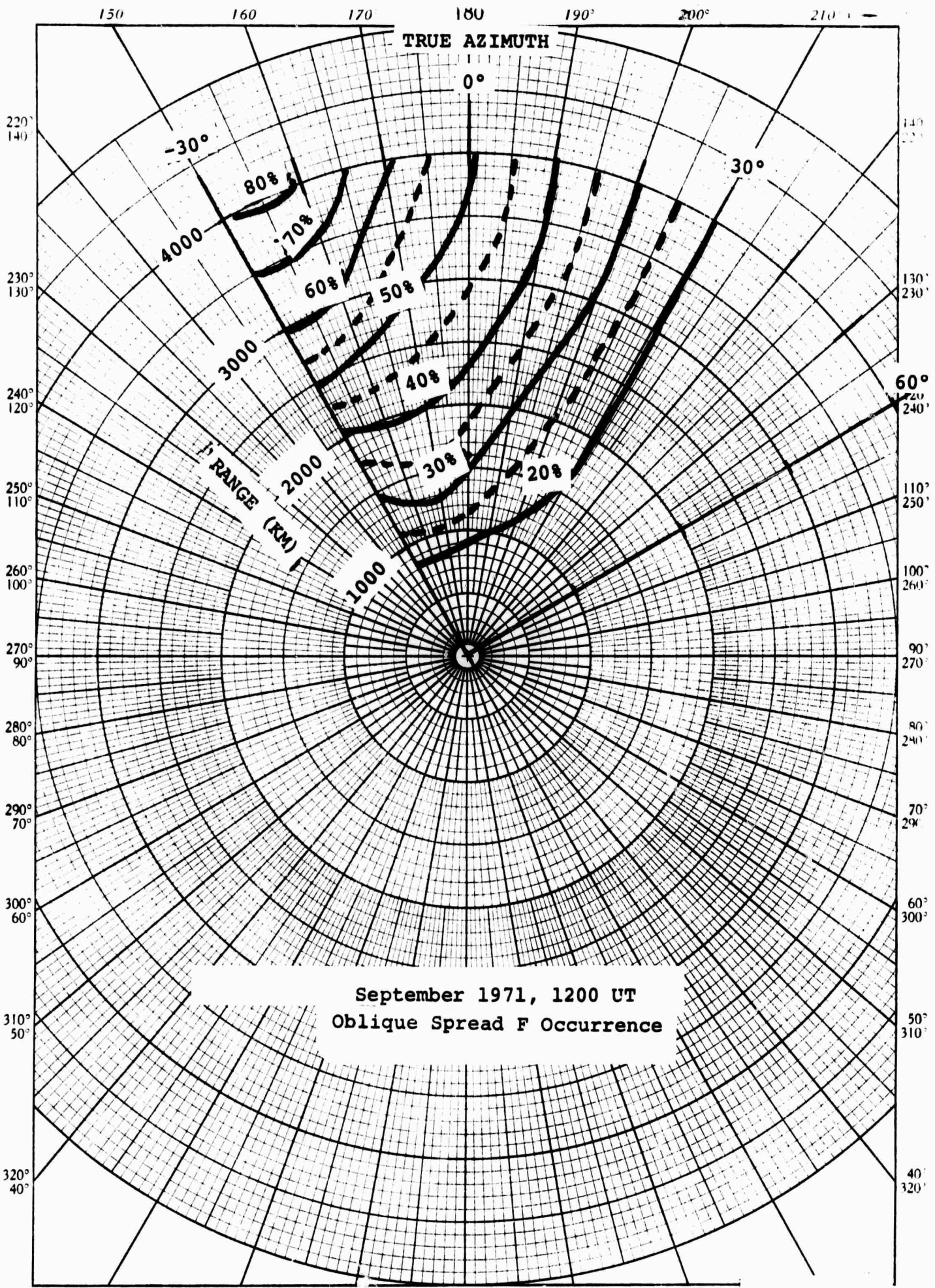


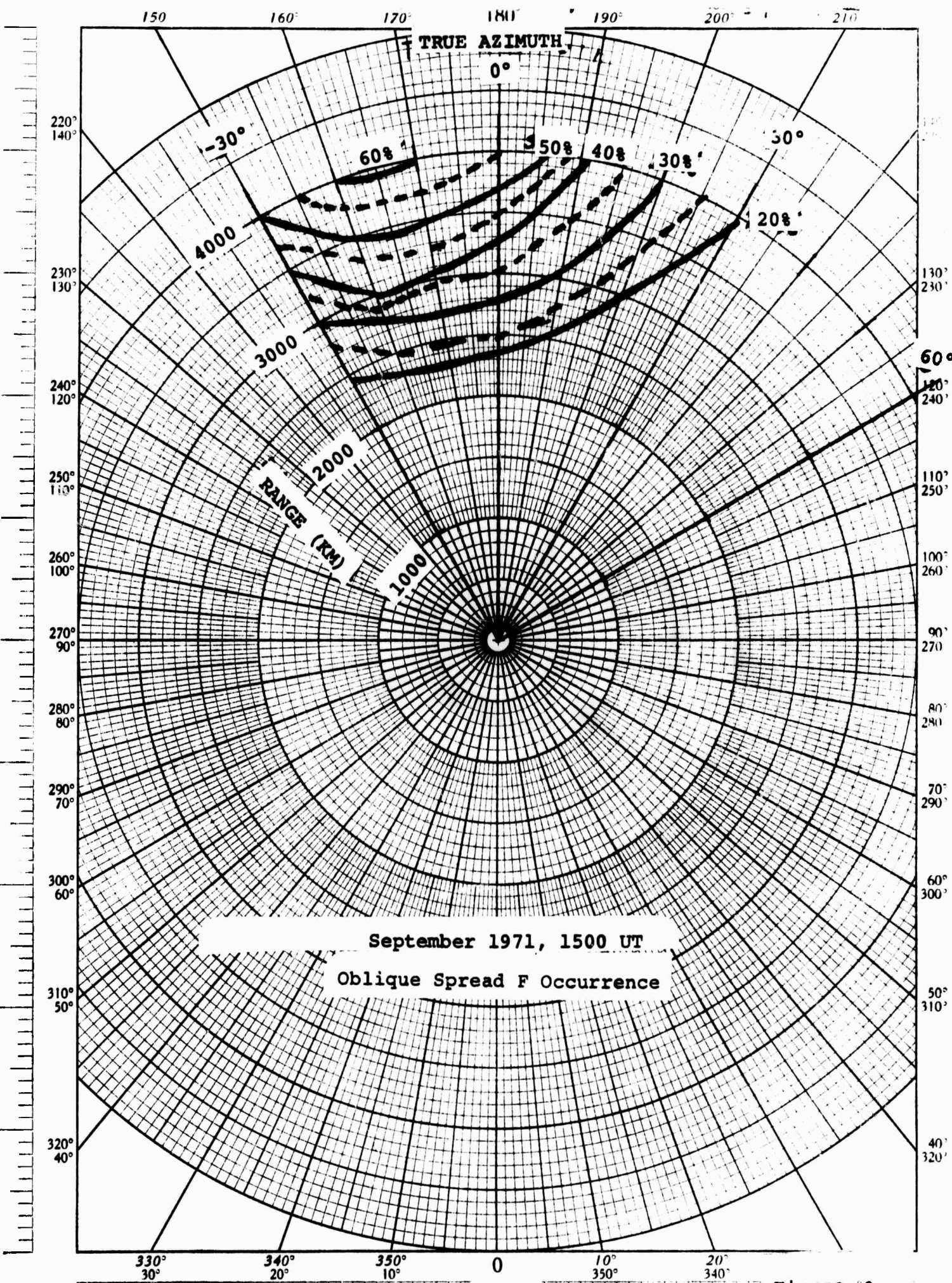
Figure 47



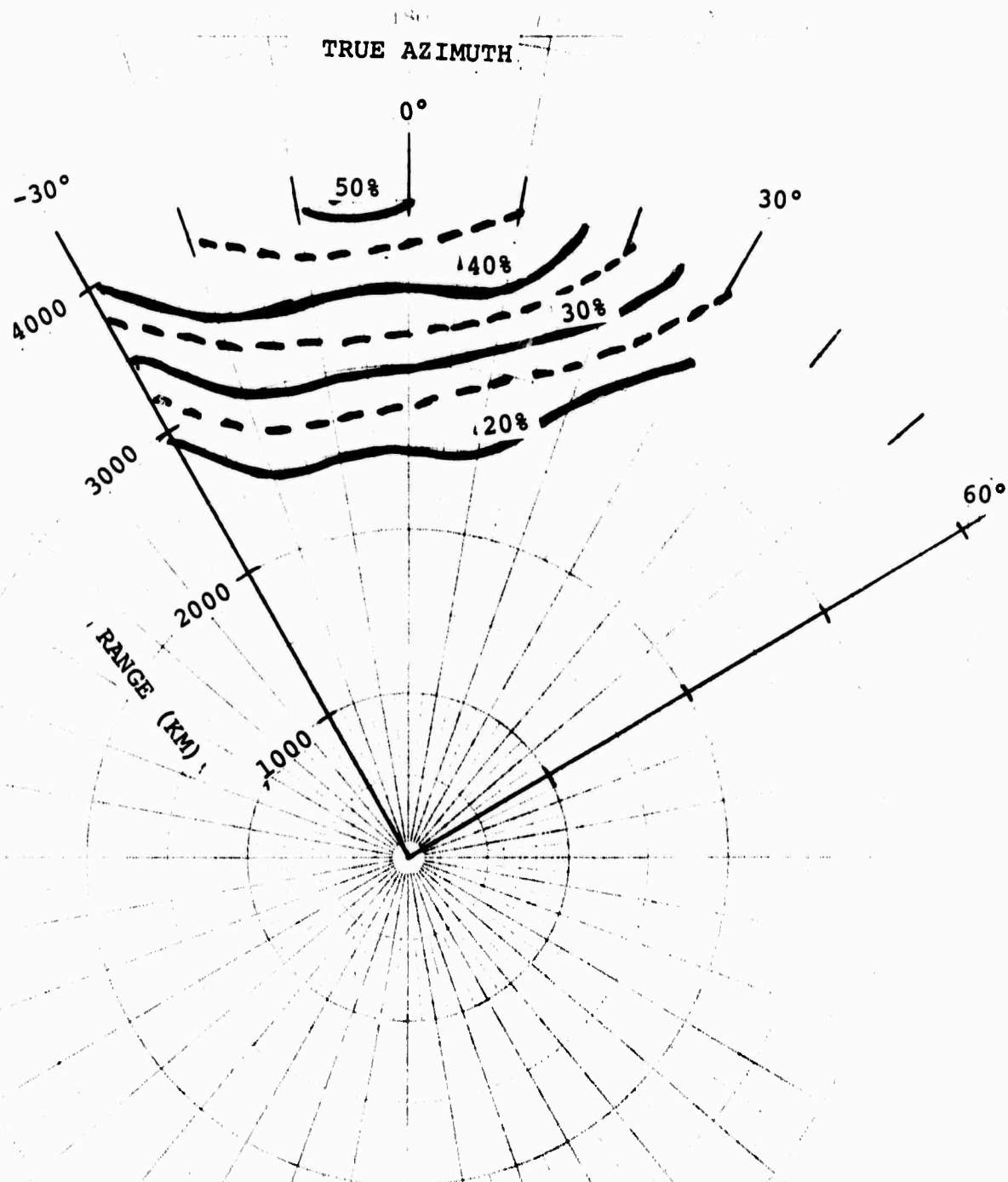
September 1971, 1200 UT
 Oblique Spread F Occurrence

Figure 40

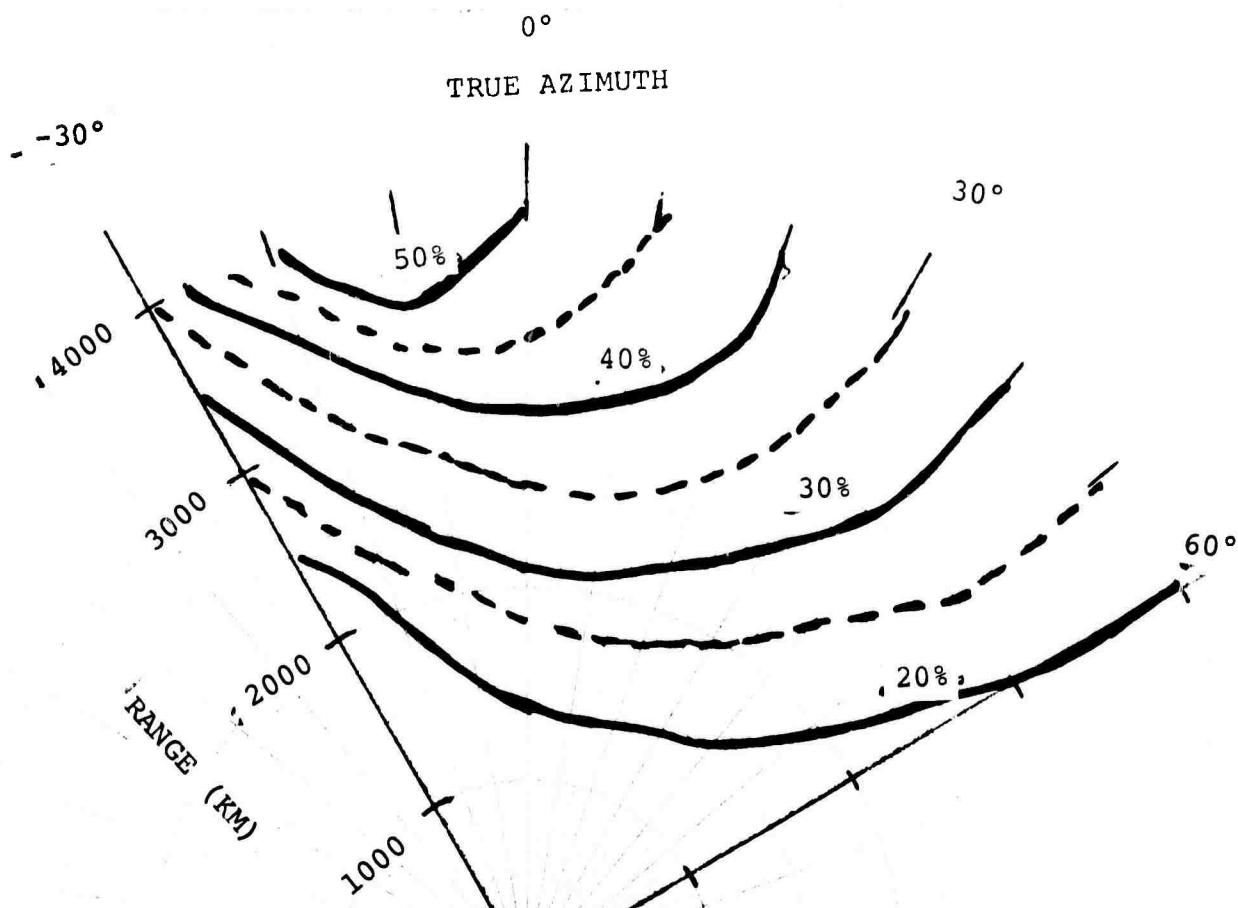
K&E POLAR CO-ORDINATE
46 4412
MADE IN U. S. A.
KEUFFEL & ESSER CO.



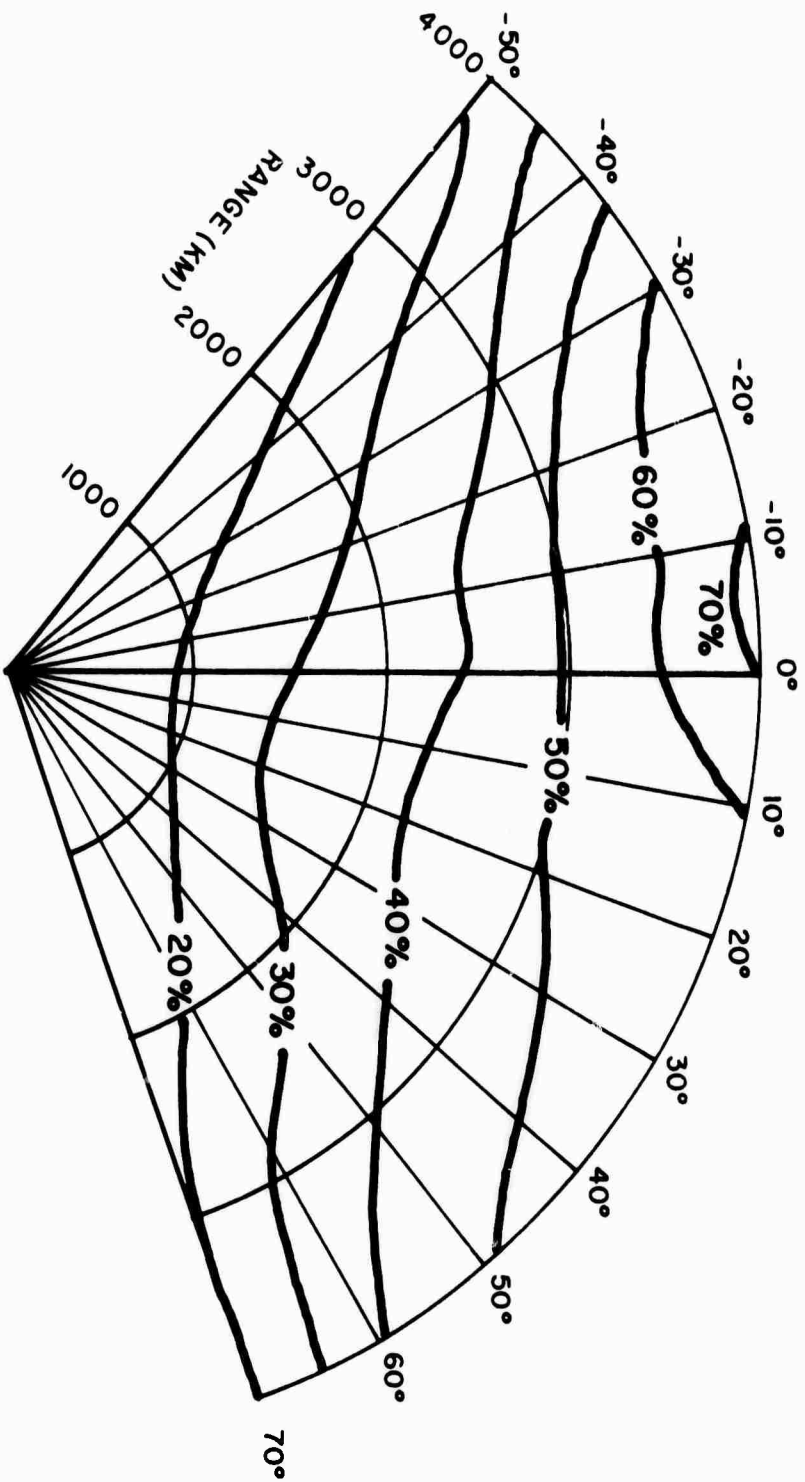
September 1971, 1500 UT
Oblique Spread F Occurrence



September 1971, 1800 UT
 Oblique Spread F Occurrence

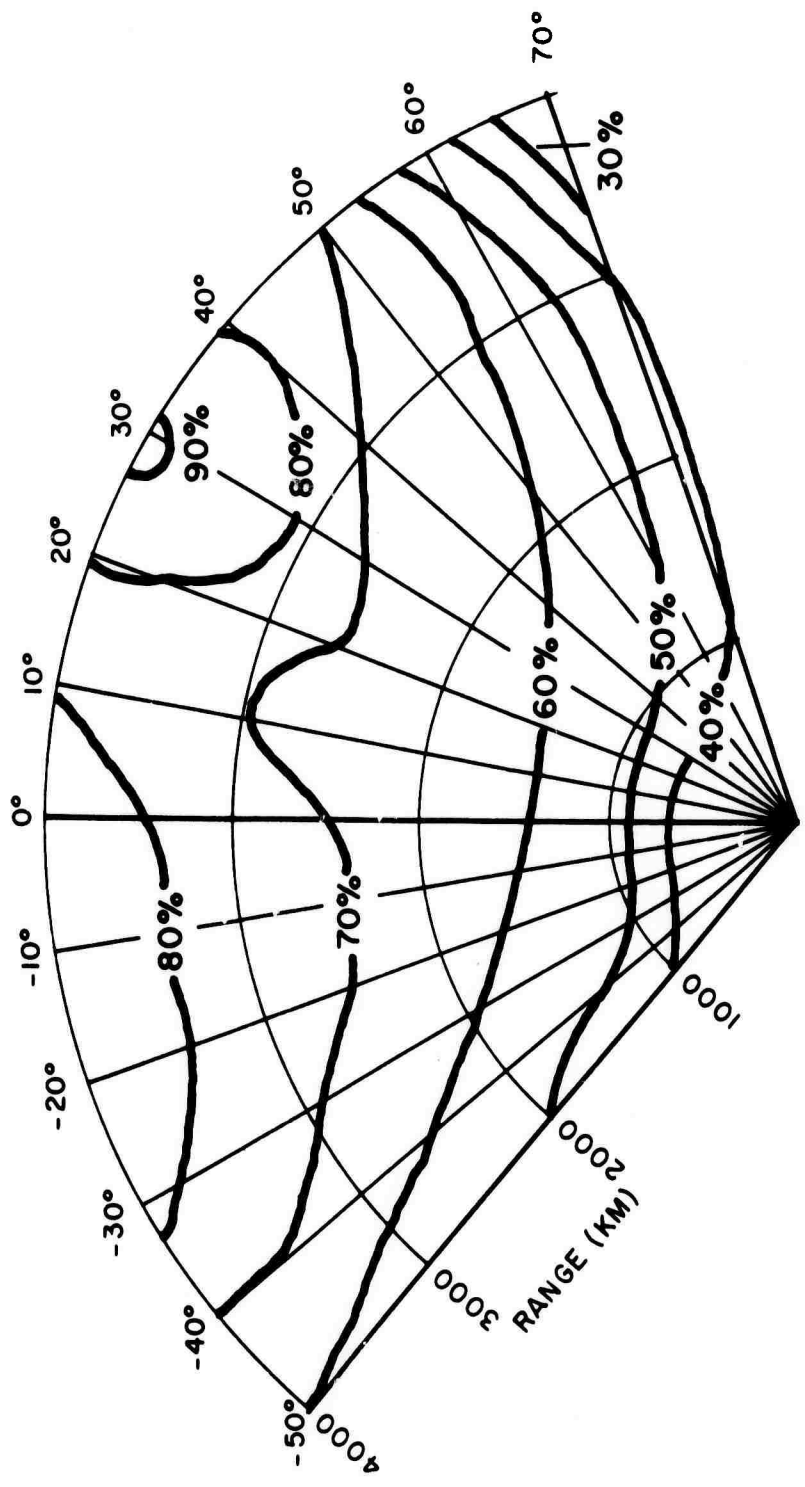


September 1971, 2100 UT
 Oblique Spread F Occurrence



00 UT WINTER

Spread F Occurrence probability at
 midpoint of path terminating at
 indicated range and azimuth.
 Projected to Winter (January 1971/72)
 for 0000 UT.

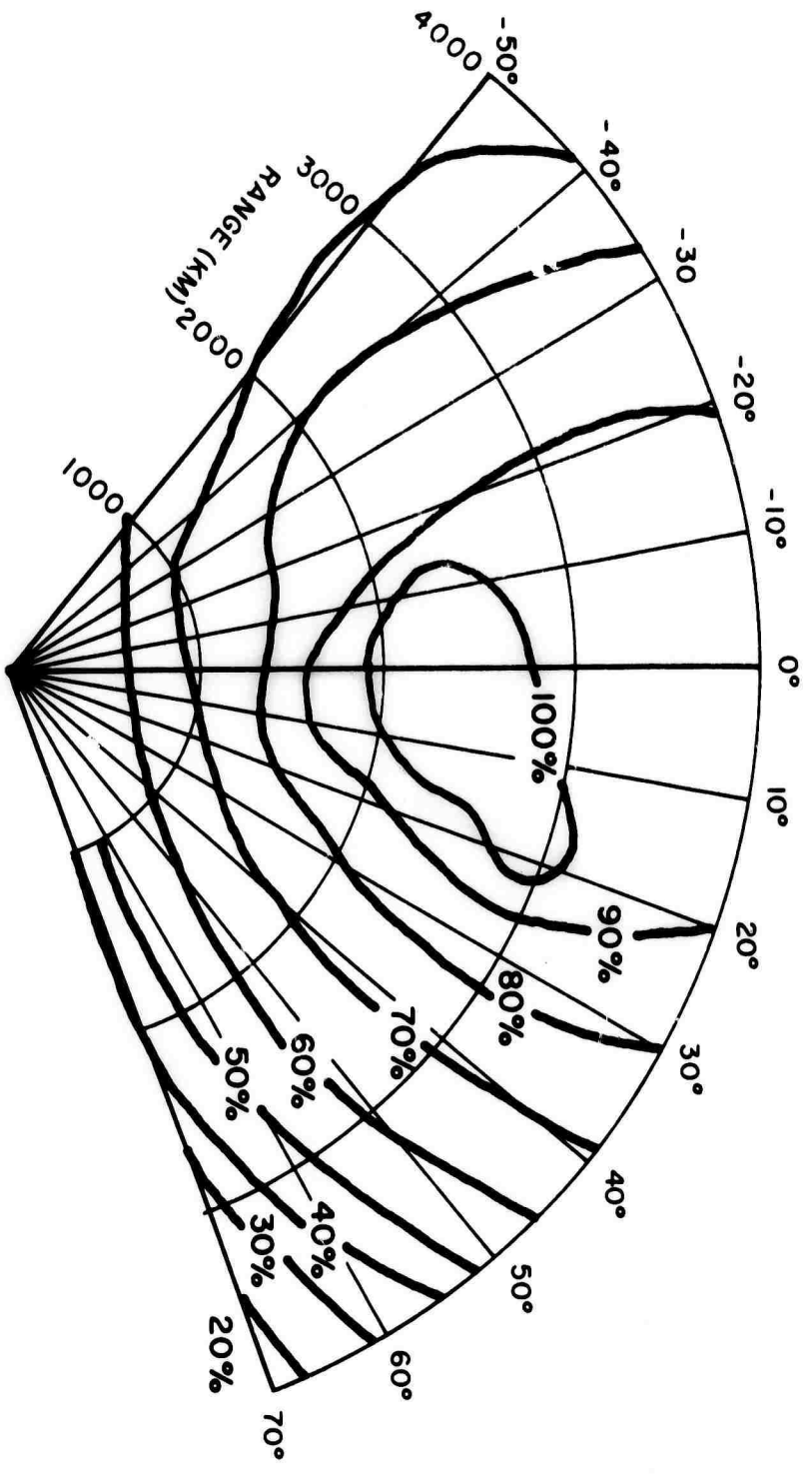


03 UT WINTER

Oblique Spread F Occurrence

I-99

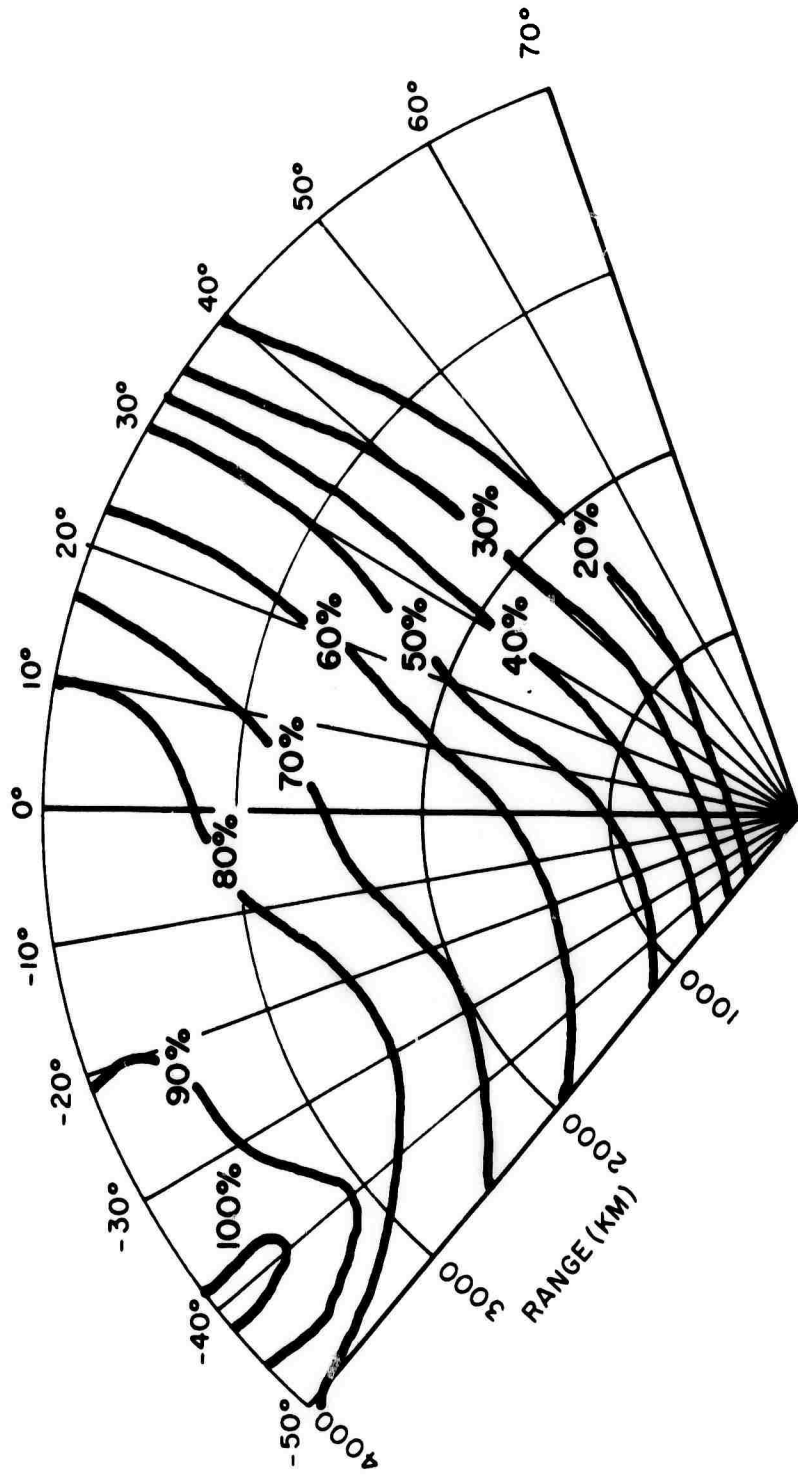
Figure 53



06 UT WINTER
 Oblique Spread F Occurrence

I-100

Figure 54

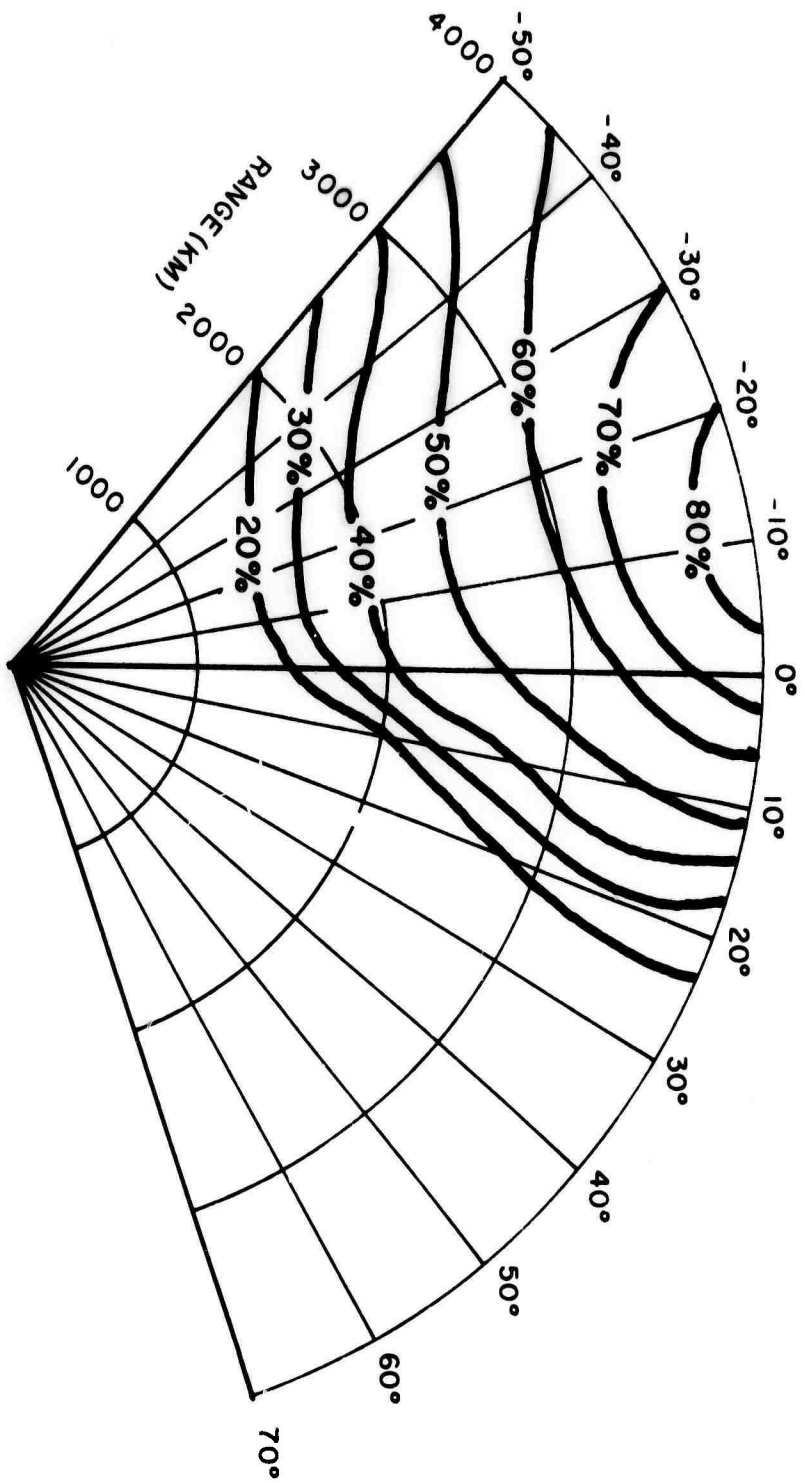


09 UT WINTER

Oblique Spread F Occurrence

Figure 55

I-101

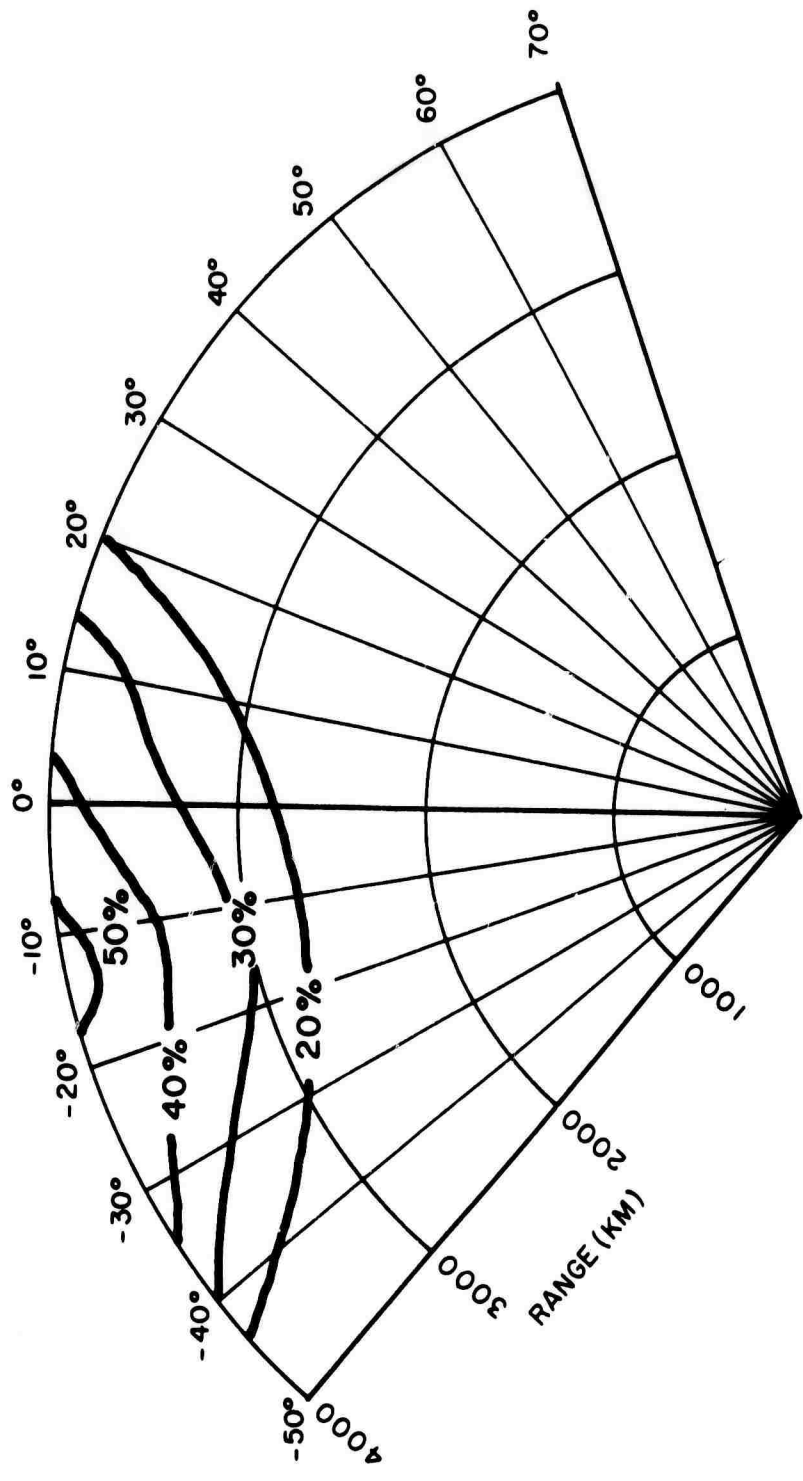


12 UT WINTER

Oblique Spread F Occurrence

I-102

Figure 56

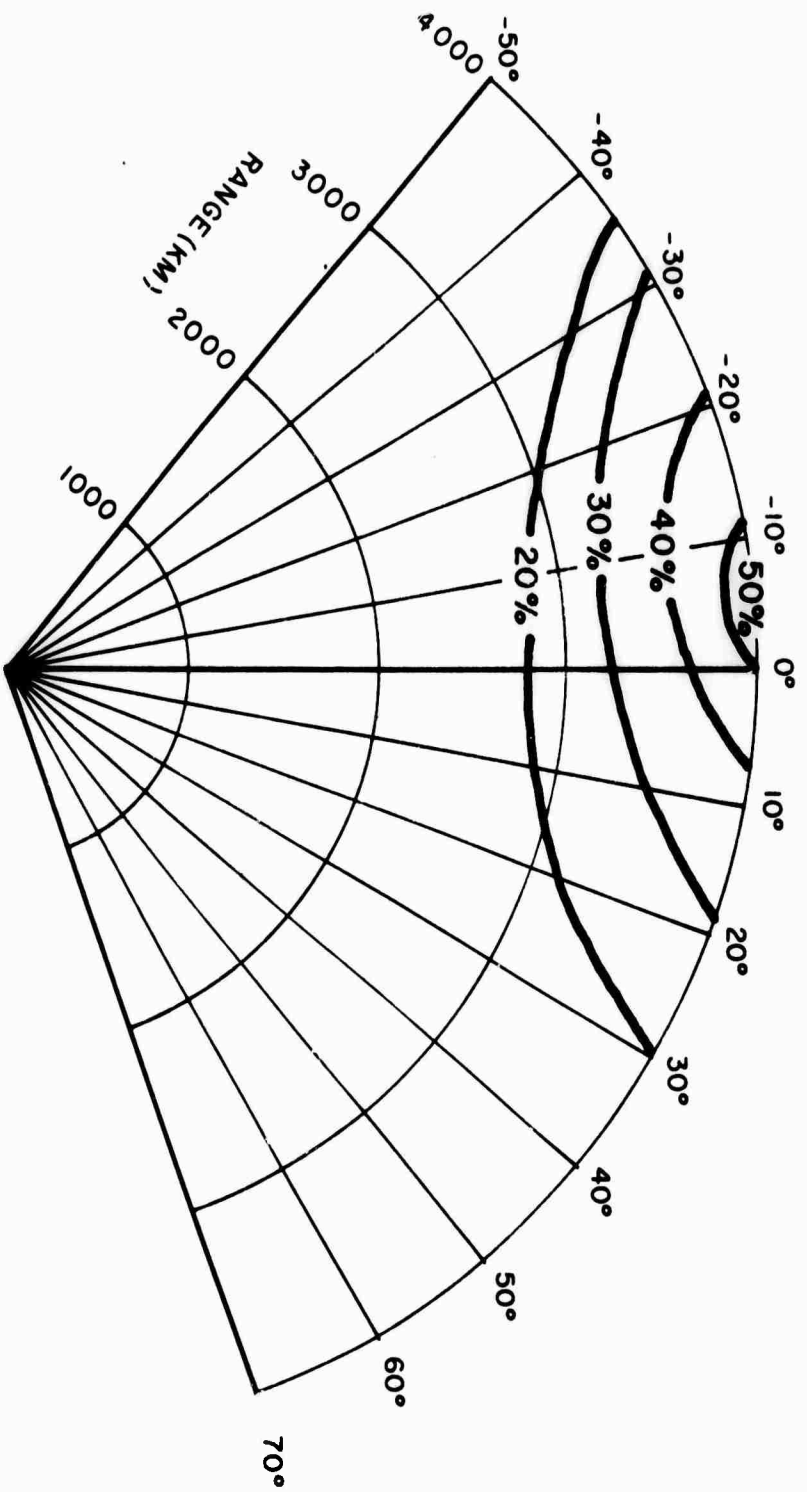


15 UT WINTER

Oblique Spread F Occurrence

I-103

Figure 57

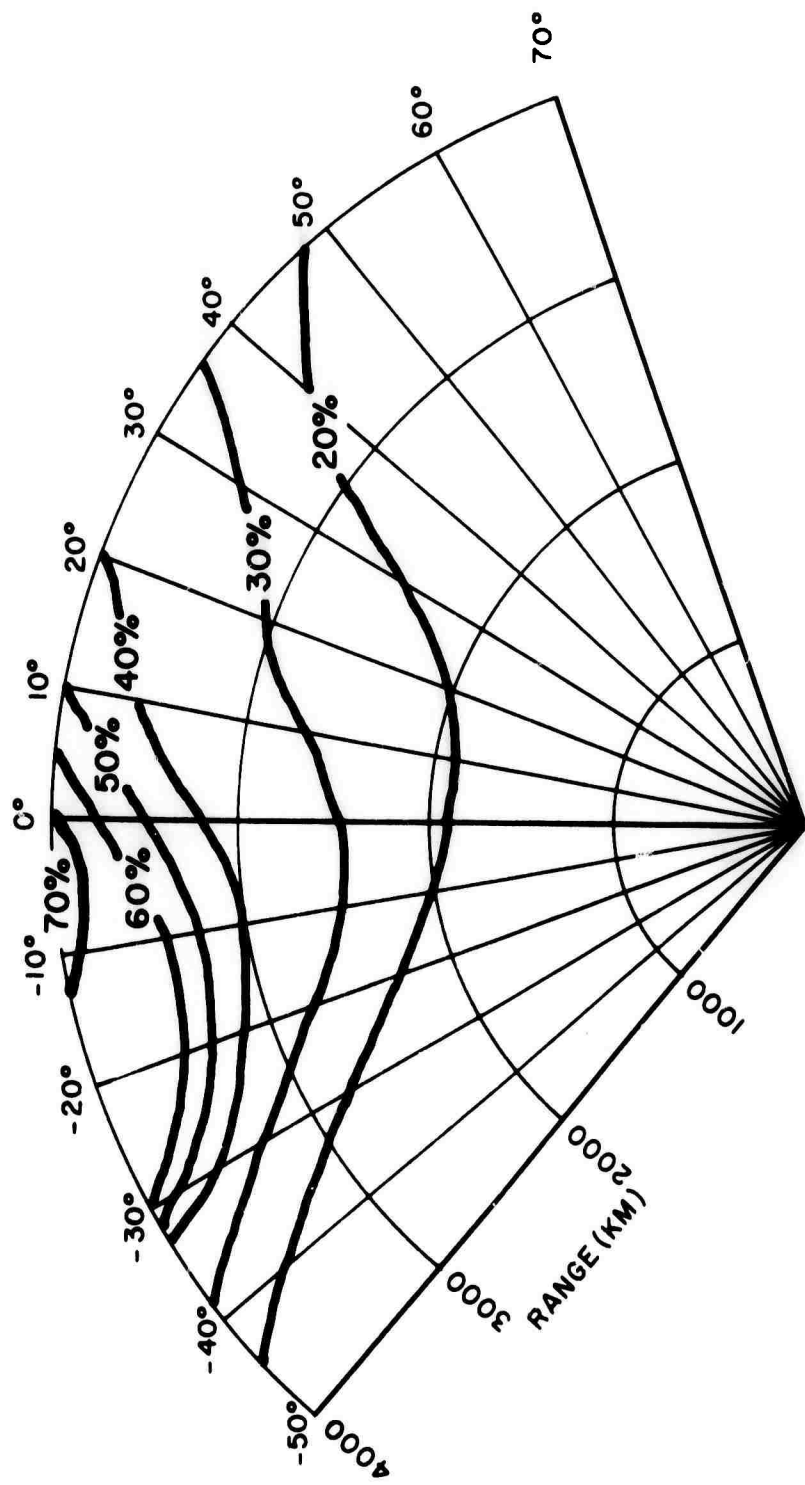


18 UT WINTER

Oblique Spread F Occurrence

I-104

Figure 58



21 UT WINTER

Oblique Spread F Occurrence

I-105

BLANK PAGE

Analytical Systems CORPORATION 

PART II: AURORAL SPORADIC E PREDICTIONS

by

R. Vargas-Vila

II-1

1. INTRODUCTION

During the nighttime hours or during sun spot cycle minimum when the critical frequency of the F layer decreases there is a corresponding decrease in maximum usable frequency range afforded by normal F layer propagation. At these times auroral sporadic E (E_s) occurs with a high enough frequency to make it a significant factor in the oblique E_s propagation of HF radio waves in the polar ionosphere. By E_s propagation is meant some mechanism that will stably support HF radio transmissions for periods of several minutes to several hours.

In this report contour plots were generated which show the probability of occurrence of the top frequency of Sporadic E, for various frequencies and conditions of magnetic activity. It is the function of these maps to give an idea of how much E_s one would expect to observe in the fan of a high latitude radar such as Polar Fox II. The data were gathered in the period of 1967 through 1970 and are used here as a prediction of the expected E_s in the period 1971-1972. The plots indicate percentage occurrence at the path midpoint expressed at the path endpoint in terms of range and azimuth from a fixed observing location to that endpoint of interest. Since the spatial correlation of E_s as a function of latitude was not known, the range coverage only extends to 2000 km (one hop propagation assumed). Propagation to greater distances requires two hops and therefore two E_s clouds; and while the occurrence of any two

clouds is not necessarily independent, neither is it necessarily simultaneous.

Oblique HF radio transmissions will be supported E_s propagation for the percentage of time indicated on the contour plots at frequencies up to approximately that given by the product of the top frequency and the secant of the incidence angle.